CRANFIELD UNIVERSITY


**Ahmed A. ABDULJABBAR**

# Energetic and Exergetic Study for Cross-Corrugated Membrane-Based Total Recovery Exchanger for Ventilation

School or Water, Energy and Environment

PhD Thesis in Mechanical Engineering
Academic Year: 2017 - 2018

Supervisors

Dr **ILAI SHER**
Dr **TAKA NISHINO**

October 2017

CRANFIELD UNIVERSITY

SCHOOL OF WATER, ENERGY AND ENVIRONMENT

PhD Thesis

Academic Year 2017 - 2018

**Ahmed A. ABDULJABBAR**

# Energetic and Exergetic Study for Cross-Corrugated Membrane-Based Total Recovery Exchanger for Ventilation

Supervisor: Dr **ILAI SHER** and Dr **TAKA NISHINO**

October 2017

This thesis is submitted in partial fulfilment of the requirements for the degree of PhD in Mechanical Engineering

# ABSTRACT

Indoor air quality is an important component of the air conditioning of buildings due to its major effect on the health of the occupants, thus the air supplied to these buildings by the ventilation system should be sufficient, clean and healthy. A most promising development was the heat recovery system which offers better thermal energy efficiency and comfort with adequate fresh air.

An energetic and exergetic analysis has been conducted on a cross-corrugated membrane based total heat exchanger core for ventilation of single dwellings. In order to enhance the sensible and latent effectiveness of the heat and mass transfer intensification was achieved by selecting Polyethersulfone for the membrane material, and a cross-corrugation arrangement of different dimensions for the primary surface exchanger.

The design was tested against a ventilation air volume flow rate for an individual household; from 85 to 100 $m^3$/hr. The dimensions of the exchanger were based on the polymer core being developed by Redring-Xpelair, Peterborough UK, with core dimensions of width and length both 250 mm, and a range of heights 100 – 500 mm. The cross-corrugated design of the test core had triangular openings with pitch lengths of 5, 10 and 25 mm. The ambient conditions were for a cold and humid winter in the UK. The ambient temperature test values were 2, 4, 6, 8 and 10 $^oC$, and the inlet air velocities in the core were 0.5, 1.0, 1.5 and 2 m/s, with Reynolds numbers not exceeding 2200.

CFD studies were conducted to investigate the thermal-fluid performance of the core, the Transition-SST model was used in the simulations within ANSYS Fluent 17.1 software and was validated using experimental data in the literature. The proposed model performed successfully in this study and proved that it was compatible with the test conditions.

The exergetic analysis was conducted using the IPSEpro modelling software, by creating a system consisting of membrane core, a domestic dwelling, fresh air and exhaust fans. The energetic analysis results were the basis of the IPSEpro modelling to determine the exergy, the exergetic efficiency and exergy destruction in the system.

The study concluded from both the energetic and the exergetic analysis that the membrane based exchanger core showed promising performance as a total heat and moisture recovery application with sensible and latent effectiveness values varying from 65% to 82%; and exergetic efficiency values varying from 30% to 60%, depending on core geometry and ambient conditions. The chemical exergy was the dominant factor in the performance in all cases, and the membrane core had the highest exergy destruction percentage comparing to the other system components.

Decreasing the pitch length of the exchanger core intensified its performance, the 5 mm case showed the best performance, but there are likely to be difficulties in manufacturing such a compact core. But, and more directly, its use would mean unpleasant compromises due to the extremely higher pressure drop across such a core even at low Reynolds numbers. The 10 mm case gave a better performance than the 25 mm, but not substantially different, therefore, the optimum choice lies between the better heat and mass transfer performance of the 10 mm case and the lower pressure drop and relative ease of manufacture of the 25 mm.

# ACKNOWLEDGEMENTS

Praise to our almighty **GOD**, the most merciful and gracious for enabling me to complete this thesis.

I would like to express my sincere thanks and deep gratitude to my supervisor **Dr. Ilai Sher** for his support, encouragement and suggestions throughout the work.

I also wish to give my utmost appreciation and thanks to my Family for their love, help, and supports through the years.

I would like also to express my gratitude to my colleagues **Dr. Abdulrahmen Almutairi**, **Dr. Abdelaziz Gamil** and **Dr. Aws Al-Akam** for their valuable help and backing, as well as all my colleagues in the Iraqi society at Cranfield University.

Special thanks to my sponsor, the Ministry of Higher Education and Scientific Research – IRAQ, whom without their sponsorship, I would not be able to achieve this piece of work.

Finally, I would like to extend my thanks and gratitude to all who had ever assisted me during the period of this research.

Author

*Ahmed Abduljabbar*

*2017*

# *Dedication*

***To ...***

My Precious Parents

*For making me who I am*

My Beloved Wife

*The symbol of sincerity*

My Gorgeous Daughter

*The flower of my life*

My Only Brother

*The best brother ever*

***Ahmed***

# TABLE OF CONTENTS

ABSTRACT ..... i
ACKNOWLEDGEMENTS ..... iii
TABLE OF CONTENTS ..... vii
LIST OF FIGURES ..... xi
LIST OF TABLES ..... xviii
NOMENCULTURE ..... xx
1 INTRODUCTION ..... 1
1.1 Background ..... 1
1.1.1 Fresh Air for Ventilation ..... 1
1.1.2 Energy Saving Prospective ..... 3
1.1.3 Types of Heat Recovery Systems ..... 4
1.2 Cross-Corrugated Exchanger Core ..... 4
1.3 Redring-Xpelair Company Meeting ..... 5
1.4 The Aim of This Study ..... 6
1.5 Objectives ..... 7
1.6 Overall Methodology ..... 7
1.7 Contribution to knowledge ..... 9
1.8 Thesis Structure ..... 9
2 LITERATURE REVIEW ..... 11
2.1 Overview ..... 11
2.2 Design Prospective ..... 12
2.3 Sizing and Ductwork ..... 14
2.4 Structure and Materials ..... 16
2.4.1 Metal Exchanger Cores ..... 17
2.4.2 Polymer-Based Exchanger Cores ..... 18
2.4.3 Fibre-Based Exchanger Cores ..... 19
2.4.4 Membrane-based Heat Exchanger Core ..... 19
2.4.5 Corrugated-plate Structure ..... 22
2.5 Air Flow Pattern ..... 24
2.6 Cross-Corrugated Membrane Exchanger Core ..... 25
2.7 Exergy in Heat Exchangers ..... 26
2.8 Exergetic Analysis for Corrugated Exchangers ..... 27
2.9 Literature Review Summary ..... 29
2.10 Current Work Approach and Contribution ..... 30
2.10.1 Energetic Analysis Contribution ..... 31
2.10.2 Exergetic Analysis contribution ..... 31
3 CROSS-CORRUGATED EXCHANGER CORE DESIGN ..... 32
3.1 Introduction and Core Description ..... 32

3.2 Triangular duct opening design ..... 35
3.3 Design Arrangement ..... 35
3.4 Ventilation Air Volume Flow Rates and Inlet Velocities Design ..... 37
3.5 Climate Design Conditions ..... 40
3.6 Hydraulic Diameter ..... 41
3.7 Reynolds Number ..... 42
3.8 Friction Factor ..... 44
3.9 Membrane-Based Exchanger ..... 45
3.9.1 Fundamental Principles of Membrane Materials ..... 45
3.9.2 Membrane Properties ..... 46
3.9.3 Membrane Material Selection ..... 47
3.10 Polyether-Sulfone (PES) Membrane Material ..... 48
3.11 Design Summary ..... 49
4 ENERGETIC ANALYSIS ..... 50
4.1 Introduction ..... 50
4.2 The Exchanger Core Geometry ..... 52
4.3 Basic Governing Equations ..... 55
4.3.1 Conservation of Mass (Continuity) ..... 55
4.3.2 Narvier-Stokes Equations (Momentum) ..... 55
4.3.3 Energy Equation ..... 56
4.3.4 Species Transport Equations ..... 56
4.3.5 Transition Flow Model (Transition-SST) ..... 57
4.4 Assumptions ..... 63
4.5 Mesh Generation ..... 63
4.5.1 Mesh Topology ..... 64
4.5.2 Three Dimensional Mesh Generation ..... 65
4.5.3 Mesh Quality and Dependency ..... 66
4.5.4 Model mesh characteristics ..... 72
4.6 Simulation Cases Setup in ANSYS Fluent 17.1 ..... 74
4.6.1 General Setup ..... 75
4.6.2 Model Setup ..... 75
4.6.3 Materials Setup: ..... 75
4.6.4 Cell Zone Conditions and Mesh Interference ..... 76
4.6.5 Boundary Conditions ..... 76
4.7 Solution ..... 79
4.7.1 Initial Conditions ..... 81
4.7.2 Solution Parameters ..... 82
4.7.3 Solution Methods ..... 82
4.7.4 Precision Solver Type ..... 82
4.7.5 Number of Iterations ..... 82
4.7.6 Convergence Criteria ..... 83
4.7.7 Under-Relaxation factors ..... 85

4.7.8 Multi-grid Parameters ..... 86
4.7.9 Linearization ..... 86
4.7.10 Discretization Scheme ..... 87
4.8 Validation Model ..... 89
4.8.1 Proposed Validation Model ..... 91
4.9 Energetic Analysis, Results and Discussion ..... 97
4.9.1 Flow Behaviour and Velocity Distribution ..... 100
4.9.2 Temperature Distribution ..... 105
4.9.3 Humidity Ratio Distribution ..... 111
4.9.4 Effectiveness Calculation ..... 117
4.9.5 Nusselt Number ..... 125
4.9.6 Sherwood number ..... 127
4.9.7 Pressure drop ..... 128
4.10 Energetic analysis summery ..... 131
5 EXERGY ANALYSIS ..... 132
5.1 History and Background ..... 132
5.2 The Theory Behind Exergy ..... 133
5.3 Ventilation Systems Thermal Analysis ..... 134
5.4 Exergetic Analysis ..... 135
5.5 Exergy Associated with Heat Transfer ..... 135
5.6 Exergy Associated with Work ..... 136
5.7 Types of Exergy ..... 136
5.7.1 Physical Exergy ..... 136
5.7.2 Chemical Exergy ..... 137
5.7.3 Kinetic Exergy ..... 138
5.7.4 Potential Exergy ..... 138
5.8 Reference and Dead State ..... 138
5.9 Waste Exergy ..... 139
5.9.1 Exergy Losses ..... 139
5.9.2 Exergy Destruction ..... 139
5.10 Exergetic Efficiencies ..... 140
5.11 Exergetic Analysis Modelling ..... 140
5.12 Total Recovery System Modelling ..... 141
5.12.1 Modelling Data of the Total Recovery System ..... 143
5.12.2 The Process Simulation Environment (PSE) ..... 143
5.12.3 Process Simulation MS Excel (PS Excel) ..... 146
5.13 Exergetic Analysis Results and Discussion ..... 146
5.13.1 Exergy Calculations ($\boldsymbol{E}$) ..... 148
5.13.2 Exergy Destruction Results ($\boldsymbol{Edes}$) ..... 156
5.14 Exergetic Efficiency Calculations ..... 164
5.15 Exergetic Analysis Summary ..... 167
6 CONCLUSIONS AND RECOMMENDATIONS FOR FURTHER WORK ..... 168

6.1 Conclusions ..... 168
6.1.1 Energetic Analysis Conclusions ..... 168
6.1.2 Exergetic analysis conclusions ..... 169
6.1.3 Final Conclusions ..... 171
6.2 Recommendations for the Future Work ..... 172
REFERENCES ..... 173
APPENDICES ..... 195
Appendix A ENERGETIC RESULTS ..... 195
Appendix B EXERGETIC RESULTS ..... 201

# LIST OF FIGURES

Figure 1-1: Typical heat recovery ventilation system for individual household. .. 2

Figure 1-2: The official Xpelair company's natural air 180 mechanical ventilation with heat recovery for domestic applications. The hexagonal flat plate polymer exchanger core (from the official website of Xpelair company ..... 2

Figure 1-3: Building energy consumption with the heat recovery system links… 3

Figure 1-4: Cross-corrugated triangular heat exchanger core arrangement [1].. 5

Figure 1-5 Overall summarised methodology..... 8

Figure 2-1: Typical membrane-based exchanger core for the energy recovery ventilator [38] ..... 13

Figure 2-2: Schematic model of heat exchanger flows [38] ..... 13

Figure 2-3: Schematic of moisture and heat transfer in a membrane core. [105] ..... 20

Figure 3-1: Cross-corrugated exchanger core. ..... 32

Figure 3-2: The supported plastic spacers for the membrane sheets..... 33

Figure 3-3: Schematic of a single channel of the membrane core showing the cross-corrugated flow pattern. ..... 33

Figure 3-4: Top view of the exchanger cores (a) Redring-Xplair's company present hexagonal flat-plate polymer core design, (b) The proposed square cross-corrugated membrane-based design ..... 34

Figure 3-5: Schematic shows the equilateral triangular duct opening with the apex angle (θ) and the pitch length (α). ..... 34

Figure 3-6: Exchanger core height vs heat transfer area. ..... 36

Figure 3-7: Exchanger core height vs number of triangular duct openings..... 37

Figure 3-8: Exchanger core height vs air velocity per opening..... 39

Figure 3-9: Exchanger core height vs total inlet area per core. ..... 39

Figure 3-10: Exchanger core height vs number of channels per core. ..... 39

Figure 3-11: Reynolds number with the inlet air velocity of the proposed cases. ..... 43

Figure 3-12: Mean friction factor with inlet air velocity. ..... 44

Figure 3-13: Hydrophilic polymer membrane selectivity [154] ..... 46

Figure 4-1: Cross corrugated triangular heat exchanger core arrangements. .. 52

Figure 4-2: Geometry of the element in CATIA 5 ..... 53

Figure 4-3: Geometric cross-sectional view of the elements in the CATIA 5 window..... 53

Figure 4-4: 25 mm model on the left with zoomed-in cross section on the right. ..... 54

Figure 4-5: 10 mm full scale model with zoomed-in cross section..... 54

Figure 4-6: 5 mm full scale model with zoomed-in cross section..... 54

Figure 4-7: (a) Triangular type element, (b) Tetrahedral type element, ..... 64

Figure 4-8: Mesh resolution test for 25 mm pitch length (mass flow rate) ..... 68

Figure 4-9: Mesh resolution test for 25 mm pitch length (Temperature)..... 68

Figure 4-10: Mesh resolution test for 25 mm pitch length (H2O mass transfer fraction)..... 69

Figure 4-11: Mesh for 25 mm pitch length model ..... 70

Figure 4-12: Zoomed-in picture of mesh for 25 mm pitch length model ..... 70

Figure 4-13: Mesh for (10 mm) pitch length model..... 70

Figure 4-14: Zoomed-in picture of mesh for (10 mm) pitch length model ..... 71

Figure 4-15: Mesh for (5 mm) pitch length model..... 71

Figure 4-16: Zoomed-in picture of mesh for (5 mm) pitch length model ..... 71

Figure 4-17: Air inlets and outlets (a) Fresh (b) Exhaust ..... 73

Figure 4-18: Sealing walls (a) Fresh air (b) Exhaust air ..... 73

Figure 4-19: (a) Upper top wall, (b) Lower bottom wall..... 73

Figure 4-20: Interference faces (a) fresh side (b) Exhaust side..... 74

Figure 4-21: SIMPLE algorithm flow chart. ..... 81

Figure 4-22: Solution residuals for (25 mm) case..... 84

Figure 4-23: Solution residuals for the (10 mm) cases ..... 84

Figure 4-24: Solution residuals for the (5 mm) cases ..... 84

Figure 4-25: Surface monitor for the mass flow rate (25 mm case) at ($T_{amb}$ = 6 $^{o}$C and $V_a$ = 1 m/s)..... 85

Figure 4-26: Schematic of Zhang's and Li's experimental setup [181]. ..... 90

Figure 4-27: Zhang's and Li's actual assembled total heat exchanger [181]. ... 90

Figure 4-28: Validation geometry (pitch length 18 mm and apex angle 60$^{o}$) .... 91

Figure 4-29: Validation (18 mm) pitch length meshed model ..... 92

Figure 4-30: zoomed-in section of the validation model in the corner of the model, pitch length (18 mm) and apex angle $60^0$. ..... 93

Figure 4-31: Fresh inlet velocity with fresh out temperature ..... 93

Figure 4-32: Exhaust inlet velocity with exhaust outlet temperature ..... 93

Figure 4-33: Fresh inlet velocity with fresh outlet humidity ratio ..... 94

Figure 4-34: Exhaust inlet velocity with exhaust humidity ratio..... 94

Figure 4-35: (a) Temperature contour on the membrane wall at 1 m/s inlet velocity for the proposed validation model (18mm), (b) Zhen-Xing Li's numerical temperature contour at the membrane wall at 1 m/s inlet velocity [181]..... 95

Figure 4-36: (a) Humidity contour on the membrane wall at 1 m/s inlet velocities in the proposed validation model (18mm), (b) Li's (18mm) numerical Humidity contour at the membrane wall and at 1 m/s inlet velocity [181]. . 95

Figure 4-37: Temperature contours in several sections for the fresh and exhaust stream for the validation model at inlet velocity 2.0 m/s..... 96

Figure 4-38: Humidity contours in several sections for the fresh and exhaust stream for the validation model at inlet velocity 2.0 m/s..... 96

Figure 4-39: 3D vectors in several sections for the fresh and exhaust stream for the validation model at inlet velocity 2.0 m/s..... 96

Figure 4-40: Velocity streamlines in several sections for the fresh and exhaust stream for the validation model at inlet velocity 2.0 m/s..... 97

Figure 4-41: Slices for 25 mm pitch length in both X and Z directions..... 98

Figure 4-42: : Slices for 10 mm pitch length in both X and Z directions..... 99

Figure 4-43: : Slices for 5 mm pitch length in both X and Z directions..... 99

Figure 4-44: (25 mm) 3D velocity vectors in X direction ..... 101

Figure 4-45: (25 mm) 3D velocity vectors in Z direction ..... 101

Figure 4-46: (25 mm) Velocity streamlines in X direction ..... 101

Figure 4-47: (25 mm) Velocity streamlines in Z direction ..... 102

Figure 4-48: (10 mm) 3D vectors in X direction ..... 102

Figure 4-49: (10 mm) 3D vectors in Z direction ..... 102

Figure 4-50: (10 mm) Velocity streamlines in X direction ..... 103

Figure 4-51: (10 mm) Velocity streamlines in Z direction ..... 103

Figure 4-52: (5 mm) 3D vectors in X direction ..... 103

Figure 4-53: (5 mm) 3D vectors in Z direction ..... 104

Figure 4-54: (5 mm) Velocity streamlines in X direction ..... 104

Figure 4-55: (5 mm) Velocity streamlines in Z direction. ..... 104

Figure 4-56: (25 mm) Temperature contours (Left) at X-AXIS and (Right) Y-AXIS at ($T_{fi}$=6$^{o}$C) and ($v_i$=0.5 m/s) ..... 106

Figure 4-57: (25 mm) Temperature contours (Left) at X-AXIS and (Right) Y-AXIS at ($T_{fi}$=6$^{o}$C) and ($v_i$=2.0 m/s) ..... 106

Figure 4-58: (25 mm) Temperature contours on the membrane's surface at ($v_i$=0.5 m/s) (Left) and ($v_i$=2.0 m/s) (Right) at ($T_{fi}$=6$^{o}$C). ..... 106

Figure 4-59: (25 mm) Temperature contours (Left) at X-AXIS and (Right) Y-AXIS at ($T_{fi}$=2$^{o}$C) and ($v_i$=2.0 m/s) ..... 107

Figure 4-60: (25mm) Temperature contours (Left) at X-AXIS and (Right) Y-AXIS at ($T_{fi}$=10$^{o}$C) and ($v_i$=2m/s) ..... 107

Figure 4-61: (10mm) Temperature contours (Left) at X-AXIS and (Right) Y-AXIS at ($T_{fi}$=6$^{o}$C) and ($v_i$=0.5m/s) ..... 107

Figure 4-62: (10mm) Temperature contours (Left) at X-AXIS and (Right) Y-AXIS at ($T_{fi}$=6$^{o}$C) and ($v_i$=2m/s) ..... 108

Figure 4-63: (10mm) Temperature contours on the membrane's surface at ($v_i$=0.5m/s) (Left) and ($v_i$=2m/s) (Right) at ($T_{fi}$=6$^{o}$C). ..... 108

Figure 4-64: (10mm) Temperature contours (Left) at X-AXIS and (Right) Y-AXIS at ($T_{fi}$=2$^{o}$C) and ($v_i$=2m/s) ..... 108

Figure 4-65: (10mm) Temperature contours (Left) at X-AXIS and (Right) Y-AXIS at ($T_{fi}$=10$^{o}$C) and ($v_i$=2m/s) ..... 109

Figure 4-66: (5mm) Temperature contours (Left) at X-AXIS and (Right) Y-AXIS at ($T_{fi}$=6$^{o}$C) and ($v_i$=0.5m/s) ..... 109

Figure 4-67: (5mm) Temperature contours (Left) at X-AXIS and (Right) Y-AXIS at ($T_{fi}$=6$^{o}$C) and ($v_i$=2m/s) ..... 109

Figure 4-68: (5 mm) Temperature contours on the membrane's surface at ($v_i$=0.5m/s) (Left) and ($v_i$=2m/s) (Right) at ($T_{fi}$=6$^{o}$C). ..... 110

Figure 4-69: (5 mm) Temperature contours in (Left) at X-AXIS and (Right) Y-AXIS at ($T_{fi}$=2$^{o}$C) and ($v_i$=2m/s) ..... 110

Figure 4-70: (5 mm) Temperature contours (Left) at X-AXIS and (Right) Y-AXIS at ($T_{fi}$=10$^{o}$C) and ($v_i$=2m/s) ..... 110

Figure 4-71: (25mm) Humidity contours (Left) at X-AXIS and (Right) Y-AXIS at ($T_{fi}$=6$^{o}$C) and ($v_i$=0.5m/s). ..... 112

Figure 4-72: (25mm) Humidity contours (Left) at X-AXIS and (Right) Y-AXIS at ($T_{fi}$=6$^{o}$C) and ($v_i$=2m/s) ..... 112

Figure 4-73: (25mm) Humidity contours on the membrane's surface at ($v_i$=0.5m/s) (Left) and ($v_i$=2m/s) (Right) at ($T_{fi}$=6$^{o}$C). ..... 112

Figure 4-74: (25mm) Humidity contours (Left) at X-AXIS and (Right) Y-AXIS at ($T_{fi}$=2$^{o}$C) and ($v_i$=2m/s) ..... 113

Figure 4-75: (25mm) Humidity contours (Left) at X-AXIS and (Right) Y-AXIS at ($T_{fi}$=10$^{o}$C) and ($v_i$=2m/s) ..... 113

Figure 4-76: (10mm) Humidity contours (Left) at X-AXIS and (Right) Y-AXIS at ($T_{fi}$=6$^{o}$C) and ($v_i$=0.5m/s) ..... 113

Figure 4-77: (10mm) Humidity contours (Left) at X-AXIS and (Right) Y-AXIS at ($T_{fi}$=6$^{o}$C) and ($v_i$=2m/s) ..... 114

Figure 4-78: (10mm) Humidity contours on the membrane's surface at ($v_i$=0.5m/s) (Left) and ($v_i$=2m/s) (Right) at ($T_{fi}$=6$^{o}$C). ..... 114

Figure 4-79: (10mm) Humidity contours (Left) at X-AXIS and (Right) Y-AXIS at ($T_{fi}$=2$^{o}$C) and ($v_i$=2m/s) ..... 114

Figure 4-80: (10mm) Humidity contours in (Left) at X-AXIS and (Right) Y-AXIS at ($T_{fi}$=10$^{o}$C) and ($v_i$=2m/s) ..... 115

Figure 4-81: (5mm) Humidity contours in (Left) at X-AXIS and (Right) Y-AXIS at ($T_{fi}$=6$^{o}$C) and ($v_i$=0.5m/s) ..... 115

Figure 4-82: (5mm) Humidity contours (Left) at X-AXIS and (Right) Y-AXIS at ($T_{fi}$=6$^{o}$C) and ($v_i$=2m/s) ..... 115

Figure 4-83: (5mm) Temperature contours on the membrane's surface at ($v_i$=0.5m/s) (Left) and ($v_i$=2m/s) (Right) at ($T_{fi}$=6$^{o}$C). ..... 116

Figure 4-84: (5mm) Humidity contours (Left) at X-AXIS and (Right) Y-AXIS at ($T_{fi}$=2$^{o}$C) and ($v_i$=2m/s) ..... 116

Figure 4-85: (5mm) Humidity contours (Left) at X-AXIS and (Right) Y-AXIS at ($T_{fi}$=10$^{o}$C) and ($v_i$=2m/s) ..... 116

Figure 4-86: (25 mm) Sensible and latent effectiveness and air inlet velocity (m/s) ..... 121

Figure 4-87: (25 mm) Sensible and latent effectiveness and ambient temperature (C$^{o}$) ..... 121

Figure 4-88: (10 mm) Sensible and latent effectiveness and air inlet velocity (m/s) ..... 121

Figure 4-89: (10 mm) Sensible and latent effectiveness and ambient temperature (C$^{o}$) ..... 122

Figure 4-90: (5 mm) Sensible and latent effectiveness and air inlet velocity (m/s) ..... 122

Figure 4-91: (5 mm) Sensible and latent effectiveness and ambient temperature ($C^o$) ..... 122

Figure 4-92: Sensible effectiveness according to the air inlet velocity (m/s) for all three pitch lengths. ..... 123

Figure 4-93: Sensible effectiveness according to the ambient temperature ($C^o$) for all three pitch lengths..... 123

Figure 4-94: Latent effectiveness according to the air inlet velocity (m/s) for all three pitch lengths ..... 124

Figure 4-95: Latent effectiveness according to the ambient temperature ($C^o$) for all three pitch lengths..... 124

Figure 4-96: The relation between Nusselt number and Reynolds number for the three pitch lengths ..... 126

Figure 4-97: The relation between Sherwood number and Reynolds number. ..... 128

Figure 4-98 Pressure drop across heat exchanger of (250 $\times$ 250 $\times$ 500 mm) dimensions for three pitch lengths with change in inlet velocity..... 129

Figure 5-1: The energy portion that cannot be converted in to work is unavailable energy ..... 132

Figure 5-2 Schematic diagram for the air conditioning system, showing the components and the thermal processes for the exergetic analysis ..... 142

Figure 5-3 Screen shot of the IPSEpro for a heat exchanger duct of pitch length 25 mm..... 144

Figure 5-4: Model for 10 mm pitch length in IPSEpro at $10^0$C ambient temperature and 2.0 m/s inlet air velocity. ..... 147

Figure 5-5: Model for 5 mm pitch length in IPSEpro at $6^0$C ambient temperature and 2.0 m/s inlet air velocity. ..... 148

Figure 5-6: Exergy and inlet air velocity for heat exchanger duct with 5 mm pitch length..... 152

Figure 5-7: Exergy and inlet air velocity for heat exchanger duct with 10 mm pitch length ..... 152

Figure 5-8: Exergy and inlet air velocity for heat exchanger duct with 25 mm pitch length ..... 152

Figure 5-9: Exergy and ambient temperature for the exchanger core (5 mm) pitch length. ..... 154

Figure 5-10: Exergy and ambient temperature for the exchanger core (10mm) pitch length ..... 154

Figure 5-11: Exergy and ambient temperature for the exchanger core with (25 mm) pitch length. ..... 154

Figure 5-12: Total exergy destruction in the system as a function of inlet air velocity..... 157

Figure 5-13: Total exergy destruction in the system with the ambient temperature. ..... 158

Figure 5-14: Exergy destruction percentage with the inlet air velocity for system components with 5 mm pitch length ..... 159

Figure 5-15: Exergy destruction percentage with the inlet air velocity for system components with 10 mm pitch length. ..... 159

Figure 5-16: Exergy destruction percentage with the inlet air velocity for system components with 25 mm pitch length. ..... 159

Figure 5-17: Membrane core's exergy destruction percentage with air inlet velocity..... 160

Figure 5-18: Exergy destruction percentage and the ambient temperature for pitch length 5 mm. ..... 162

Figure 5-19: Exergy destruction percentage and the ambient temperature for pitch length 10 mm. ..... 162

Figure 5-20: Exergy destruction percentage and the ambient temperature for pitch length 25 mm. ..... 162

Figure 5-21: Membrane core's exergy destruction percentage with ambient temperature ..... 163

Figure 5-22: Exergetic efficiency with inlet air velocity for all three duct geometries..... 165

Figure 5-23: Exergetic efficiency with ambient temperature ..... 166

# LIST OF TABLES

Table 3-1: Corrugated sheets: dimensions and areas. ..... 35

Table 3-2 Heat exchanger dimensions, number of layers (*n*) and heat exchange area (*A*)..... 36

Table 3-3: Heat exchanger designs with their dimensions (Average velocity calculated using flow rate of 100 $m^3$/h [0.0278 $m^3$/s]). ..... 38

Table 3-4: Humidity ration values in (kg/kg) for given ambient temperature and relative humidity..... 40

Table 3-5: Hydraulic diameter for equilateral triangle duct opening..... 41

Table 3-6: Reynolds number values for the designed inlet air velocities ..... 43

Table 3-7: Mean friction factor for the designed air inlet velocities. ..... 44

Table 3-8: Properties of some common membrane materials [155] ..... 47

Table 4-1: Mesh details for the all three pitch lengths ..... 67

Table 4-2: Mesh study for the 25 mm pitch length..... 68

Table 4-3: The geometric parameters ..... 72

Table 4-4: Properties of membrane material ..... 75

Table 4-5: Properties of working fluid (Air) ..... 76

Table 4-6: Thermal boundary conditions ..... 78

Table 4-7: Momentum boundary condition summary ..... 79

Table 4-8: Under relaxation factor (r ) for 25mm cases ..... 86

Table 4-9: Li and Zhang's physical parameters [181] ..... 91

Table 4-10: Slice position for all the cases according the axis ..... 98

Table 4-11: Percentage decrease in heat exchanger effectiveness with changes in air inlet velocity and humidity. ..... 119

Table 4-12: Inlet and outlet air mass flow rate 25mm at 6$^o$C ambient. ..... 120

Table 4-13: Inlet and outlet air temperature 25mm at 6$^o$C ambient. ..... 120

Table 4-14: Inlet and outlet FRESH air composition rate 25mm at 6$^o$C ambient. ..... 120

Table 4-15: Inlet and outlet EXHAUST air composition rate 25mm at 6$^o$C ambient. ..... 120

Table 4-16: selection table for the presented exchanger core designs. ..... 130

Table 5-1 Comparison between ENERGY and EXERGY [133,183]..... 133

Table 5-2: Air states points through the system ..... 147

Table 5-3: Reference composition and air states 25 mm, 6$^{o}$C and 0.5 m/s.... 149

Table 5-4: Chemical exergy rate calculations and results (25mm, 6$^{o}$C and 1.5m/s)..... 150

Table 5-5 Equations used in the fuel-product method. ..... 156

Table 5-6: The differences in the exergy destruction percentage for each component when increasing the inlet air velocity from 0.5 m/s to 2.0 m/s 161

Table 5-7: The percentage of difference in the exergy destruction percentage for each component when increasing the ambient temperature from 2$^{o}$C to 10$^{o}$C..... 164

# NOMENCULTURE

## LATIN SYMBOL

| SYMBOL | DESCRIPTION | UNIT |
|---|---|---|
| $A$ | Heat transfer membrane area | $m^2$ |
| $\bar{A}$ | Surface area vector | $m^2$ |
| $a_p$ , $a_{nb}$ | Linearized coefficients | - |
| $C_a$ , $C_e$ | Constants | - |
| $C_p$ | Specific heat | J/kg.k |
| $D_h$ | Hydraulic diameter | m |
| $D_{ima}$ | Diffusion coefficient | $m^2/s$ |
| $D_{va}$ | Moisture diffusivity of air | $m^2/s$ |
| $D_{vm}$ | Effective moisture diffusivity in membrane | $m^2/s$ |
| $d_p$ | Pore diameter in membrane | mm |
| $E_{ch}$ | Molar chemical exergy | J/mol |
| $e_{k^{-ch}}$ | Standard molar chemical exergy | J/mol |
| $\dot{E}_{ch}$ | Chemical exergy rate | Watt |
| $\dot{E}_d$ | Exergy destruction rate | Watt |
| $\dot{E}_e$ | Exergy destruction exit | Watt |
| $\dot{E}_f$ | Fuel supplied exergy rate | Watt |
| $\dot{E}_i$ | Exergy destruction input | Watt |
| $\dot{E}_{ke}$ | Kinetic exergy rate | Watt |
| $\dot{E}_l$ | Exergy loss | Watt |
| $\dot{E}_p$ | Product exergy rate | Watt |
| $\dot{E}_{pe}$ | Potential exergy rate | Watt |
| $\dot{E}_{ph}$ | Physical exergy rate | Watt |
| $\dot{E}_x$ | Total exergy rate | Watt |
| $f_D$ | Mass friction factor | - |
| $F_{length}$ | Empirical control correlation | - |
| $F_{turb}$ | Turbulence empirical correlation | - |
| $G_k^*$ | Modified production for turbulence kinetic energy | |
| $\tilde{G}_k$ | Original production term of SST model | |
| $H$, $h$ | Enthalpy | J |
| $h$ | Convection heat transfer coefficient | $W/m^2.K$ |

| | | |
|---|---|---|
| J | Mass transfer flux | kg/s |
| $\vec{J_i}$ | Diffusion flux | kg/s |
| $k$ | Mass transfer coefficient | kg/m$^2$.s |
| k | Turbulence kinetic energy | m$^2$/s$^2$ |
| $\dot{m}$ | mass flow rate | kg/s |
| $N_{face}$ | number of faces enclosing the cell in the mesh. | - |
| $n$ | Number of channels | - |
| $P$ | Pressure | Pa |
| $P_{\gamma 1}$ , $E_{\gamma 1}$ | Transition sources | - |
| $P_{\gamma 2}$ , $E_{\gamma 2}$ | Destruction/relaminerization sources | - |
| $R$ | Ideal gas constant | J/mol.K |
| $Re$ | Reynolds number | - |
| $Re_v$ | Vorticity Reynolds number | - |
| $Re_{\theta c}$ | Critical Reynolds number | - |
| $\widetilde{Re}_{\theta c}$ | Transition Reynolds number | - |
| $R_T$ | Vorticity ratio | - |
| r | Under-relaxation factor | - |
| S | Strain rate magnitude | - |
| s | Entropy | J/k |
| $S_k$ | User-defined source term | m$^2$/ s$^2$ |
| T | Temperature | $^o$C |
| U | Local velocity | m/s |
| $u, v \; and \; w$ | Cartesian velocity components | m/s |
| $V$ | velocity | m/s |
| $\bar{v}$ | Velocity vector | m/s |
| $\vec{v}$ | Velocity field | m/s |
| $\dot{V}_a$ | Air volume flow rate | m$^3$/s |
| $w$ | Humidity ratio | kg/kg |
| x, y and z | Cartesian coordinates | - |
| $y$ | Wall distance | m |
| $y^+$ | Non-dimensional distance | - |
| $y_k$ | Molar fraction | mol/mol |
| $Y_i$ | local mass fraction | mol |
| $Y_k$ | Original destruction term of SST model | |
| $Y_k^*$ | Modified dissipation rate | |

## GREEK SYMBOLS

| SYMBOL | DESCRIPTION | UNIT |
|---|---|---|
| $\alpha$ | Pitch length | mm |
| $\beta$ | Thermal expansion coefficient | 1/K |
| $\Gamma$ | Diffusion coefficient | N.s/m$^2$ |
| $\gamma$ | Intermittency | 1/s |
| $\Delta T_m$ | Log mean temperature difference | $^o$C |
| $\Delta w_v$ | Log mean humidity ratio difference | kg/kg |
| $\delta$ | Thickness | m |
| $\varepsilon$, $\omega$ | Dissipation rate of kinetic energy | 1/s |
| $\varepsilon_S$, $\varepsilon_L$ | Sensible and latent effectiveness | - |
| $\eta_{ex}$ | exergetic efficiency | - |
| $\theta$ | Apex angle | Degree |
| $\nu$ | Kinematic viscosity | m$^2$/s |
| $\lambda$ | Thermal conductivity | W/m.K |
| $\mu$ | Viscosity | kg/m.s |
| $\mu_t$ | Eddy viscosity | kg/m.s |
| $\rho$ | Density | kg/m$^3$ |
| $\Phi$ | Primary variable | - |
| $\varphi$ | Relative humidity | - |
| $\Omega$ | Vorticity magnitude | - |
| $\psi$ | Correction factor | - |

## ABBREVIATIONS

| | |
|---|---|
| ASHRAE | American Society of Heating, Refrigeration and Air Conditioning Engineers |
| CAD | Computer Aided Design |
| CFD | Computational Fluid Dynamics |
| CIBSE | Chartered Institution of Building Services Engineers |
| COP | Coefficient of Performance |
| CPU | Central Processing Unit |
| CSLM | Composite Supported Liquid Membrane |
| EGM | Entropy Generation Minimization |
| FLT | First Law of Thermodynamics |
| HVAC | Heating, Ventilation and Air Conditioning |
| MDK | IPSEpro Model Development Kit |

| | |
|---|---|
| MDL | Model Description Language |
| Nu | Nusselt Number |
| QRST | Quality, Resolution, Smoothness and Total cell count |
| PES | Polyethersulfone membrane |
| PSE | Process Simulation Environment |
| PSExcel | Process Simulation Microsoft Excel |
| RAMEE | Run-Around Membrane Energy Recovery |
| Re | Reynolds number |
| SIMPLE | Semi-Implicit Method for Pressure-Linked Equations |
| Sh | Sherwood number |
| SLT | Second Law of Thermodynamics |
| SST | Shear Stress Transport |

## SUBSCRIBTIONS

| SYMBOL | DESCRIBTION |
|---|---|
| 0 | Reference state |
| a | Air |
| amb | Ambient |
| e | Exhaust |
| f | Fresh, Face |
| i | Inlet |
| o | outlet |
| mem | Membrane |
| nb | Neighbour cell |
| s | Specified state |
| tot | TOTAL |

## SUPERSCRIPTIONS

| SYMBOL | DESCRIPTION |
|---|---|
| * | Guessed quantity or quantity from last iteration |
| ‘ | Corrected quantity |
| + | Dimensionless |

# 1 INTRODUCTION

## 1.1 Background

Air conditioning is an area where sciences and engineering meet, primarily, to produce comfortable living and working conditions for humans, though there is an extensive range of additional applications, ranging from the cooling of electronic devices to animal husbandry and food preservation. Air conditioning has a multidisciplinary character, including mechanical engineering, electrical engineering, civil engineering, chemical engineering, chemistry, physics and even, occasionally, food engineering. The air conditioning systems industry has dramatically expanded during the past years to play a significant role in societies throughout the world. Its social and economic impact is ever more impressive and this will continue because of the increasing number and extent of its applications. It would be expected that due to the increase in the temperature of the earth due to global warming this technology will serve to improve living conditions in further countless ways [1].

### 1.1.1 Fresh Air for Ventilation

One of the most important aspects in air conditioning is indoor air quality [2–7]. The health and comfort of the occupants is essential, so the fresh air supplied by the ventilation system should be adequate. The most traditional and easy way to access fresh air is by opening a window and this the reason why, traditionally, buildings have been provided with openable windows. Today, however, this arrangement would ruin the concept of constructing insulated buildings [8]. One of the alternative solutions is heat recovery systems which offer fresh air, better thermal comfort and high energy efficiency [9].

Heat recovery systems can be considered as processes of recovering energy (heat/mass) from a high temperature flow and transferring it to a low temperature flow in a manner which is both functionally effectively and economically useful [10]. With air conditioning this would normally be a device that extracts, recovers or removes heat or mass from a flow of warmer air and

transfers it to another cooler flow of air [11]. Figure 1-1 shows a typical heat recovery ventilator for an individual household.

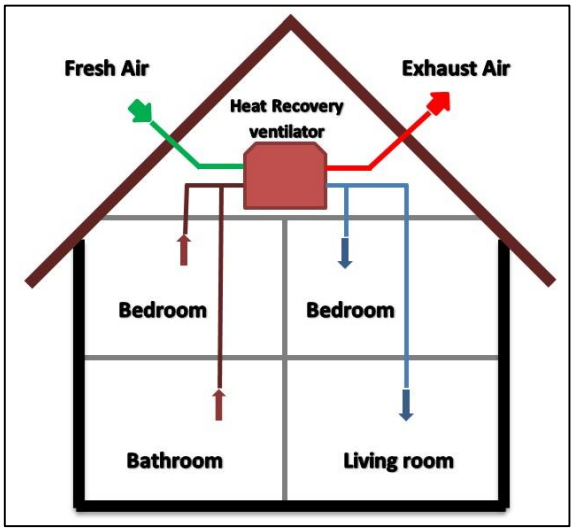


**Figure 1-1: Typical heat recovery ventilation system for individual household.**

**Figure 1-2: The official Xpelair company's natural air 180 mechanical ventilation with heat recovery for domestic applications. The hexagonal flat plate polymer exchanger core (from the official website of Xpelair company**

### 1.1.2 Energy Saving Prospective

Energy consumption for the last 30 years has increased exponentially due to economic and population growth [1]. Most research surveys have concluded that a major reason for this is the increase in the number of buildings[9]. Typically, 40% of total energy needed in Europe is consumed by heating, ventilation and air conditioning systems (HVAC), and in the UK total domestic energy consumption fell over the last five years due to government sponsored insulation programmes [12]. Domestic buildings are invariably built to last for decades, even generations, so it is very important to make the right decisions in the design phase to achieve long term environmental balance and energy control. Figure 1-3 is a schematic showing building energy consumption with a heat recovery system.

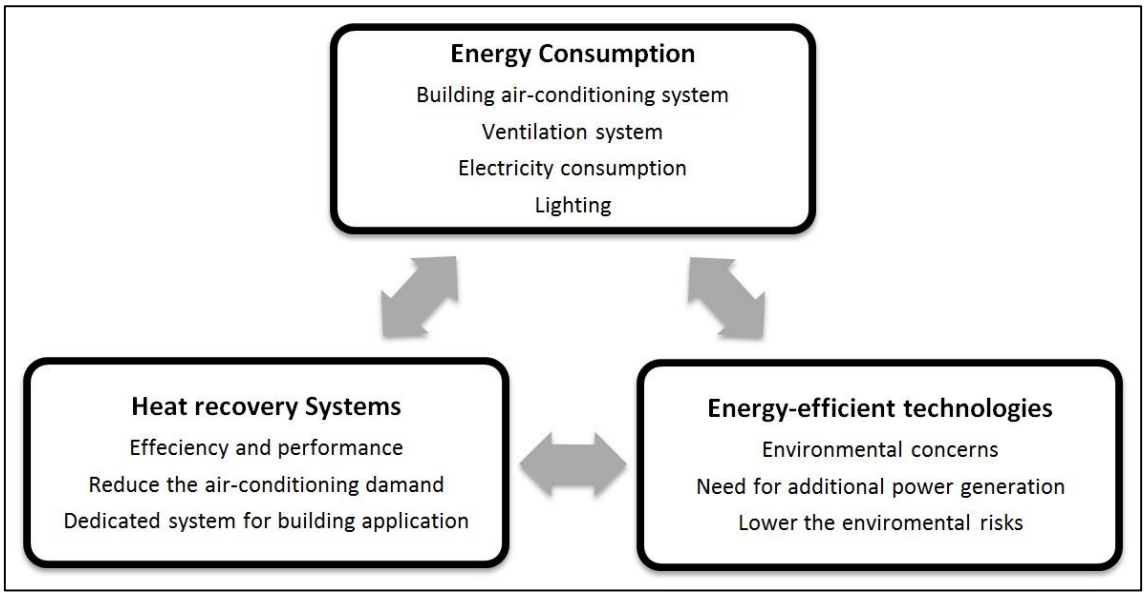


**Figure 1-3: Building energy consumption with the heat recovery system links.**

The design of many HVAC systems in current use did not take in consideration the large amounts of energy that are being wasted, beside which these systems are responsible for large $CO_2$ emissions that contribute to global warming. Additionally such systems can pollute the indoor air and turn the building into a “Sick Building” that adversely affects the health of the occupants [13]. Fortunately, heat recovery systems promise a solution to these problems, especially the waste energy which needs to be recovered.

### 1.1.3 Types of Heat Recovery Systems

Available heat recovery systems include: sensible heat exchangers [14–16], heat pipes [17], energy wheels [18–26], run-around systems [27,28], liquid desiccant systems [6,7,29], solid desiccant systems [30,31], phase change materials [32] and membrane-based total heat exchangers [33–38]. The most important component part in all of these heat recovery technologies is the heat exchanger because it has a big influence on the overall efficiency, the size of the system and the total cost of the system: both capital and running costs [13].

The membrane based heat exchanger has a number of distinct advantages [8]:

1. Compact.
2. Very efficient.
3. Both the sensible and the latent effectiveness can be as high as 0.8.
4. The running and capital costs are reasonable and affordable.
5. Its performance declines over time less than other exchangers
6. No cross-contamination problems.
7. Simple with no moving parts.

## 1.2 Cross-Corrugated Exchanger Core

To increase sensible and latent effectiveness of a stationary total heat exchanger with limited transfer area, heat and mass transfer intensification is needed. There are two general methods for heat/mass transfer intensification: material side intensification and air side intensification. It has been shown that cross corrugated triangular ducts are a structure that will intensify heat/mass transfer in air to air exchangers [39].

Due to the finite fin conductance both for sensible heat and latent heat, fin efficiency is quite limited [39]. To substantially enhance the heat/mass transfer, the structure known as the cross-corrugated triangular membrane duct is proposed [40–42]. This is classed as a primary surface heat exchanger, which is widely used for air-to-air sensible heat exchange [8,43]. The concept is shown in Figure 1-4.

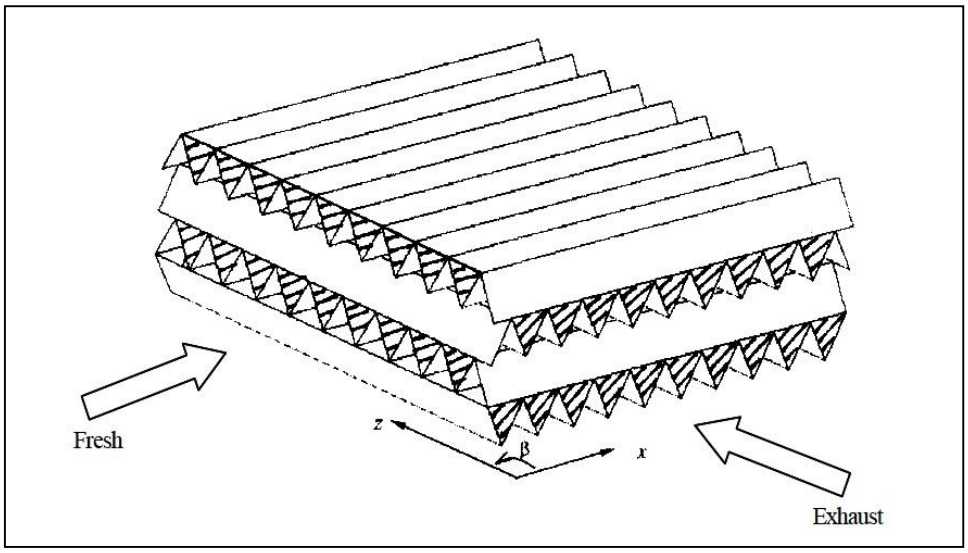


**Figure 1-4: Cross-corrugated triangular heat exchanger core arrangement** [1]**.**

## 1.3 Redring-Xpelair Company Meeting

The UK based ventilation company Redring-Xpelair [44] use the polymer cores in their heat recovery units, and this research project on overcoming the problems encountered with the polymer cores is based on their polymer core design with the same membrane material. The problems to be overcome are the low thermal efficiency of the core and the condensation problem (water accumulation in the bottom of the exchanger that causes unwanted complications and problems).

A couple of meetings was held with one of the company's representative and one engineer in the company's head quarter in Peterborough (UK), and discussed the problems with their commercialized polymer heat recovery ventilator unit for small ventilation application and it was agreed there was a need to develop a new choice of materials other than was raised to overcome the existing problem with the current polymer one such as the thermal efficiency and, condensation and water accumulation in the bottom of the exchanger core and needed to be tested in the UK weather.

As a profitable company, the pressure drop is essential to reduce the fans sizes, but an agreement was reached to have some compromises in order to reach a common ground between the promising thermal performance of the cross-corrugated total exchanger core and the relatively higher pressure drop comparing to their polymer flat plate exchanger. The last thing they needed to do, is to investigate the economic feasibility of this core in order to consider it within their existing ventilation systems, even though the proposed membrane in considerably cheaper than the polymer in addition to its multiple advantages over the polymer.

## 1.4 The Aim of This Study

Given the European climate, heat recovery is becoming increasingly important as energy demands grows, HVAC technologies develop, and the demand for energy conservation increase, especially with the recent revolution in the construction of buildings and houses which can be described as “air-tight”, i.e. well insulated, zones.

The aim of this research project is to develop an advanced heat recovery ventilator for use by individual households. To design a membrane-based, light, efficient and affordable heat exchanger core, that could have a positive impact on the UK construction industry.

## 1.5 Objectives

The current study is focused on the cross-corrugated membrane exchanger for the reasons given in Section 1.1.3. It will conduct a thermal energetic analysis of the exchanger performance, and establish an exergetic analysis of the quality of energy and describe the losses in detail for the whole system. The main objectives are summarized as follows:

1. To carry out a heat recovery performance assessment via a full numerical study of the cross-corrugated membrane-based heat exchanger core, using a three-dimensional CFD model for heat and moisture transfer, the ANSYS Fluent 17.1 software package.
2. Enhance the full cross-corrugated design of the heat exchanger core for a heat recovery ventilation system by investigating more versatile geometries based on different pitch length for the duct opening, and identify the most efficient design for heat transfer enhancement.
3. Analyse the influence of the physical design parameters of the exchanger, and the physical properties of the two air streams, on the core effectiveness.
4. Develop an exergetic analysis model using IPESPro software to evaluate the performance of proposed exchanger cores designed from a purely thermodynamic perspective and evaluate the exergetic efficiency and exergy destruction in the system.
5. Use the exergetic model to examine the heat exchanger as a system, i.e. the exchanger core and its fans, determine the power losses in the system, and provide solutions for these losses, especially pressure drop losses.

## 1.6 Overall Methodology

In order to achieve the objectives of this study to reach to its aim, two different approaches (heat transfer and thermodynamic point of view) were considered to solve the problem and by combining them, they contribute to the heat exchanger design realm. The flow chart below summarizes the methodology of the current study:

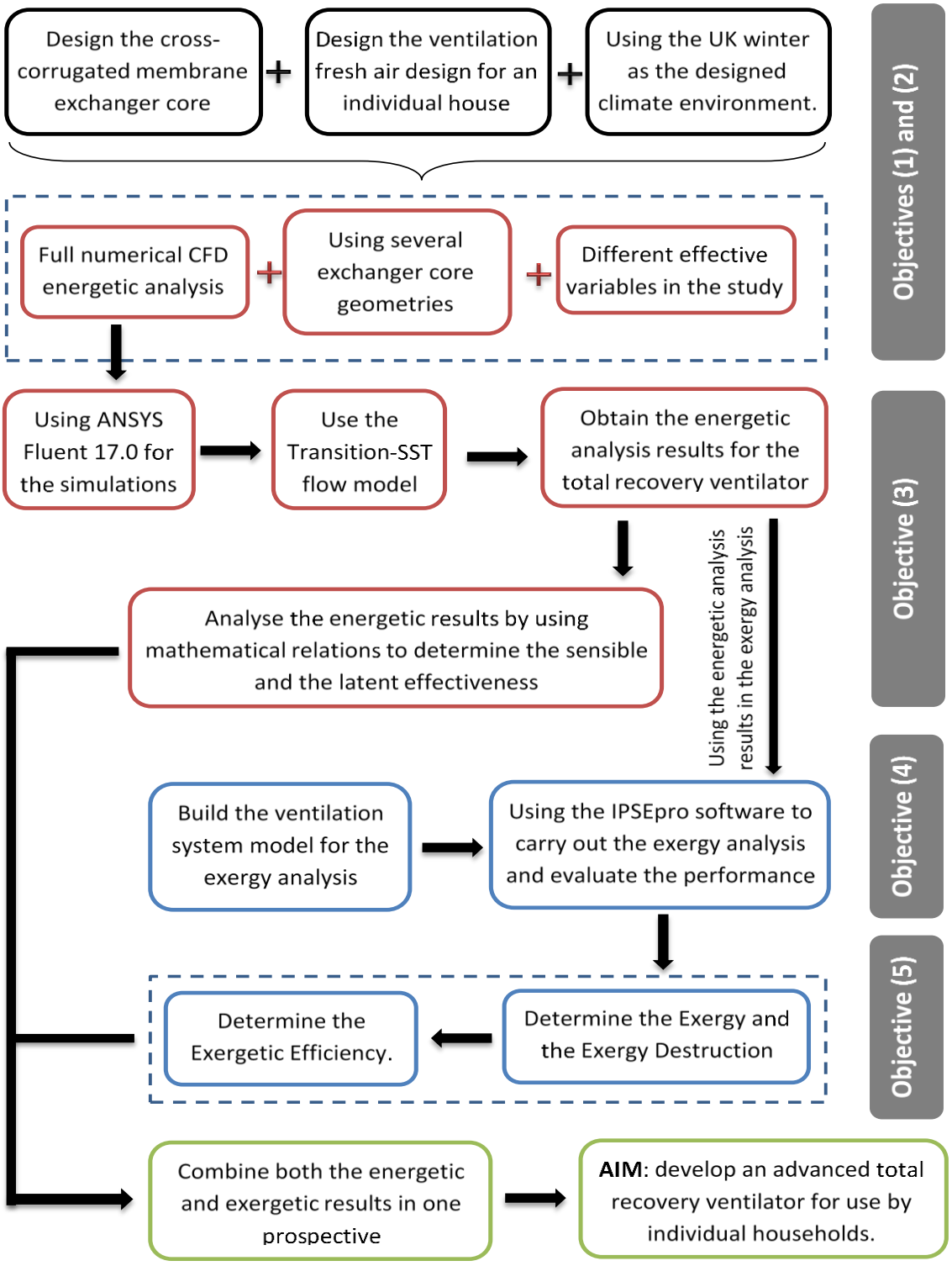


**Figure 1-5 Overall summarised methodology**

## 1.7 Contribution to knowledge

The conservation of energy has two fundamental laws; the first law represents energy consumption and utilization in a quantitative manner. The second law states that the energy can be represented in a qualitative way as well as quantitatively. This brings to light energy quality destruction, which takes place in the actual heat and mass transfer processes. Based on the second law, exergy analysis will be conducted to estimate and assess the available work destruction.

The contribution to knowledge of this study is the comprehensive evaluation of combining the energy and exergy findings for the three designed cross-corrugated total recovery exchangers and their whole system, including the proposed house and the air blowers in the UK weather, and the identification of the quality of the energy losses and the useful work within the system. According to the open literature as well as the researcher knowledge in the previous researches, this method of combining the exergetic and energetic analysis on such exchanger as well as using the IPSEpro software in exergy analysis for total recovery system, have not been covered and investigated yet. Furthermore, the process of utilising the waste heat energy of a cross-corrugated membrane core in an individual heat recovery ventilation application has not been covered in existing literature as well.

## 1.8 Thesis Structure

This thesis consists of six chapter that describe every work stage carried out and also covers the scientific and industrial challenges for the designed exchanger core that might prove obstacles for the European market. **Chapter One** introduces the general ideas behind this thesis as well as highlighting the problem. Then it introduces the main focus of the work. The chapter ends with identifying the aim and objectives of the work and its contribution to knowledge.

**Chapter Two** is a review of literature relevant to the research. Firstly, the chapter previews the different types of heat recovery systems and discusses them according to several defined parameters. It also discusses the cross-corrugated membrane heat recovery exchanger. The literature on the exergy analysis of heat exchangers is then reviewed and, lastly, a summary of the existing literature is given with an assessment of where the current study is positioned amongst them.

**Chapter Three** presents the design prospective of the proposed exchanger core arrangement and focuses on the membrane material and the reasons behind its selection as the main heat and mass transfer material in the exchanger core.

**Chapter Four** is the heart of the thesis. This chapter presents the energetic analysis of the exchanger core, the heat and mass transfer methodology, the CFD numerical modelling, the results and the discussion. The parameters resulting from the work in this chapter form the bases of the exergetic analysis in the next chapter.

**Chapter Five** introduces exergy analysis of the proposed exchanger and presents the thermodynamic methodology used. A new software tool, IPSEpro, is introduced and used to analyse the energetic results and obtain the exergetic parameters. The achievements of this study become clear at the end of this chapter.

Finally, **Chapter Six** summarize the research findings and the conclusions from the energetic and exergetic analyses as well as the novel factors of the study. It also presents recommendations for the future work relating to the current heat recovery system.

# 2 LITERATURE REVIEW

## 2.1 Overview

The total energy consumed by buildings increased in the last year; the most important factors being increased demand for personal comfort, the increased installation of gas central heating and HVAC systems, the increase in economic activity and growth of the construction sector [45]. However the average age of many dwellings and buildings in present use is more than 50 years, which means it is difficult for them to conserve energy and makes it important to plan a strategy to recover waste energy and help reduce consumption [46].

The literature review revealed the importance of recovering the heat that is currently being lost by UK dwellings, and which could be achieved by adopting heating systems which contained not only heat recovery but also supply fresh air. Such systems can not only provide better thermal comfort and climate control but are considered to be relatively energy efficient [47]. Such heat recovery systems have been introduced to northern Europe in such countries such as Sweden and Germany [48,49].

Heat recovery technologies have become important components of many buildings, because modern regulation and policies about conserving the energy encourage minimizing energy consumption as much as possible. In Germany, for example, modern buildings are well insulated and air tight, this reduces the energy demand for the air conditioning to almost 60% of the total energy annual demand [50]. Energy consumption rates can be reduced by 20% in cold weather areas by using heat recovery systems [49]. However in relatively hot climates such as China, the use of these system have increased in the last couple of years in domestic building and even in single small houses which use air-to-air heat exchangers as a heat recovery ventilation system to conserve the energy and recover it from the exhaust air streams [34].

The UK Directive on the Energy Performance of Building (EPBD) came into force in January 2003, and was “Recast” in July 2010; it required the government to “set minimum energy performance requirements for new buildings, for buildings subject to major renovation, as well as for the replacement or retrofit of building elements as a part as the building services.” In November, 2016, the European Commission published “Clean Energy For All Europeans”, which made a number of important proposals and calls for action: “(To) put energy efficiency first and support cost-effective building renovation”, for individual governments “to improve the energy efficiency of buildings ... (including setting) minimum energy performance requirements for new buildings, for buildings subject to major renovation, as well as for the replacement or retrofit of building elements” [51].

To have a comfortable and healthy indoor environment for the occupant, and at the same time to save energy requires an energy efficient technology. Obviously there is a need to develop heat recovery systems to conserve energy and also make a genuine contribution to reducing $CO_2$ emissions. Such systems should include an alternative or replacement for existing systems or might be used as an addition to existing systems [43].

## 2.2 Design Prospective

The physical parameters for the heat recovery system are essentially what determines its performance and makes its operation distinctive. These parameters are what control the behaviour of the system. Standard heat recovery systems consist of a heat exchanger core, ducts for inlet and outlet, and one or more fans [9]. Hu et al., [38,52] described the basic design of the heat recovery system as shown in Figure 2-1 and Figure 2-2. Heat recovery systems can be classified according to type, size and flow arrangement [10,27,53–59].

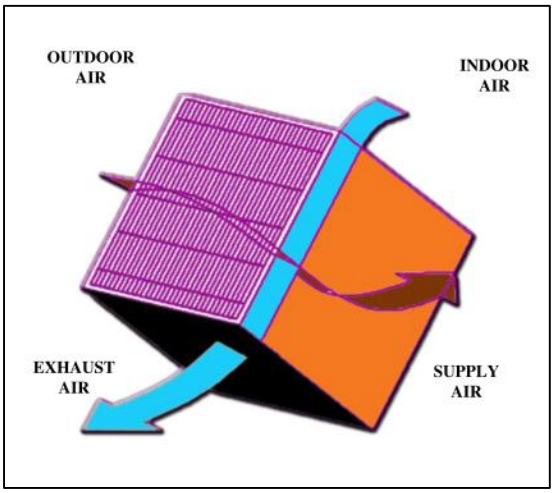


**Figure 2-1: Typical membrane-based exchanger core for the energy recovery ventilator** [38]

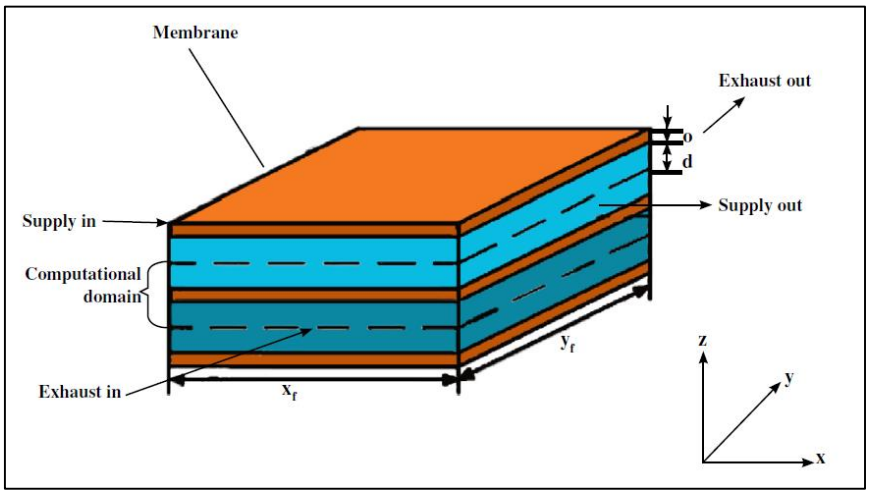


**Figure 2-2: Schematic model of heat exchanger flows** [38]

Researchers have showed great interest in heat exchanger technologies for building applications, and the majority of their studies have been concerned with these design parameters. Huynh et al., [60] have developed a numerical model of an energy recovery application and emphasized the importance of the design parameters on the HVAC performance.

## 2.3 Sizing and Ductwork

The most important single parameter in the heat recovery system is the heat transfer area of the heat exchanger core, which is considered the heart of the system. Thus, all the sizing parameters are critical and important in determining the cost and the overall efficiency of the system: these parameters are length, width and height of the exchanger and overall heat transfer area. In the last 20 years numerous researchers have investigated the effect of the size and heat transfer area on cost and performance and explored the basic heat recovery designs [61–64] with the aim of optimising existing systems [65,66].

Heat exchangers can be classified according to their flow arrangement into three different types: counter-flow, parallel flow and single fluid. Soylemeyz [63] made an attempt to optimise the heat transfer area for these systems, developed a thermo-economic analysis and concluded that there is an increase in effectiveness with increase in area. Manz and Huber [67] also considered the effect of exchanger size and area on the effectiveness and their findings agreed with Soylemeyz. However, Manz and Huber worked on heat pipe recovery and demonstrated that an increase in the number of rows could be considered as an increase in the area which increased the effectiveness [47,68,69].

That the increase of the area of the rotary heat exchanger has a significant effect on the effectiveness of the exchanger, was demonstrated by Dalkilic et al., [70] in their numerical optimisation of a rotary heat recovery system. Recently, rotary heat recovery exchangers have become a promising and successful alternative to dehumidification systems [71].

The literature does not focus only on the thermal efficiency of heat recovery systems, but recognises it is essential to also make economic savings, as emphasized by [72]. The financial effects of using heat recovery systems instead of conventional ventilation systems have been estimated by Adamski [16,73]. Dalkilic et al., [70] used a new model to estimate the exchanger's core area for maximum gain of heat recovery systems. They concluded that the exchanger with the highest NTU compared with its effectiveness would be best exchanger.

In the last couple of years, researchers have included the extended surface concept (i.e. fins) in heat recovery technologies. It was found that there is an enhancement in the net heat transfer because there is a reduction in the thermal resistance when using fins [74]. Experimental work by Pongsoi et al., [65] on optimising a finned exchanger core with different row configurations, arrangements and pitch sizes concluded that higher convective heat transfer could be achieved by increasing the fin-pitch. Tang et al., [75] conducted both simulation and experimental work examining the air-side of a heat exchanger for five different kinds of fin arrangements. Their investigations showed that the pressure-drop across the exchanger was a parameter which affected the air-side heat transfer.

It is very important to take into account the fan size and ducting system as well as the heat exchanger core. Much literature can be found concerning fan and duct sizing. The global fan efficiency of a heat recovery system as a function of power consumed has been investigated in an earlier study by Routlet et al., [76], who concluded that there were significant differences between fans within the same power class used for heat recovery system. Recently, Laverge and Janssen have pointed out that fans used for heat recovery would consume an electrical load rate which is connected to both fan and ductwork specifications [77]. They carried out a study on the energy and exergy of a ventilation and heat recovery system for different European climates, and concluded that only a low fan power would make the heat recovery system beneficial if saving energy is the only concern. El-Fouith [78] conducted simulations to examine the effect of the efficiency of an exchanger and fan power on the heat recovery system from the perspective of energy performance for a variety of buildings and climatic conditions in France. They found that the fan power is affected by three factors: (1) fan overall efficiency; (2) pressure drop in the exchanger; and (3) air velocity of the flow within the ductwork.

From the literature, several researchers have investigated heat recovery system performance and energy saving as a function of its physical parameters, for several different climates [79,80]. Kang et al., [81] conducted a study on the

effects of using a fresh air fan with variable speed on a heat recovery system which also supplied fresh air to buildings in different locations in China. The results showed that the coefficient of performance (COP) of a fan - which is the ratio of net heat recovered by the system to the electrical load consumed by the fan - has only a small influence on whole system. Kang et al., found that when the COP of a variable speed fan was around 2.5, the system was still able to function at maximum efficiency and energy saving as well.

Much experimental and numerical work can be found concerning the investigation of ductwork design as one of the important physical parameters of heat exchanger heat recovery systems [82–84]. Research investigating the effect of duct sizing on such system characteristics as temperature, humidity, air flow rate and pressure drop in heat recovery ventilation systems for buildings [85].

However, despite all the work that has been done on optimizing exchangers for total recovery applications from the point of view of sizing and arrangement of the exchanger core, a firm connection between research findings and actual heat recovery applications is still missing. The design of any heat recovery system should consider the balance between initial and running costs of the total recovery system. More research is needed which includes additional operating parameters and for different climates, such as the UK. Hence, some of this research will focus on the design of a heat recovery system for different climatic conditions.

## 2.4 Structure and Materials

Heat recovery systems have evolved significantly in the last 10 years with the development of advanced heat and mass transfer technologies, especially exchanger core structures and materials. The base line for selecting an efficient and efficacious structural design with suitable materials is how well the selections perform and work together in combination, and how well a proposed exchanger core would function in its local environment and how would the core affect the environment.

For moisture transfer, the porosity and pore diameter are crucial in determining the quality of a material. Liu, [86] for instance, concluded that high porosity materials are directly proportional to the value of the mass transfer. Another parameter for selecting the material is the thickness, which represents heat and mass transfer resistance. The durability of the material will also play a major role in determining the core performance from both the optimization and economic perspectives. The literature review has shown that many researchers have investigated and developed structures and materials for heat/mass recovery exchangers. This section will review the existing research including materials and structure of heat/mass recovery systems.

### 2.4.1 Metal Exchanger Cores

Most heat exchangers are based on fin-and-tube or plate-fin designs for the exchanger core with a high dependence on the properties of materials such as copper, aluminium and steel. However, these materials can only transfer sensible heat from one stream to another, they cannot cope with the latent heat transfer. The lack of the capability of these metallic materials to transfer moisture is due to their non-porous nature and inability to allow moisture to travel through them. To meet market demand several studies have conducted both simulations and experiments on heat recovery exchangers to optimize the metallic core and maximise the heat/mass recovery by increasing the heat transfer surface area by, for example, increasing the roughness of the metallic surfaces [87–89]. The literature shows that this type of core suffers limitations when included in a total recovery systems and, as a result, there is a need to develop an exchanger core with a structure and material which can overcome the problem of moisture transfer.

### 2.4.2 Polymer-Based Exchanger Cores

Their high resistance to fouling and corrosion make polymers very promising candidates for use in heat recovery applications, especially in integrated heat recovery system containing humidification or dehumidification systems. T'joen et al., [90] reviewed the use of polymer materials in HVAC systems, and concluded that polymer materials could be suitable, subject to certain compromises.

Polycarbonate, which belongs to the thermoplastic polymers group is well known as a material for heat exchangers cores. Polycarbonate has good chemical resistance to acids but poor resistance to alkalis and solvents, can withstand temperatures from -4 to 135 $^{o}$C, but has a low thermal conductivity, between about 0.19-0.22 W/mK. However, it retains significant promise for heat exchanger applications, especially in HVAC and heat recovery ventilation technologies [90–92].

The compromises which are needed when selecting polymer materials for heat/mass recovery systems centre around their low thermal conductivity. Gendebien et al., [93,94] investigated the low thermal conductivity of one of the most common polymers (polystyrene) and concluded that this weakness could be compensated for by enlarging the size of the exchanger by, for example, increasing the number of its layers. This is possible because polymers are lighter than most metallic materials. The problems with the polymer materials was discussed in chapter one about Redring-Xpelair company that it tried to discuss different material choices and test it in the UK.

### 2.4.3 Fibre-Based Exchanger Cores

Fibrous hydrophilic materials, can be effective at transferring both heat and moisture at the same time. However, the downside is that the fibres give these materials low thermal conductivities, ranging from 0.01 to 0.3 W/mK [95,96]. Fibres with narrow pores and a decent absorption ability have the capability to transfer both heat and moisture with less resistance. But fibres have a very significant disadvantage, low material hardness and insufficient strength to be used in a plate type heat exchanger. Studies conducted by Idicula et al., [97] and Fend et al., [98], concluded that the lifespan of fibre exchangers is likely to be short, its performance seriously degrades as, in time, it becomes soaked with water (condensate). Several researchers [99–101] have tried to optimize or enhance the performance of fibre materials and conducted several studies on their performance in total recovery systems. It was concluded that the fibres showed promising results that could attract industrial companies especially in the rotary wheel recovery systems. In practice, however, the disadvantages of the fibres have overcome their initial promising performance. Consequently, the need of a replacement material that could handle both heat and moisture transfer with minimum compromises remains a necessity.

### 2.4.4 Membrane-based Heat Exchanger Core

Currently, one of the most promising and competitive technologies in air-to-air heat recovery systems is the membrane-based heat exchanger core. The reason is its high performance in enthalpy recovery, i.e. moisture recovery, which could transfer both sensible and latent heat at the same time [36,43,102,103]. These membranes have the capability of transferring heat and moisture from the inlet fresh air stream to the exhaust returned air from the air conditioned zone (hot and humid China). Such an heat exchanger might be constructed from a vapour permeable membrane such as treated paper and micro-porous polymeric membranes [104].

Membrane based materials have been used for several years in different types of heat exchangers due to the advantages mentioned above, and have gained considerable attention in both research and industry [8]. These membrane exchangers have a primary heat transfer surface area which separates the two air streams without the need for the existence of a secondary resistance layer as in some other exchangers. Consequently, the membrane materials can have high sensible and even latent heat recovery as well as relatively high energy effectiveness and have proved to perform economically [43]. Error! Reference source not found. shows the heat and moisture transfer through a membrane core.

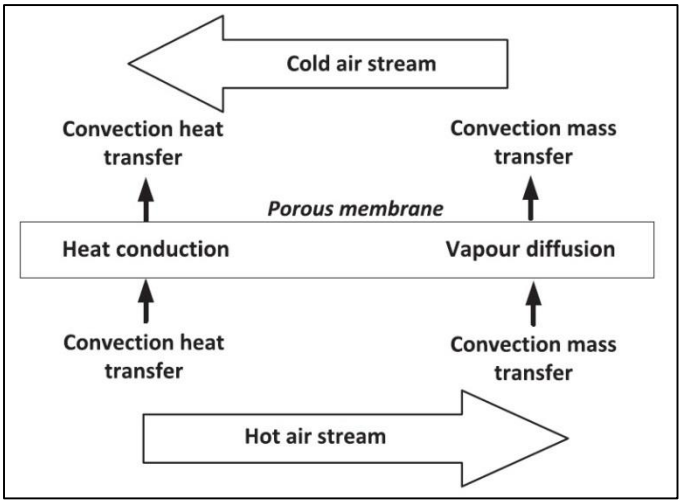


**Figure 2-3: Schematic of moisture and heat transfer in a membrane core. [105]**

Niu and Zhang [106] developed a theoretical model to investigate the performance of an energy recovery ventilation system based on a membrane heat exchanger and to examine the effect of changes in the conditions and the properties at the two inlets. Zhang and Niu [103] produced correlations to predict the enthalpy effectiveness of the membrane based heat recovery heat exchanger. Likewise, numerical work by Min and Su [104] examined the influence of the thickness of the membrane layer and the pitch between them, on performance; they concluded that the use of thin layers of membrane is necessary to achieve high performance of the energy recovery system (used for ventilation).

Experimental work carried out by [107] to study the effect of a variety of airflow support spacers on the performance of energy recovery systems found an enhancement of both heat and mass transfer. A novel material of composite supported liquid membrane (CSLM) was presented by Zhang [108] who used a liquid membrane for moisture transfer; he tried this novel approach because current heat exchanger cores of energy recovery ventilators have a relatively low latent effectiveness [109,110]. CSLM was used as the plate material to solve the problem of the impairment of the current fin and plate materials which are using hygroscopic paper. Moreover, in his investigation Zhang [108] compared CSLMs to paper-fin and paper-plates, and paper-fin and membrane-plates. The results showed the membrane plate heat exchanger core had a 60% higher latent effectiveness than the paper-fin and paper plate current cores by virtue of the CSLM's high moisture diffusivity.

A performance study was carried out by Zhang and Jiang [111] to investigate different materials for the heat exchanger core and the flow arrangement for energy recovery ventilation systems. Different core types were compared; paper, membrane and even sensible cores. The results demonstrated that the lowest enthalpy effectiveness was achieved by the sensible exchanger core whereas the highest enthalpy effectiveness with the best performance was achieved be the counter flow arrangement with membrane-based core.

On the other hand, Hemingson et al., [112] investigated the effect of variation in the outdoor conditions on a run-around membrane energy exchanger (RAMEE); and conducted a steady-state performance study. The results confirmed that outdoor conditions play major role in heat recovery performance and have substantial influence on the effectiveness values; where the value of the effectiveness might vary between less than 0% to higher than 100% for some cases of the outdoor conditions examined. Likewise, Ge et al., [113] proposed an analytical model, based on Hemingson's results [112], for developing and optimising both the heat and moisture exchanger core size and the desiccant solution flow rate in the RAMEE. The annual energy recovery could be enhanced up to 7% by optimisation control of the solution flow rate.

Liu et al., [114] have proposed a new hybrid membrane, poly-vinyl chloride/sodium montmorillonite (Na+-MMT), with varied content of Na+- MMT and casting process, for use in energy recovery ventilation systems. Although these hybrid membranes are promising materials for heat or energy recovery systems, they still face serious challenges such as low permeability of water vapour, low moisture and enthalpy exchange effectiveness compared to polymeric ionic or cellulose membranes.

Most recent studies have emphasized the importance of the membrane materials and how applicable it is to use them in ventilation applications. These studies include a review by O'Connor et al., [115] on passive heat recovery ventilation applications; Chang et al., [116] in a study of the effectiveness of a membrane total recovery ventilator; and Chang, [117] who carried out an experimental analysis of a membrane dehumidifier for ventilation applications.

### 2.4.5 Corrugated-plate Structure

The flat-plate and the fin-plate remain the most common structures of heat exchangers but the corrugated-plate arrangement is growing in popularity and today can be considered a common fix-plate exchanger core. The corrugations in the core give the capability and flexibility to have different flow patterns compared to the conventional flat plat exchanger. The flow inside the corrugated exchanger is forced to have continuous changes in direction due to the changes of shape of the flow area. This type of arrangement has the advantages of having higher energy effectiveness, stronger build quality (even if constructed from very thin layers) and better heat/mass transfer capability [42,91,118].

Several attempts have been made throughout the years to evaluate and examine the performance of the corrugated arrangement in total energy recovery systems using different materials and design parameters. In 2010, Han et al., [119] developed a numerical and experimental chevron corrugated-plate heat exchanger, and in 2013, Forooghi et al., [120] used numerical methods to estimate the effect of buoyancy on turbulent convection heat transfer in corrugated channels. They all concluded, in agreement with

Islamoglu et al., [121], that the corrugated structure improved heat transfer. They also pointed out that other factors in the corrugated structure may affect the performance, such as the thickness of the plate layer, the exchanger core geometry, the spacing between the layers and lastly, and most significant, the pitch length of the corrugations. All these factors are crucial in the design phase of the exchanger core.

A CFD study was conducted by Doo et al., [122] to develop a quantitative evaluation of the thermal performance of a cross-corrugated heat exchanger by considering parameters such as the plate thickness and its effect on longitudinal heat conduction. Design optimization study was carried out by Qi et al., [123] using corrugated louvered fins, they concluded that the performance was affected by several parameters such as the flow depth and the material thickness. Zhang et al., [124] examined the effect of physical parameters (such as?) on fluid-side fouling by conducting numerical and experimental studies. Woods and Kozubal, [107] considered an open channel simple polypropylene triangular spacer and carried out a theoretical pressure drop study on the heat recovery system.

Elshafei et al., [125] discussed the effect of channel spacing on both heat transfer and pressure drop in a corrugated structure, and showed the heat transfer performance was enhanced but pressure drop compromised. A cross-counterflow arrangement for an air-to-air heat recovery exchanger was designed by Gendebien et al., [93] who, with Fernandez-Seara et al., [126], considered the same air flow ratio in order to examine the exchanger performance.

The literature review has shown that several parameters have been investigated, but further investigation of different geometries and arrangements are needed in order to fully evaluate the benefits of a corrugated structure, and provide greater understanding of modelling the thermal performance of such structure when used in heat recovery applications.

## 2.5 Air Flow Pattern

The flow pattern has a very important effect on exchanger performance, this has been extensively covered in the literature. It has been proven that exchanger effectiveness is significantly influenced by the flow arrangement, especially when both streams have different directions of flow [11]. In heat recovery applications several researchers have conducted studies concerning the flow arrangement, and proved that the exchanger effectiveness of the cross-flow pattern in slightly lower than the counter-flow arrangement by around 10%, see Mardiana and Riffat, [9]. For instance, in 2013, Yaici et al., [127] carried out a numerical study of a total membrane heat recovery exchanger, and compared the performance of counter-flow and co-current arrangements under typical Canadian weather conditions, they found that the counter flow has better performance. Researchers are eager to optimize the existing arrangements as well as developing new ones by manipulating the design structure of the exchanger, see Zhang [128] who developed a quasi-counter flow and proved its superiority over the standard counter-flow arrangement by almost 5%. Further, Nasif et al., [129] examined a Z-flow arrangement in the heat recovery exchanger to maximize the heat transfer area leading to increase in the heat/mass transfer. Al-Waked et al., [105] conducted a CFD study on enthalpy for an air-to-air membrane recovery exchanger using a hybrid type flow arrangement (named cross-counter-flow) and investigated the conjugate heat and mass transfer problem.

Some of the most recent studies highlight the effect of the flow pattern on performance, the first was conducted in 2016, by Deshko et al., [130] who carried out a numerical simulation to evaluate heat and the mass transfer in an air-to-air, cross-flow membrane exchanger in heating mode, the second was by Koester et al., [131] in 2017 who investigated the cross-counter flow arrangement in an enthalpy exchanger.

All the literature reviewed has demonstrated that the effectiveness of any heat exchanger depends extensively on airflow pattern, configuration of the exchanger, and the condition and parameters of the inlet and outlet air streams. The need for new developments in heat exchanger design has become a major focus of research seeking to enhance the performance of these exchangers. One such development could be the cross-corrugated exchanger that has a unique type of flow pattern that might enhance both the heat and the moisture transfer in the exchanger core.

## 2.6 Cross-Corrugated Membrane Exchanger Core

Overcoming the weaknesses and limitations in heat and mass transfer performance of conventional exchangers such as parallel-plate and plate-fin with the need to add spacers within these exchangers to support the material layers due to aging of the membrane and its possible collapse or contraction due to the passage of air, is a priority for the HVAC industry. Research has focused on enhancing the heat and mass transfer [40,41], and has resulted in a structure named the cross-corrugated triangular membrane duct. This design was proposed. Zhang, [42] who conducted a study to evaluate the convective mass transfer in a cross-corrugated membrane exchanger, and stated that this arrangement belongs to a type of primary surface heat exchangers, which have been used for air-to-air sensible heat exchangers.

Recently, Li et al. [132] have carried out a numerical and experimental study on a membrane based cross-corrugated heat exchanger with a triangular duct with internal corrugations, they focused on the effect of the flow pattern on the heat and mass transfer. The pitch length of the equilateral triangle duct opening in their design was 18 mm and the aspect angle of the triangular duct was $60^{o}$. Liang et al.., [132] focused on the laminar flow region of the cross-corrugated exchanger and examined the effect of low Reynolds numbers on performance and pressure drop.

The cross-corrugated design showed promising results in transferring both heat and moisture especially when using a membrane as the primary material, so further work on different and more complex designs needs to be conducted to achieve better understanding and better evaluation of this structure in order to determine the exchanger core performance in recovery applications.

## 2.7 Exergy in Heat Exchangers

In the last 20 years, the use of the first and second laws of thermodynamics and their combination to evaluate any system has caught the attention and interests of researchers worldwide, with extensive literature based on entropy generation and exergy [133,134]. In 2000, Hesselgreaves [135] established that the exergy analysis of heat exchangers could highlight performance criteria by using evaluation of exergy destruction and exergetic efficiency.

Several researchers have worked on exergetic optimization for different heat exchangers. Cornelissen and Hirs, [136] conducted a study using exergy analysis to achieve optimum design of a counter-flow domestic heat exchanger, using a life cycle analysis method. Yilmaz et al., [137] have presented a second-law based performance evaluation criterion to assess the performance of heat exchangers. Naphon, [138] has carried out experimental and theoretical investigations of entropy generation and exergy loss in a horizontal concentric micro-fin tube heat exchanger.

Feng et al., [139] have studied cumulative exergy consumption theory and the cumulative exergy contribution of heat exchanger processes. The theory was able to not only analyse the process energy performance, but also to optimize both the process parameters and the size of equipment at the same time.

In the matter of heat recovery systems, Sukhodub and Deshko [140] established an exergy analysis of ventilation systems with energy recovery for the ventilation system of a room in Kiev and included the effect of climate change during the year as well as the variation of the effect of the thermal and chemical components of the exergy through the summer and winter. A new

approach to the evaluation of heat recovery devices in mechanical ventilation systems was proposed by Mroz and Dotka [141], they conducted an evaluation based on exergy balance and economic analysis, that required the application of a multi-criteria decision aid method (weighted sum method). Ghazikhani et al., [142] have carried out an investigation to clarify the differences between exergy consumption and exergy destruction in both of the humidification methods: Constant Enthalpy Humidification (CEH) and Constant Temperature Humidification (CTH) in HVAC systems.

## 2.8 Exergetic Analysis for Corrugated Exchangers

Very few papers were found in the literature review concerning energetic and exergetic analysis of corrugated exchangers, and especially few for total recovery applications. One of the few available papers is by Durmus et al., [143] an experimental investigation of three types of plate heat exchanger; flat-plat, asterisk-plate and corrugated plate. They studied the effect of these surface geometries on the heat transfer but did not consider mass transfer in their exchangers. Another experimental study was conducted by Pandey and Nema [144] in order to determine the exergy destruction in a corrugated plate heat exchanger. Both of these studies considered exergetic efficiency as the main describer for exchanger performance.

Tiwari et al. [145] conducted an experimental investigation on a corrugated plate heat exchanger, using a combination of exergy and energy analyses with water as the working fluid. They studied the effect of the physical parameters (such as the water velocity and temperature conditions), on the exchanger performance - its energetic and exergetic efficiency.

Most recently in 2017, Martinaitis et al., [146] researched the application of exergy analysis to evaluate the performance of building mechanical systems. A method was developed for exergetic analysis of the HVAC system’s thermal processes when the reference point of the properties was assumed to be above, below or equal to the operating state of the working fluid. Using a

derivative status parameter from enthalpy and entropy, a method for calculating the exergy efficiency for HVAC equipment was proposed. The most recent study found was conducted by Al-Sulaiman [147], he compared the energetic and the exergetic analyses for an air conditioning system with and without a membrane total exchanger. This research considered several parameters including the COP of the system, evaporative cooling rate, exergetic efficiency, exergy destruction and compressor power input. He concluded that the presence of a membrane enhanced the exergetic efficiency, but has minimal effect on the COP. The exergy destruction was decreased with the use of the membrane, while the evaporator has the highest exergy destruction value compared with the other components. The total exergy destruction decreases, on average, by more than 50% when a membrane was used compared with the case when no membrane was used. I.e., the second law efficiency increases when a membrane is used and this study reveals that it increases by more than 5%.

As no reports were found in the literature review of exergetic analysis of a membrane total recovery exchanger, it is concluded that more research effort is needed in this area especially with its potential benefits for individual households in the UK

## 2.9 Literature Review Summary

The literature on the energetic analysis of heat and mass transfer recovery applications, has clearly proven that there are a number of parameters that directly and significantly affect the thermal performance of recovery ventilation systems.

These parameters include the physical parameters that significantly influence the effectiveness of the exchanger, the core of the system, both its sensible and latent performance because the effectiveness of an exchanger is the most significant evaluator of the system's thermal performance. The physical parameters were categorized under several headings: (i) sizing perspective, (ii) sizing and duct work, (iii) structure and materials, (iv) air flow pattern and (v) the design physical conditions such as the temperature and pressure.

The flow pattern has been extensively studied using numerical methods supported by experimental investigations. All have emphasized the importance of the flow arrangement in the design phase (including fans and ducting) and demonstrated that with a flat-plate exchanger, the counter-flow arrangement has the highest effectiveness. However, the cross corrugated scheme showed very promising results especially when the working material is a membrane which maximizes the total effectiveness by boosting the latent effectiveness.

Different geometric structures and materials were used in the literature, and it was proven that they directly affect the air flow patterns inside the exchangers and consequently their effectiveness. Structure and material are considered as the most important factors in determining the heat/mass transfer performance. Membrane-based materials showed very competitive results, especially in energy recovery applications for ventilation systems due their capability to transfer heat and moisture at the same time.

The cross-corrugated exchanger has long been a research topic in the literature, and more recently it was proposed that such heat recovery systems be built from membrane-based materials. Their effectiveness proved to be

higher than for other conventional structures but they suffered a high pressure drop across the exchanger core.

Exergy analysis is a quite new approach to heat exchanger optimization, but recently this issue has attracted researchers to investigate the quality of the energy as well as the quantity because exergy analysis can offer a more in-depth analysis and fuller assessment of heat exchangers. The main findings of the literature were the importance of exergetic efficiency and exergy destruction rate. The present need is for exergy analysis of a membrane-base recovery ventilator and this is part of the current work.

## 2.10 Current Work Approach and Contribution

Since the literature has not properly covered the topic of the energy recovery ventilation system, this study contains an energetic analysis by conducting a full CFD numerical simulation for a proposed new design of a cross-corrugated membrane based exchanger core to evaluate its thermal performance and determine the latent and sensible effectiveness. The main variables to be studied are the air flow velocity and the ambient temperature. This study also combines energetic analysis with a full exergetic analysis to investigate the quality of the energy and determine energy losses in the system and their location. The system was constructed specially to work with the exergy analysis software.

### 2.10.1 Energetic Analysis Contribution

The contribution and originality in the current study of the energetic analysis are:

1. Three new geometries for a cross-corrugated exchanger core with equilateral triangular cross-section with 5 mm, 10 mm and 25 mm pitch length and $60^{o}$ apex angle.
2. Using the Transition-SST model in the CFD simulation with low Reynolds number, to evaluate where the air flow is in the transitional region.
3. Using UK typical winter weather as the working conditions.
4. The design air ventilation rate was for an individual household.

### 2.10.2 Exergetic Analysis contribution

The contribution and originality in the exergetic analysis are:

1. Combining and using the energetic results in the exergetic analysis for the cross-corrugated membrane total recovery ventilation system.
2. Using the IPSEpro and PSExcel software in the current application.
3. Create a closed system for the exchanger core by including the house as the main heat source as well as the fresh and exhaust fans as the power consumers in the system.
4. Using the fuel-product method to determine the exergy destruction values and to validate these value when using the exergy method.

# 3 CROSS-CORRUGATED EXCHANGER CORE DESIGN

## 3.1 Introduction and Core Description

The design of the heat exchanger core plays the main role in exchanger performance, especially when estimating the sensible and latent effectiveness respectively. However, achieving an optimum design represents a challenge to researchers. Many types of cores, including plate-fin and parallel plate are used in the construction of the exchanger because of their simplicity and ease of manufacture, their strength, stability and compactness, however their downside is their limited capacity for heat and mass transfer, for both sensible and latent heats.

The cross-corrugated exchanger core, see Figure 3-1, with duct openings of triangular shape, and could be a means of significantly enhancing both heat and mass transfer. This design belongs to the family of primary surface heat exchangers which most air-to-air type sensible heat exchangers are using.

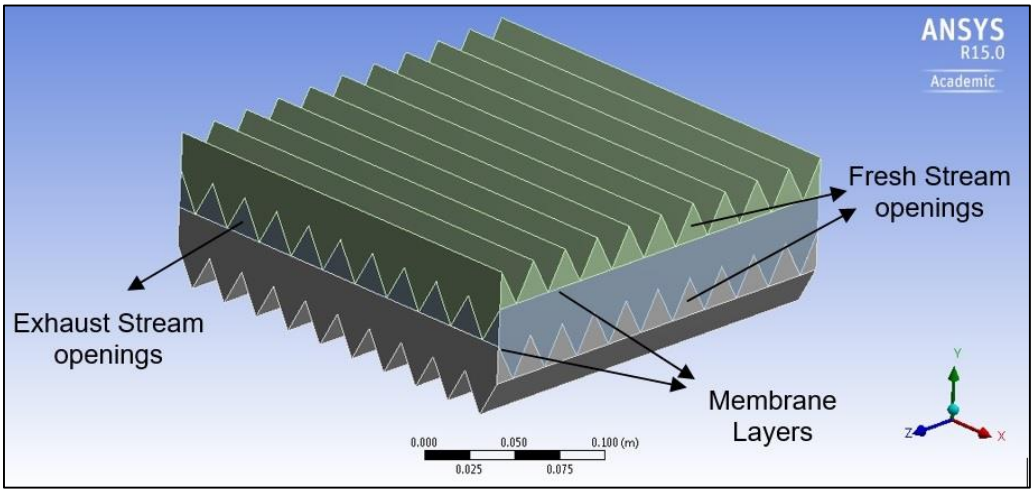


**Figure 3-1: Cross-corrugated exchanger core.**

The use of hydrophilic membrane materials is increasing becoming a practical option in the air conditioning industry due to their low cost, their surface selectivity and their being weight efficient. The membrane material sheets are used to add the latent heat effect to the overall exchanger effectiveness.

Figure 3-1 shows that in a heat exchanger thin hydrophilic membrane sheets are corrugated to form a series of small equilateral triangular ducts, and the corrugated sheets then arranged and stacked together in layers each at 90$^{o}$ to the layers immediately above and below it. The angle was chosen to be 90$^{o}$ for two reasons; this arrangement gives a cross flow type of exchanger, and to have the same flow pattern in the exchanger for both fluids.

The Triangular shapes in Figure 3-1 represents the openings for the fresh and exhaust streams. The membranes are very thin and soft, which requires plastic frame cases to support them, as seen in Figure 3-2. Consequently, with a pre-designed plastic frame, triangular shaped duct walls are formed to construct the required geometry. The structure gives better heat mass transfer. This efficiency improvement is attributed to the pattern of flow that undergoes abrupt turnaround, contraction, and expansion as shown in Figure 3-3 which shows a single channel of the membrane exchanger core.

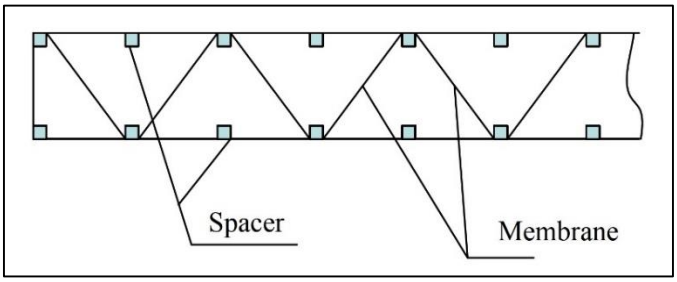


**Figure 3-2: The supported plastic spacers for the membrane sheets**

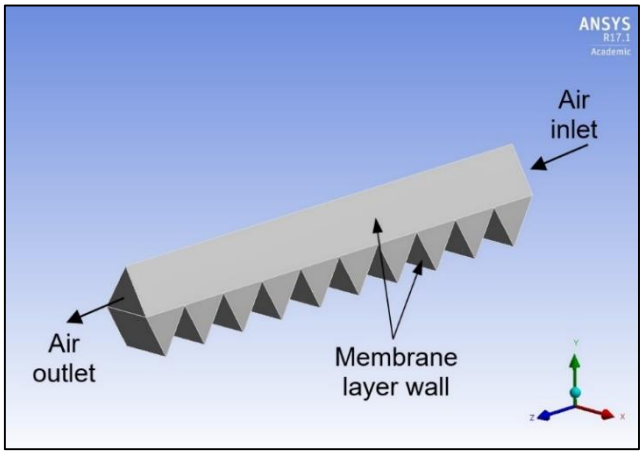


**Figure 3-3: Schematic of a single channel of the membrane core showing the cross-corrugated flow pattern.**

Redring-Xpelair (UK based ventilation company in Peterbourough) Company produces heat recovery systems though it buys the exchanger core from another company. These heat exchangers are flat-plate polymer based exchangers, and in this project the design of the proposed membrane core is based on the dimensions of these units. The company's present exchanger core is hexagonal in shape, see Figure 3-4, and for continuity and convenience this research will use the same outer dimension of the 350 mm but convert the core to a square shape (250 mm X 250 mm) because that is how the cross-corrugated core should be constructed according to the membrane sheets alliance, and in order to fit the company's ventilator housing. Several pitch lengths were chosen according to the company standards as well as the possibility of corrugating the membrane sheets.

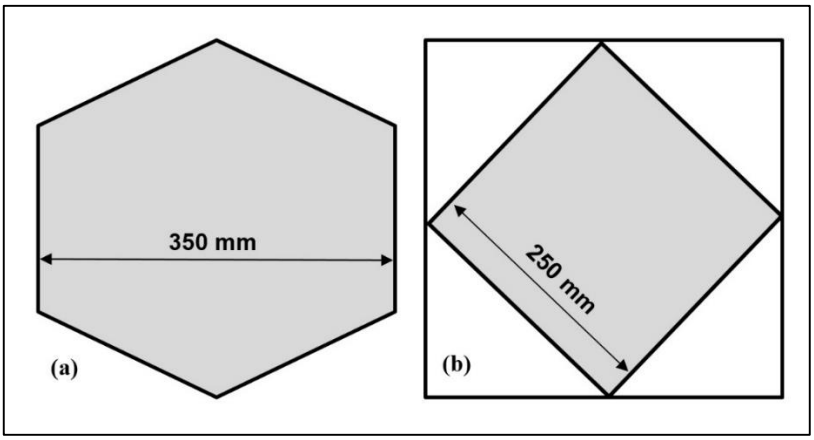


**Figure 3-4: Top view of the exchanger cores (a) Redring-Xplair's company present hexagonal flat-plate polymer core design, (b) The proposed square cross-corrugated membrane-based design**

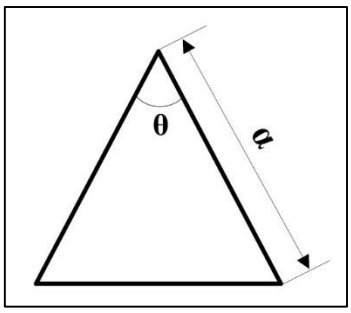


**Figure 3-5: Schematic shows the equilateral triangular duct opening with the apex angle (θ) and the pitch length (α).**

## 3.2 Triangular duct opening design

As mentioned earlier, the smooth membrane sheets were corrugated to form triangular ducts, and in this study an equilateral triangle design was proposed with one of three pitch lengths, see Figure 3-5. The first and main design is with 25 mm pitch length and the other two cases are 10 mm and 5 mm. The small hydraulic diameter of triangular duct openings comparing to its length negate the effect of the dead zones in the inlets and the flow become fully developed shortly after the inlet. Table 3-1 below shows the areas of the inlets for each pitch length (α). By choosing to have the sheets corrugated in the form of equilateral triangles the area of the sheet in contact with the flow is effectively doubled compared to a sheet laid flat. The areas and the channel heights were calculated using the well-known equations below.

$$Area\ of\ Equilateral\ Triangle = \frac{\sqrt{3}}{4} * \alpha^2 = 0.433\ \alpha^2 \qquad 3.1$$

$$Height\ of\ Equilateral\ Triangle\ = \frac{\sqrt{3}}{2} * \alpha = 0.866\ \alpha \qquad 3.2$$

**Table 3-1: Corrugated sheets: dimensions and areas.**

| **Pitch length (α)** | **5 mm** | **10 mm** | **25 mm** |
|---|---|---|---|
| **Opening area (mm²)** | 11 | 43 | 271 |
| **Corrugated sheet area (m²)** | 0.125 | | |
| **Flat sheet area (m²)** | 0.0625 | | |

## 3.3 Design Arrangement

In order to establish the design of the entire exchanger core, a new parameter was introduced: the height of the exchanger. This will determine the number of layers, *n*, that can be laid one on top of one-another. The total number of ducts/channels will be the number of layers multiplied by the number of ducts per layer. Different exchanger heights could be used for different applications, depending on the desired ventilation loads. Table 3-2 Heat exchanger dimensions, number of layers (*n*) and heat exchange area (*A*).and Figures (3-3) and (3-4) show the relation between the core height, total heat transfer area (*A*) and number of layers. *n* = INT (height of heat exchanger core/$0.866\ \alpha$) and INT because there must be an integer number of layers.

The heat transfer area of the membrane sheets per exchanger core is equal to $A$ = 0.125 x n, $m^2$, since the area of each layer is 0.125 $m^2$. While, the number of individual triangular channels carrying either fresh air or exhaust air = $n$ x (Height/ $0.866\,\alpha$). The total number of the total channels will be twice this. The exchanger core heights were also considered depending on Redring-Xpelair exchangers heights to match the commercialized polymer exchanger cores with their heat recovery units depending on the ventilation needed.

**Table 3-2 Heat exchanger dimensions, number of layers (*n*) and heat exchange area (*A*).**

| | | Heat exchanger core height (mm) | | | | | |
|---|---|---|---|---|---|---|---|
| | | **100** | **200** | **300** | **400** | **500** | |
| **Pitch length (mm)** | **5** | 22 | 44 | 68 | 90 | 112 | ***n*** |
| | | 2.75 | 5.625 | 8.50 | 11.25 | 14.00 | ***A*** ($m^2$) |
| | **10** | 10 | 22 | 34 | 44 | 56 | ***n*** |
| | | 1.375 | 2.75 | 4.25 | 5.625 | 7 | ***A*** ($m^2$) |
| | **25** | 4 | 8 | 12 | 18 | 22 | ***n*** |
| | | 0.50 | 1.125 | 1.625 | 2.25 | 2.75 | ***A*** ($m^2$) |

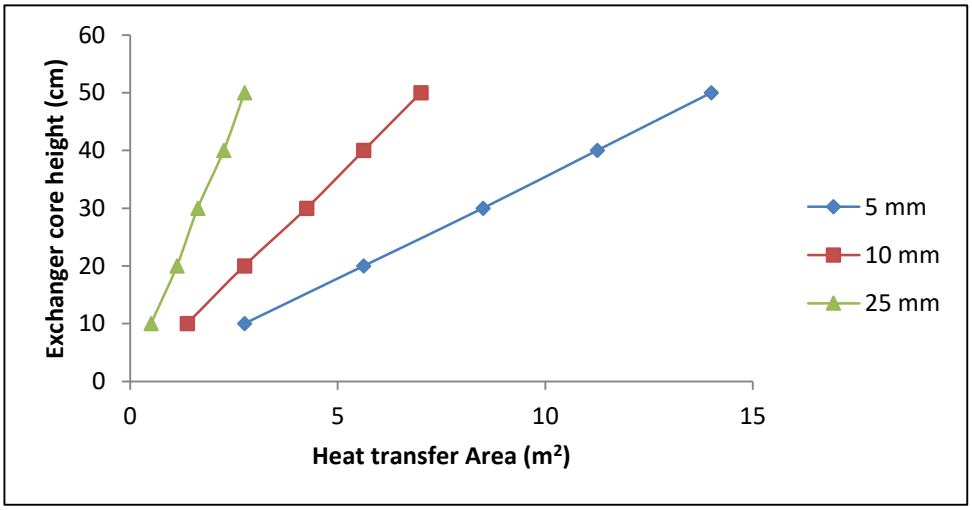


**Figure 3-6: Exchanger core height vs heat transfer area.**

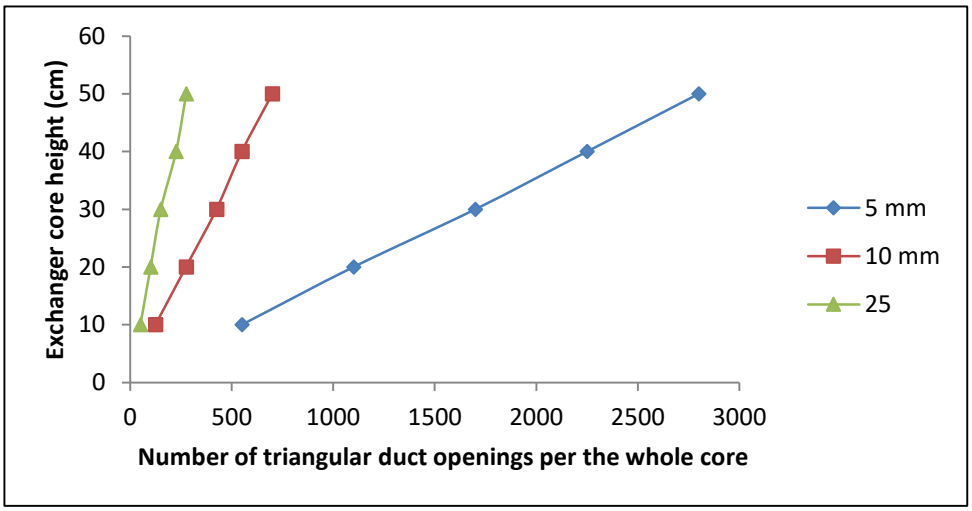


**Figure 3-7: Exchanger core height vs number of triangular duct openings**

## 3.4 Ventilation Air Volume Flow Rates and Inlet Velocities Design

One of the main focuses of this study is to supply the needed amount of fresh ventilation air, and as the air is to ventilate an individual household - and according to the American Society of Heating, Refrigeration and Air-Conditioning Engineers (Fundamentals volume of the ASHRAE *Handbook*, 2005) - the amount of ventilation air needed for two people in a two-bedroom house with living room and kitchen, and a floor area of 100 $m^2$ would be between 85 and 100 $m^3$/hr (0.0236 to 0.0278 $m^3$/s). Chartered Institution of Building Services Engineers (CIBSE) guide has almost the same values for the needed fresh air for ventilation.

Knowing the required volumetric flow rate and total area of the duct inlet openings, and assuming that all the required air flows through that area, the velocity of the air flow through each triangular ducts can be calculated. Table 3-3 lists the number of triangular openings and their cross-sectional areas, for each heat exchanger core and the required air velocity through each triangular duct.

Ventilation air volumetric flow rate ($m^3/s$) : $\dot{V}_a$ = area of opening x average velocity of flow through opening: Table 3-3 presents design options for the number of openings for each design of the exchanger core and the calculated air velocity through each triangular duct opening, with its area.

**Table 3-3: Heat exchanger designs with their dimensions (Average velocity calculated using flow rate of 100 $m^3/h$ [0.0278 $m^3/s$]).**

| | | Heat exchanger core height (mm) | | | | | |
|---|---|---|---|---|---|---|---|
| | | **100** | **200** | **300** | **400** | **500** | |
| **Pitch length (mm)** | **5** | 22 | 44 | 68 | 90 | 112 | No. of sheets |
| | | 2.75 | 5.625 | 8.5 | 11.25 | 14.00 | Total sheet area ($m^2$) |
| | | 550 | 1100 | 1700 | 2250 | 2800 | No. of triangular duct openings |
| | | 4.6 | 2.3 | 1.5 | 1.1 | 0.9 | Average velocity (m/s) |
| | | 0.0061 | 0.0121 | 0.0187 | 0.025 | 0.03 | inlet total Area ($m^2$) |
| | **10** | 10 | 22 | 34 | 44 | 56 | No. of sheets |
| | | 1.375 | 2.75 | 4.25 | 5.625 | 7.00 | Total sheet area ($m^2$) |
| | | 125 | 275 | 425 | 550 | 700 | No. of triangular duct openings |
| | | 5.1 | 2.3 | 1.5 | 1.2 | 0.9 | Average velocity (m/s) |
| | | 0.0054 | 0.012 | 0.0182 | 0.023 | 0.03 | inlet total Area ($m^2$) |
| | **25** | 4 | 8 | 12 | 18 | 24 | No. of sheets |
| | | 0.5 | 1.125 | 1.625 | 2.25 | 2.75 | Total sheet area ($m^2$) |
| | | 50 | 100 | 150 | 225 | 275 | No. of triangular duct openings |
| | | 2.0 | 1.0 | 0.7 | 0.5 | 0.4 | Average velocity (m/s) |
| | | 0.0135 | 0.027 | 0.04 | 0.06 | 0.07 | inlet total Area ($m^2$) |

Figures from Figure 3-8 to Figure 3-10 show the relation between the height of the core with the air velocity per opening, total inlet area per core and the number of channels per core. From the figures below, a first impression might be obtained regarding which of them would be the best design because higher inlet velocities mean higher pressure drops and higher energy consumption. The 5 mm and the 10 mm showed almost the same average velocity per opening because the 5 mm cases will have the same total inlet area as the 10 mm cases for the same exchanger core height.

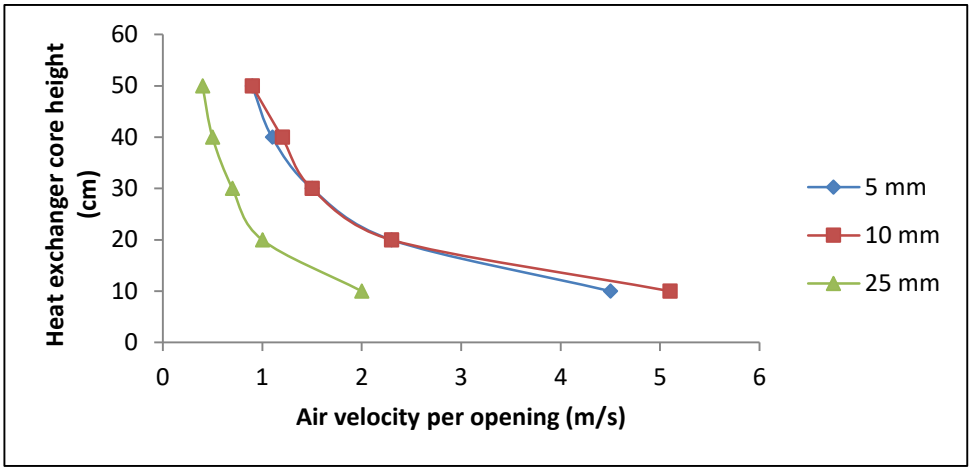


**Figure 3-8: Exchanger core height vs air velocity per opening**

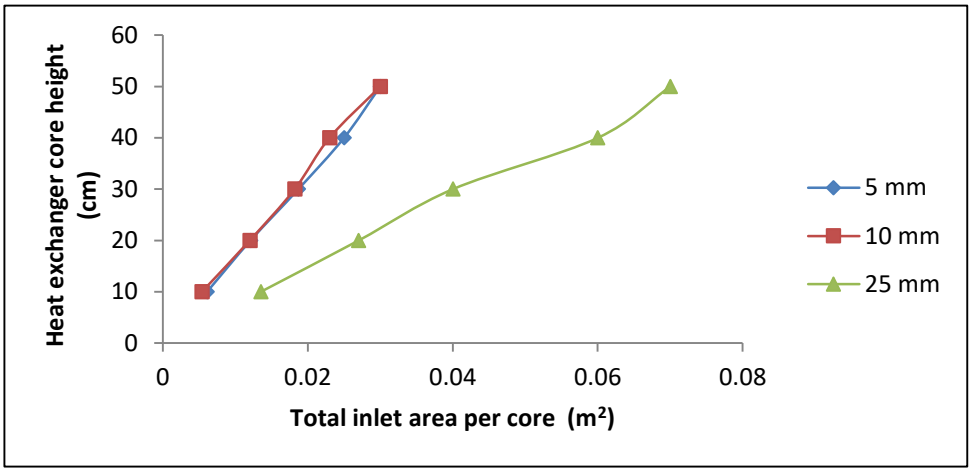


**Figure 3-9: Exchanger core height vs total inlet area per core.**

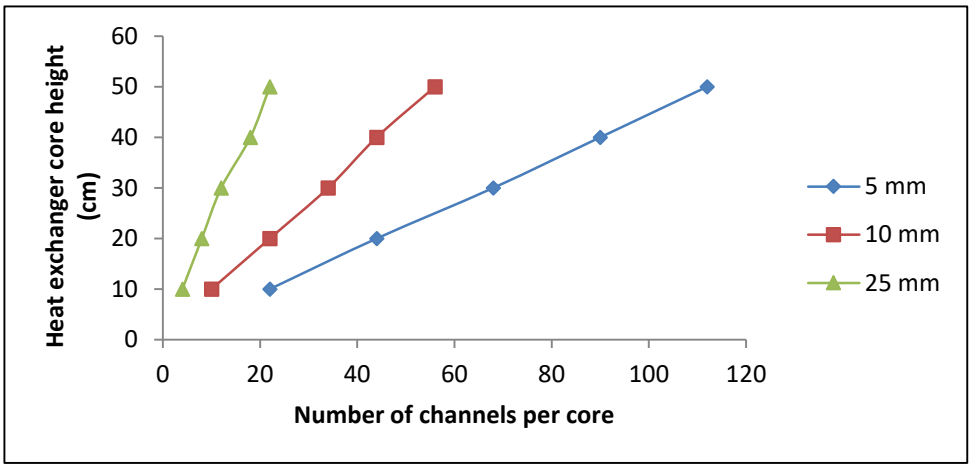


**Figure 3-10: Exchanger core height vs number of channels per core.**

## 3.5 Climate Design Conditions

The current exchanger core was designed in order to work under the UK climate conditions. According to UK climate projection office report [148] and for winter months (December, January and February) the average high/low temperature in the UK varies between 2ºC - 10ºC, and the relative humidity ($\phi$) varies between 65% - 95%. In order to evaluate the latent effectiveness for the proposed energy recovery exchanger, the humidity ratio *w* ($kg_{H2O}/kg_{Dry\ air}$) is the most essential parameter. The range of the ambient temperature which is considered in this study is (2ºC, 4ºC, 6ºC, 8ºC and 10ºC), while the range of the relative humidity ($\phi$) is (65%, 75%, 85% and 95%). Table 3-4 show the calculated values for the humidity ratio from the psychrometric chart for air status conditions, and the values at the 85% relative humidity where considered in this study (0.00371, 0.00427, 0.00492, 0.00565 and 0.00647) according to the specified ambient temperature, and this will be fully explained in Chapter Four in section 4.6.5.5 in the species boundary conditions for the fresh inlet air. The reason behind choosing the 85% relative humidity is because it most frequent range in the UK winter conditions according to [148].

**Table 3-4: Humidity ration values in (kg/kg) for given ambient temperature and relative humidity**

| | **Ambient temperature** | | | | | | |
|---|---|---|---|---|---|---|---|
| | **2** ºC | **4** ºC | **6** ºC | **8** ºC | **10** ºC | | |
| **Humidity ratio (*w*)** (kg/kg) | 0.00283 | 0.00326 | 0.00375 | 0.00431 | 0.00493 | **65%** | **Relative Humidity ($\phi$)** |
| | 0.00327 | 0.00377 | 0.00434 | 0.00498 | 0.00570 | **75%** | |
| | **0.00371** | **0.00427** | **0.00492** | **0.00565** | **0.00647** | **85%** | |
| | 0.00414 | 0.00478 | 0.00550 | 0.00632 | 0.00724 | **95%** | |

## 3.6 Hydraulic Diameter

In order to estimate other design parameters, the hydraulic diameter is necessary, e.g. for evaluating the Reynolds number and then to calculate friction factor and Nusselt number. The hydraulic diameter, $D_h$, is commonly used with non-circular pipes, holes or ducts. As can be seen in Figure 3-5, The hydraulic diameter depends on the pitch length of the triangular duct opening (α) and the apex angle (θ). However, it could be calculated also by using the area of the inlet triangular duct divided it by the perimeter of the duct. Table 3-5 show the values of the hydraulic diameter which were calculated using one of following equations [149]:

$$D_h = \frac{\alpha \sin\theta}{1 + sin\left(\frac{\theta}{2}\right)} = \frac{4 * Inlet\ Area}{Perimeter} \qquad 3.3$$

where $\theta$ = 60°, $\alpha$ = 5,10 and 25 mm

**Table 3-5: Hydraulic diameter for equilateral triangle duct opening.**

| **Pitch length** mm | **Inlet Area** ($m^2$ x $10^6$) | **Perimeter** mm | **$D_h$** (mm) |
|---|---|---|---|
| **5** | 10.8 | 15 | 2.88 |
| **10** | 43.3 | 30 | 5.77 |
| **25** | 271 | 75 | 14.4 |

## 3.7 Reynolds Number

The Reynolds number (Re) is a dimensionless quantity commonly used in fluid mechanics as the main guide to identify whether a flow is laminar, turbulent or transitional and to help predict fluid behaviour. Re is a function of several parameters including the flow velocity.

It is well known that roughening surfaces can increase the heat transfer rate, and that increasing the Reynold's number of a flow over a surface can promote heat transfer due to increase in turbulence and swirl and the disruption and thinning of the boundary layer [150]. The flow of the air streams through the triangular ducts which considered to smooth internal duct walls, that means the effects of turbulence will be to disrupt the stagnant layer of the wall surface, bringing the hotter air in closer contact with the wall surface and increasing heat and mass transfer. For non-swirl flow regimes enlarging the surface area of the heat transfer surface (the corrugated plate) is an established means of enhancing heat transfer but is significantly less effective than increasing flow disruption [151].

Reynolds number can be evaluated from the equation below, the minimum temperature in this study is (2$^{o}$C) which is the lowest considered ambient temperature, while the maximum temperature is the exhaust outlet temperature from the conditioned room which is (22$^{o}$C). Consequently, the kinematic viscosity of air ($\nu$) values vary from (13.43x10$^{-6}$ m$^2$/s to 15.56x10$^{-6}$ m$^2$/s) and the density of air ($\rho$) vary from (1.284 kg/m$^3$ to 1.177 kg/m$^3$), these values were taken from the air properties table in [149] and for the 2$^{o}$C and 22$^{o}$C temperature respectively.

$$Re = \frac{\rho V_a D_h}{\nu} \qquad 3.4$$

where $V_a$ is the velocity of the air, and the values for $\nu$ and $\rho$ where 14.5 m$^2$/s and 1.2 kg/m$^3$ respectively as an average values and the minimal effect that the difference of these values on Reynold number values.

As shown in Table 3-3, the average inlet velocities for proposed cases varies from (0.4 m/s to 4.6 m/s) and after 2 m/s the Re values exceeded 2000 which means the flow inside the core channels become turbulent, despite the benefits of turbulent flow on the heat transfer but it suffers from compromises like way higher pressure drop, noise and vibration in the exchanger core according to Redring-Xpelair. Consequently, four main cases are considered in this study taking a range of inlet velocity which are (0.5 m/s, 1 m/s, 1.5 m/s and 2 m/s) to determine the most efficient design point and how the affected by the increasing inlet velocity. In addition, the flow in the cross corrugated tends to transform to the transition region in lower Reynolds numbers than 2000 due the nature of the channel structure as was proven by [105,152], and because of this reason the Transition-SST model was used to simulate the current cases in the CFD part as it will explained in Chapter four later. Table 3-6 and Figure 3-11 show the Reynolds number values with the selected air inlet velocities.

**Table 3-6: Reynolds number values for the designed inlet air velocities**

| | | Calculated duct air velocity (m/s) | | | | |
|---|---|---|---|---|---|---|
| | | **0.5** | **1** | **1.5** | **2** | |
| **Pitch length** | **5 mm** | 118 | 235 | 353 | 470 | **Reynolds Number** |
| | **10 mm** | 236 | 471 | 706 | 942 | |
| | **25 mm** | 587 | 1175 | 1763 | 2351 | |

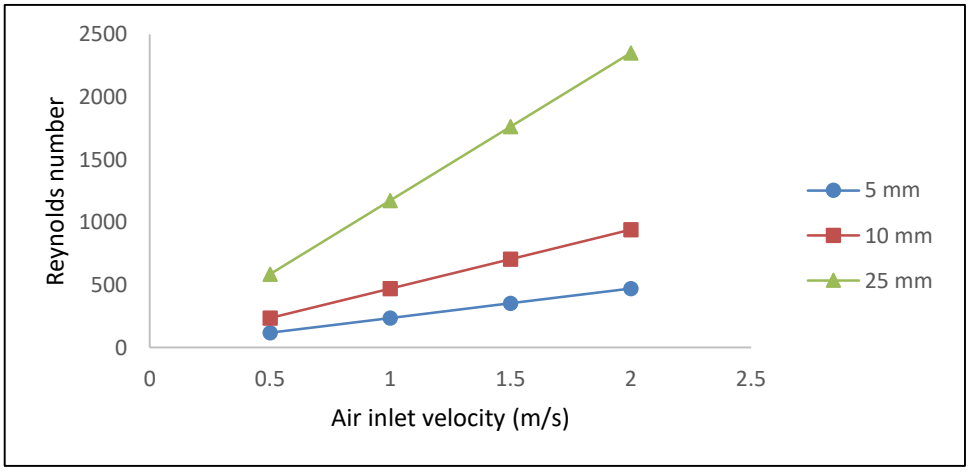


**Figure 3-11: Reynolds number with the inlet air velocity of the proposed cases.**

## 3.8 Friction Factor

For the cross-corrugated triangular ducts, the mean friction factor ($f_D$) is significant parameter which affect the heat exchanger core design, because it depends on the pressure drop in the exchanger core and plays a major role in determining the need fan power to overcome the core's pressure drop. Table 3-7 and show the mean friction factor for each of the velocity cases along the flow direction, for three pitch lengths. A correlation was proposed by Zhang [1] to establish the relations between the periodically mean friction factor of the cross-corrugated triangular duct with Reynolds numbers, and this equation is valid for the low Reynolds number as (10 ≤ Re ≤ 2000). As shown, the mean friction factor is higher at the low velocities, decreasing with increase in flow velocity.

$$f_{D=}11.03\ Re^{-0.5121} \qquad 3.5$$

**Table 3-7: Mean friction factor for the designed air inlet velocities.**

| | | Calculated duct air velocity (m/s) | | | | |
|---|---|---|---|---|---|---|
| | | **0.5** | **1** | **1.5** | **2** | |
| **Pitch length** | **5 mm** | 1.027 | 0.72 | 0.585 | 0.5 | **Friction Factor** |
| | **10 mm** | 0.74 | 0.52 | 0.42 | 0.36 | |
| | **25 mm** | 0.46 | 0.32 | 0.26 | 0.22 | |

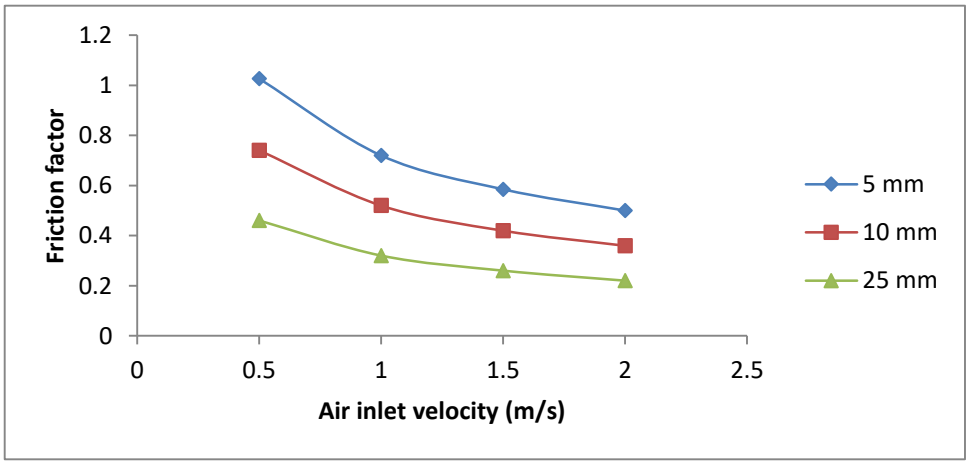


**Figure 3-12: Mean friction factor with inlet air velocity.**

## 3.9 Membrane-Based Exchanger

Membrane materials, generally in HVAC systems are used for dehumidification purposes. To select the most suitable membrane material for this study, several parameters have to be considered and this section will focus on material suitable for the heat exchanger design [153].

### 3.9.1 Fundamental Principles of Membrane Materials

Membrane-based heat and moisture recovery is an innovative means for energy recovery from the exhaust air expelled from occupied buildings. While the water vapor content of the exhaust air is small, only about tens grams per cubic meter of air it has a very high heat of vaporization, which means the latent heat contained in the exhaust air can be of the same order of magnitude as the sensible heat.

Membrane-based heat recovery systems are usually represented as a mass transfer problem based on the humidity ratio transfer between the two sides of the membrane: the feed side and the permeate side. The water vapour partial pressure difference is the main driving force of the mass transfer process, and this includes the difference in the humidity ratio. The mass transfer flux $J$ (kg/s) can be calculated as follows [153]:

$$J = k\Delta wA \tag{3.6}$$

where $k$ is the mass transfer coefficient (kg/m$^2$.s); $w$ is the humidity ratio (kg/kg$_{\text{dry air}}$) and $A$ is the total heat transfer area of the membrane (m$^2$).

### 3.9.2 Membrane Properties

The main two properties which play the major roles in determining the performance and quality of the membrane are; selectivity and permeability. Selectivity in a humid environment could be defined as the amount of water vapour that transfers through the membrane, while the passage of air was blocked. In other words, selectivity is how efficient the membrane material is in selecting only water vapour and separating it from anything else in the air mixture. However, absolute separation is almost impossible, and a few air particles might infiltrate the membrane material through its pores, though the quantity can generally be neglected. Thus, the porous hydrophilic membrane was introduced into heat recovery systems. Figure 3-13 shows the membrane selectivity [154].

The permeability represents the relation between the porosity of the membrane to the speed of the mass transfer: higher porosity leads to faster water vapour transfer and higher permeability.

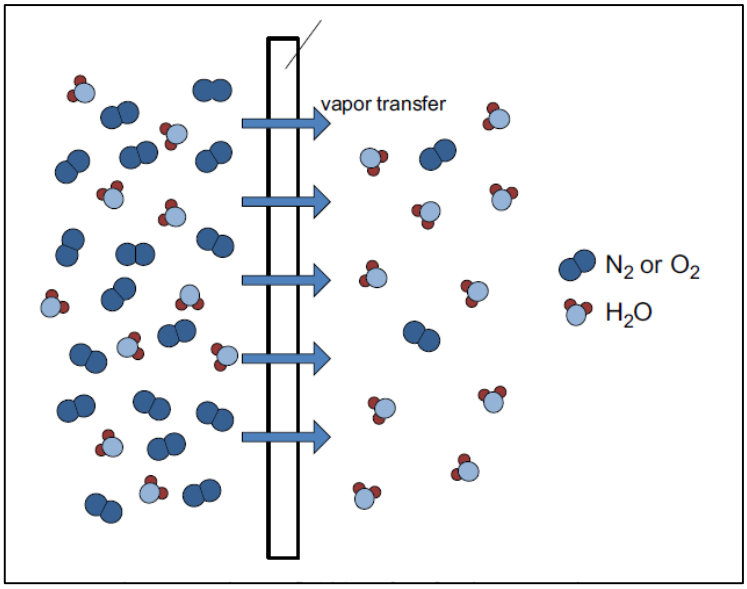


**Figure 3-13: Hydrophilic polymer membrane selectivity** [154]

### 3.9.3 Membrane Material Selection

The membrane materials used in heat recovery systems include organic materials such as polymers (which are the most commonly used), and inorganic materials such as silicates. As the main component of air is Nitrogen (it comprises almost 76% of atmospheric air) membrane performance is measured according to its $H_2O/N_2$ separation ability. Table 3-8 shows the permeability and selectivity of some of the more common membrane materials.

**Table 3-8: Properties of some common membrane materials** [155]

| **Polymer membrane** | **Water vapour permeability** $10^{-18}$ ($m^2$/s.Pa) | **Selectivity** $H_2O/N_2$ |
|---|---|---|
| PEBAX 1074 | 1,216,000 | 200,000 |
| PBT/PEO block copolymer | 649,800 | 40,500 |
| Sulfonated poly (ether ether ketone) | 463,600 | 10,200,000 |
| Polydimethylsiloxane | 304,000 | 143 |
| Sulfonated poly (ether sulfone) | 114,000 | 214,000 |
| Ethyl cellulose | 152,000 | 6060 |
| Cellulose acetate | 45,600 | 24,000 |
| Poly (phenylene oxide) | 30,856 | 1068 |
| **Poly (ether Sulfone)** | **19,912** | **10,500** |
| Natural rubber | 19,760 | 299 |
| Polysulfone | 15,200 | 8000 |
| Polycarbonate | 10,640 | 4670 |
| Polystyrene | 7372 | 388 |
| Polyimide | 4860 | 5,330,000 |
| Polyacrylonitrile | 2280 | 1,880,000 |
| Poly (viny1 chloride) | 2090 | 12,500 |
| Polyamide 6 | 2090 | 11,000 |
| Polypropylene | 517 | 227 |
| Poly (viny1 alcohol) | 144 | 33,300 |
| Polyethylene | 91 | 6 |

However, Table 3-8 also shows the unfortunate fact that very few membranes possess both good selectivity and permeability at the same time. Even if some of these materials have high water vapour permeability as well as high $H_2O/N_2$ selectivity, they tend to be very expensive or not compatible or relevant to heat recovery applications. The simultaneous achievement of good selectivity and permeability is difficult using simply structured and readily available materials, so manufacturers tend to fabricate heat exchange modules with composite membranes. These composite membranes are usually constructed in two parts; the first one is a thin high hydrophilic skin layer made of dense membrane that covers the second part, which is the supportive layer. Together the membranes form a material with good mass transfer capability and enhanced mechanical strength.

## 3.10 Polyether-Sulfone (PES) Membrane Material

PES is considered a good hydrophilic membrane material due its promising $H_2O/N_2$ selectivity and water vapour permeability [156]. In addition, this material has excellent mechanical and chemical stability. A wet inversion process is usually used to prepare PES membranes. Polymer PES is also one of the most widely used polymers for making the membrane support, is available commercially and is relatively inexpensive. PES membrane selectivity and permeability is shown in.

Researchers such as Abbdalla et al. [157], they have undertaken a variety of work on polymers such as PES, including developing PES to fabricate it as a hydrophobic material to use as the main material for a distillation unit. However, Kochan et al. [158] have investigated modifying the PES ultrafiltration membrane with polyelectrolytes in order to assemble a novel material to use for wastewater treatment for a bioreactor. Ouyang et al. [156] have proposed a novel use for PES as an ultrafiltration membrane by enhancing its permeability by blending it with cobalt oxide/graphene oxide nanocomposites. This work was also on the hydrophobic properties of PES. In accordance with, and continuation of, these studies hydrophilic PES membrane was selected and used in this study.

## 3.11 Design Summary

The cross-corrugated exchanger core is the main component of the heat recovery system, so this chapter has focused on considering an established and widely used set of geometries for three different pitch lengths (25 mm, 10 mm and 5 mm). The chapter has taken into consideration several heat exchanger design parameters such as; the ventilation load needed for an individual small house, the weather conditions selected were for winter in the UK and the material chosen to be used is PES.

# 4 ENERGETIC ANALYSIS

## 4.1 Introduction

With the advancement of computer technology, numerical methods have become accepted in the scientific community and are widely used, especially in the area of fluid dynamics. Today numerical methods, often in the form of commercially available software packages, complement the traditional approaches of theory and experiment [159,160].

Numerical simulations allow the analysis of complex phenomena without resorting to expensive prototypes and difficult experimental measurements. During the last few years Computational Fluid Dynamics (CFD) has become one of the most powerful and useful tools for the accurate prediction of such factors as temperature distribution and air flow behaviour in heat exchangers. Numerical modelling of flow, heat transfer, and related phenomena is of great importance in a number of industrial applications [161].

CFD simulation for the purpose improving cross-corrugated exchanger core design is appropriate and timely in view of the increasing competitiveness and other pressures being faced by the air conditioning industry. Computational Fluid Dynamics is now one of the most powerful and useful tools for predicting the performance of such heat exchangers. Experimental rigs and prototypes are only necessary during the initial stages of an exchanger design, once these initial experimental results are validated by a suitable CFD code, further development can be largely computationally performed. With these computational methods the time involved for model making, mounting, and testing at each and every stage is no longer required. Design modification can be performed with the available CAD software and analysed using the available CFD tools. Repeating this cycle enables achieving an optimal design with less development cost. Therefore, a complete numerical analysis is used in the present work to simulate the flow, temperature and humidity distribution in the proposed exchanger core and predict the performance and thermal outcomes [162,163].

In the present work, CFD was used to analyses the three main core geometric parameters according the pitch length (5 mm, 10 mm and 25 mm) as described in Chapter three. This chapter will cover the following:

- **Geometry**: In this section, the physical geometry of the exchanger core is constructed and used in the CFD numerical simulations.
- **Governing Equations**: The characteristics of the fluid flow in the exchanger core is simulated based on several equations and assumptions.
- **Mesh Generation**: Specifying an appropriate mesh for the physical domain is of great importance since mesh size can strongly influence the accuracy of the solution. The mesh should be sized such that it can accurately compatible with the boundary conditions, and simulate the cases and converged with minimum number of iterations. A good mesh is very essential in order to the governing equation be evaluated with ease to obtain the required results precisely.

  Mesh is generated using ANSYS WORKBENCH 17.1 [164], mesh smoothness, quality, resolution and dependency are checked prior to run.
- **Solution Method**: CFD is used in this study to simulate flow through a cross-flow corrugated heat and mass exchanger. The computations are performed using the ANSYS Fluent 17.1 [165] code. The solution method, algorithm and solution parameters are presented in this section.
- **Boundary conditions**: The most important role is played in the CFD simulations by the boundary conditions, therefore, determining accurate and precise boundary conditions is essential to solve the case numerically. All the boundary conditions in this research are described in details in this section.

## 4.2 The Exchanger Core Geometry

The basic heat exchanger geometry considered in the current study is as shown in Figure 4-1. Where F and EX refer to fresh and exhaust air streams.

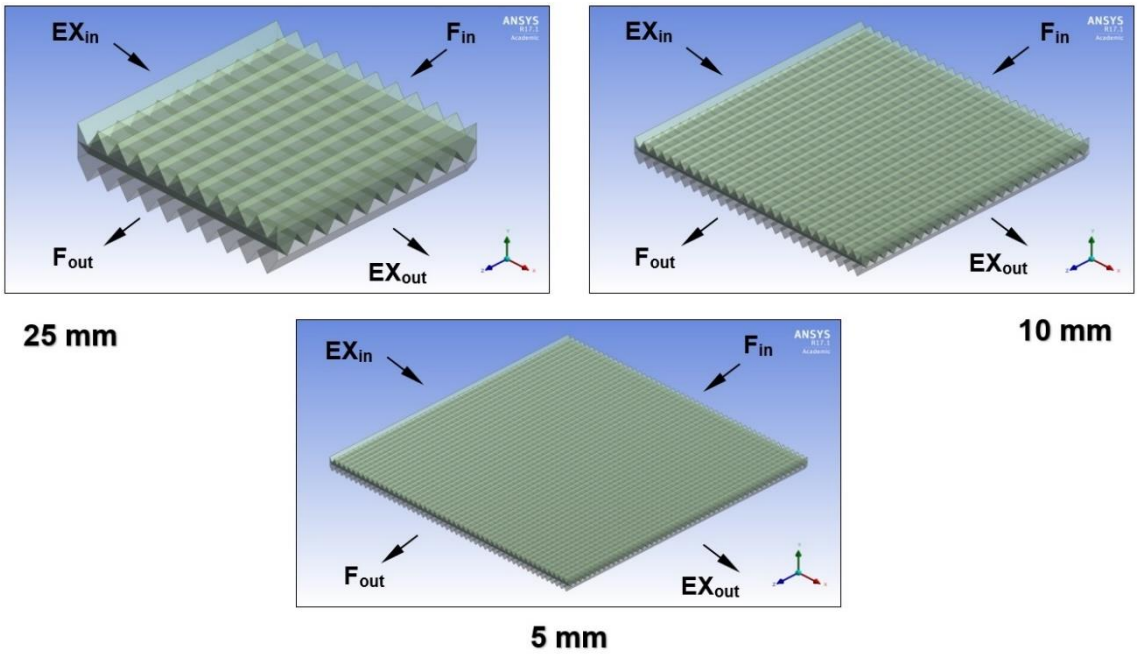


**Figure 4-1: Cross corrugated triangular heat exchanger core arrangements.**

**For the computational model,** the geometry is generated through the following steps:

1. Since the geometry is quite complex, it is not useful to create the geometry for the whole core. Therefore, only one active membrane layer between two air streams was considered in the study and the thermal performance of this single layer provided the data needed for the exergetic analysis
2. The geometries were built in **CATIA V5** [166] with equilateral triangular duct openings for both fresh and exhaust air inlets.
3. Finally, the solid model generated in CATIA V5 is exported to ANSYS Workbench 17 and meshed for the solution stage (details are described in Section 3-4).

Figure 4-2 and Figure 4-3 show how the geometry was built in CATIA V5 and explains the three elements which were created to represent the membrane and the two air streams. The grey element carries the fresh air, the green element is the separating membrane, and the red element represents exhaust air. The difference in thickness between the green element (the membrane thickness is 0.1 mm) and the air streams can be seen.

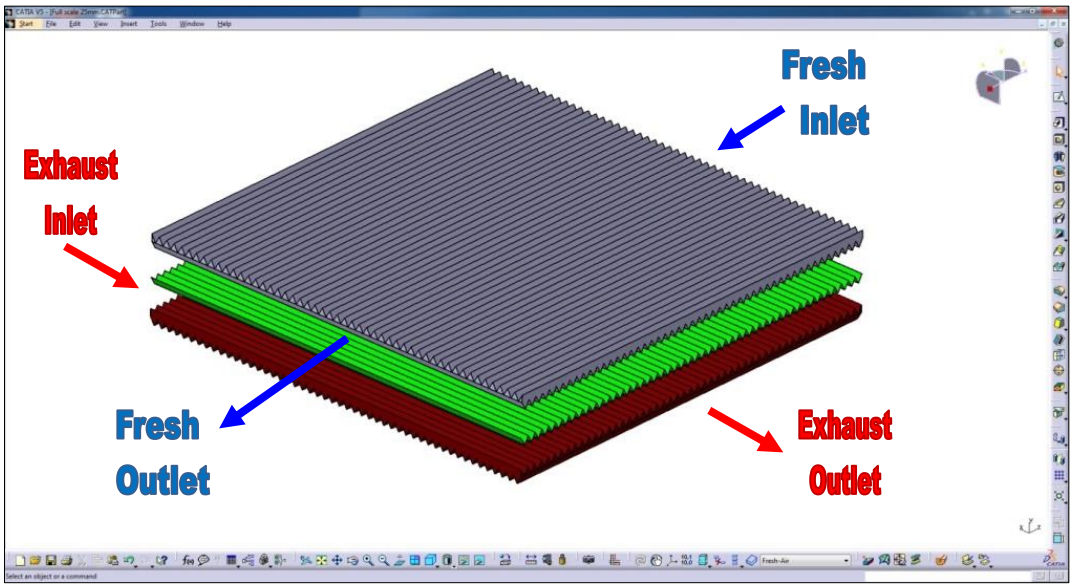


**Figure 4-2: Geometry of the element in CATIA 5**

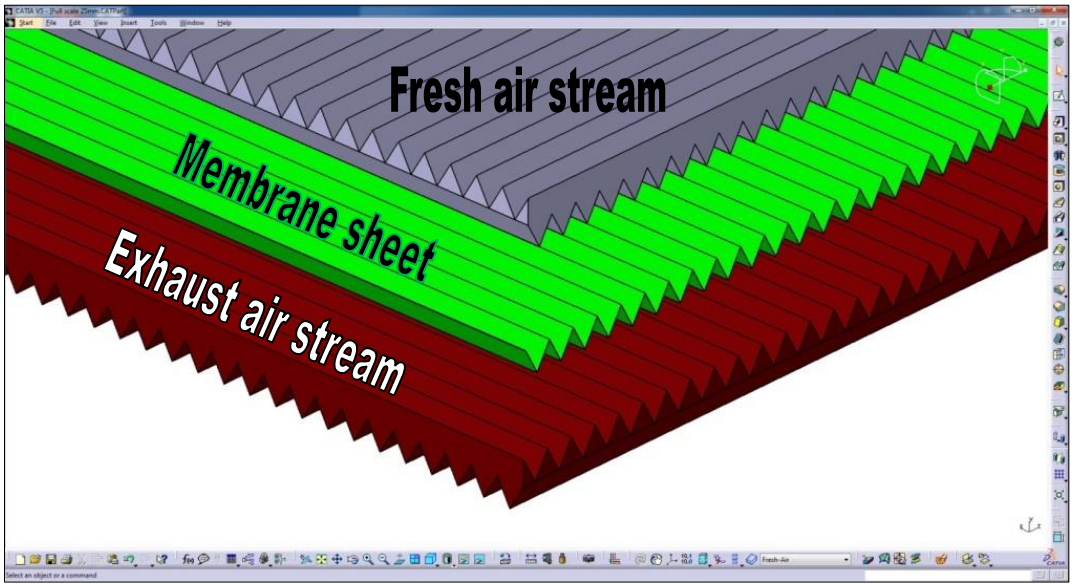


**Figure 4-3: Geometric cross-sectional view of the elements in the CATIA 5 window**

As mentioned in Chapter 3, the pitch lengths of 25 mm, 10 mm and 5 mm correspond, respectively to the 10, 25 and 50 openings per layer for a heat exchanger width of 250 mm, for both the fresh and the exhaust air streams. Figure 4-4, Figure 4-5 and Figure 4-6 show the three bodies (membrane, fresh and exhaust streams) in which were created in CATIA V5 and exported to Workbench 17. The horizontal green line represents the membrane layer, while the other bodies represent the fresh and exhaust computational bodies.

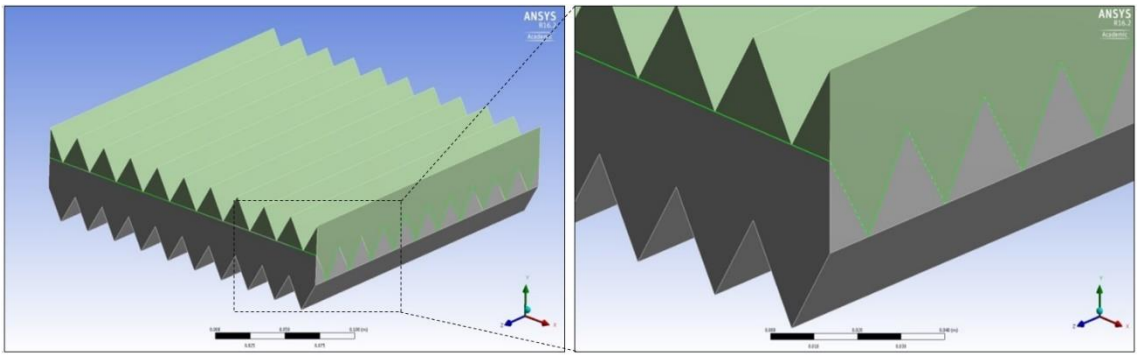

**Figure 4-4: 25 mm model on the left with zoomed-in cross section on the right.**

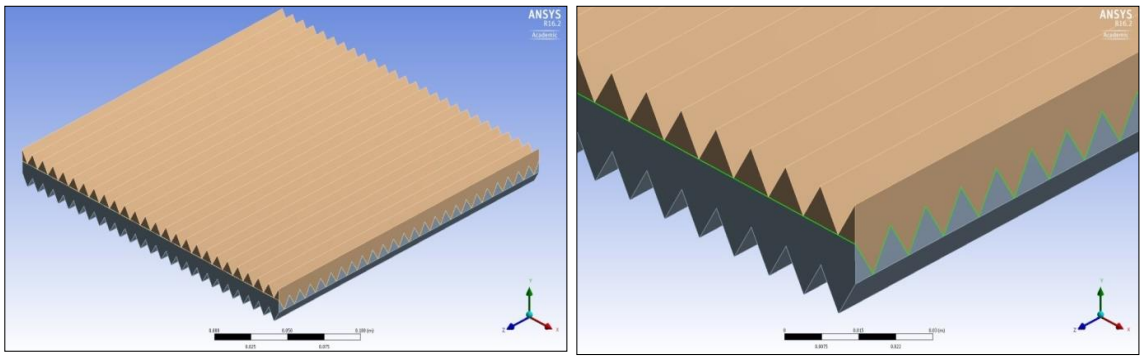

**Figure 4-5: 10 mm full scale model with zoomed-in cross section.**

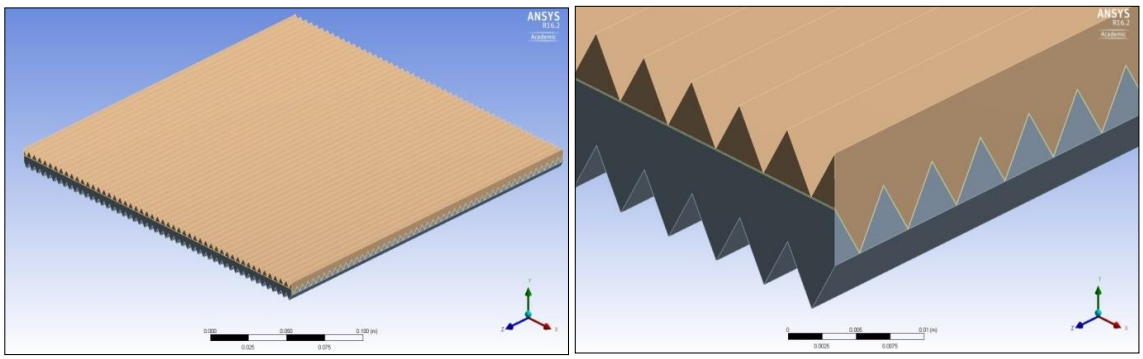

**Figure 4-6: 5 mm full scale model with zoomed-in cross section.**

The reason behind constructing three exchangers with different pitch lengths is to simulate different flows inside the membrane; considering it as a standalone porous zone, and obtaining the heat and vapour transfer through it. Four of the layers' faces (The upper and lower membrane layer surfaces, the lower surface of the fresh stream body and the upper surface of the exhaust stream) will be considered as interference surfaces, where an interference surface is the surface between the air streams and the membrane surfaces, their purpose is to connect the membrane mesh with the air stream meshes in ANSYS Fluent.

## 4.3 Basic Governing Equations

The conservation of mass equations for continuity, momentum, energy and transition flow are described below according to [167]**:**

### 4.3.1 Conservation of Mass (Continuity)

For a control volume, the difference in the mass flow rate between the inlet and the outlet should be zero. For an incompressible flow and under the law that stated the mass cannot be created from nothingness nor can destroyed, the continuity equation can be expressed as follow:

$$\frac{\partial u}{\partial x}+\frac{\partial v}{\partial y}+\frac{\partial w}{\partial z}=0 \qquad 4.1$$

where ***u***, ***v*** and ***w*** are the Cartesian velocity component within the Cartesian axes x, ***y*** and ***z*** respectively.

### 4.3.2 Narvier-Stokes Equations (Momentum)

Newton's second law of motion is the base of the momentum equations and all Narvier-Stokes equation can be derived from it, the equations of the conservation of momentum with the assumption of an incompressible fluid are:

$$\frac{\partial(\rho uu)}{\partial x}+\frac{\partial(\rho vu)}{\partial y}+\frac{\partial(\rho wu)}{\partial z}=-\frac{\partial p}{\partial x}+\mu[\frac{\partial^2 u}{\partial x^2}+\frac{\partial^2 u}{\partial y^2}+\frac{\partial^2 u}{\partial z^2}] \qquad 4.2$$

$$\frac{\partial(\rho uv)}{\partial x}+\frac{\partial(\rho vv)}{\partial y}+\frac{\partial(\rho wv)}{\partial z}=-\frac{\partial p}{\partial y}+\mu\left[\frac{\partial^2 v}{\partial x^2}+\frac{\partial^2 v}{\partial y^2}+\frac{\partial^2 v}{\partial z^2}\right] \qquad 4.3$$

$$\frac{\partial(\rho uw)}{\partial x}+\frac{\partial(\rho vw)}{\partial y}+\frac{\partial(\rho ww)}{\partial z}=-\frac{\partial p}{\partial z}+\mu[\frac{\partial^2 w}{\partial x^2}+\frac{\partial^2 w}{\partial y^2}+\frac{\partial^2 w}{\partial z^2}] \quad 4.4$$

where ***u***, ***v*** and ***w*** are the Cartesian velocity components along the Cartesian axes ***x***, ***y*** and ***z*** respectively . $S_{bj}$ is a buoyancy source or sink term.

### 4.3.3 Energy Equation

The following equation represents the transport of heat energy within the flow field:

$$\rho\frac{\partial}{\partial x}(uT)+\rho\frac{\partial}{\partial y}(vT)+\rho\frac{\partial}{\partial z}(wT) = \frac{\partial}{\partial x}\left(\Gamma_{eff}\frac{\partial T}{\partial x}\right)+\frac{\partial}{\partial y}\left(\Gamma_{eff}\frac{\partial T}{\partial y}\right)+\frac{\partial}{\partial z}\left(\Gamma_{eff}\frac{\partial T}{\partial z}\right)+S_T \quad 4.5$$

where the symbols have their usual meanings and $\Gamma_{eff}$ is the effective diffusion term.

### 4.3.4 Species Transport Equations

For solving the conservation equations for air and water vapour species, the local fraction of mass, $Y_i$, can be predicted by ANSYS Fluent 17.1 for each species by solving a convection-diffusion equation for a specified species ($i^{th}$). The general form of the conservation equation is as follows:

$$\nabla.\left(\rho\vec{V}Y_i\right)=\nabla.\vec{J}_i \quad 4.6$$

where $Y_i$ is local mass fraction, $\vec{V}$ is the velocity field that the quantity is moving with, it is function of time and space and $\rho$ is the local density of the air flow.

#### 4.3.4.1 Mass Diffusion in Laminar Flows

The diffusion flux, $\vec{J}_i$, of $i^{th}$ species (i.e. air or water vapour) which form due to concentration gradients is given by Equation 4.7. Fluent 17.1 uses the dilute approximation, so the diffusion flux is written as:

$$\vec{J}_i = \rho D_{i.ma} \nabla Y_i \quad 4.7$$

where $D_{i.ma}$ is the diffusion coefficient for $i^{th}$ species in the air-vapor mixture.

### 4.3.5 Transition Flow Model (Transition-SST)

The flow model is essential in any CFD simulation problem. The Reynold's numbers were calculated for each of the three pitch lengths and the range of Re associated with each of them determined for the given ventilation rates. In this study it was required that the Re was lower than 2000. This normally means the flow in the exchanger is laminar flow. However, at this value of Re the Fluent simulations were unstable and kept diverging because as mentioned in Chapter 3 in section 3.7 that the cross-corrugated arrangement tends to transform from laminar to turbulence in lower Reynolds number values than 2000 as proved by [161].

At that point, a flow model study was conducted using two turbulence models, the first one was the k-ε (k-epsilon) and the second was the k-ω (k-omega). Both models consist of two equation solvers, and two transition models, the first one of which was the Transition-k-kl-ω which consists of three equation solvers and the latter was the Transition-SST model which consists of four equation flow solvers, as well as this model has the strength of the k-ε near the walls and the strength of the k-ω in the free stream [161]. The "transition" expression is referring to the change in conditions of the flow from laminar to turbulence.

As the geometry of the duct that the flow takes place is not uniform and the corrugations are underneath the air, therefore the boundary layer does not have the time to be created properly as well as the flow takes longer to develop completely, all of that because of the eddies that accrues inside the corrugations casing the flow to be disturbed and goes toward the transition region even on lower Re numbers than 2000.

The transition shear stress (SST) model was used for this study because it gave the best flow pattern and smoothly converged solution. Four equation were combined in order to form the Transition-SST model, the intermittency transport

equation, transition criteria equation that based on the momentum thickness Re and the two transport equations of SST k-ω.

The empirical correlations in ANSYS Fluent 17.1 were conducted by Menter and Langtry [168–170] and were established to deal with standard transitions flows in addition to the flows in low free-stream turbulence region.

#### 4.3.5.1 Transition-SST Model's transport equations

All the sets of equation in this model where taken from ANSYS Fluent 12.0 user's guide [167]. The intermittency (γ) transport equation is:

$$\frac{\partial(\rho\gamma)}{\partial t}+\frac{\partial\left(\rho U_j\gamma\right)}{\partial x_j}=P_{\gamma1}-E_{\gamma1}+P_{\gamma2}-E_{\gamma2}+\frac{\partial}{\partial x_j}\left[\left(\mu+\frac{\mu_t}{\sigma_\gamma}\right)\frac{\partial\gamma}{\partial x_j}\right] \quad 4.8$$

where U is local velocity, $\mu$ and $\mu_t$ are the molecular viscosity and the eddy viscosity respectively.

The transition sources are defined as follows:

$$P_{\gamma1}=C_{a1}F_{lngth}\rho S[\gamma F_{onset}]^{C_{\gamma3}} \quad 4.9$$

$$E_{\gamma1}=C_{a1}P_{\gamma1}\gamma \quad 4.10$$

where $C_{a1}$ and $C_{e1}$ are constants equals to 2 and 1, respectively, an empirical equation $F_{length}$ is presented to controls the transition region's length, $S$ is the strain rate.

The source terms of the destruction/re-laminarization are:

$$P_{\gamma2}=C_{a2}\rho\Omega\gamma F_{turb} \quad 4.11$$

$$E_{\gamma2}=C_{e2}P_{\gamma2}\gamma \quad 4.12$$

where Ω is the vorticity, and $F_{turb}$ is turbulence empirical correlation.

The following set of equation and functions are presented to control the transition onset:

$$Re_v = \frac{\rho y^2 S}{\mu}$$

$$R_T = \frac{\rho k}{\mu \omega} \qquad 4.13$$

$$F_{onset1} = \frac{Re_v}{2193 Re_{\theta c}}$$

$$F_{onset2} = min\left(max\left(F_{onset1}, F_{onset1}^4\right), 2.0\right) \qquad 4.14$$

$$F_{onset3} = \max\left(1 - \left(\frac{R_T}{25}\right)^3, 0\right)$$

$$F_{onset} = max(F_{onset2} - F_{onset3}, 0) \qquad 4.15$$

$$F_{turb} = e^{-\left(\frac{R_T}{4}\right)^4}$$

where $Re_v$ and $R_T$ are vorticity Re and vorticity ratio respectively, $S$ is the strain rate, $y$ is the wall distance, and $Re_{\theta c}$ represent the critical value of Reynolds number in the start of the boundary layer when the intermittency begins to increase. This happens opposite to the transition Reynolds number $\widetilde{Re}_{\theta t}$ and the empirical correlation determines the difference between them both. The $F_{length}$ and $Re_{\theta c}$ are functions of $\widetilde{Re}_{\theta t}$.

The intermittency equation's constants are:

$$C_{a1} = 2; C_{e1} = 1; C_{a2} = 0.06; C_{e2} = 50; c_{\gamma 3} = 0.5;\ \sigma_\gamma = 1.0 \qquad 4.16$$

The transport equation for the transition momentum thickness Reynolds number $\widetilde{Re}_{\theta t}$ is:

$$\frac{\partial\left(\rho \widetilde{Re}_{\theta t}\right)}{\partial t} + \frac{\partial\left(\rho U_j \widetilde{Re}_{\theta t}\right)}{\partial x_j} = P_{\theta t} + \frac{\partial}{\partial x_j}\left[\sigma_{\theta t}(\mu + \mu_t)\frac{\partial \widetilde{Re}_{\theta t}}{\partial x_j}\right] \qquad 4.17$$

The source term is presented as:

$$P_{\theta t} = c_{\theta t}\frac{\rho}{t}\left(Re_{\theta t} - \widetilde{Re}_{\theta t}\right)(1.0 - F_{\theta t})$$

$$t = \frac{500\mu}{\rho U^2} \qquad 4.18$$

$$F = min\left(max\left(F_{wake}e^{\left(-\frac{y}{\delta}\right)^4}, 1.0 - \left(\frac{\gamma - 1/50}{1.0 - 1/50}\right)^2\right), 1.0\right) \qquad 4.19$$

$$\theta_{BL} = \frac{\widetilde{Re}_{\theta t}\mu}{\rho U}$$

$$\delta_{BL} = \frac{15}{2}\theta_{BL} \qquad 4.20$$

$$\delta = \frac{50\Omega y}{U}\delta_{BL}$$

$$Re_{\omega} = \frac{\rho\omega y^2}{\mu}$$

$$F_{wake} = e^{-\left(\frac{Re_{\omega}}{1E+5}\right)^2} \qquad 4.21$$

the constants for $\widetilde{Re}_{\theta t}$ equation are:

$$c_{\theta t} = 0.03;\ \ \sigma_{\theta t} = 2.0 \qquad 4.22$$

Zero flux boundary condition at a wall is considered for the $\widetilde{Re}_{\theta t}$. While at the inlet, the inlet turbulence intensity empirical correlation can determine the boundary conditions for $\widetilde{Re}_{\theta t}$.

The Transition-SST model has three empirical correlations. The experiment determined the first one which is the transition onset $Re_{\theta t}$, and was modified by Menter et al. [169] to enhance the forcast estimation of the natural transition. The second correlation is the transition zone length $F_{length}$, and in order to match both $Re_{\theta t}$ and $F_{length}$, the model is activated at $Re_{\theta c}$. Langtry and Menter [171] have developed and proposed these empirical correlations.

$$Re_{\theta t} = f(Tu, \lambda)$$

$$F_{length} = f\left(\widetilde{Re}_{\theta t}\right) \quad 4.23$$

$$Re_{\theta t} = f\left(\widetilde{Re}_{\theta t}\right)$$

The first empirical correlation is a function of the local turbulence intensity, $Tu$:

$$Tu = \frac{100}{U}\sqrt{\frac{2}{3}k} \quad 4.24$$

where $k$ is the turbulent kinetic energy.

The Thwaites' pressure gradient coefficient $\lambda_\theta$ is defined as:

$$\lambda_\theta = \left(\frac{\theta^2}{v}\right)\frac{dU}{ds} \quad 4.25$$

where *dU/ds* is the acceleration in the stream-wise direction.

#### 4.3.5.2 Separation-Induced Transition Correction

The modification for separation-induced transition is:

$$\gamma_{sep} = min\left(C_{s1} max\left[\left(\frac{Re_v}{3.235 Re_{\theta c}}\right) - 1{,}0\right] F_{reattch}, 2\right) F_{\theta t}$$

$$F_{reattch} = e^{-\left(\frac{R_T}{20}\right)^4} \quad 4.26$$

$$\gamma_{eff} = max\left(\gamma, \gamma_{sep}\right)$$

here, the constant $C_{s1}$ is equal to 2.

Menter et al. [169] have modified the constants of the model in Equation 4.26 to enhance the estimated separation in the transition flow.

The controlling constant of the relationship between both $Re_v$ and $Re_{\theta c}$ are different and was increased from 2.193 to 3.235 and these values are for the Blasius boundary layer and at the separation point respectively, the shape factor in this case is 3.5 [169]. The boundary condition for the intermittency $\gamma$ boundary condition is zero normal flux at the wall, while the intermittency $\gamma$ is equal to 1.0 at the inlet.

#### 4.3.5.3 Combining the Transition Model with the SST Transport Equations

The interaction between the transition model and the SST transport model is achieved by modifying the turbulence $k$-ω equation, as follows:

$$\frac{\partial}{\partial t}(\rho k) + \frac{\partial}{\partial x_i}(\rho k u_i) = \frac{\partial}{\partial x_i}\left( \Gamma_k \frac{\partial k}{\partial x_i}\right) + G_k^* - Y_k^* + S_k \qquad 4.27$$

$$G_k^* = \gamma_{eff}\widetilde{G_k} \qquad 4.28$$

$$Y_k^* = min\left(max\left(\gamma_{eff}, 0.1\right), 1.0\right)Y_k \qquad 4.29$$

where the modified parameters of the turbulence kinetic energy $G^*_k$ is production, $Y^*_k$ is dissipation while $S_k$ is user-defined source term. $\widetilde{G_k}$ and $Y_k$ are the original production and destruction terms for the SST model. Note that the production term in the ω-equation is not modified. The rationale behind the above model formulation is given in detail in Menter et al. [169].

In order to capture the laminar and transitional boundary layers correctly, the mesh must have a $y^+$ of approximately one. If the $y^+$ is too large (that is, > 5), then the transition onset location moves upstream with increasing $y^+$. It is recommended that you use the bounded second order upwind based discretization for the mean flow, turbulence and transition equations.

## 4.4 Assumptions

The working fluid is air with the following assumptions:

- Steady flow rate,
- Incompressible fluid,
- Newtonian fluid, and
- Fluid structure interaction can be neglected.

## 4.5 Mesh Generation

Standard CFD methods require a mesh that fits the boundaries of the computational domain. The generation of a computational mesh suitable for the discretized solution of the three dimensional Navier-Stokes equations has always been the subject of intensive research because it is relevant to a wide range of engineering applications and there is no single mesh generation technique that fits the whole range of problems [161,172]. It is usual to employ a technique that is specific to a given engineering application.

For a complex geometry, the generation of such a mesh is time consuming and often requires modifications to the model geometry. However, there are main two types of approaches to volume meshing, **structured** and **unstructured** meshing [173].

In a structured mesh, the governing equations are transformed into a curvilinear coordinate system aligned with the surface. This is trivial for simple shapes but becomes extremely inefficient and time consuming for complex geometries. Thus, this approach has been excluded in this research as the geometry being considered is relatively complex and contains significant details. In the unstructured approach, the integral form of the governing equations is discretized and either a finite-volume or finite-element scheme is used. The information regarding the grid is directly incorporated into the discretization process. While unstructured grids are generally more successful for complex geometries the quality of these grids deteriorates with shape complexity. In addition, there is a large computational overhead owing to the large number of operations per node [174–176].

### 4.5.1 Mesh Topology

For unstructured mesh, Fluent 17.1 uses a solver which is unstructured as well, by using data structures to allocate an arrangement to the element, faces, and mesh of nodes in a grid to achieve the contact between neighbouring cells and elements. This leads to using the best mesh topology for complex geometries with ease, this gives the flexibility to the solver not force an overall topology on the grid without the need of i, j and k parameters for indexing to trace adjacent cells). The Fluent 17.1 has several cell types for mesh topology.

The type of element specifies the number of mesh nodes and the node pattern associated with element shapes. The current study uses a higher order element type for the generation of the mess as seen in Figure 4-7, to estimated more accurately the boundaries with high curvatures, this included the following:

- For the membrane body a standard **rectangular** element was used because of the small thickness of the layer.
- The **triangular** element shape is used as a higher order type for the surface mesh.
- The **tetrahedral** element which considered a higher order as well and was used for the 3D mesh.

Triangular Element Tetrahedral Element

**Figure 4-7: (a) Triangular type element, (b) Tetrahedral type element, the dots represent the hanging nodes** [173]**.**

### 4.5.2 Three Dimensional Mesh Generation

The mesh was generated using ANSYS Workbench 17.1. This included the following:

- **Surface mesh generation**, and
- **Volume mesh generation.**

#### 4.5.2.1 Surface Mesh Generation

A mesh on the surfaces was built for the heat exchanger core geometry including the membrane, fresh air, and exhaust air by the following steps:

1. Every boundary that consist of a specified dimension is considered an edge and given a mesh with a specific interval size for each one of them.
2. The meshed edges then organised by specifying as arranging pattern for each one of them.
3. The triangular elements then generated as soon as all the edges are meshed by linking between them to form the unstructured surface mesh.

#### 4.5.2.2 Volume Mesh Generation

After all the surfaces (each individual area) had been meshed, a volume mesh was generated for each surface having a specified closed loop area. The construction of a good mesh needs fine elements in areas near the membrane surface, suitable for characterizing flow wake and separation. However, using the same element size throughout the whole CFD domain can cause a huge number of elements. Thus, a fine mesh is used in the area close to the membrane surface and coarser mesh as the distance from the surface increased. The mesh could be manipulated and controlled manually in ANSYS Workbench 17.1 to ensure smooth mesh transition, while maintaining a sufficiently precise mesh for a 3D geometry domain seeking to minimize the computational process expenses. Thus was accomplished by:

- Multi zone mesh (Membrane, fresh steam and exhaust stream bodies).
- Using a size function (finer mesh in the fresh and exhaust stream bodies near the membrane layer).

### 4.5.3 Mesh Quality and Dependency

In order to obtain accurate simulations results successfully, the evaluation of the quality and the dependency of the mesh is essential before making the solution run. Several guidelines where established by [159,177] and were governed by QRST (Quality, Resolution, Smoothness, and Total cell count), these guidelines stated that in order to achieve a good mesh, the mesh elements should be sufficient and its convenient distributed is very important as well as not exceeding the computer limits for simulation.

#### 4.5.3.1 Mesh Quality

The examination of the quality of the mesh is crucial. Several quality factors need to be investigated, the first one is the **face alignment** which has the ability to evaluate the elements' skewness because the cells with high skewness suffer from severe distortion, and these distorted cells must not be present in critical regions. Apart from the effect on the solution accuracy, the highly skewed cells can force the solution to diverge. The second factor for the mesh quality is the **aspect ratio**. All the week and slim elements should be evaded. The third mesh quality factor is the **volume quality** of elements. The very fine mesh with extremely small elements might cause the solution to struggle with convergence unless a smooth transition from fine to coarse mesh is considered [172].

#### 4.5.3.2 Mesh Dependency and Resolution

The choice of the mesh resolution usually depends on the user. However, the mesh needs to be sufficiently fine to properly and accurately simulate the flow behaviour, and the final solution results should not depend on the mesh. The mesh independent solution represents a solution which its results will not change as the mesh becomes finer. The evaluation if the solution dependence on the mess, several finer meshes need to be created and tested to a point there is no effect of the finer meshes on the results. The mesh evaluation study showed that a mesh size of around 8-10 million cells for the current geometries can provided sufficient accuracy and resolution to be adopted as the standard for all three cases (pitch lengths 5, 10 and 25 mm).

A mesh was constructed for each 3D body, and several parameters were considered when determining a good and reliable mesh. These parameters were the element size, number of mesh layers and the growth rate which determined the fine mesh near the source face (in this case the face is the membrane surface) and how the element size increased with distance from the membrane.

A mesh study was conducted to examine mesh independency and its effect on the simulation and on the solution as a final output, and for all the three test cases (in addition to the validation model). The study was based on the number of the elements in each proposed mesh and monitored the changes in the physical properties of the exchanger outlet; e.g. mass flow rate, temperature and humidity ratio. A set of cases were conducted for the 25 mm pitch length at ($T_{amb}$ = 6 $^{o}$C and $V_a$ = 2m/s) in a range of (1.4 mm – 0.8 mm) element size and (2.32 – 9.88 million) number of elements. The results show that for 2.32 million and 4.43 million elements cases, the solution tend to diverge and give extreme values for the properties. However, the solution began to stay the same for 7.7 million elements case and above and becomes completely converged as shown in figures from Figure 4-8 to Figure 4-10. Table 4-1 below shows the total considered number of elements and the element size in each case in this study. While Table 4-2 shows the mesh study for the 25 mm case.

**Table 4-1: Mesh details for the all three pitch lengths**

| Pitch length | Number of elements | Element size (mm) |
|---|---|---|
| 25 mm | 7,701,046 | 0.9 |
| 10 mm | 8,248,294 | 0.7 |
| 5 mm | 8,677,143 | 0.7 |

**Table 4-2: Mesh study for the 25 mm pitch length**

| Pitch length | Number of elements | Element size (mm) |
|---|---|---|
| **25 mm**<br><br>At ($T_{amb}$ = 6 °C)<br>($V_a$ = 2 m/s) | 2,320,049 | 1.4 |
| | 4,431,078 | 1.2 |
| | 6,084,022 | 1.0 |
| | 7,701,046 | 0.9 |
| | 8,951,416 | 0.85 |
| | 9,885,391 | 0.8 |

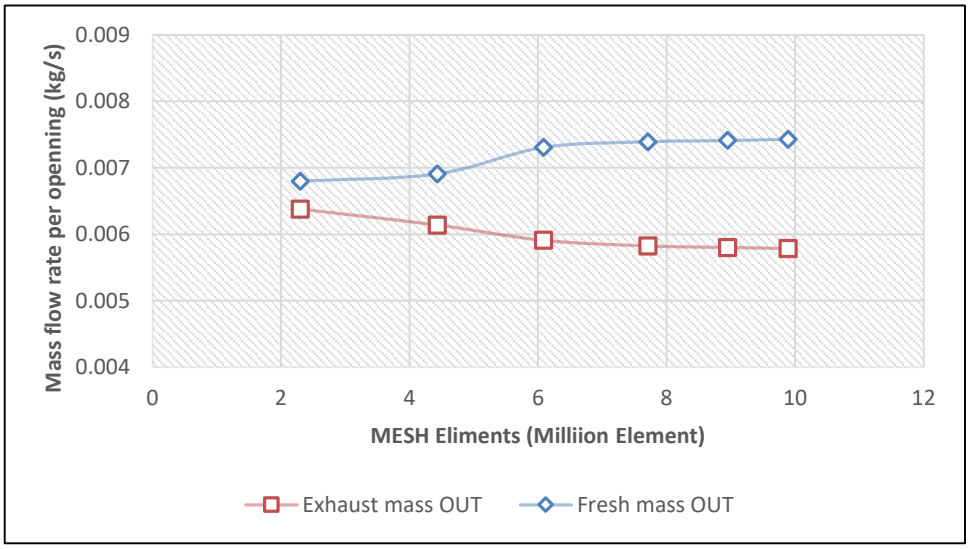


**Figure 4-8: Mesh resolution test for 25 mm pitch length (mass flow rate)**

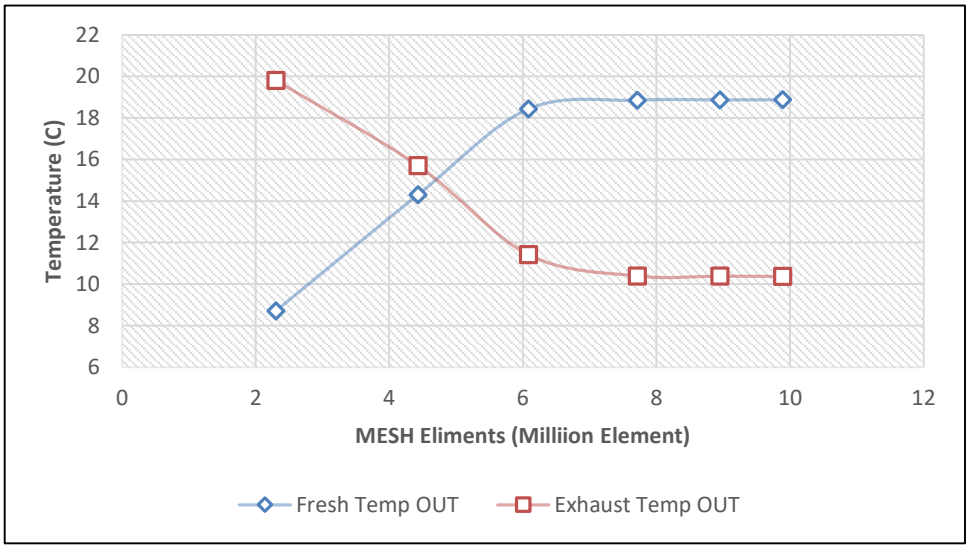


**Figure 4-9: Mesh resolution test for 25 mm pitch length (Temperature)**

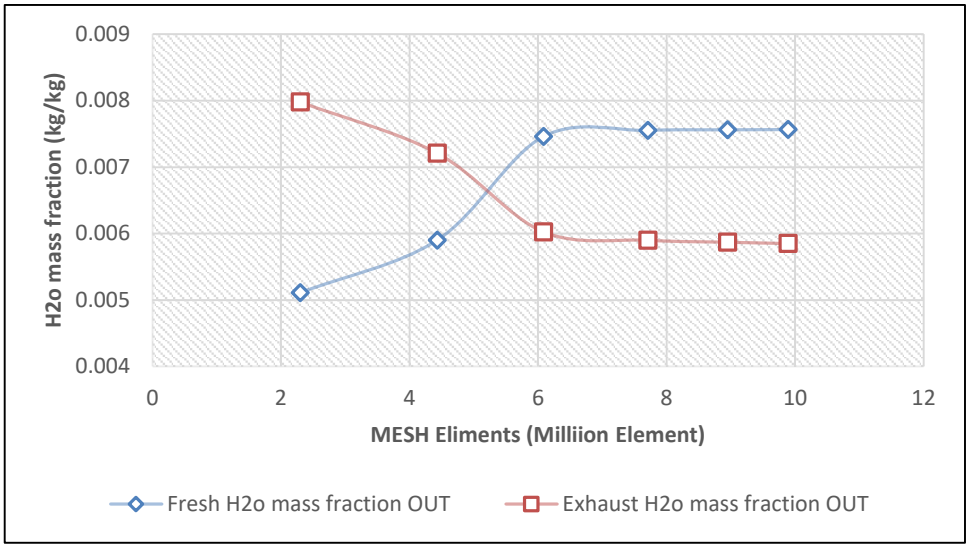


**Figure 4-10: Mesh resolution test for 25 mm pitch length (H2O mass transfer fraction)**

#### 4.5.3.3 Total Cell Count

Finally, it is vital to have a sufficient number of cells for good resolution, but memory requirements increase as the numbers of cells increase. Current computer resources do not allow more than 20 million cells on a single processor on Windows platforms. Here the present cases used an average of 8 million cells as shown in Table 4-1 above. Figures from 4-11 to 4-16 show the meshes for the three pitch lengths and the zoomed-in section taken from the corner of the modelled geometry (in order to clarify the mesh near the membrane layer) of the meshes for the different pitch lengths. As can be seen also in the zoomed-in pictures below, the distribution of the mesh of the 25 mm model near the membrane layer is better than the 10 mm and 5 mm. This was because to reach the same mesh resolution of the 25 mm model, the number of element exceeded 20 million for both 5 mm and 10 mm models. Accordingly, after mesh studies for both the 5 mm and the 10 mm models, the 8 million mash was enough and any more increase in the mess will not affect the final outcome of the simulations.

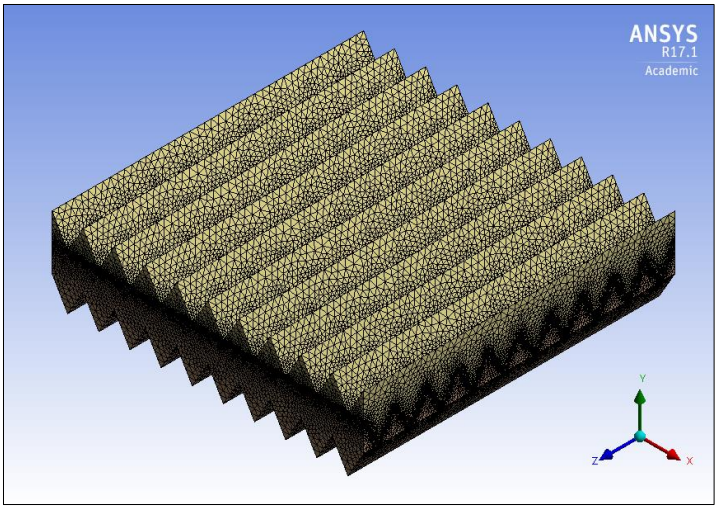


**Figure 4-11: Mesh for 25 mm pitch length model**

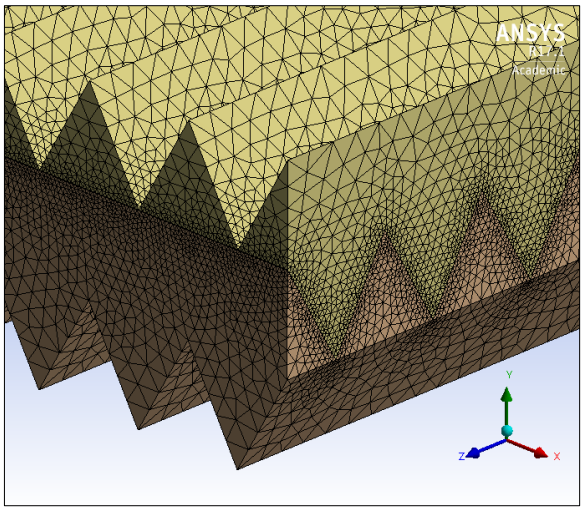


**Figure 4-12: Zoomed-in picture of mesh for 25 mm pitch length model**

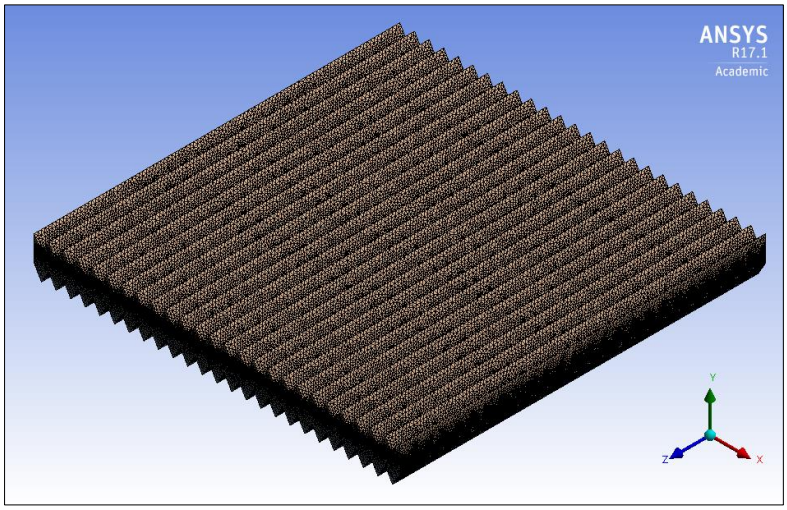


**Figure 4-13: Mesh for (10 mm) pitch length model**

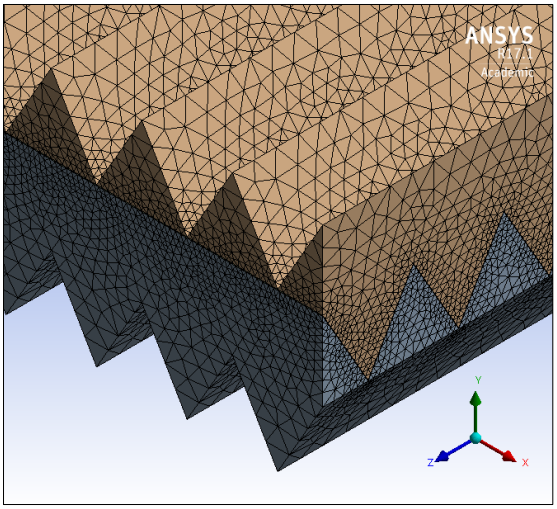


**Figure 4-14: Zoomed-in picture of mesh for (10 mm) pitch length model**

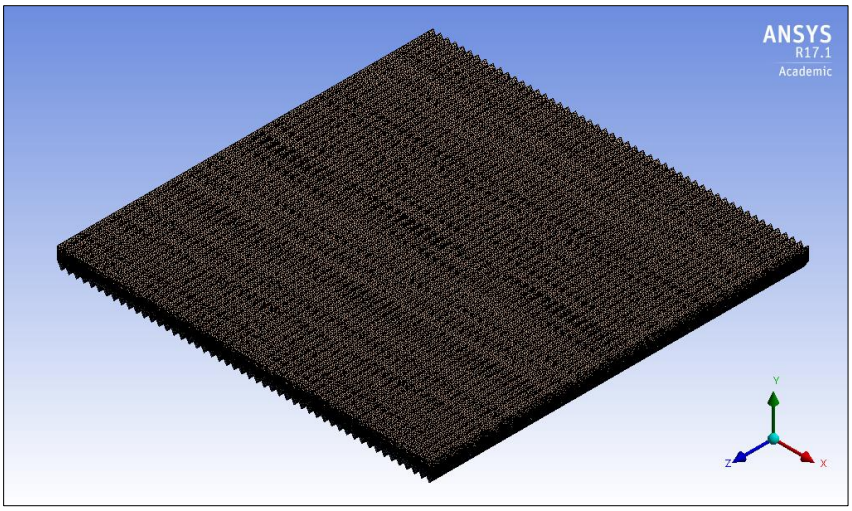


**Figure 4-15: Mesh for (5 mm) pitch length model**

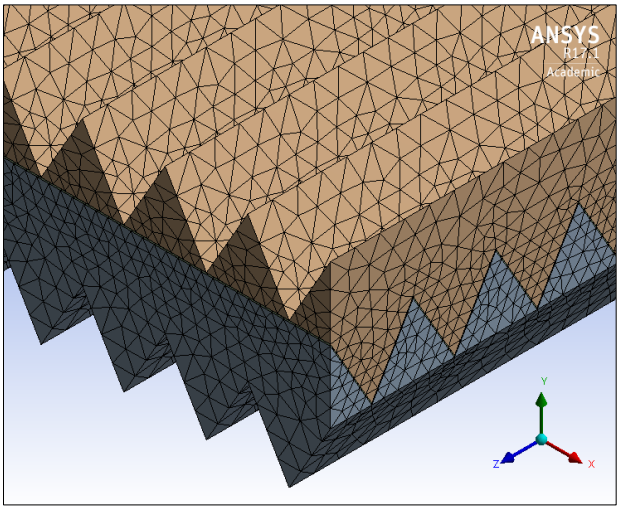


**Figure 4-16: Zoomed-in picture of mesh for (5 mm) pitch length model**

### 4.5.4 Model mesh characteristics

In order to solve the mesh geometry with Fluent 17.1, several setup steps are needed. The component parts and faces should be named as well as the geometric parameters, such as the inlets, outlets and interference surfaces.

The geometry is divided into distinct areas, such as air inlets and outlets as well as walls and boundaries. The fresh air inlet, fresh air outlet, exhaust air inlet and exhaust air outlet were identified by selecting the appropriate triangular faces in the geometry and considering them as a single entity. The side walls of the membrane body are considered as a single entity. Table 4-3 shows the actual geometric features and their abbreviated names for ANSYS Workbench 17.1. Figures from Figure 4-17 to Figure 4-20 illustrate every parameter in the geometry.

**Table 4-3: The geometric parameters**

| Parameter | Description |
|---|---|
| FRESH-IN | Inlet openings for the fresh air for ventilation. |
| FRESH-OUT | Outlet openings for the fresh air. |
| Fresh-seal | The two imaginary walls, one either side of the fresh air stream. |
| Fresh-UPPER-wall | The wall above the fresh air stream. |
| EX-IN | Inlet openings for the exhaust return air. |
| EX-OUT | Outlet openings for the exhaust air. |
| EX-seal | The two imaginary walls on both sides of the exhaust air stream. |
| EX-Lower-wall | The wall under the exhaust air stream. |
| Membrane wall | The side wall of the membrane layer. |
| Interference-1 | The lower wall of the fresh stream. |
| Interference-2 | The upper wall of the membrane layer. |
| Interference-3 | The lower wall of the membrane layer. |
| Interference-4 | The upper layer of the exhaust stream. |

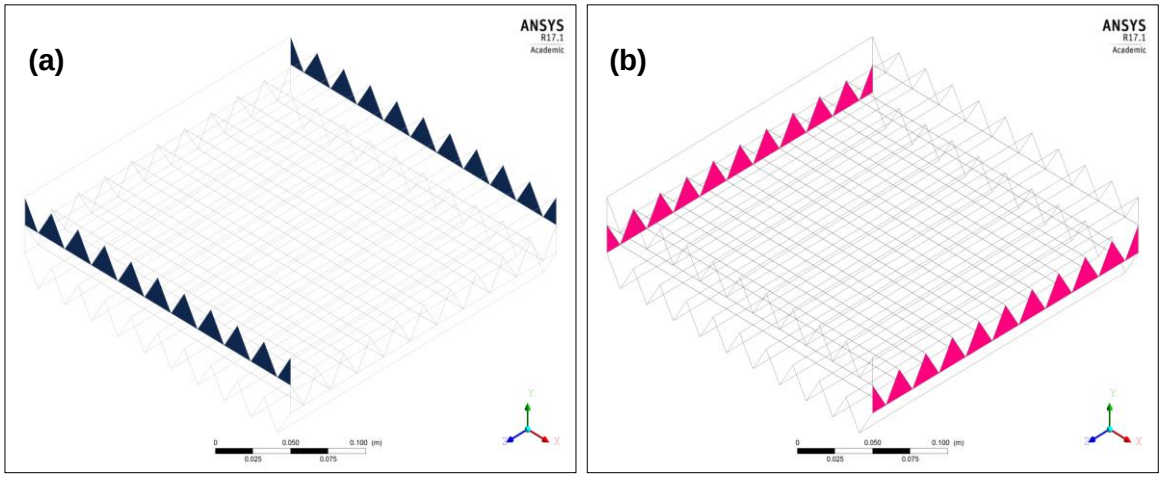


**Figure 4-17: Air inlets and outlets (a) Fresh (b) Exhaust**

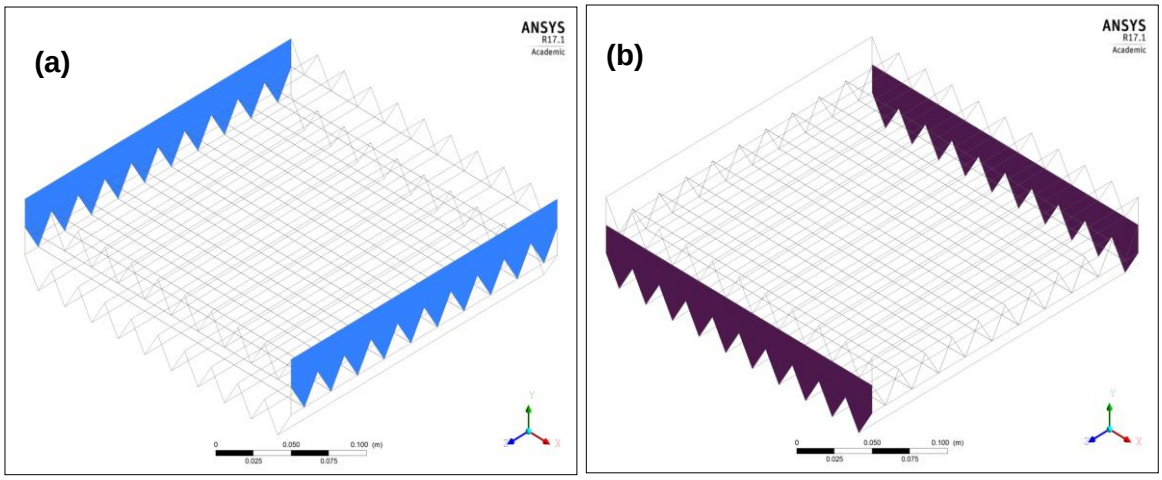


**Figure 4-18: Sealing walls (a) Fresh air (b) Exhaust air**

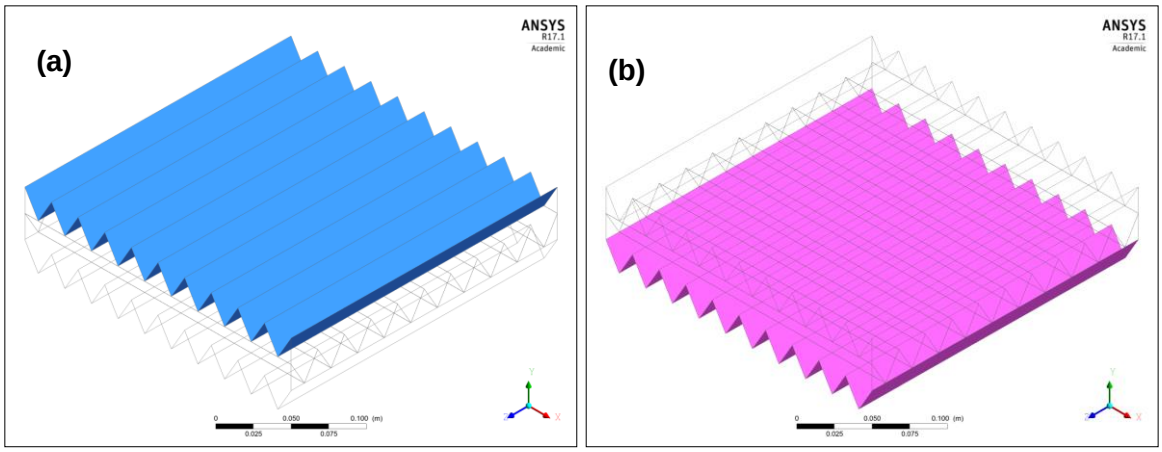


**Figure 4-19: (a) Upper top wall, (b) Lower bottom wall**

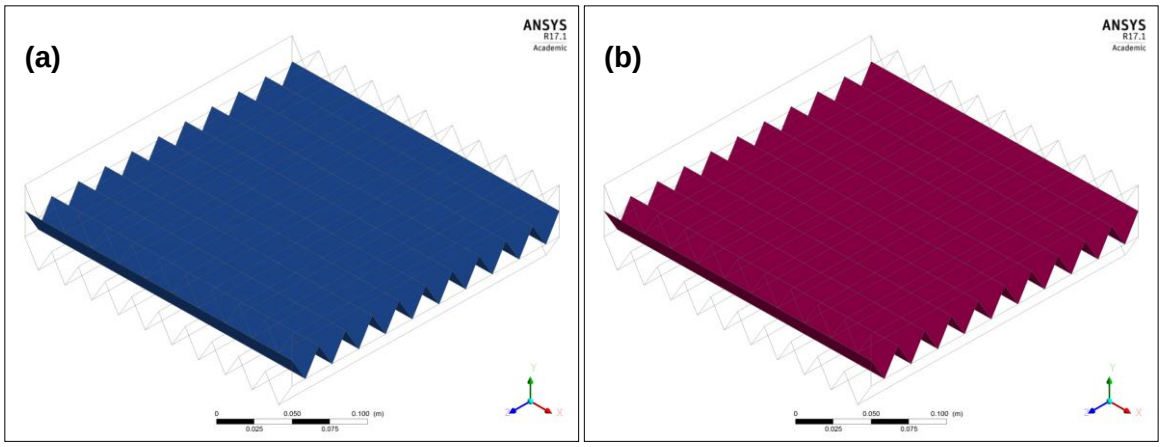


**Figure 4-20: Interference faces (a) fresh side (b) Exhaust side**

In Figure 4-20, the membrane layer is very thin (0.1 mm) and the membrane faces represent interference surfaces 2 and 3 respectively as explained in Table 4-3 above. In order to achieve the most precise and smoothest mesh, an interference technique was used to associate the meshes with each of the three surfaces. This process was conducted by joining the common faces between the fresh and exhaust air streams with the membrane body by creating an interference between the walls. This technique was processed using both Workbench17.1 and Fluent 17.1, with interference walls 1 and 2 combined into one mesh interference which represented the connection between the fresh air stream and the membrane body, similarly interference walls 3 and 4 were combined into one mesh interference which represents the connection between the exhaust air stream and the membrane body.

## 4.6 Simulation Cases Setup in ANSYS Fluent 17.1

The first step in any CFD problem is how set up properly before proceeding to the solution, and Fluent 17.1 is no different. To setup the simulation solution, several things need to be taken into consideration and they are discussed below. Moreover, it is very important to accurately specify the parts of the model construction, material properties and the properties of the fluid medium (moist air in this case).

### 4.6.1 General Setup

The general set up of the case is to identify some general assumptions that can be made by the user such as the solver type, velocity formulation as well as either the flow is in steady state or not. The general setup selections for the current study are shown below

- **Pressure-Based** solver.
- **Absolute** velocity formulation.
- **Steady** state for time considerations.

### 4.6.2 Model Setup

To analyse the heat transfer within the heat exchanger, the energy equation was activated with the flow inside the exchanger assumed viscous. The Transition-SST model was also activated; as mention earlier this consisted of four equations. Since determining the mass transfer of the humidity is fundamental, the species transport equation was also activated. In addition to the above, the momentum equation was also activated.

### 4.6.3 Materials Setup:

It's very important to specify the material properties of the component parts of the model as well as the properties of the medium fluid. Table 4-4 shows the model's parts with its types and properties, and Table 4-5 shows the properties of the air in that flows through the heat exchanger.

**Table 4-4: Properties of membrane material**

| Part | Material Type | Density (ρ) | Specific Heat ($C_p$) | Thermal Conductivity ($k$) |
|---|---|---|---|---|
| | | (kg/m$^3$) | (J/kg.K) | (W/m.K) |
| Membrane body | Polyethersulfone | 1370 | 1100 | 0.13 |

**Table 4-5: Properties of working fluid (Air)**

| Parameter | Unit | Value | | |
|---|---|---|---|---|
| Density ($\rho$) | ($kg/m^3$) | Piecewise-Linear Profile | | |
| | | Point | $T_a$ ($^oC$) | $\rho$ |
| | | 1 | 0 | 1.293 |
| | | 2 | 2 | 1.284 |
| | | 3 | 8 | 1.256 |
| | | 4 | 12 | 1.239 |
| | | 5 | 16 | 1.222 |
| | | 6 | 20 | 1.205 |
| | | 7 | 24 | 1.188 |
| Specific Heat ($C_p$) | (J/kg.K) | 1006.43 | | |
| Thermal Conductivity ($\lambda$) | (W/m.K) | 0.0242 | | |
| Viscosity ($\mu$) | kg/m.s | $17.894\times10^{-6}$ | | |
| Thermal Expansion Coefficient ($\beta$) | 1/K | $3.47\times10^{-3}$ | | |

### 4.6.4 Cell Zone Conditions and Mesh Interference

As mentioned earlier in this chapter, the three model heat exchangers were built with pitch lengths 25 mm, 10 mm and 5 mm. The Polyethersulfone membrane as the main corrugated sheets, was treated as a porous medium with specified porosity and diffusivity. The air streams, fresh air and exhaust air were considered as normal air. For the mesh interference, the meshes of these bodies were connected and associated which each other by connecting to the walls separating the air flows.

### 4.6.5 Boundary Conditions

In this section, the focus is on the boundary condition at each of the model components. The boundary conditions for the exchanger core are important in obtaining an accurate solution and, as is the case here, are normally divided into momentum, thermal and species boundary conditions. Boundary conditions are specified for each zone of the computational domain. However, the internal domains (zones) that share common areas (faces), do not require any separate boundary condition. The membrane sheet body considered as pours medium zone and was assigned as a fluid.

#### 4.6.5.1 Velocity inlet boundary conditions

Velocity inlet boundary conditions are used to define the flow velocity, along with all relevant scalar properties of the flow at the inlet. The current heat exchanger core has fresh air and exhaust air inlets, each inlet consisting of a number of openings depending on the specific case, see Table 3-3 in Chapter Three, which also provides the calculated average duct velocity in m/s for each openings for a typical ventilation rate of 0.0278 $m^3$/s (100 $m^3$/h).

#### 4.6.5.2 Pressure Outlet Boundary Conditions

Pressure at the outlet for exhaust air is assumed to be atmospheric for undisturbed flow. This case has two pressure outlets which are the fresh and exhaust air outlets. All other dependent variables are extrapolated from the nearest grid-point at the outlet assuming zero gradient normal to the boundary according to [159,178,179].

#### 4.6.5.3 Wall Boundary Conditions

The no slip boundary condition is specified for the membrane core which is set as a wall. These conditions are used to bound the fluid and solid regions. For all the outer wall, a no slip wall boundary condition is prescribed.

#### 4.6.5.4 Interior Boundary Conditions

The interior boundary conditions are assigned to the fresh and exhaust air streams and the membrane is located midway between them. Since the main purpose of constructing a three zones model is to allow different meshing strategies at different parts of the domains such that the boundary conditions do not affect or obstruct the flow in any manner. Hence, for the current case the walls that divide the zones are assigned interior boundary conditions.

#### 4.6.5.5 Species Boundary Conditions

These boundary conditions are related to the transfer of mass through the porous membrane, and as the working fluid is air, the two main parameters, mass fraction of the oxygen and the humidity ratio must be specified. The oxygen mass fraction in the fresh and exhaust inlets assumed to be constant with a value of (0.23 kg/kg), while the humidity ratio ($H_2O$ mass fraction) for the fresh inlet are where taken from the designed UK winter weather conditions as explained in Table 3-4 in Chapter Three / section 3.5. Accordingly, the $H_2O$ mass fraction boundary conditions in fresh inlet air are **(0.00371, 0.00427, 0.00492, 0.00565 and 0.00647 kg/kg)** for the (2, 4, 6, 8 and 10 $^oC$) ambient temperature boundary conditions respectively. The value for the humidity ratio in the exhaust air inlet considered constant, since the indoor house is considered to be conditioned at standard comfort level of 22 $^oC$ temperature and 50% relative humidity. The value for $H_2O$ mass fraction at the exhaust air inlet is **(0.00822 kg/kg)**.

Table 4-6 and Table 4-7 shows thermal and the momentum boundary conditions respectively for all parameters of the model, where the seal refers to the side walls in both fresh and exhaust streams and considered as insulators with zero heat flux boundary condition.

**Table 4-6: Thermal boundary conditions**

<table>
<tr><th>Parameter</th><th>Type</th><th colspan="2">Thermal Conditions</th></tr>
<tr><td>FRESH-IN</td><td rowspan="2">Velocity Inlet</td><td colspan="2" rowspan="2">- Temperature 2, 4, 6, 8 and 10 $^oC$</td></tr>
<tr><td>EX-IN</td></tr>
<tr><td>FRESH-OUT</td><td rowspan="2">Pressure outlet</td><td colspan="2" rowspan="2">- Back total temperature specified automatically</td></tr>
<tr><td>EX-OUT</td></tr>
<tr><td>Fresh-seal</td><td rowspan="6">Wall</td><td rowspan="5">1 mm</td><td rowspan="5">- Heat Flux = 0 (W/m$^2$).<br>- Heat Generation Rate = 0 (W/m$^3$).</td></tr>
<tr><td>Fresh-UPPER-wall</td></tr>
<tr><td>EX-seal</td></tr>
<tr><td>EX-Lower-wall</td></tr>
<tr><td>Membrane wall</td><td>0.1 mm</td></tr>
</table>

**Table 4-7: Momentum boundary condition summary**

| Parameter | Type | Momentum Conditions |
|---|---|---|
| FRESH-IN | Velocity Inlet | - Velocity Magnitude = (**0.5, 1, 1.5** and **2 m/s**), [constant]. |
| EX-IN | | |
| FRESH-OUT | Pressure outlet | - Gauge Pressure = (**0 pascal**), [constant]<br>- Backflow Direction Specification Method : **(Normal to Boundary).** |
| EX-OUT | | |
| Fresh-seal | Wall | - Wall motion: Stationary<br>- Sheer condition: No slipping |
| Fresh-UPPER-wall | | |
| EX-seal | | |
| EX-Lower-wall | | |
| Membrane wall | | |
| Interference-1 | Wall | Interference |
| Interference-2 | | |
| Interference-3 | | |
| Interference-4 | | |

## 4.7 Solution

Fluent 17.1 solves the governing equations for the continuity, momentum, energy and the Transition-SST. A **control-volume based technique** is used on the following steps [159,162]:

- A mesh is created on the computational domain, see Section 04.5.
- Sets of integrated equation is generated from the main governing equations for every control volume, in order to obtain the results for velocity, pressure and the other conserved scalars.
- The equations then discretized and linearized and solved using an iterative method.

The segregated solver [167] is the solution algorithm used by Fluent 17.1 and is adopted in the present work. For compressible high velocity fluid flows, the “coupled solver” might be used as well in Fluent 17.1 but as temperatures are not high and the assumption has been made of incompressibility this method will not be used. The governing equations are solved successively by the segregated solver method. Because of the non-linearity and the coupling of the governing equations, plenty of iterations are needed in order to achieve a converged solution. The SIMPLE algorithm [162] is used in the current study and every iteration goes through the steps outlined as follow:

1. The solution firstly initialized to obtain an initial iteration for the fluid flow properties, then the values of the next iteration updated depending on the first one and so on.
2. Narvier-Stokes equations are solved one by one depending on the current pressure and mass flow rate to update the velocity values for the next iteration
3. The velocities may not satisfy the continuity equation locally; therefore, a pressure correction equation is derived from the continuity equation and momentum equations. This equation is then solved to obtain the necessary corrections to the pressure and velocity fields and the face mass fluxes so that the continuity condition is satisfied.
4. Using the previously solved variables, the turbulence equation is solved.
5. Following these steps, a convergence check is done. These steps are continued until the convergence criteria are met.

Figure 4-21 illustrates a flow chart for the process above for the SIMPLE algorithm, showing how the iterations in the solution works in Fluent 17.1 based on the CFD fundamentals.

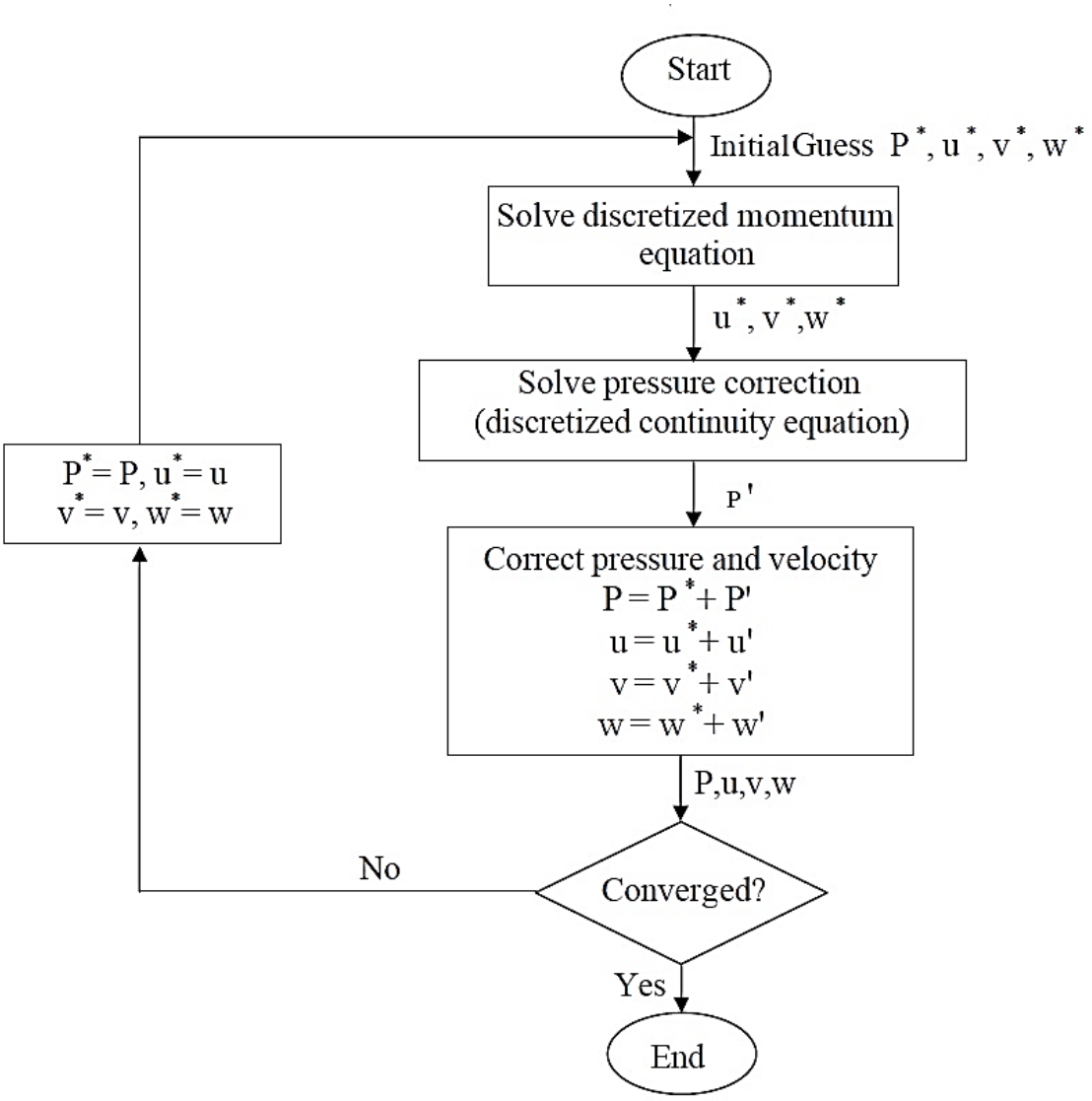


**Figure 4-21: SIMPLE algorithm flow chart.**

### 4.7.1 Initial Conditions

The first estimation of the properties is crucial due to the ignoramus of the flow field. Therefore, the initialization is essential for a converged solution. The convergence time is also dependent on the properly considered initial conditions and in some cases the poor initial conditions leads the solution to diverge. In the current, all variables properties are initialized from the fresh air inlet boundary conditions values as explained in section 4.6.5.

### 4.7.2 Solution Parameters

Precision solver type, number of iterations, convergence criteria, under-relaxation factors, multi-grid parameters, linearization, and discretization scheme are defined. This is the last step before obtaining the solution.

### 4.7.3 Solution Methods

The Pressure-Velocity Coupling is solved using the **SIMPLE** algorithm with the **Second Order Upwind** scheme for momentum and energy equations, and **Least Squares Cell Based** gradient. The pressure equation was the solver **Second Order** scheme, while Transition-SST model equations (Turbulent kinetic energy, specific dissipation rate, intermittency and momentum thickness Re) were solved by **First Order Upwind**. The solution after these selection tends to converge faster.

### 4.7.4 Precision Solver Type

The solvers in the Fluent 17.1 divided into two precision parts, single and double. The infinite precision computers have the ability to decrease the residuals to zero for the convergence, the actual computers however, declines the residuals to a very small value called (round-off) until stop declining to a value called (level-out). The residuals in the single precision solver could decline to 6 magnitude orders before reaching the round-off, while the residuals in the double precision solver could decline to 12 magnitude orders. The CFD solution in the current study is based on the single precision solver in order to reduce the time of the simulations without the need for complicated solution.

### 4.7.5 Number of Iterations

The Fluent 17.1 solver stops at user-defined maximum number of iteration. In the current study, 1000 iterations were setup before proceeding to run the solution. Fortunately, all the cases converged in lower number of iterations even with high number of elements in each model, which means that the cases are well constructed especially with the Transition-SST model which was used in this study.

### 4.7.6 Convergence Criteria

This refers to the residual values, below which, the solver terminates the program. Residuals are the error of the computational simulations. It is accepted that when the residuals for flow, including continuity, momentum, species and Transition-SST variables to fall below $1*10^{-4}$, the residuals could be neglected after that due to its minimal value [177,179]. In most cases, these residuals are insignificant. However, there might be some scalar values which could not converged even though their residuals declines below $1*10^{-4}$. Therefore, a convergence monitor in addition is presented in this case.

In the present model, the mass flow rate in the outlet considered one of the important outputs of the CFD model, since it can represent the moisture transfer from one stream to the other. When the mass flow rate value monitor converged, it was unnecessary to go further with those iterations, even if the residuals do not fall below $1*10^{-4}$ [172-175]. Figure 4-22, Figure 4-23 and Figure 4-24 ,were taken from ANSYS Fluent 17.1, show the convergence histories for continuity, momentum, and Transition-SST and species equations for the 25 mm, 10 mm and 5 mm pitch lengths, respectively. It can be seen for the 25 mm case that the residual for the momentum and equations fell below $1*10^{-4}$ after about 300 iterations while the residual for continuity dropped to about $1*10^{-4}$ after 520 iterations and stayed there even when number of iterations increased. The Transition-SST equations reached the value of $1*10^{-4}$ after about 270 iterations.

However, this does not mean the solution has not converged, as mentioned above, a mass flow rate can be used to track solution convergence and it has been shown, see Figure 4-25 that iterations were terminated after 518 iterations due to convergence in the continuity equation. However, the mass flow rate at the fresh outlet tends to oscillate heavily until 42 iterations and then decreased gradually until it stabilised at an average value at the iteration number 182 and then it became stable completely.

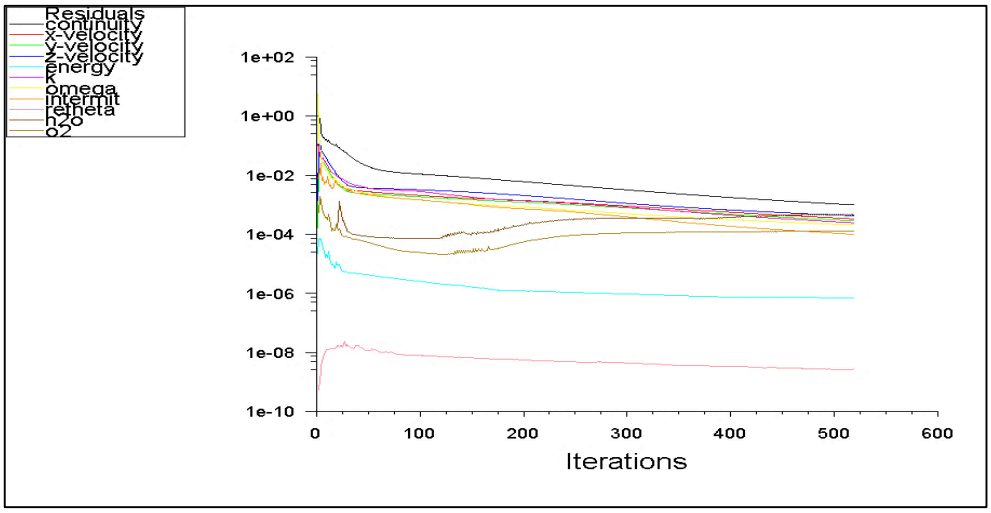


**Figure 4-22: Solution residuals for (25 mm) case**

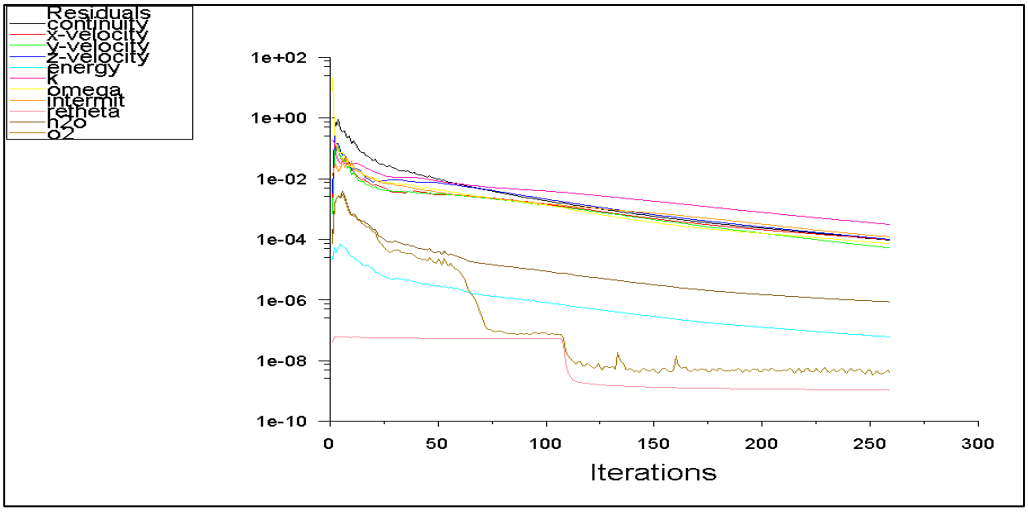


**Figure 4-23: Solution residuals for the (10 mm) cases**

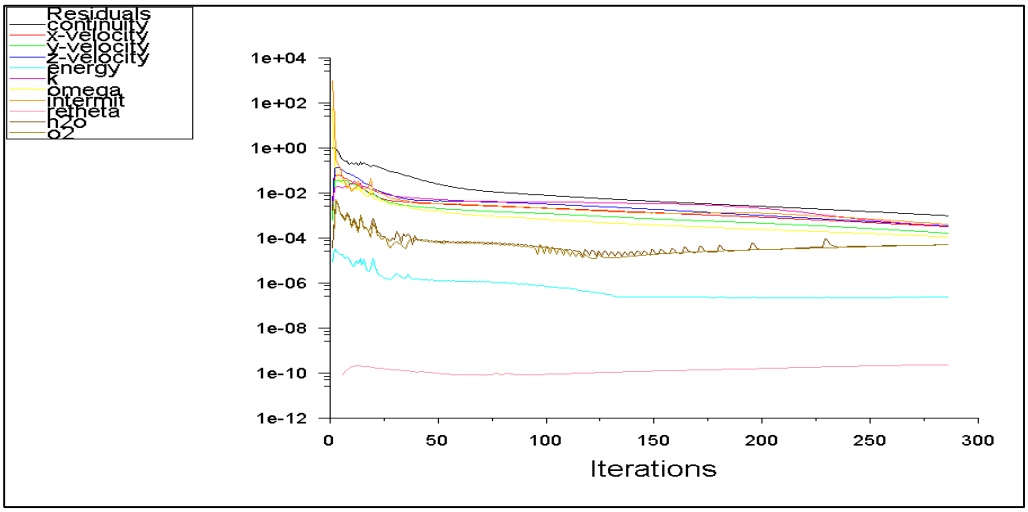


**Figure 4-24: Solution residuals for the (5 mm) cases**

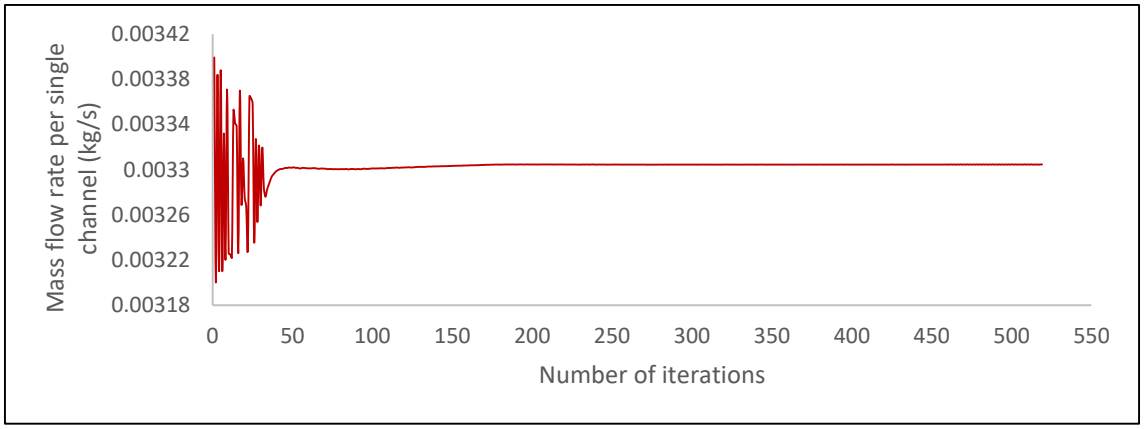


**Figure 4-25: Surface monitor for the mass flow rate (25 mm case) at ($T_{amb}$ = 6 °C and $V_a$ = 1 m/s)**

### 4.7.7 Under-Relaxation factors

Because of the nonlinearity of the equation set being solved by FLUENT17, it is necessary to control the change of the primary variable $\Phi$. This is typically achieved by under-relaxation, which reduces the change of $\Phi$ produced during iteration. In a simple form, the new value of the variable $\Phi$ within a cell depends upon the old value, ($\Phi_{old}$); the computed change in $\Phi$ and the under-relaxation factor α are given as follows [167]:

$$\Phi = (1 - r)\Phi_{old} + r\Delta\Phi \qquad 4.30$$

Because the computational domain may comprise regions of high curvature and separation, due to the structure of the exchanger, a high velocity gradient persists in this flow region. Consequently, the reduction the value of $\boldsymbol{r}$ is essential for getting the results to reach convergence. The used values of under-relaxation factor $\boldsymbol{r}$ in the current study to solve the needed governing equations are listed in Table 4-8.

**Table 4-8: Under relaxation factor (r ) for 25mm cases**

| Equation | *r* | Equation | α |
|---|---|---|---|
| Pressure | 0.1 | Intermittency | 0.8 |
| Density | 1 | Momentum Thickness, Re | 0.8 |
| Body force | 1 | Turbulent Viscosity | 1 |
| Momentum | 0.3 | $H_2O$ | 1 |
| Turbulent Kinetic Energy | 0.8 | $O_2$ | 1 |
| Specific Dissipation rate | 0.8 | Energy | 1 |

### 4.7.8 Multi-grid Parameters

Fluent 17.1 is using the multi-gridding to accelerate the convergence. It is also using a solver which called point implicit and based on Gauss-Seidel scheme. Gauss-Seidel scheme can quickly deal with the local computational errors with high frequency in the solution, the global errors with low-frequency however, decreased at a rate indirectly related to the mesh size. Consequently, for a huge mesh and complex geometry, the Fluent solver “stalls’’ and the residual declination rate becomes very low. What multi-gridding does is to coarsen the mesh successively, removing the global error, and then returning the mesh back to its original condition.

### 4.7.9 Linearization

The segregated solver in Fluent 17.1 is an implicit solver. A set linear equations are used to compute the unknown value of any variable. Every equation of them is used for single element in the computational domain. The new variable is linked to the known and unknown values from the adjacent elements. Accordingly, the new element exists in multiple equation in the solver. A solver of point implicit (Gauss-Seidel) linear equation is used in combination with an algebraic multi-grid (AMG) method to solve the consequential set of equations for the dependent variable in each element. Since there exists one equation per cell, this set of equations is called scalar system of equations. Segregated solver solves for a single variable field in a matrix form [167].

### 4.7.10 Discretization Scheme

In order to convert the set of the integral equations to algebraic forms, the finite volume method is used. A general variable (Φ) with steady state equation is used to presents the descritization [167]:

$$\oint \rho \Phi \bar{v}.\, d\bar{A} = \oint \Gamma_{\Phi} d\bar{A} + \int_{V} S_{\Phi}\, dV \qquad 4.31$$

where $\rho$ is the density, $\bar{v}$ is velocity vector, $\bar{A}$ is surface area vector, $\Gamma_{\Phi}$ is diffusion coefficient for $\Phi$, $\nabla\Phi$ is gradient of $\Phi$ per unit volume and $S_{\Phi}$ is source of $\Phi$ per unit volume. This equation is applied to each control volume in the computational domain. The discretization of Equation 4.31 on a given cell yields:

$$\sum_{f}^{Nfaces} \rho_f\, \bar{v}_f\, \Phi_f\, .\bar{A}_f = \sum_{f}^{Nfaces} \Gamma_{\Phi}\, (\nabla\Phi)_n .\bar{A}_f + S_{\Phi} V \qquad 4.32$$

where $Nfaces$ is number of faces enclosing the cell, $\Phi_f$ is value of $\Phi$ convected through face f, $\rho_f\, \bar{v}_f .\bar{A}_f$ is mass flux through the face, $\bar{A}_f$ is area of face, $(\nabla\Phi)_n$ is magnitude of $\nabla\Phi$ normal to face f and $V$ is cell volume.

The Fluent 17.1 could solves such general equations which are valid in the three-dimensional unstructured mesh cases. According to the finite volume method, the values of the general variable $\Phi$ are kept at the element centres. But, the values of $\Phi$ is at the element faces for the convective terms in the discretised equation. Accordingly, an interpolation scheme is required to determine the values at the faces depending on the values at the elements. This is achieved by using an upwind scheme. Fluent 17.1 offers several schemes for up-winding, first-order upwind, second-order upwind and QUICK. In current study, first-order and second order up-winding are used depending on the variable and its equation.

The diffusion terms are central-differenced and are always second-order accurate. A linearized form of discretised equation can be written as follows:

$$a_p \Phi = \sum_{nb} a_{nb} \Phi_{nb} + b \qquad 4.33$$

where the subscript $nb$ refers to neighbor cells, and $a_p$ and $a_{nb}$ are the linearized coefficients for $\Phi$ and $\Phi_{nb}$ respectively. This kind of equation is written for each cell in the computational grid which results in a set of algebraic equations. In case of considering the discretization of momentum equation, then the momentum equation in one direction may be written as:

$$a_p u = \sum_{nb} a_{nb} u_{nb} + S \qquad 4.34$$

by setting $\phi = u$ at the general Equation 4.33. In this equation, pressure and mass flow rate are unknown, and as a part of the solution, they must be calculated. Consequently, pressure interpolation schemes are used. The Fluent 17.1 has several schemes interpolated the pressure; standard scheme, linear, second order, body-force weighted and PRESTO. In the current study simulations, the **standard scheme** is used due to the low velocities that were considered for all of the cases with low Reynolds number and this scheme is suitable for most of such kind of problems. The standard scheme based on using the interpolation of the pressure values at the faces using the coefficient of the momentum equation [167].

The solution then after all the steps is completed, and the results were extracted by using ANSYS CFDPost 17.1 software. This software has the capability to present the contours and vectors of the heat and mass transfer in the exchanger core. The results as a values were extracted by the same software above using the function calculator feature. All the results values tables are listed in Appendix A.

## 4.8 Validation Model

In order to ensure the accuracy of the CFD work, validation with previous numerical or experimental work is needed. Consequently, a CFD model has been built for a cross-corrugated membrane-based total heat exchanger which was proposed by Zhang and Chen [118] in 2011. They conducted an experimental study on a hydrophilic Polyether-sulfone (PES) membrane-based heat exchanger core supported by a CFD simulation to obtain the effect of the flow arrangement in the triangular exchanger duct under uniform heat flux boundary conditions. The results demonstrated that the highest effectiveness could be achieved with the highest percentage of the cross flow arrangement. The membrane material was PES which, as mentioned earlier, is considered an important polymeric material usually used in applications such as separation of fields. PES-based membranes have very good oxidative, thermal and hydrolytic stability combined with excellent physical properties [180].

Zhang and Chen [118] built a test rig to examine the heat and mass transfer of a cross-corrugated heat exchanger core, see Figure 4-26 which shows a schematic diagram of his system. Figure (4-26) shows a picture of the experimental rig. Zhang and Chen designed the air-to-air exchanger core in the shape of a rectangular parallelepiped, having dimensions of 182 mm * 182 mm * 462 mm high, with the inlets and outlets being equilateral triangles with pitch length 18 mm.

Zhen-Xing Li et al. [181] completed Zhang's work in 2015, proposed a CFD model for the experimental work and validated the simulations results with Zhang and Chen's experimental results. In this study the validation will use both, Li's numerical results and Zhang's experimental results. Fortunately, the model presented this work gives results that were very close to those of Li and Zhang. This gives the proposed model more authenticity and strength.

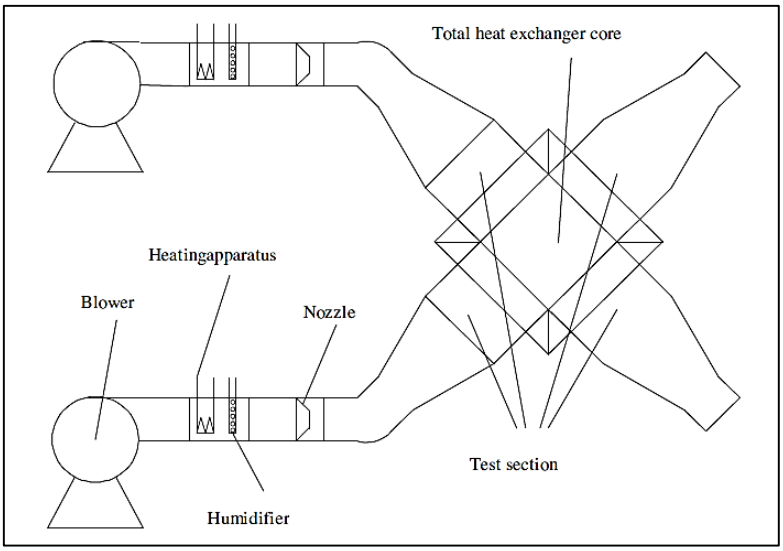


**Figure 4-26: Schematic of Zhang's and Li's experimental setup** [181]**.**


**Figure 4-27: Zhang's and Li's actual assembled total heat exchanger** [181]**.**

Table 4-9 shows the physical properties of Zhang's membrane total heat exchanger that was used by Zhen-Xing Li.

**Table 4-9: Li and Zhang's physical parameters** [181]

| Property | Symbol | Unit | Value |
|---|---|---|---|
| Model dimensions | x * y * z | $mm^3$ | 182*182*462 |
| Number of channels for each stream | - | - | 33 |
| Membrane thickness | δ | mm | 0.1 |
| Moisture diffusivity in air | $D_{va}$ | $m^2/s$ | $2.82 \times 10^5$ |
| Pore diameter of the membrane | $d_p$ | µm | 0.45 |
| Membrane porosity | - | - | 0.75 |
| Effective moisture diffusivity in membrane | $D_{vm}$ | $m^2/s$ | $3.77 \times 10^{-6}$ |
| Thermal conductivity of membrane | $\lambda_{mem}$ | W/(m.K) | 0.127 |

A set of different inlet air velocities were considered by Zhang (1.0, 1.5, 2.0, 2.5 and 3.0 m/s) and he included the effect of change of ambient temperature on the performance of his proposed exchanger core. He also tested it in the hot and humid weather in south China.

### 4.8.1 Proposed Validation Model

In order validate the proposed CFD model, the work of Zhang needed to be repeated using the same proposed simulation method and the exact same parameters and boundary conditions. The geometry of the system was modelled using CATIA 5, see Figure 4-28.

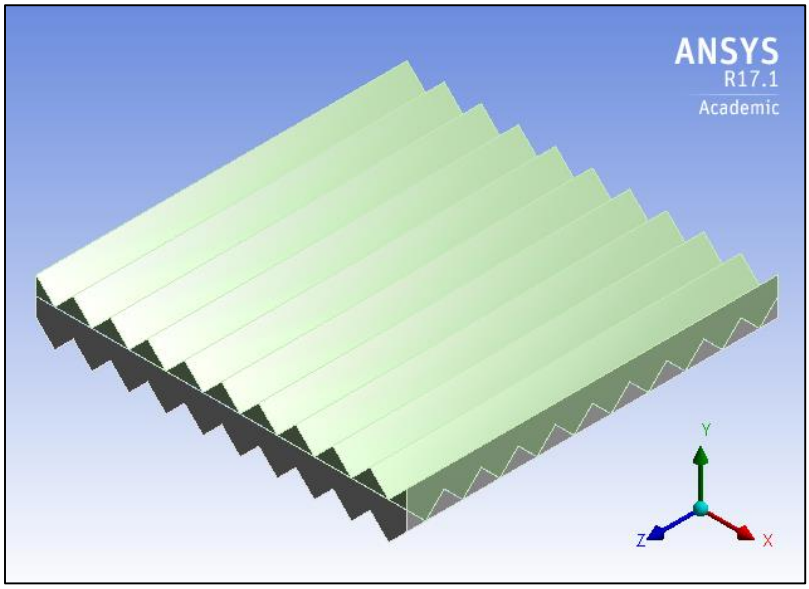


**Figure 4-28: Validation geometry (pitch length 18 mm and apex angle 60º)**

The exchanger with 18 mm pitch length was meshed using ANSYS Workbench 17.1 in the same way as discussed earlier this chapter. The meshed geometry is shown in the Figure 4-29 and Figure 4-30. A mesh study was also conducted for the proposed model, with the same range of element numbers as discussed above; from 4-12 million. After reaching 9 million elements, the results stabilised and did not change further, accordingly 9 million elements was chosen for validation in this study.

The solution was completed using ANSYS Fluent 17.1 and the results obtained from the proposed model were almost the same as those obtained by Zhen-Xing Li. Three main parameters were compared, temperature, humidity ratio and velocity vectors. Figure 4-31 and Figure 4-32 show the relation between the inlet air velocity for the fresh supply air to the house (fresh air out) and the exhaust out air stream.

The other parameter that was compared was the humidity ratio in the fresh and exhaust outlets, where the humidity ratio represented the mass fraction of the water vapour in the air. Figure 4-33 and Figure 4-34 shows the comparison between the proposed validation model and Zhang's simulated results and Zhen-Xing Li's experimental work.

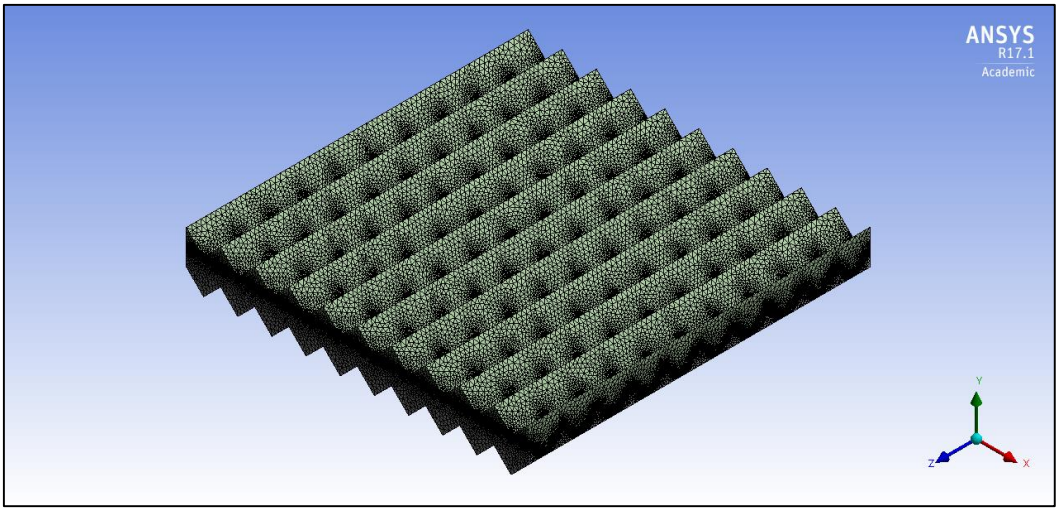


**Figure 4-29: Validation (18 mm) pitch length meshed model**

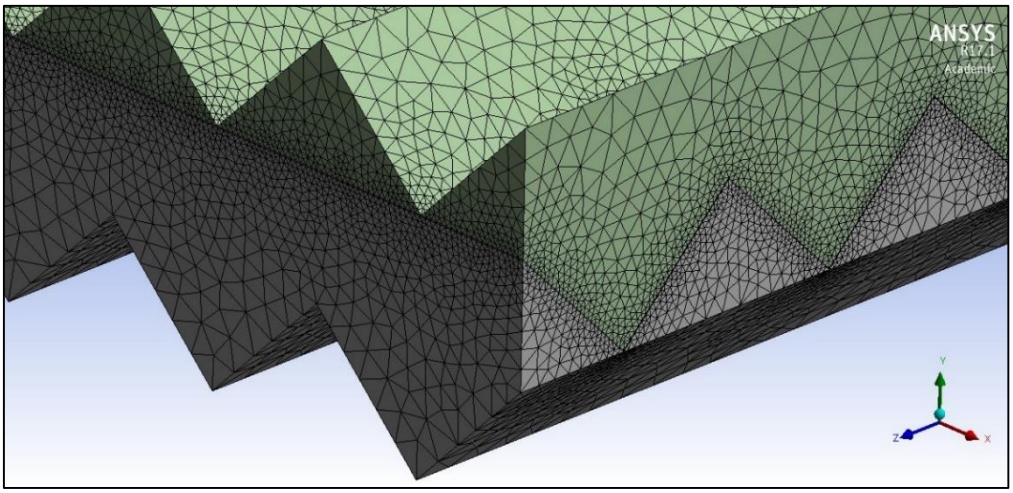


**Figure 4-30: zoomed-in section of the validation model in the corner of the model, pitch length (18 mm) and apex angle $60^0$.**

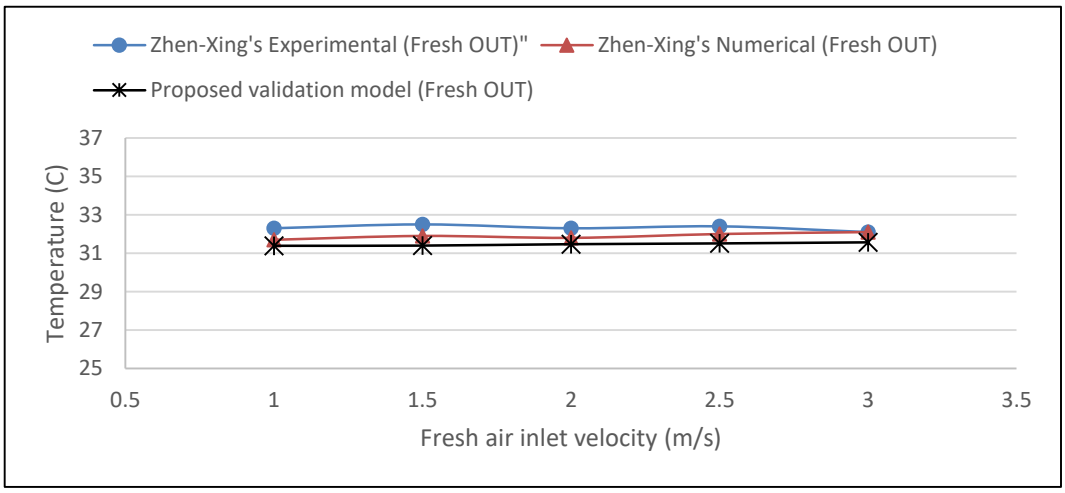


**Figure 4-31: Fresh inlet velocity with fresh out temperature**

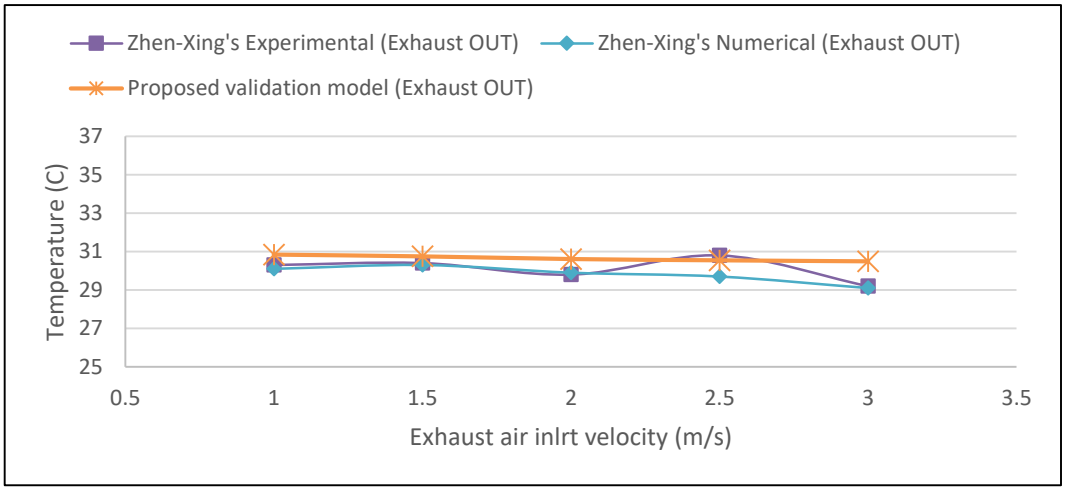


**Figure 4-32: Exhaust inlet velocity with exhaust outlet temperature**

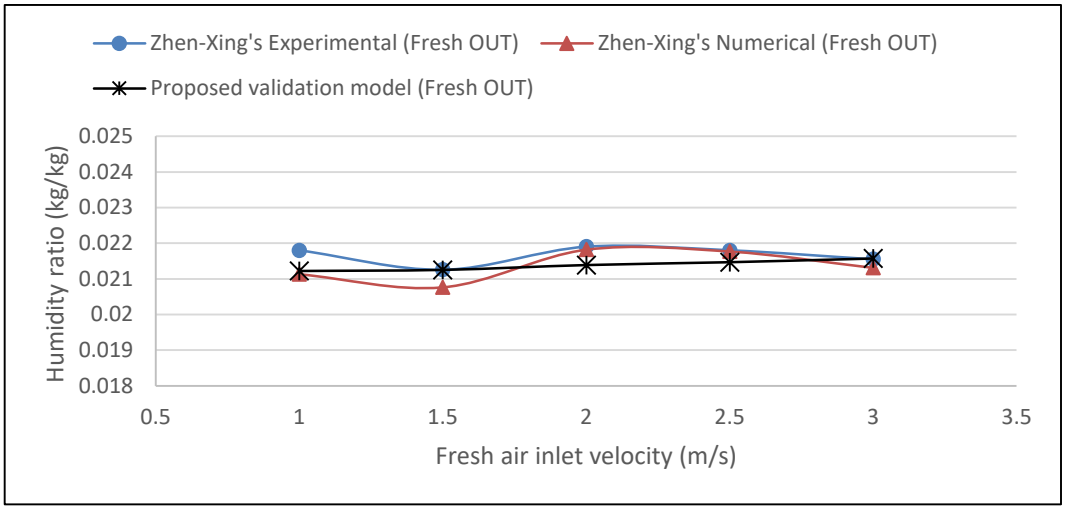


**Figure 4-33: Fresh inlet velocity with fresh outlet humidity ratio**

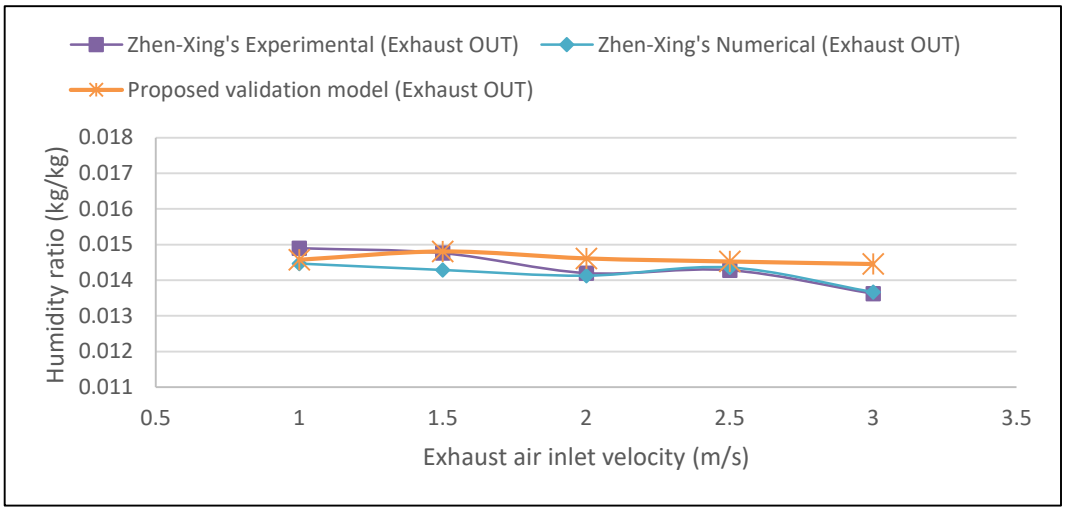


**Figure 4-34: Exhaust inlet velocity with exhaust humidity ratio**

In order to complete the validation properly, a comparison of the physical behaviour in terms of temperature and humidity contours was essential. The comparison shows the similarity between the proposed model and the Zhen-Xing Li's numerical model in the behaviour and giving the same average results at the fresh and exhaust outlets, even though they don't have exact same distribution in the contours due to the use of the Transition-SST flow model in Fluent 17.1. The results for the current validation were taken at the outlets and as an average values and they gave very similar values as that of Li, in addition, the membrane layer were considered as a whole 3D zone rather than single wall in Li's work and that what normally gave the deviation in the temperature and the humidity distribution contours on the surface of the membrane.

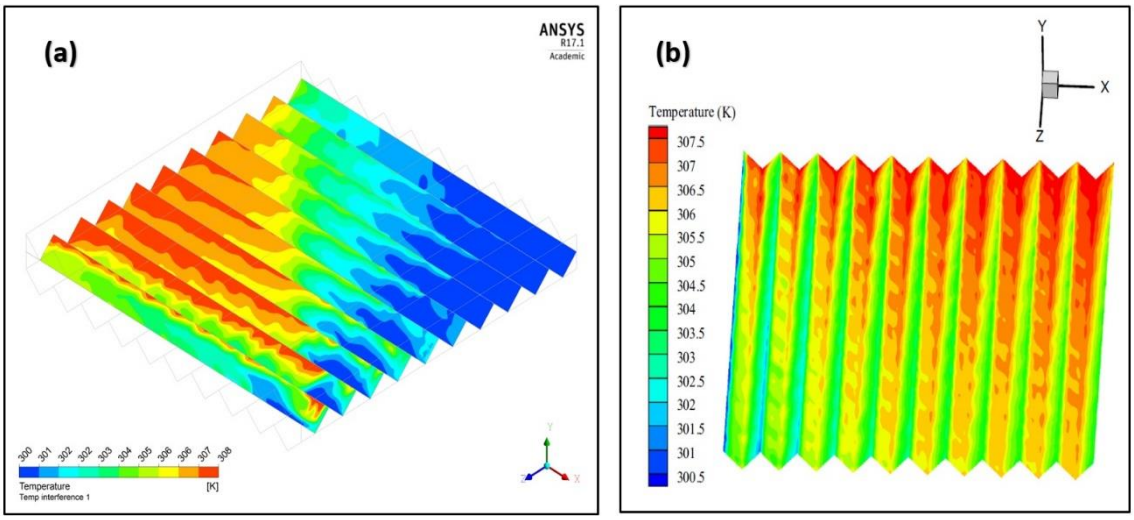


**Figure 4-35: (a) Temperature contour on the membrane wall at 1 m/s inlet velocity for the proposed validation model (18mm), (b) Zhen-Xing Li's numerical temperature contour at the membrane wall at 1 m/s inlet velocity** [181]**.**

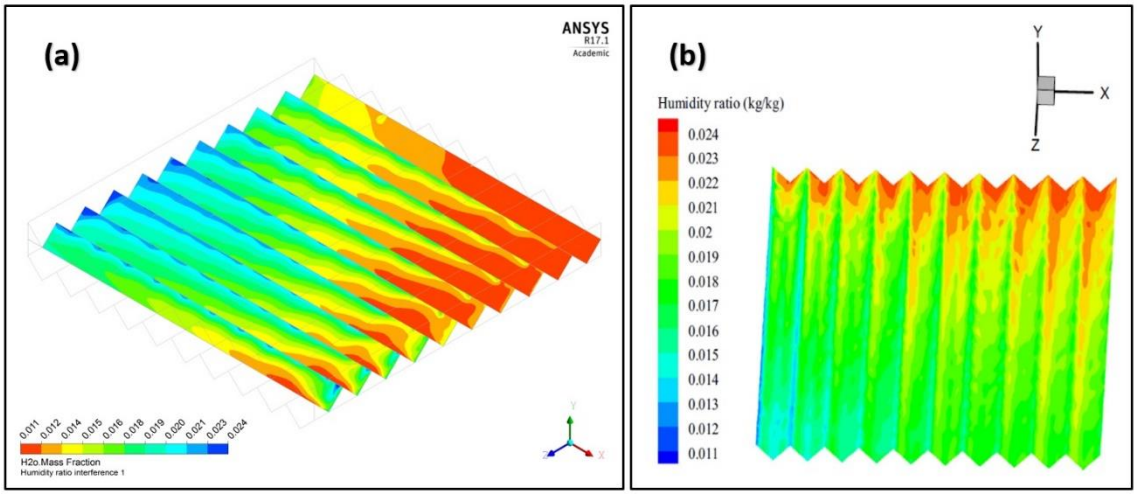


**Figure 4-36: (a) Humidity contour on the membrane wall at 1 m/s inlet velocities in the proposed validation model (18mm), (b) Li's (18mm) numerical Humidity contour at the membrane wall and at 1 m/s inlet velocity** [181]**.**

Figure 4-37 shows the temperature distributions over several cross-sections for the fresh and exhaust streams at air inlet velocity of 2.0 m/s. Figure 4-38 shows the humidity contours for the same case. Figure 4-39 and Figure 4-40 show the results for the velocity vectors and streamlines for the proposed validation model.

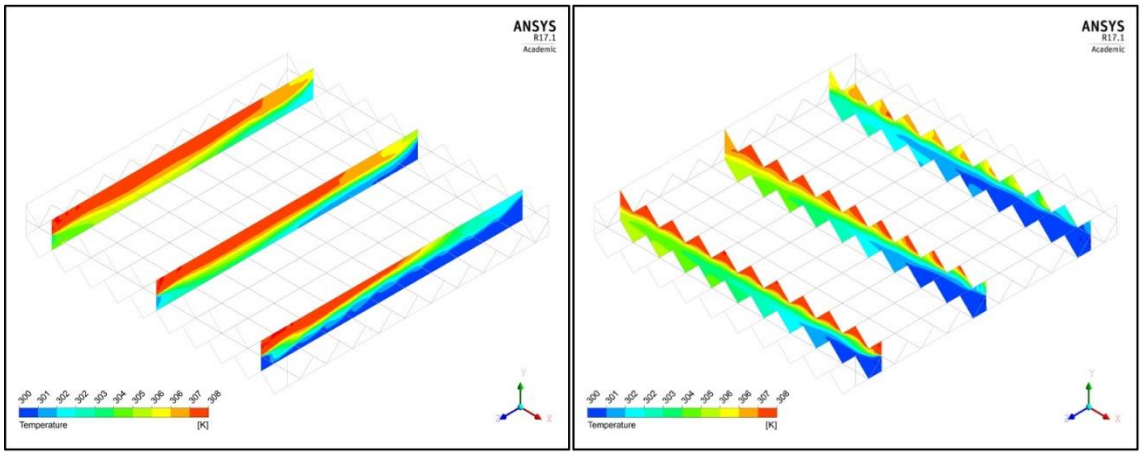


**Figure 4-37: Temperature contours in several sections for the fresh and exhaust stream for the validation model at inlet velocity 2.0 m/s.**

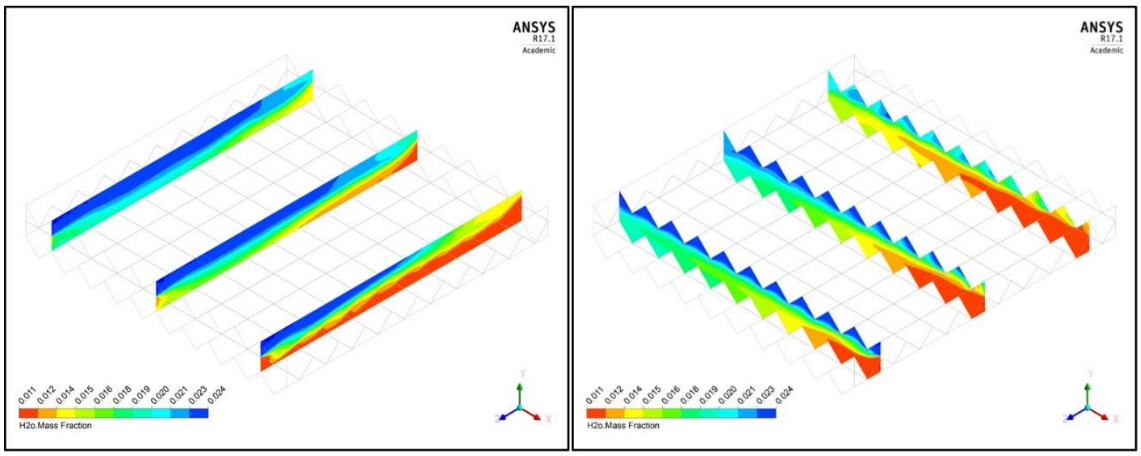


**Figure 4-38: Humidity contours in several sections for the fresh and exhaust stream for the validation model at inlet velocity 2.0 m/s.**

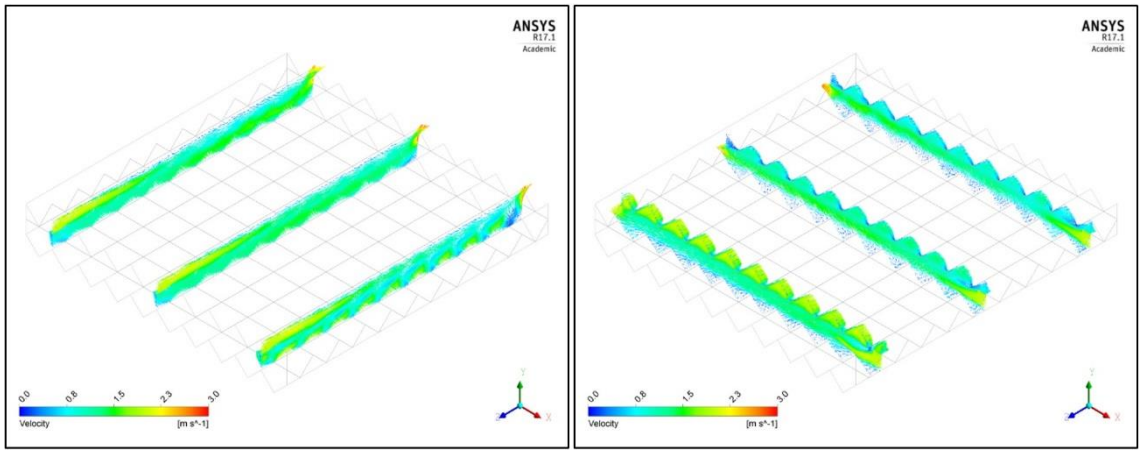


**Figure 4-39: 3D vectors in several sections for the fresh and exhaust stream for the validation model at inlet velocity 2.0 m/s.**

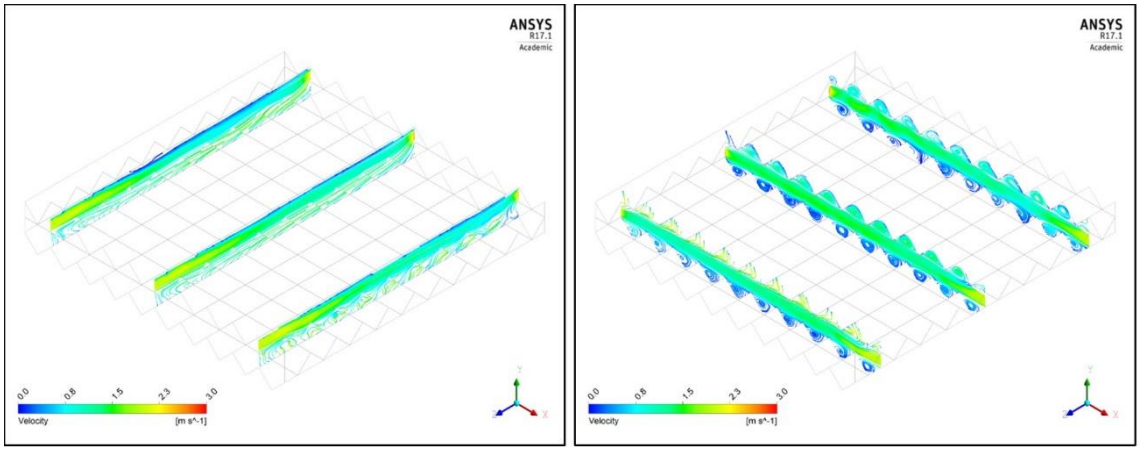


**Figure 4-40: Velocity streamlines in several sections for the fresh and exhaust stream for the validation model at inlet velocity 2.0 m/s.**

## 4.9 Energetic Analysis, Results and Discussion

This section will present the simulated results for the three geometric cases (25 mm, 10 mm and 5 mm pitch lengths). The test boundary conditions took into consideration the weather of the UK in winter when determining the ambient air properties, and the standard air conditioned room environment thermal comfort zone. Nine simulations were conducted for each geometry, four of them with changed inlet air velocity (which means change in the ventilation air volume flow rate) the linear average velocities through the heat exchanger were (0.5, 1.0, 1.5 and 2.0 m/s), and the five simulations with ambient (inlet) temperatures of 2, 4, 6, 8 and 10 $^{o}$C. This section will discuss the effects of each parameter separately on the performance of the exchanger core, including sensible heat transfer and mass of water vapour transferred from one stream to the other (as represented by the humidity contours) and with latent effectiveness an indicator of the performance of the core.

One way of presenting data graphically is to show **slices** (planes) of the flow in which one of the (X, Y and Z) coordinates is held constant. All graphic results are plotted on one of the planes, as shown in Figure 4-41, Figure 4-42 and Figure 4-43 which describe the positions of each plot sections (slices) according to the axis. Table 4-10 shows the positions of the slices according the axis and for all the cases, in mm, according to the whole dimension of a square exchanger core of 250 mm external dimension.

**Table 4-10: Slice position for all the cases according the axis**

| Pitch length | Axis | Dimensions (mm) | | |
|---|---|---|---|---|
| 25 mm | X | 25 | 125 | 225 |
| | Z | 12.5 | 112.5 | 212.5 |
| 10 mm | X | 20 | 120 | 230 |
| | Z | 25 | 115 | 215 |
| 5 mm | X | 22.5 | 132.5 | 242.5 |
| | Z | 12.5 | 122.5 | 232.5 |

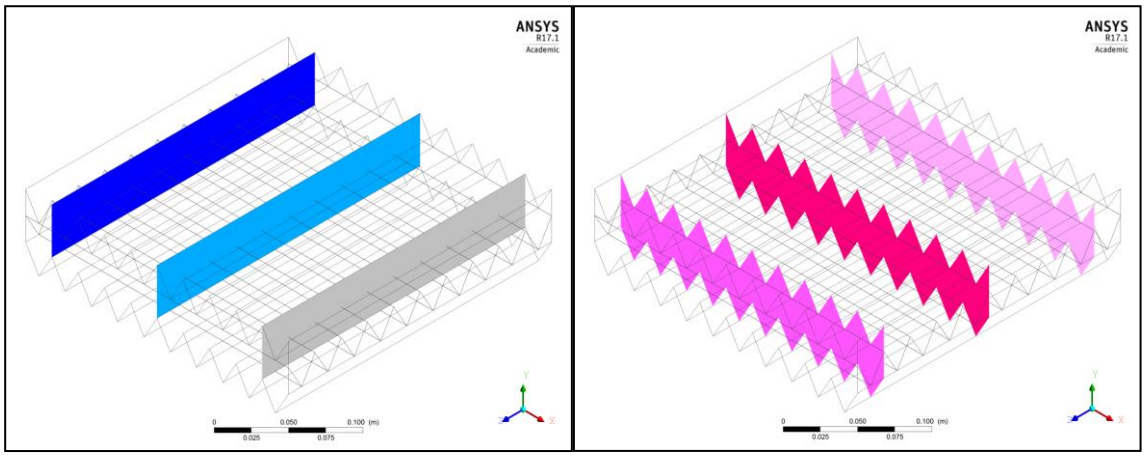


**Figure 4-41: Slices for 25 mm pitch length in both X and Z directions.**

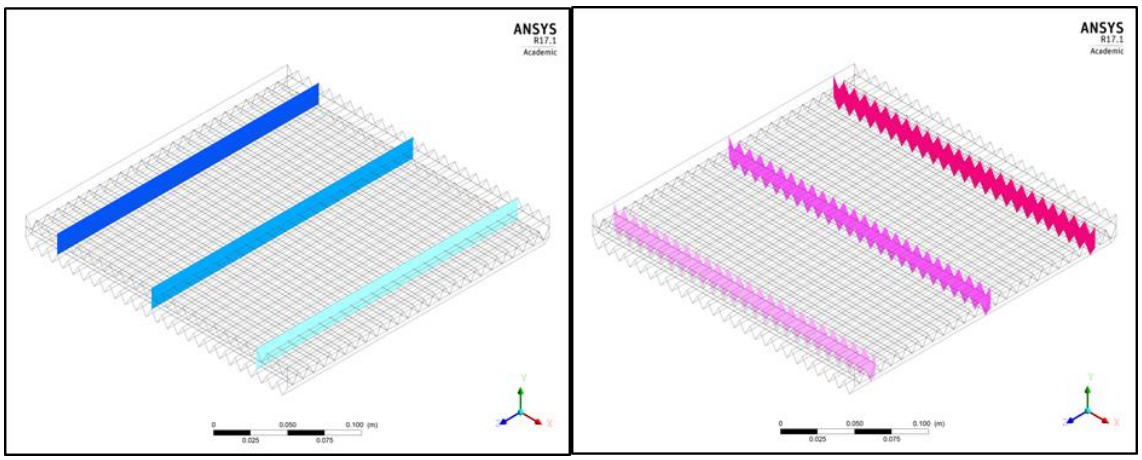


**Figure 4-42: : Slices for 10 mm pitch length in both X and Z directions**

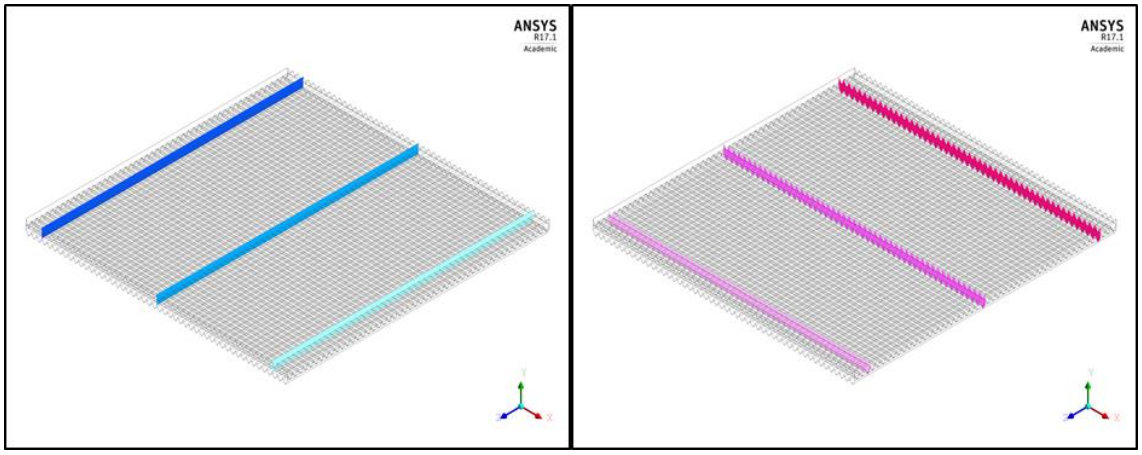


**Figure 4-43: : Slices for 5 mm pitch length in both X and Z directions**

### 4.9.1 Flow Behaviour and Velocity Distribution

The flow behaviour is presented in two different ways, the 3D streamline to show the distribution of the flow, and the velocity vectors to describe the velocity inside the corrugated heat exchanger channel. These contours were in the YZ plane for the fresh air stream, and in the XY plane for the exhaust stream, both according to the slice scheme shown above.

The results show that the flow behaviour divided into two different patterns, the first occurs in the upper half of the channel where the flow is steady, smooth and parallel to the walls, and develops fully in all cases after few corrugations. The other pattern occurs in the lower half of the channel, due to the rise and fall of the lateral corrugations below the flow. The fluid separates from the first edge formed by the lower lateral corrugation and is directed downwards, creating a swirl-like flow and recirculates towards the second edge formed by the corrugations. After few cycles the swirls have very similar shapes and intensities. The maximum velocity values occur in the upper half of the channel especially near the apex of the longitudinal channel. The smallest value of the velocity occurs close to the walls in the upper “half” of the channel at the base of the isosceles triangle, where the channel was widest.

Thus, the corrugations play a major role in shaping the flow pattern in the duct/channel, swirls and vortices occur due to the edges present, and the contractions and expansions of the channel work to enhance transfer of momentum. As these swirls are local recirculation of the flow and exert a force on the air, the air attains the flow transition region at a Re number less than 2000. As a result, the cross-corrugated exchanger has an advantage over the flat plate; the stagnant insulating layer on the wall is disturbed with the result of enhanced heat and moisture transfer.

Figures from Figure 4-44 to Figure 4-55 show the 3D velocity vectors for all cases and for highest and lowest values of the velocity and the other graphs will be shown in Appendix A.

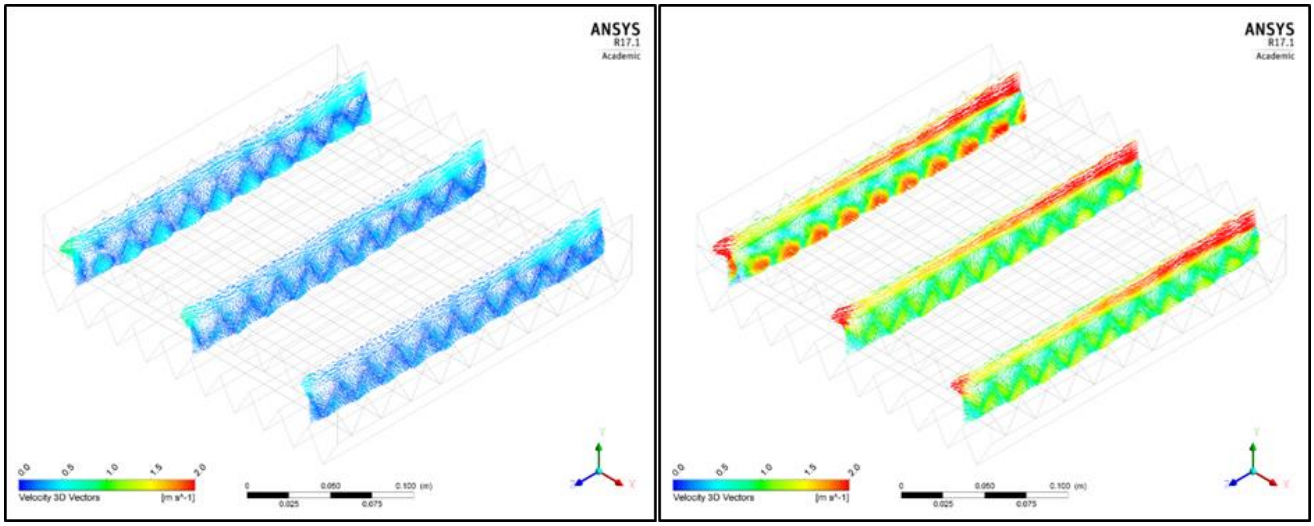


**Figure 4-44: (25 mm) 3D velocity vectors in X direction**

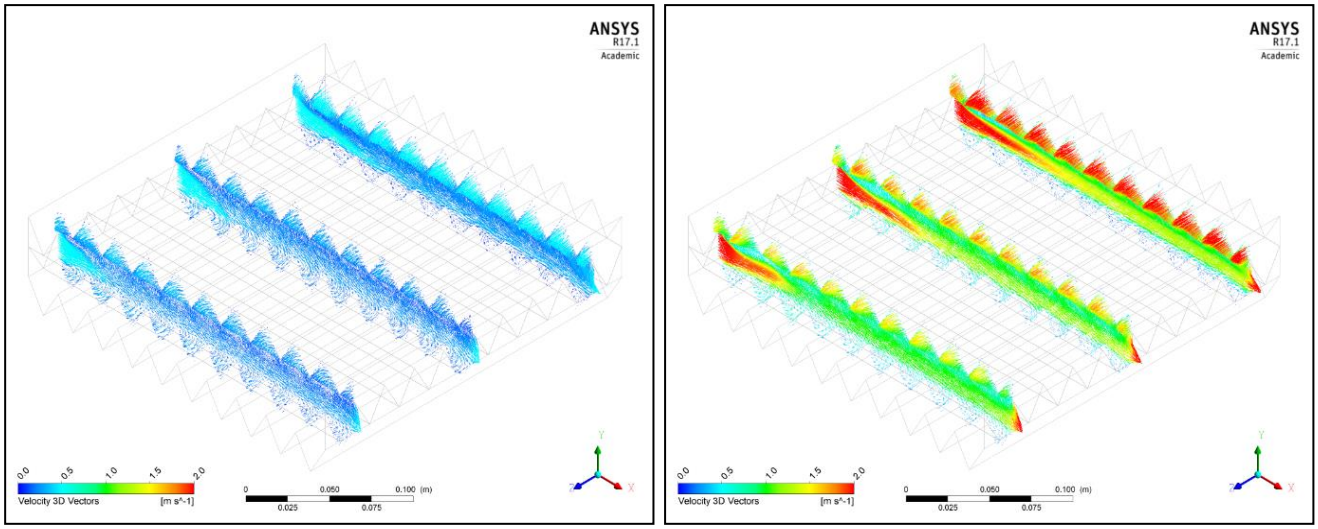


**Figure 4-45: (25 mm) 3D velocity vectors in Z direction**

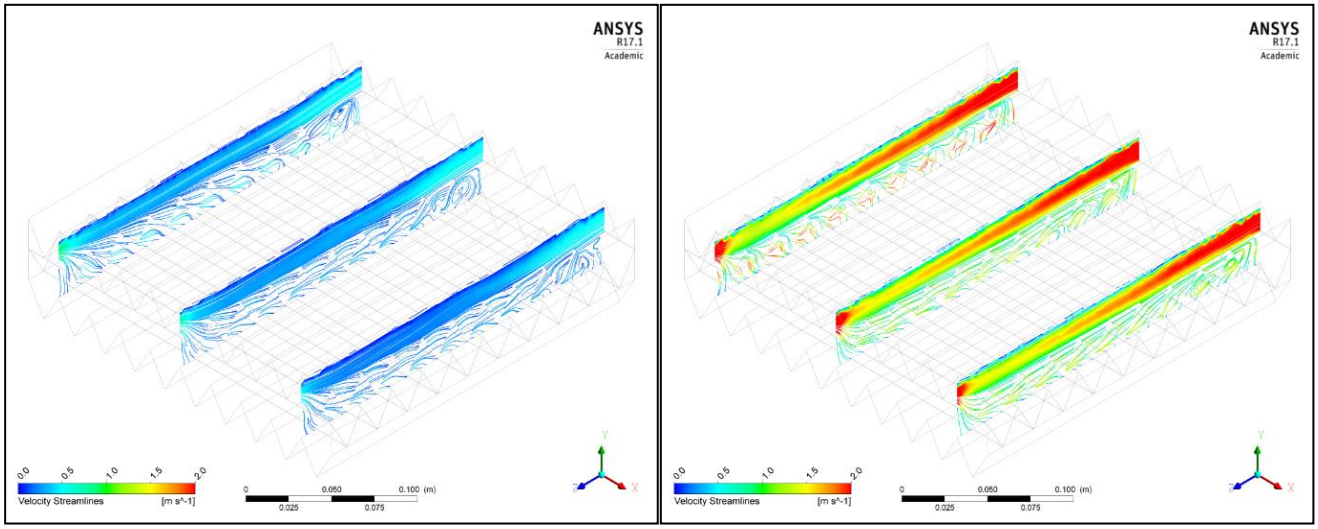


**Figure 4-46: (25 mm) Velocity streamlines in X direction**

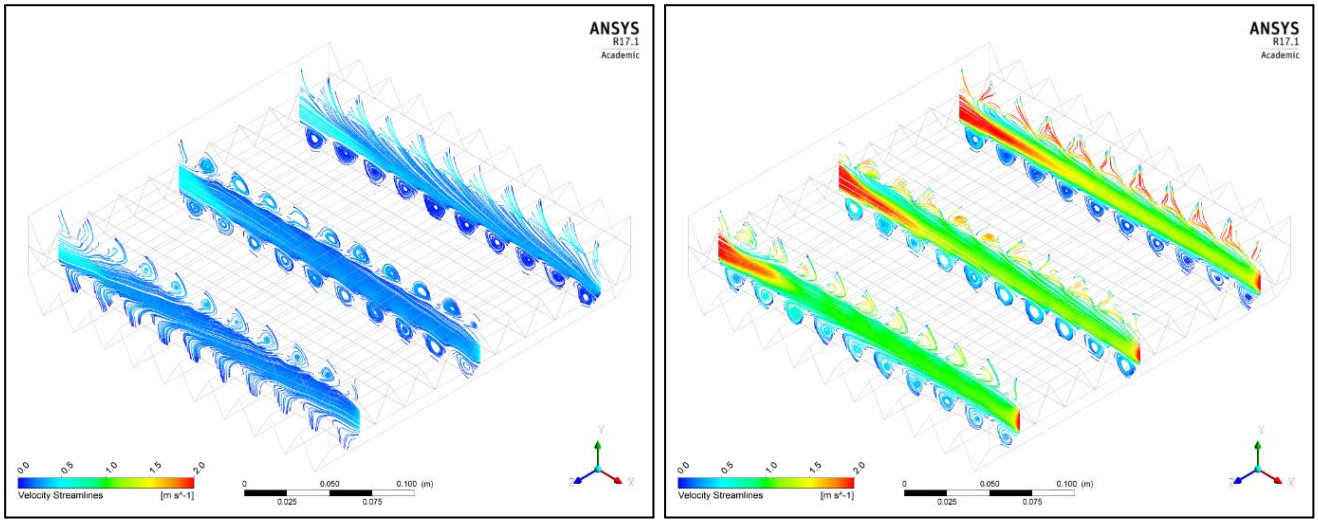


**Figure 4-47: (25 mm) Velocity streamlines in Z direction**

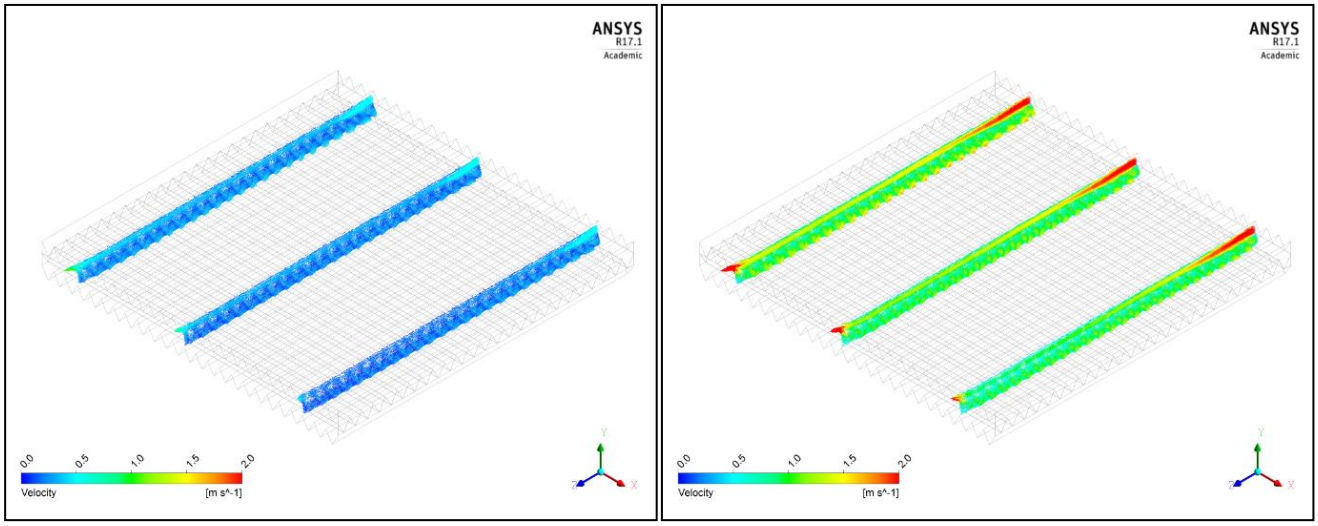


**Figure 4-48: (10 mm) 3D vectors in X direction**

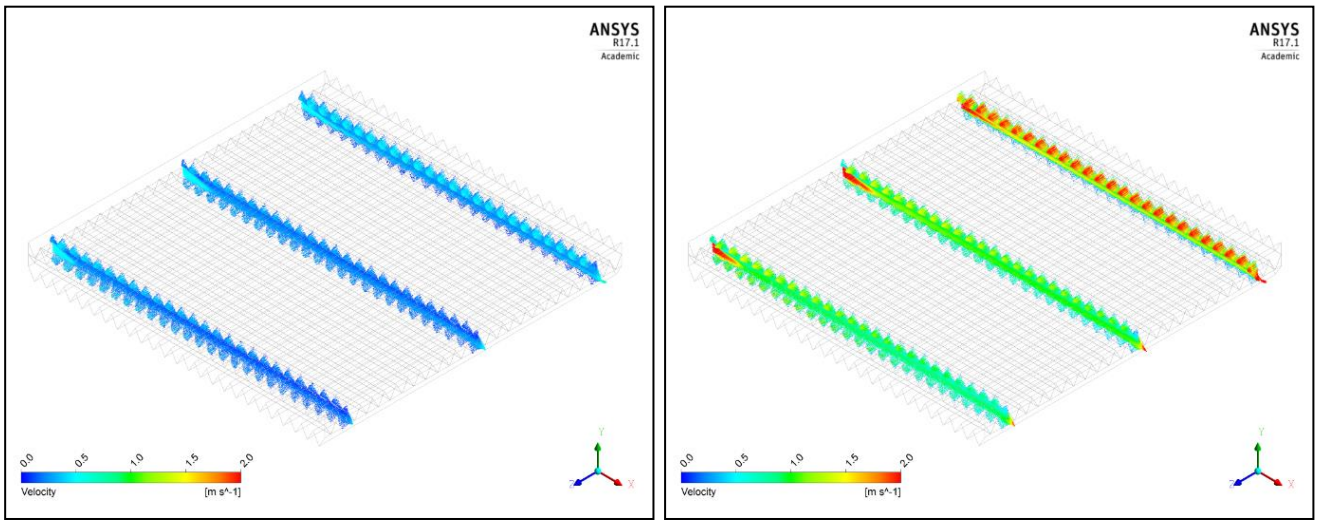


**Figure 4-49: (10 mm) 3D vectors in Z direction**

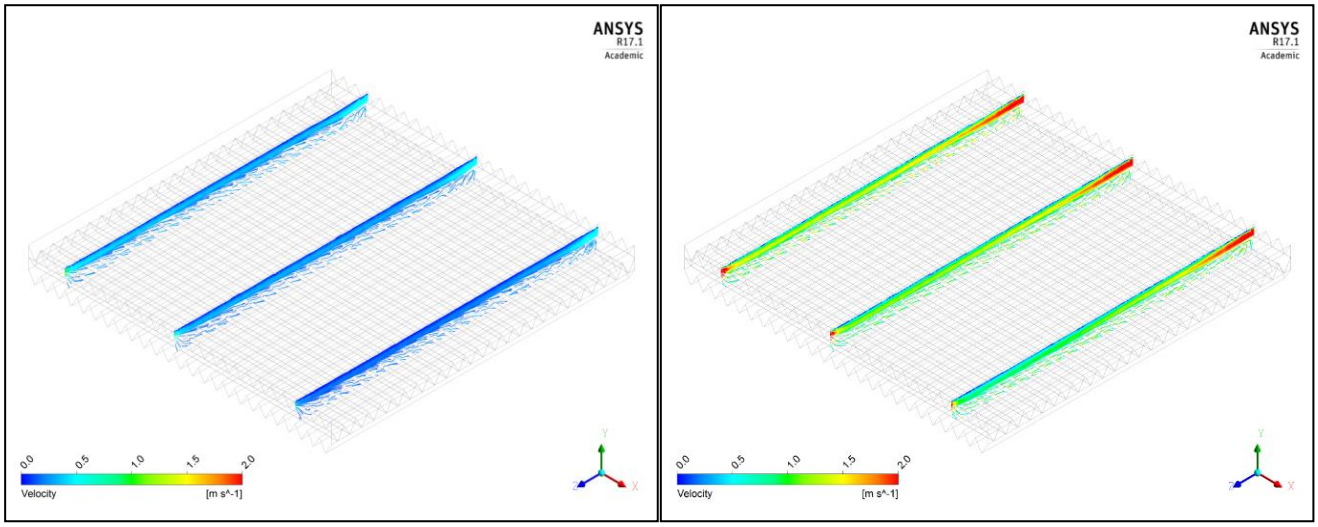


**Figure 4-50: (10 mm) Velocity streamlines in X direction**

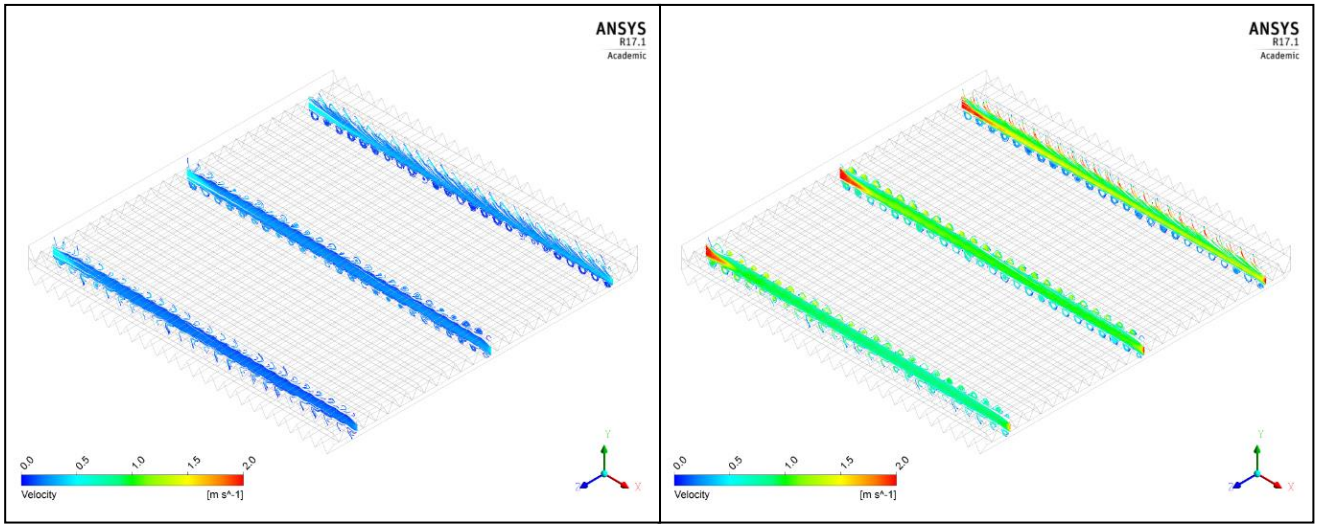


**Figure 4-51: (10 mm) Velocity streamlines in Z direction**

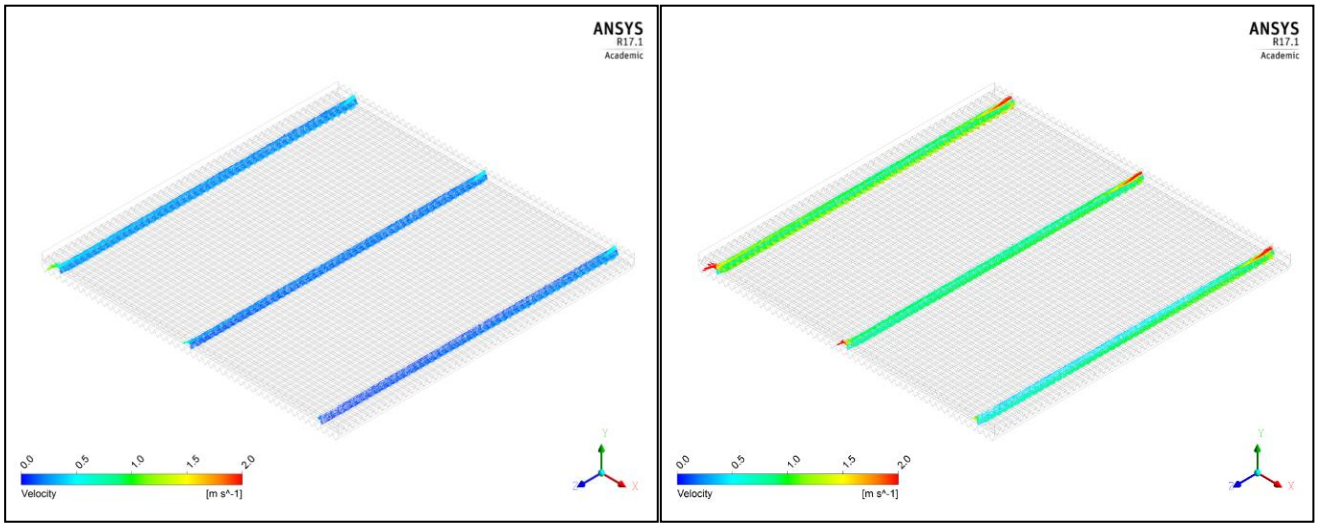


**Figure 4-52: (5 mm) 3D vectors in X direction**

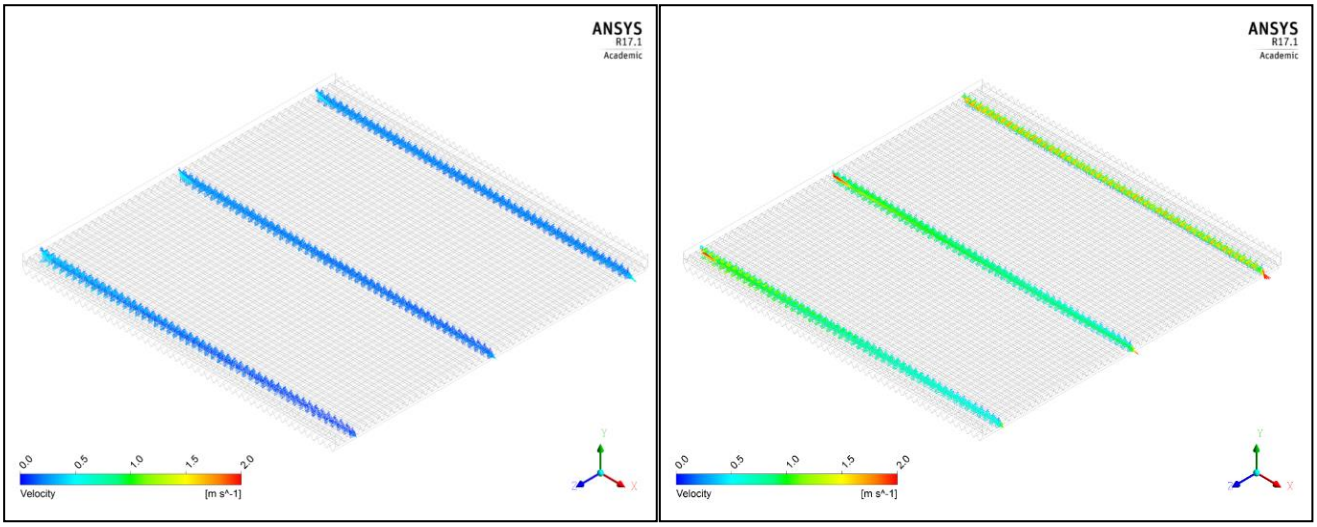


**Figure 4-53: (5 mm) 3D vectors in Z direction**

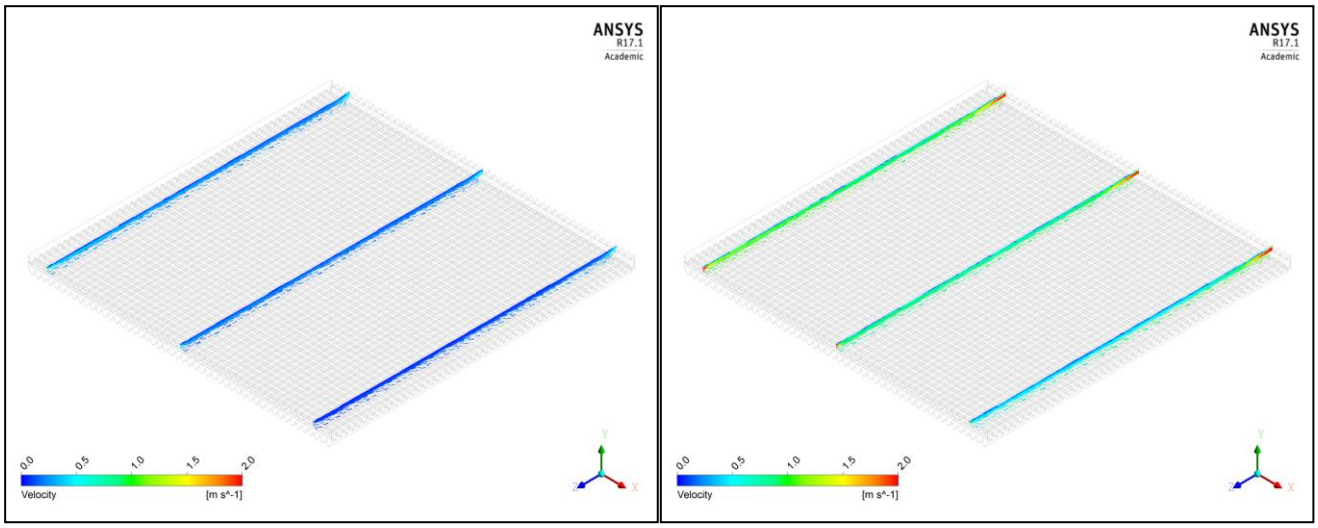


**Figure 4-54: (5 mm) Velocity streamlines in X direction**

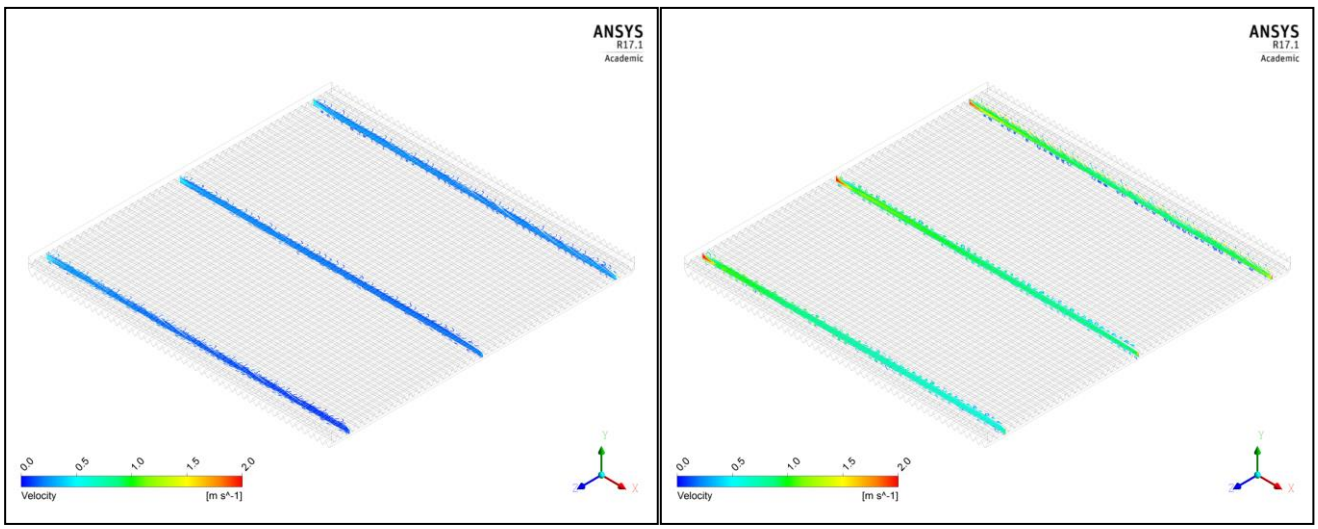


**Figure 4-55: (5 mm) Velocity streamlines in Z direction.**

### 4.9.2 Temperature Distribution

The simulated temperature values in the outlet of the fresh and exhaust air streams were obtained using the CFDPost17 function calculator. One way to present the temperature distribution inside the exchanger core is by using the temperature contours on the membrane surface as well as on the proposed slices.

The temperature contours show the heat flow pattern clearly, which is seen to be fully developed after few cycles. “Cycle” is used here to mean the flow over a corrugation lip and its travel to the next lip. The flow pattern affects the temperature distribution which is seen to be uniform and parallel to the walls in the upper half of the channel. However, with the flow over the corrugations, the temperature gradient demonstrates the effect of the swirls formed in the lower half of the duct/channel due to the separation of the air flow and recirculation of the flow.

With increased inlet velocity and higher Re numbers, the swirls became more intense giving better sensible heat transfer which is shown in temperature contours.

Figures from Figure 4-56 to Figure 4-70 show the temperature contours for all the cases, but, only the highest and lowest values of the inlet velocities and ambient temperature will be presented in this section, and all the other contours will be presented in Appendix A.

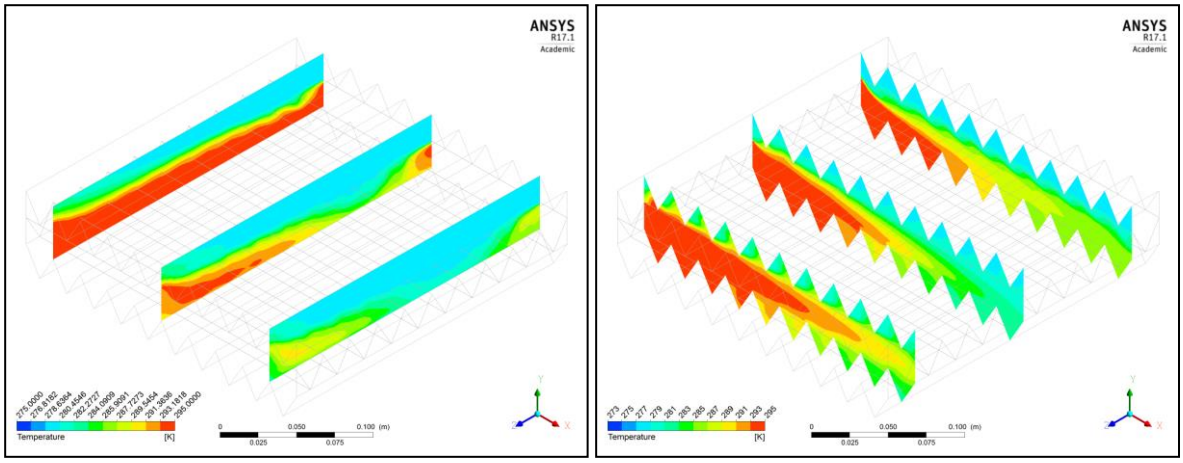


**Figure 4-56: (25 mm) Temperature contours (Left) at X-AXIS and (Right) Y-AXIS at ($T_{fi}$=6°C) and ($v_i$=0.5 m/s)**

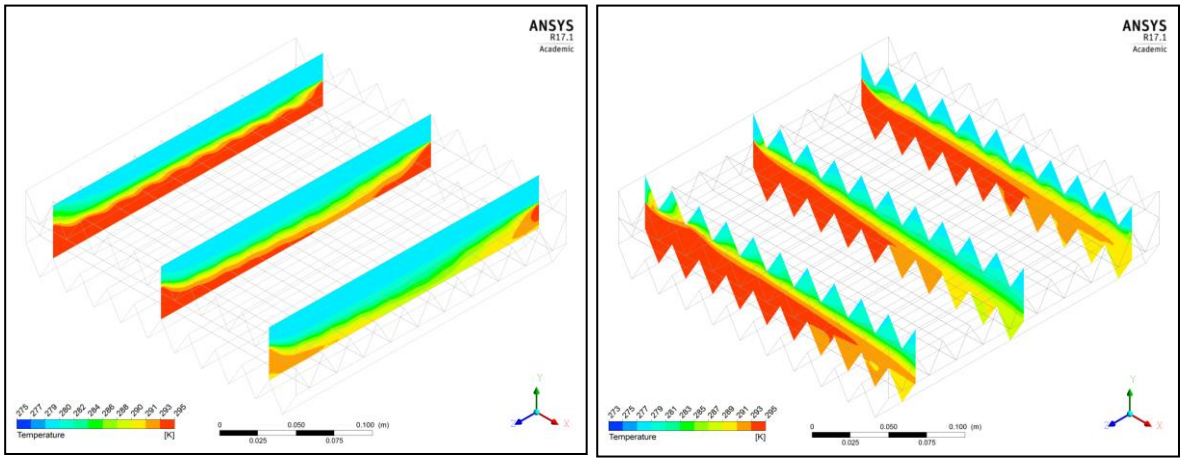


**Figure 4-57: (25 mm) Temperature contours (Left) at X-AXIS and (Right) Y-AXIS at ($T_{fi}$=6°C) and ($v_i$=2.0 m/s)**

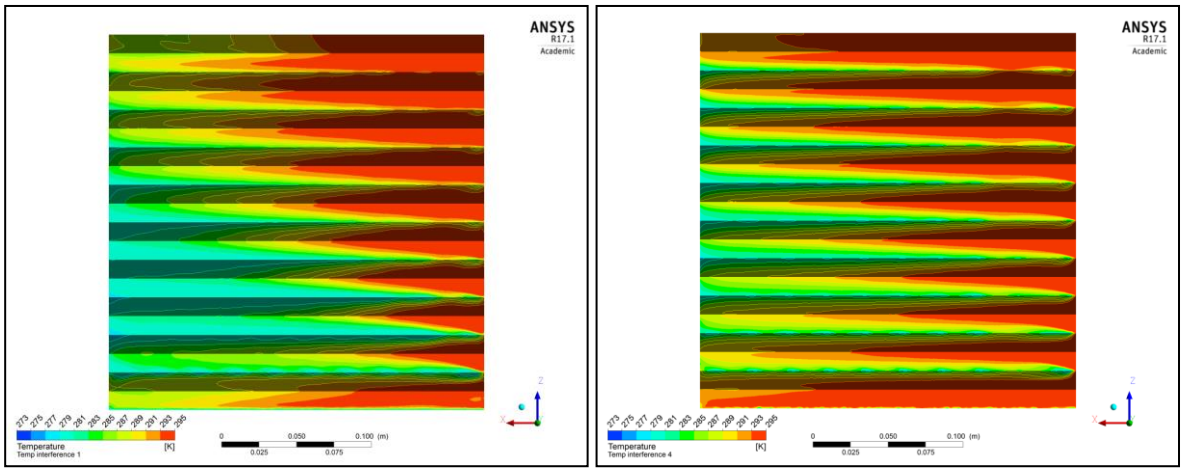


**Figure 4-58: (25 mm) Temperature contours on the membrane's surface at ($v_i$=0.5 m/s) (Left) and ($v_i$=2.0 m/s) (Right) at ($T_{fi}$=6°C).**

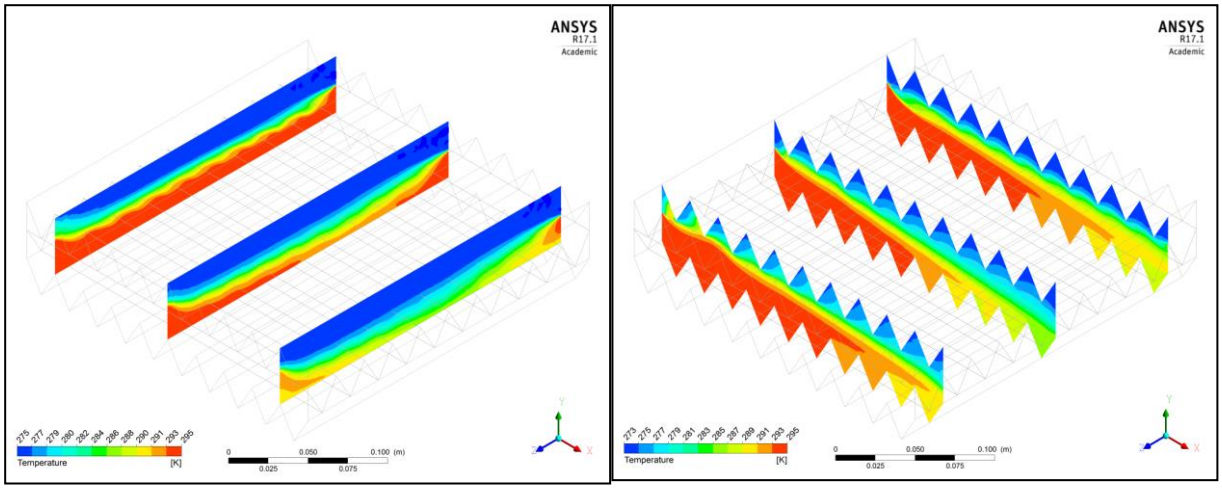


**Figure 4-59: (25 mm) Temperature contours (Left) at X-AXIS and (Right) Y-AXIS at ($T_{fi}$=2°C) and ($v_i$=2.0 m/s)**

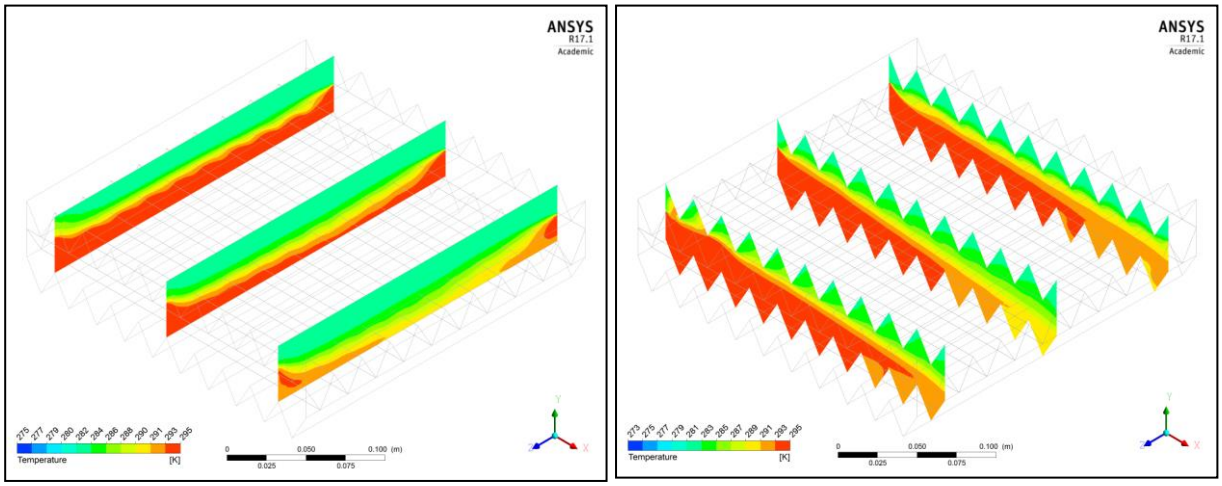


**Figure 4-60: (25mm) Temperature contours (Left) at X-AXIS and (Right) Y-AXIS at ($T_{fi}$=10°C) and ($v_i$=2m/s)**

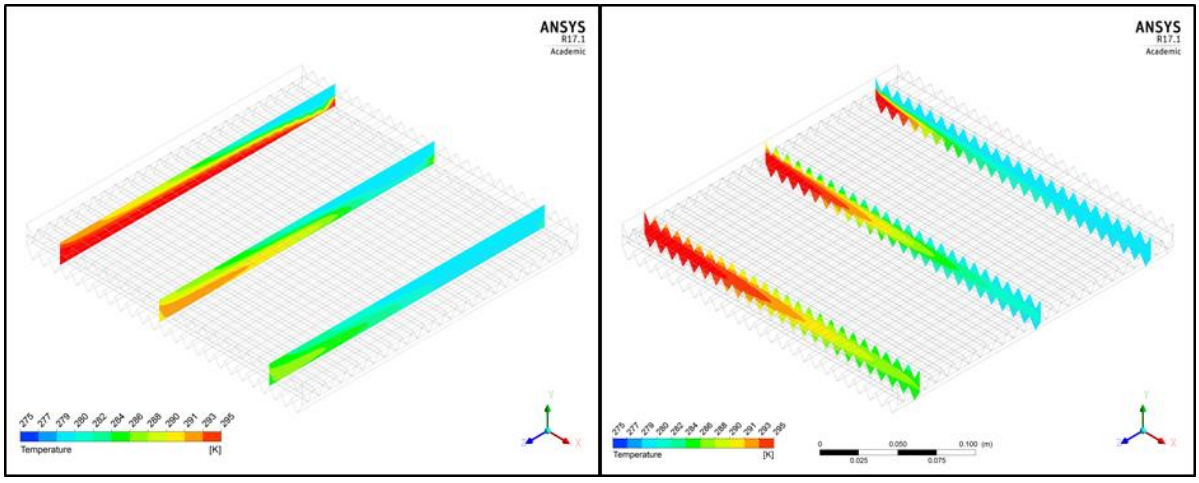


**Figure 4-61: (10mm) Temperature contours (Left) at X-AXIS and (Right) Y-AXIS at ($T_{fi}$=6°C) and ($v_i$=0.5m/s)**

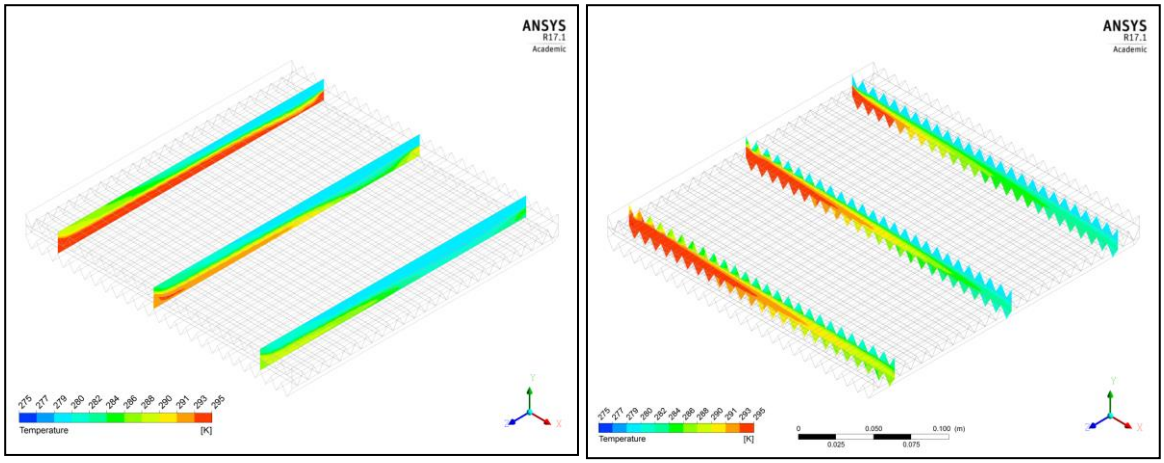


**Figure 4-62: (10mm) Temperature contours (Left) at X-AXIS and (Right) Y-AXIS at ($T_{fi}$=6°C) and ($v_i$=2m/s)**

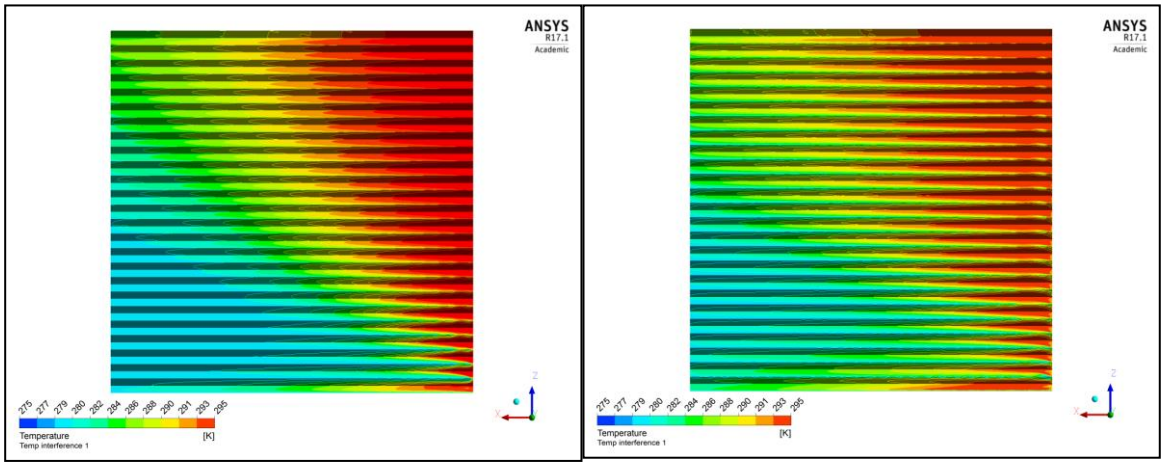


**Figure 4-63: (10mm) Temperature contours on the membrane's surface at ($v_i$=0.5m/s) (Left) and ($v_i$=2m/s) (Right) at ($T_{fi}$=6°C).**

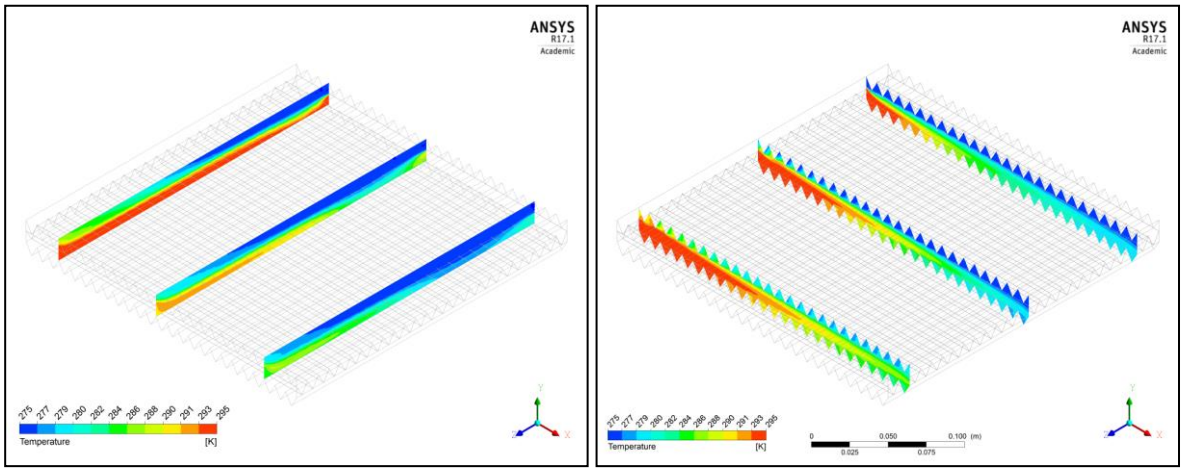


**Figure 4-64: (10mm) Temperature contours (Left) at X-AXIS and (Right) Y-AXIS at ($T_{fi}$=2°C) and ($v_i$=2m/s)**

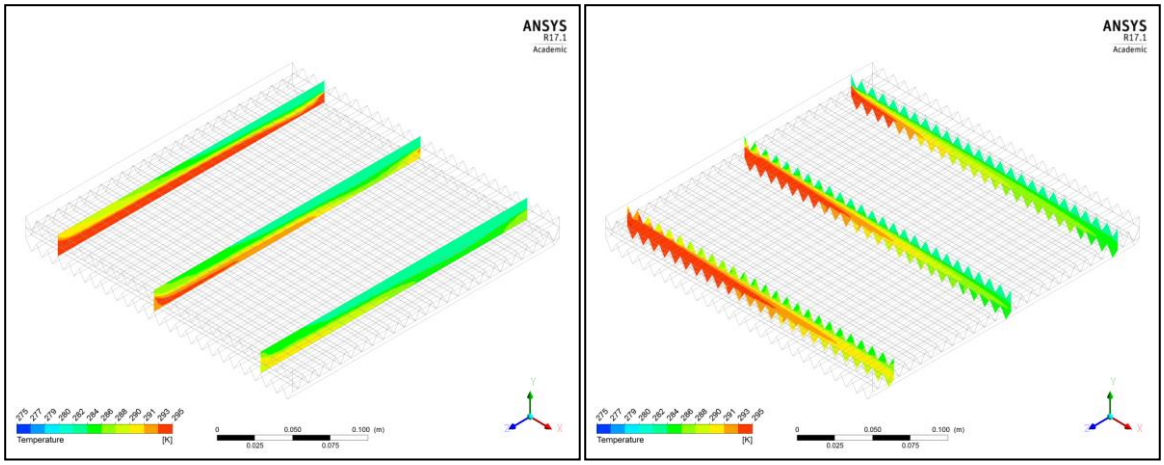


**Figure 4-65: (10mm) Temperature contours (Left) at X-AXIS and (Right) Y-AXIS at ($T_{fi}$=10°C) and ($v_i$=2m/s)**

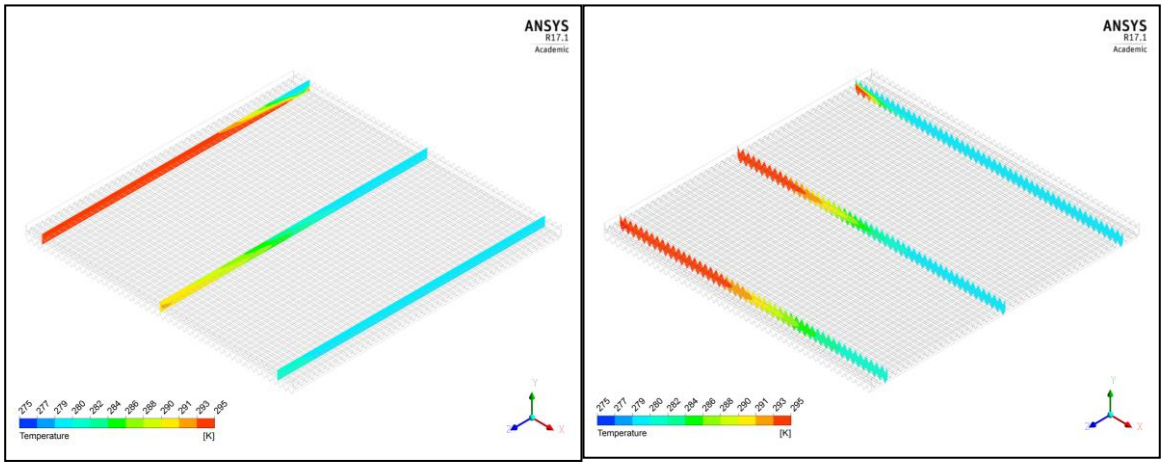


**Figure 4-66: (5mm) Temperature contours (Left) at X-AXIS and (Right) Y-AXIS at ($T_{fi}$=6°C) and ($v_i$=0.5m/s)**

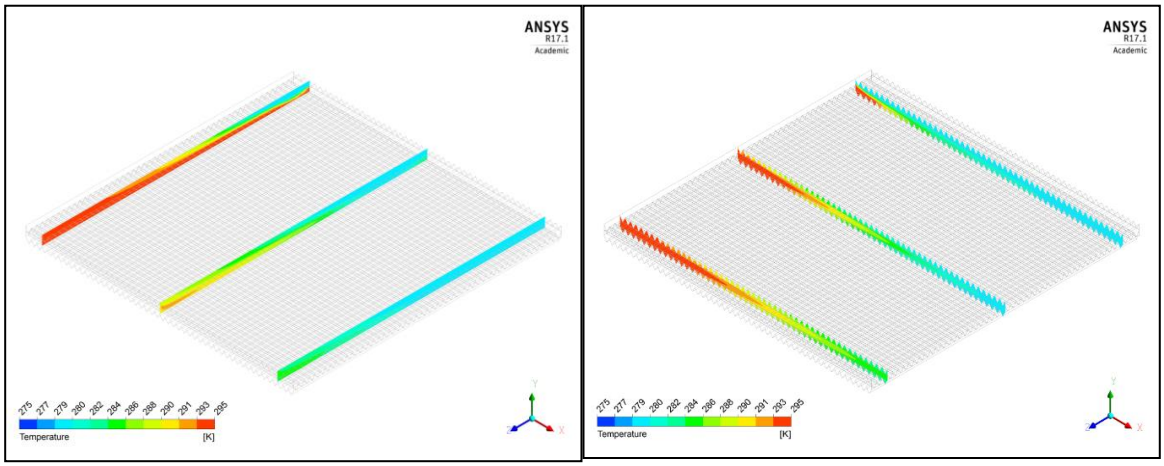


**Figure 4-67: (5mm) Temperature contours (Left) at X-AXIS and (Right) Y-AXIS at ($T_{fi}$=6°C) and ($v_i$=2m/s)**

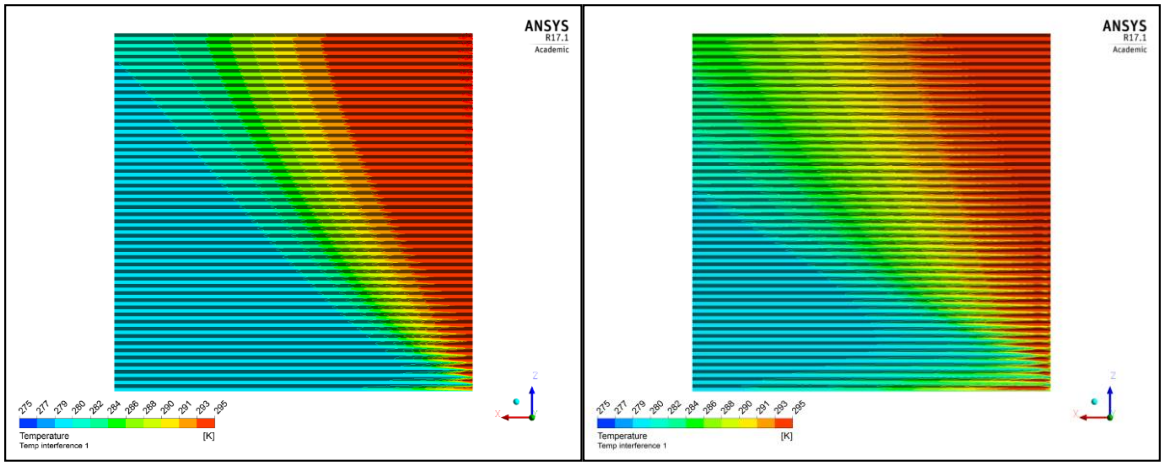


**Figure 4-68: (5 mm) Temperature contours on the membrane's surface at ($v_i$=0.5m/s) (Left) and ($v_i$=2m/s) (Right) at ($T_{fi}$=6°C).**

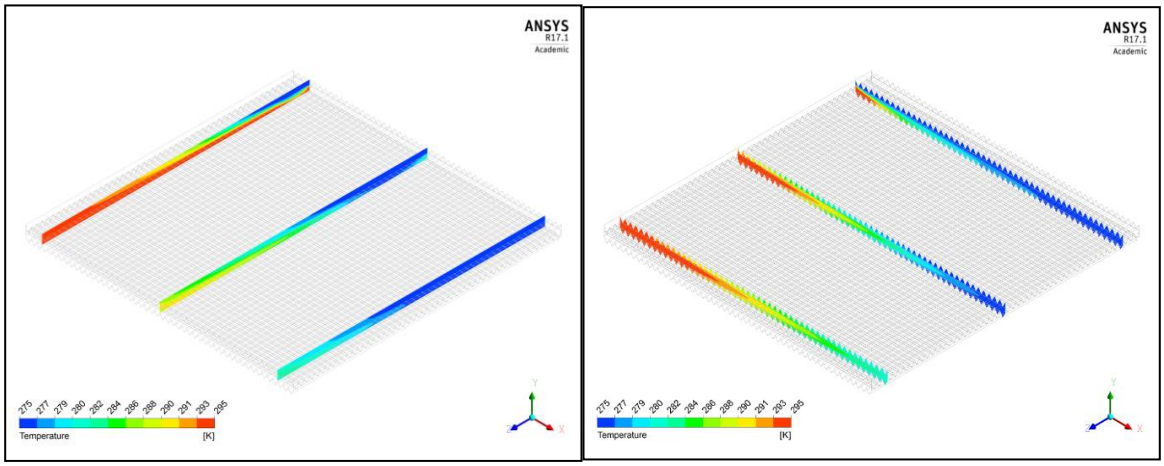


**Figure 4-69: (5 mm) Temperature contours in (Left) at X-AXIS and (Right) Y-AXIS at ($T_{fi}$=2°C) and ($v_i$=2m/s)**

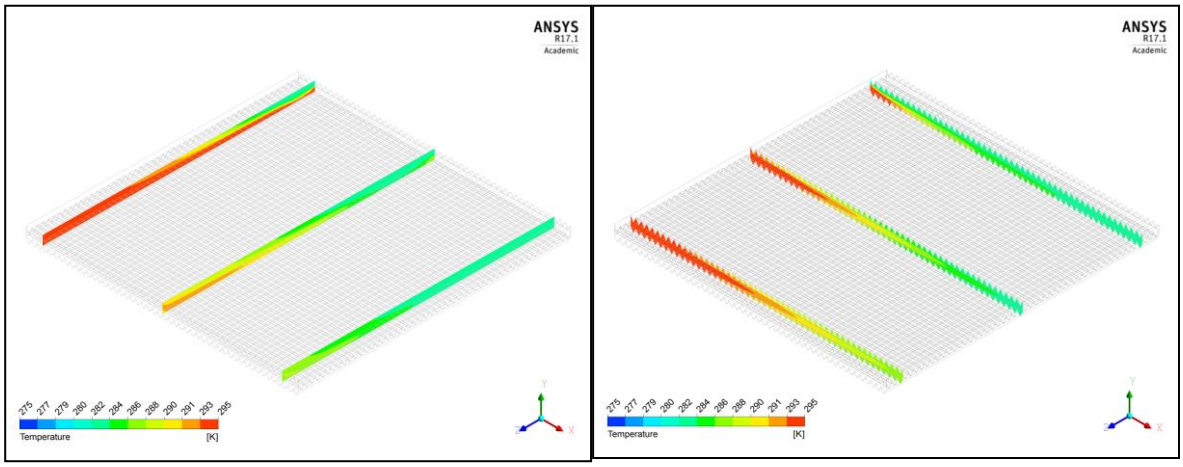


**Figure 4-70: (5 mm) Temperature contours (Left) at X-AXIS and (Right) Y-AXIS at ($T_{fi}$=10°C) and ($v_i$=2m/s)**

### 4.9.3 Humidity Ratio Distribution

One of the main purposes of using a membrane as the main material for the heat exchanger core is to recover the latent heat contained in the water vapour in the exhaust air, in other words, to recover moisture from the exhaust air to a degree depending on the application. Accordingly, the physical problem in this study is considered as a conjoint heat and mass transfer problem, with the mass transfer equally as significant as the sensible heat transfer. This section focuses on the humidity ratio transfer and presents the findings as humidity and temperature contours on the membrane surface, as well as slices in X and Z directions as shown in Figure 4-41, Figure 4-42 and Figure 4-43 earlier.

The humidity contours show that the effect of increasing the inlet air velocities in both or either fresh and exhaust streams is very noticeable and significantly increases the humidity exchange between the streams. The distribution of humidity ratio in the cross-corrugated core as shown in the contours has almost the same pattern and is quite similar to the temperature contours. The corrugations and resulting air flow patterns inside the duct/channel have a very noticeable impact on the humidity transfer between the streams.

Figures (4-70) to (4-84) show the humidity contours for both the highest and lowest inlet velocity and ambient temperatures. Comparing the results for the three geometries, the 5 mm cases show the most uniformity in humidity distribution due to the relatively smaller size of the corrugations. However, the mass transfer tends to be enhanced because of the higher number of corrugations per layer.

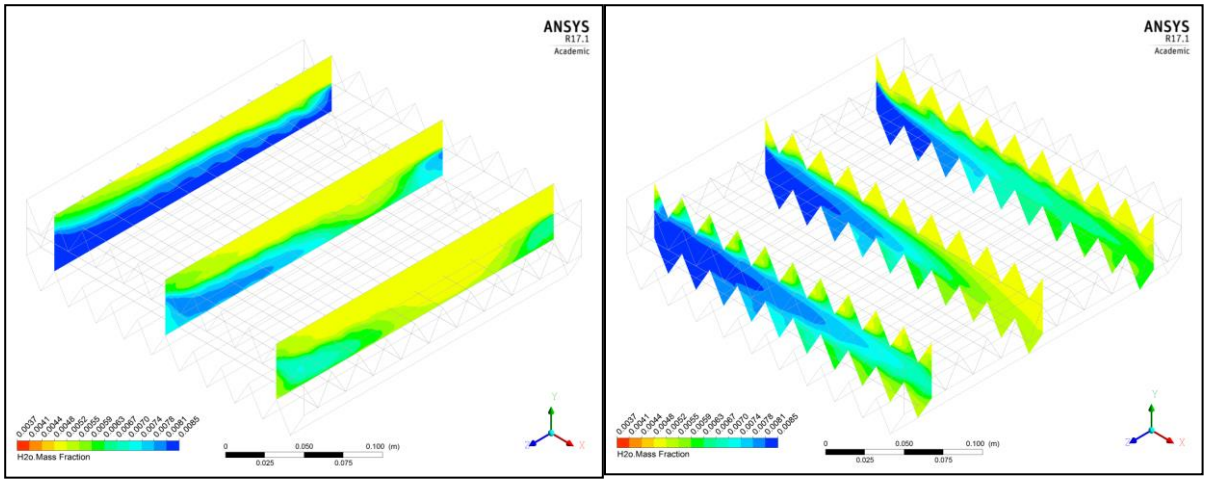


**Figure 4-71: (25mm) Humidity contours (Left) at X-AXIS and (Right) Y-AXIS at ($T_{fi}$=6°C) and ($v_i$=0.5m/s).**

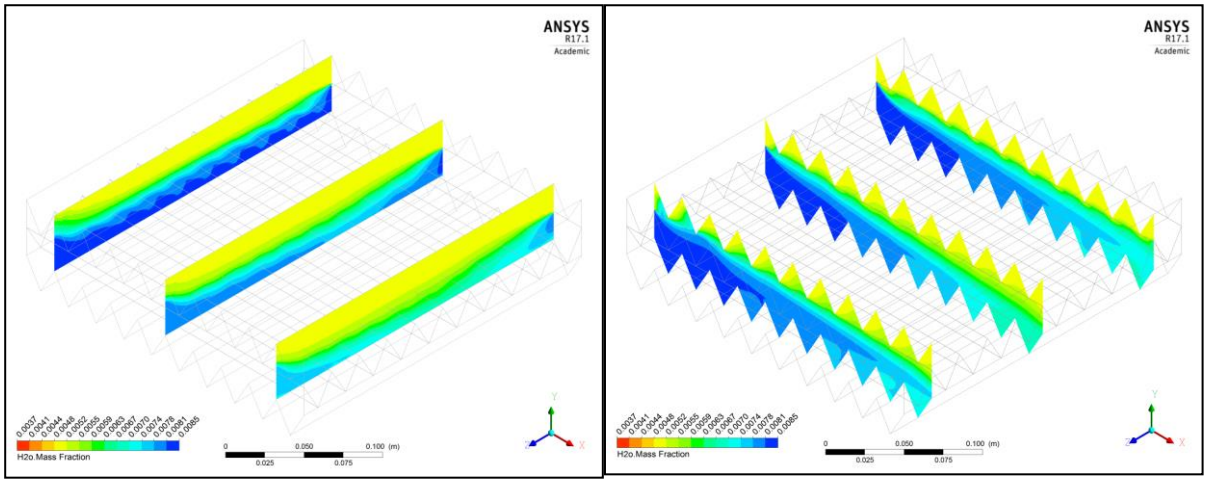


**Figure 4-72: (25mm) Humidity contours (Left) at X-AXIS and (Right) Y-AXIS at ($T_{fi}$=6°C) and ($v_i$=2m/s)**

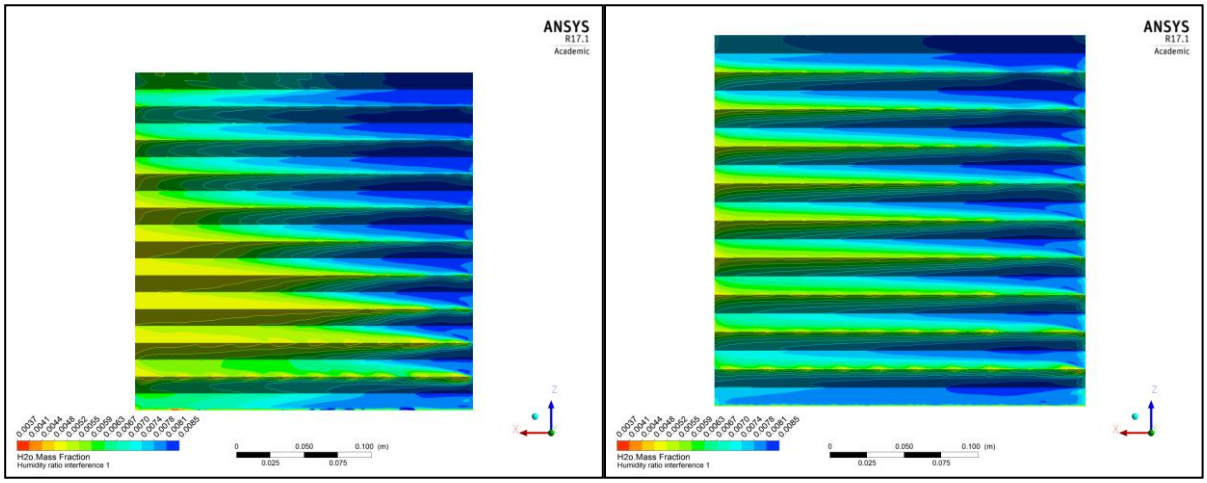


**Figure 4-73: (25mm) Humidity contours on the membrane's surface at ($v_i$=0.5m/s) (Left) and ($v_i$=2m/s) (Right) at ($T_{fi}$=6°C).**

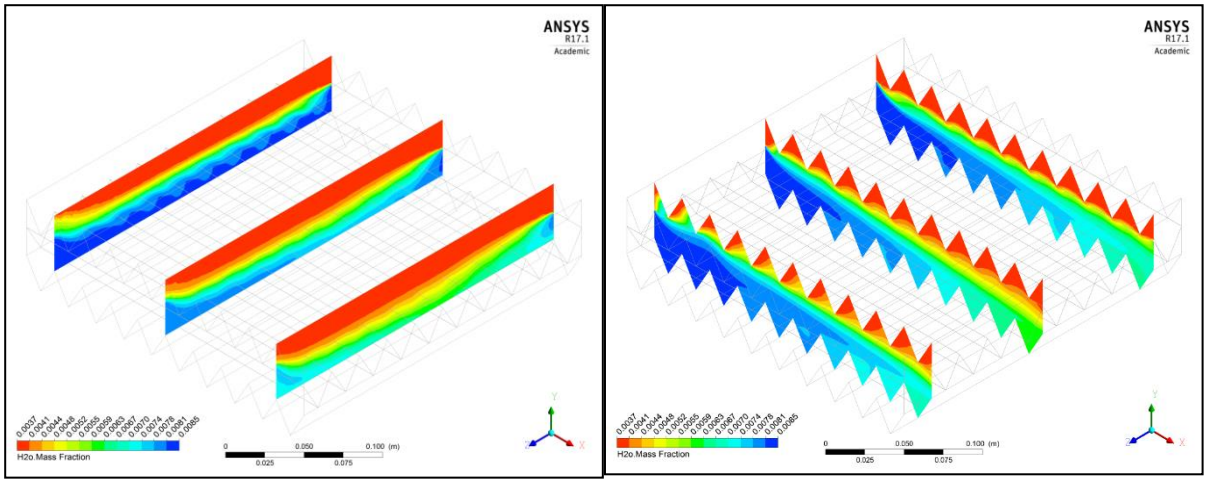


**Figure 4-74: (25mm) Humidity contours (Left) at X-AXIS and (Right) Y-AXIS at ($T_{fi}$=2°C) and ($v_i$=2m/s)**

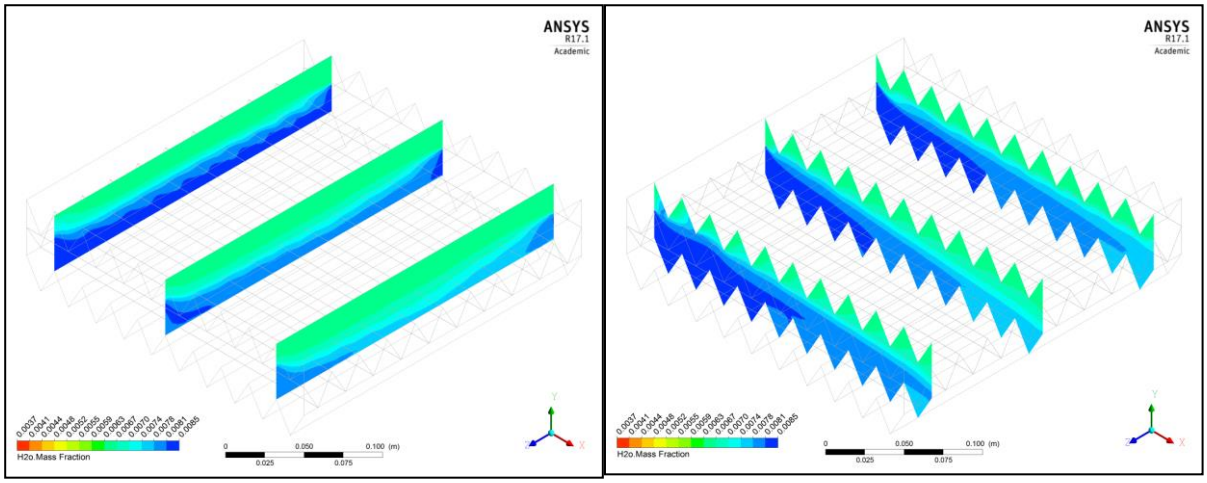


**Figure 4-75: (25mm) Humidity contours (Left) at X-AXIS and (Right) Y-AXIS at ($T_{fi}$=10°C) and ($v_i$=2m/s)**

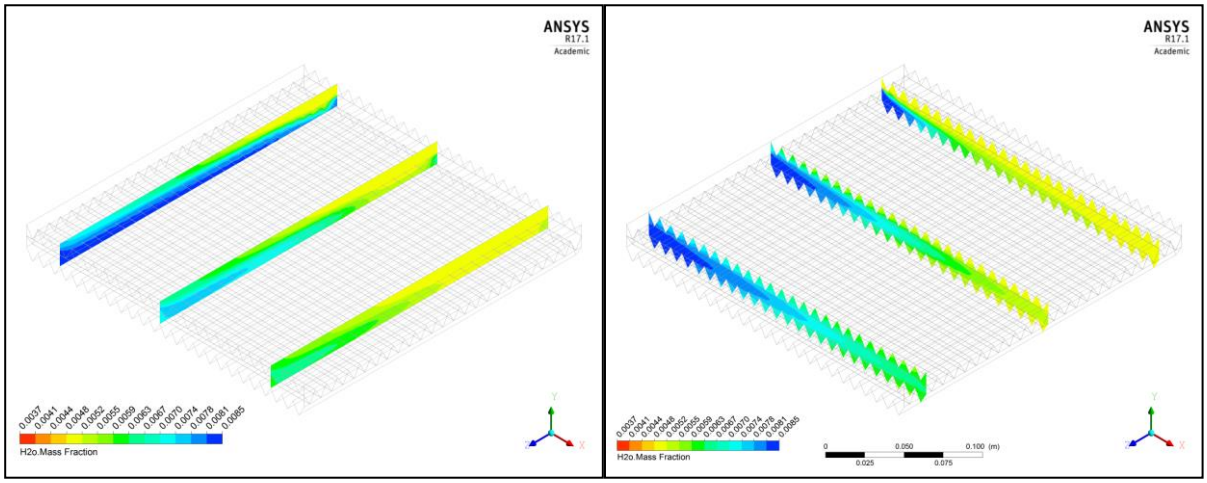


**Figure 4-76: (10mm) Humidity contours (Left) at X-AXIS and (Right) Y-AXIS at ($T_{fi}$=6°C) and ($v_i$=0.5m/s)**

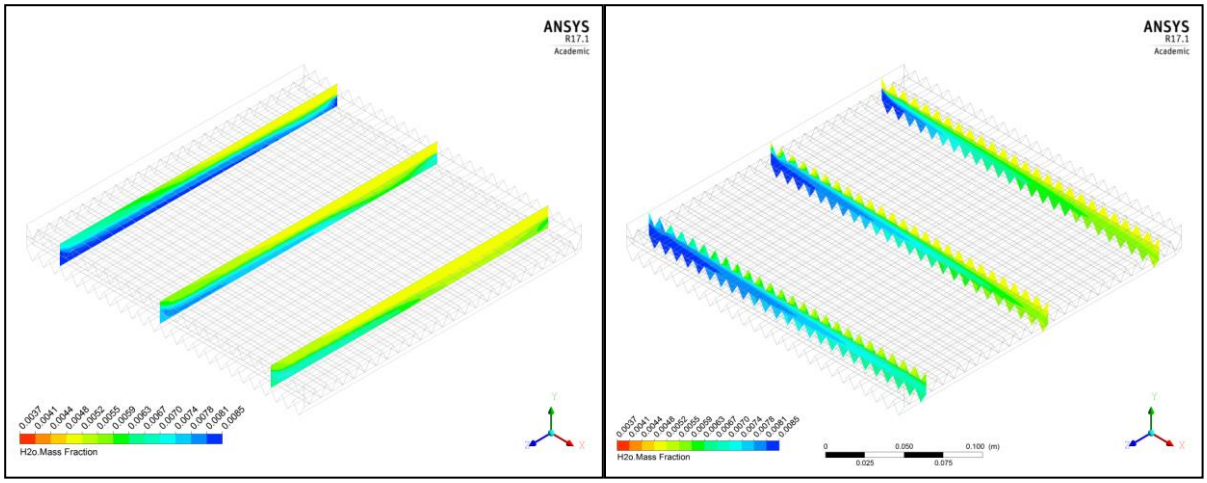


**Figure 4-77: (10mm) Humidity contours (Left) at X-AXIS and (Right) Y-AXIS at ($T_{fi}$=6ºC) and ($v_i$=2m/s)**

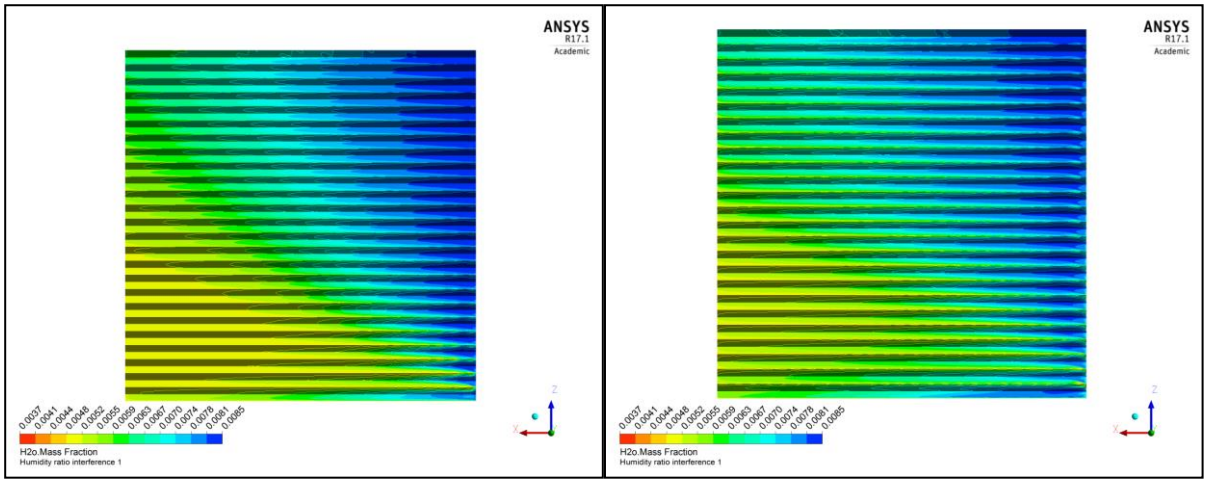


**Figure 4-78: (10mm) Humidity contours on the membrane's surface at ($v_i$=0.5m/s) (Left) and ($v_i$=2m/s) (Right) at ($T_{fi}$=6ºC).**

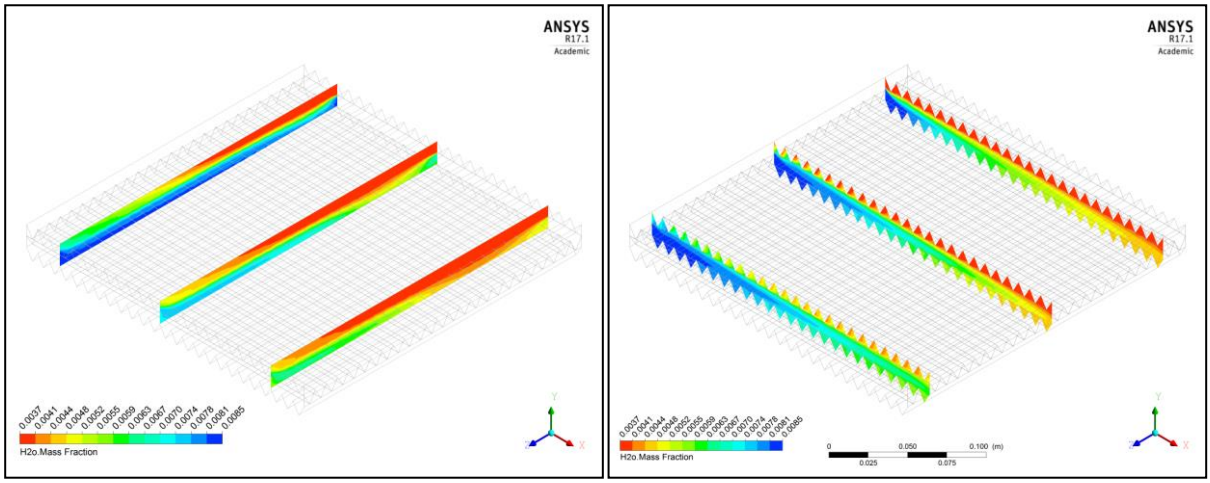


**Figure 4-79: (10mm) Humidity contours (Left) at X-AXIS and (Right) Y-AXIS at ($T_{fi}$=2ºC) and ($v_i$=2m/s)**

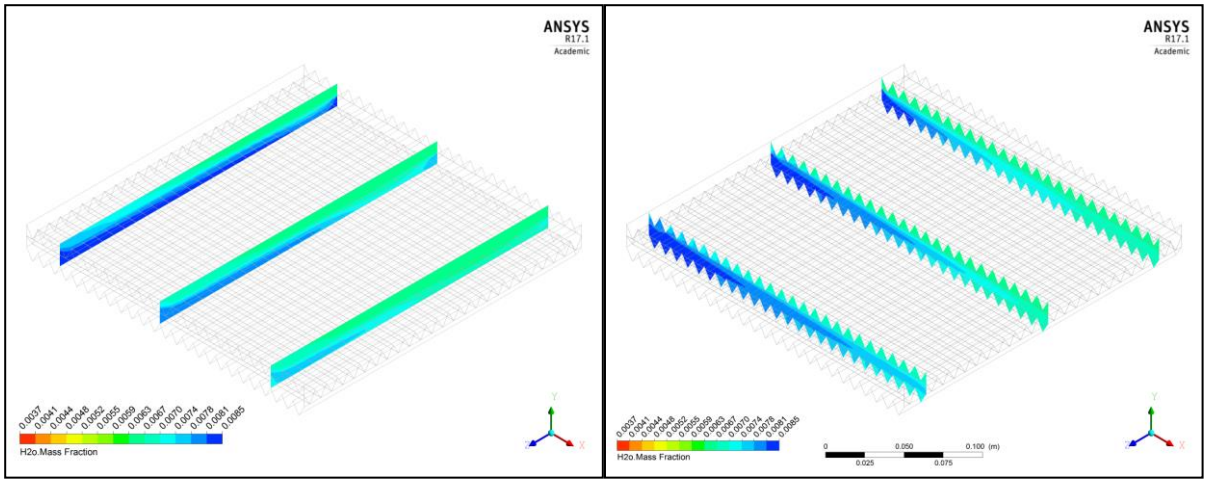


**Figure 4-80: (10mm) Humidity contours in (Left) at X-AXIS and (Right) Y-AXIS at ($T_{fi}$=10°C) and ($v_i$=2m/s)**

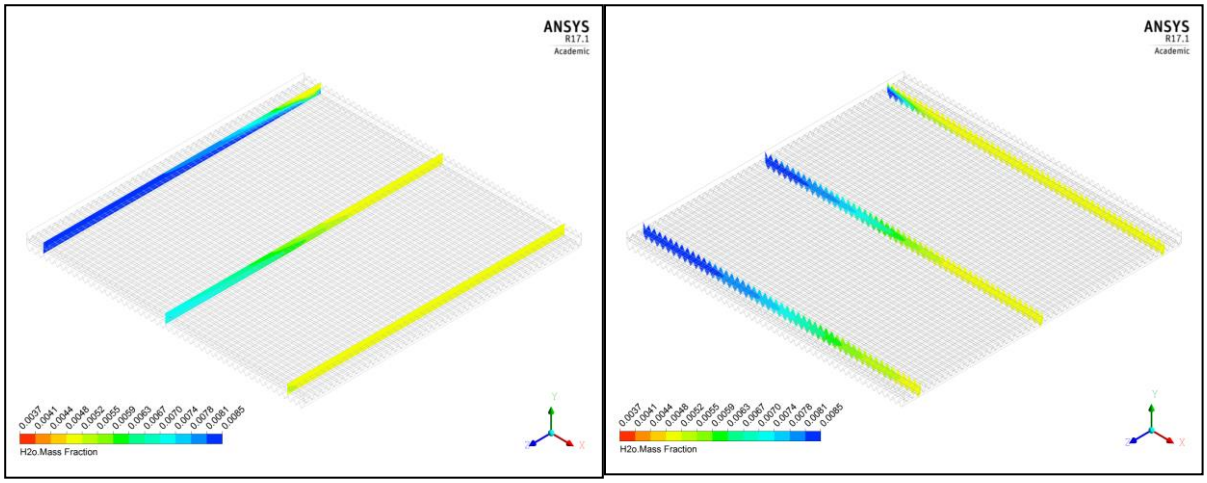


**Figure 4-81: (5mm) Humidity contours in (Left) at X-AXIS and (Right) Y-AXIS at ($T_{fi}$=6°C) and ($v_i$=0.5m/s)**

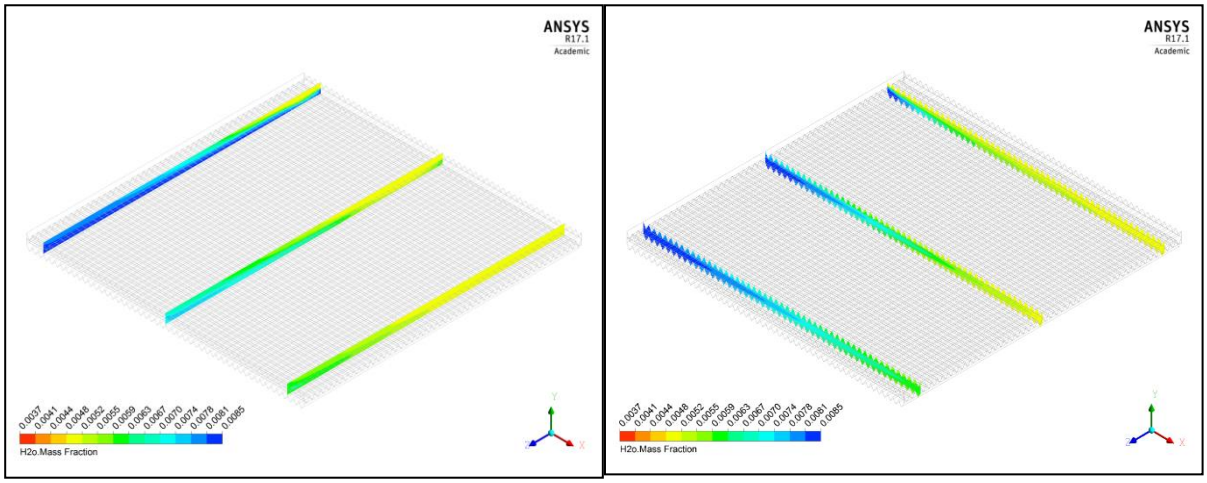


**Figure 4-82: (5mm) Humidity contours (Left) at X-AXIS and (Right) Y-AXIS at ($T_{fi}$=6°C) and ($v_i$=2m/s)**

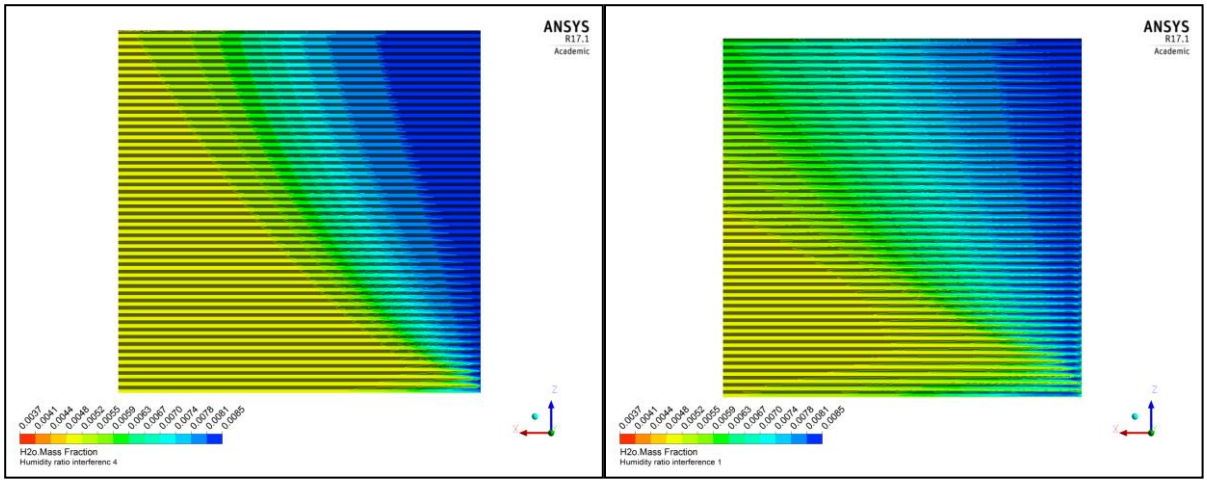


**Figure 4-83: (5mm) Temperature contours on the membrane's surface at ($v_i$=0.5m/s) (Left) and ($v_i$=2m/s) (Right) at ($T_{fi}$=6°C).**

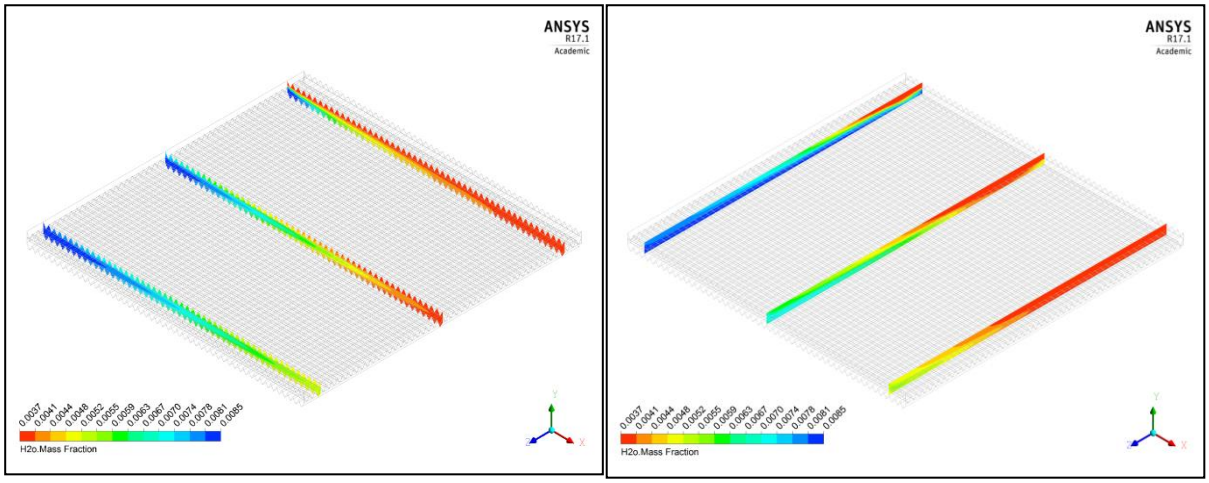


**Figure 4-84: (5mm) Humidity contours (Left) at X-AXIS and (Right) Y-AXIS at ($T_{fi}$=2°C) and ($v_i$=2m/s)**

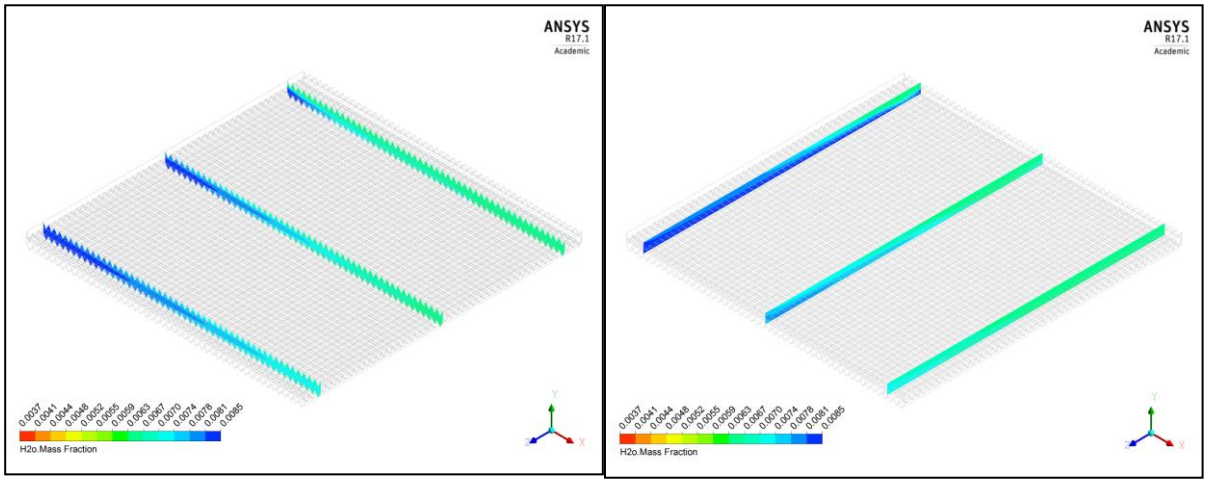


**Figure 4-85: (5mm) Humidity contours (Left) at X-AXIS and (Right) Y-AXIS at ($T_{fi}$=10°C) and ($v_i$=2m/s)**

### 4.9.4 Effectiveness Calculation

The effectiveness is considered as the most important parameter to evaluate the performance of a heat exchanger, and in the case of a membrane-based heat exchanger, there is a sensible effectiveness for the heat transfer and a latent effectiveness for the mass transfer. The values of effectiveness can be obtained from the equations [182]:

$$\varepsilon_S = \frac{T_{fi} - T_{fo}}{T_{fi} - T_{ei}} \quad 4.35$$

$$\varepsilon_L = \frac{w_{fi} - w_{fo}}{w_{fi} - w_{ei}} \quad 4.36$$

where T and *w* are the temperature and humidity fraction respectively, and the subscripts (f, e, i and o) represent fresh, exhaust, inlet and outlet, respectively. The inlet temperature and humidity for the fresh and exhaust air were given as boundary conditions, while the values in the outlet of the fresh steam where obtained from the CFD model, and were calculated using the function calculator in CFDpost17 with the outlets for each stream as average values. The sensible and latent effectiveness were calculated using the equations above.

Figures from Figure 4-86 to Figure 4-91 show the effect of the ambient temperature and the inlet velocity on the effectiveness of the exchanger, and every figure shows that when these parameters increase, the effectiveness decreases slightly, according to the individual case. Table 4-11 shows the decrease of effectiveness in details and for each case. The effect of the inlet velocity on the effectiveness is significantly higher than the effect of the ambient temperature, which is physically authentic because an ambient temperature difference range from (2 – 10 $^{o}$C) is considered relatively small and should not affect the heat exchanger performance that much and this gives the exchanger the flexibility in dealing with good range of ambient temperature without affecting the performance. This was demonstrated in this study by the simulation results and the calculated effectiveness.

This study shows that the increase in inlet velocity has the major effect on the performance of the exchanger core. The ventilation requirements to be supplied by the exchanger were based on several factors, see Chapter Three, the main two factors were the air conditioning load of the house, and to have low flow rates inside the core so that the local Reynold number did not exceed 2000, to avoid a high pressure drop across and turbulence within, the exchanger. Nevertheless, the decrease in effectiveness was still noticeable, even though this decrease was smaller the smaller the pitch length.

For the very simple case of a duct of constant cross-section the heat transfer will be (approximately) proportional to the circumference (3*a* for an equilateral triangle) while the average flow velocity will be inversely proportional to the cross-sectional area (0.444 $a^2$ for an equilateral triangle). So as the pitch length increases, the perimeter increases proportional to *a,* but the area increases proportional to $a^2$. Thus for this simple case we would expect the effectiveness [very approximately] to be inversely proportional to *a*, to increase as *a* decreased. It appears that although the structure of the current exchanger ducts is complex in shape, the same general rule holds true.

It was notices also from the effectiveness figures appointed above that the sensible effectiveness is always higher than the latent effectiveness, this is due to the existence of the moisture resistance of the Polyethersulfone membrane. The moisture resistance has different effect from the conduction thermal resistance, which is very small and has only a minor effect on the overall heat transfer resistance of the membrane and can be ignored due to the small thickness of the Polyethersulfone. For all the cases, both sensible and latent effectiveness values are close to each other in the current study, the reasons behind this are because the Polyethersulfone membrane has very low thermal conductivity of (0.13 W/m.k) with relatively high water vapour permeability and selectivity of (19,912×10-18 m2/s.Pa) and (10,500 H2O/N2) respectively, so the mass transfer parameters' effect counterpart the effect of the heat transfer ones enclosing the effectiveness values to each other.

Figures (4-91) to (4-94) show the comparison of the effectiveness between the three proposed geometries, the 5 mm case shows the highest effectiveness values next comes the 10 mm cases and, finally, the 25 mm. The highest sensible effectiveness value in this study was 81.5% and that was for the 5 mm pitch length at 6$^{o}$C ambient temperature and 0.5 m/s average inlet velocity. However, the lowest sensible effectiveness value was 65.9% and that was for the 25 mm pitch length at 10$^{o}$C ambient temperature and 2.0 m/s inlet velocity.

The latent effectiveness ranged from 81% for the 5 mm case (6$^{o}$C ambient temperature and 0.5 m/s inlet velocity) to 65% for the 25 mm case (10$^{o}$C ambient temperature and 2.0 m/s inlet velocity). The reason behind that was the contours of temperature and humidity were most uniform for the 5 mm pitch length and, as such, opposed the negative effect of increasing the inlet air velocity.

**Table 4-11: Percentage decrease in heat exchanger effectiveness with changes in air inlet velocity and humidity.**

| | | 25 mm | 10 mm | 5 mm |
|---|---|---|---|---|
| Variable inlet velocity cases | Sensible Eff. | 11% | 5% | 3.5% |
| | Latent Eff. | 13% | 4% | 3.7% |
| Variable ambient temperature cases | Sensible Eff. | 0.4% | 0.03% | 0.02% |
| | Latent Eff | 0.5% | 0.03% | 0.02% |

In order to have the have the full indication about how the physical properties simulate the effectiveness values, a sample set of tables from Table 4-12 to Table 4-15 show the extracted data from Fluent 17.1 for the (25 mm case) at (6 $^{o}$C) ambient temperature and variable inlet air velocities (0.5 m/s, 1.0 m/s, 1.5 m/s and 2.0 m/s). While the rest full tables of the properties of all of the cases are found in Appendix A.

**Table 4-12: Inlet and outlet air mass flow rate 25mm at 6°C ambient.**

| | FRESH | | EXHAUST | |
|---|---|---|---|---|
| **Velocity** | $\dot{m}_{fi}$ | $\dot{m}_{fo}$ | $\dot{m}_{ei}$ | $\dot{m}_{eo}$ |
| m/s | kg/s | kg/s | kg/s | kg/s |
| **0.5** | 0.467453 | 0.526488 | 0.441271 | 0.382261 |
| **1** | 0.934904 | 1.015185 | 0.882538 | 0.802266 |
| **1.5** | 1.402357 | 1.505411 | 1.323809 | 1.220764 |
| **2** | 1.869808 | 1.995296 | 1.765077 | 1.639602 |

**Table 4-13: Inlet and outlet air temperature 25mm at 6°C ambient.**

| | FRESH | | EXHAUST | |
|---|---|---|---|---|
| **Velocity** | $T_{fi}$ | $T_{fo}$ **average** | $T_{ei}$ | $T_{eo}$ **average** |
| m/s | C° | C° | C° | C° |
| **0.5** | 6 | 17.98 | 22 | 10.089 |
| **1** | 6 | 18.441 | 22 | 11.682 |
| **1.5** | 6 | 18.44 | 22 | 12.444 |
| **2** | 6 | 18.283 | 22 | 13.101 |

**Table 4-14: Inlet and outlet FRESH air composition rate 25mm at 6°C ambient.**

| | FRESH AIR STREAM | | | | | |
|---|---|---|---|---|---|---|
| **Velocity** | $H_2O_{fi}$ | $H_2O_{fo}$ **average** | $O_{2\,fi}$ | $O_{2\,fo}$ **average** | $N_{2\,fi}$ | $N_{2\,fo}$ **average** |
| m/s | kg/kg | kg/kg | kg/kg | kg/kg | kg/kg | kg/kg |
| **0.5** | 0.00492 | 0.00726 | 0.23 | 0.23007 | 0.76508 | 0.76267 |
| **1** | 0.00492 | 0.00747 | 0.23 | 0.22999 | 0.76508 | 0.76254 |
| **1.5** | 0.00492 | 0.00748 | 0.23 | 0.22999 | 0.76508 | 0.76253 |
| **2** | 0.00492 | 0.00744 | 0.23 | 0.23 | 0.76508 | 0.76256 |

**Table 4-15: Inlet and outlet EXHAUST air composition rate 25mm at 6°C ambient.**

| | FRESH AIR STREAM | | | | | |
|---|---|---|---|---|---|---|
| **Velocity** | $H_2O_{fi}$ | $H_2O_{fo}$ **average** | $O_{2\,fi}$ | $O_{2\,fo}$ **average** | $N_{2\,fi}$ | $N_{2\,fo}$ **average** |
| m/s | kg/kg | kg/kg | kg/kg | kg/kg | kg/kg | kg/kg |
| **0.5** | 0.00822 | 0.00553 | 0.23 | 0.229 | 0.76178 | 0.76483 |
| **1** | 0.00822 | 0.00604 | 0.23 | 0.23 | 0.76178 | 0.76394 |
| **1.5** | 0.00822 | 0.00623 | 0.23 | 0.23 | 0.76178 | 0.76376 |
| **2** | 0.00822 | 0.00637 | 0.23 | 0.23 | 0.76178 | 0.76363 |

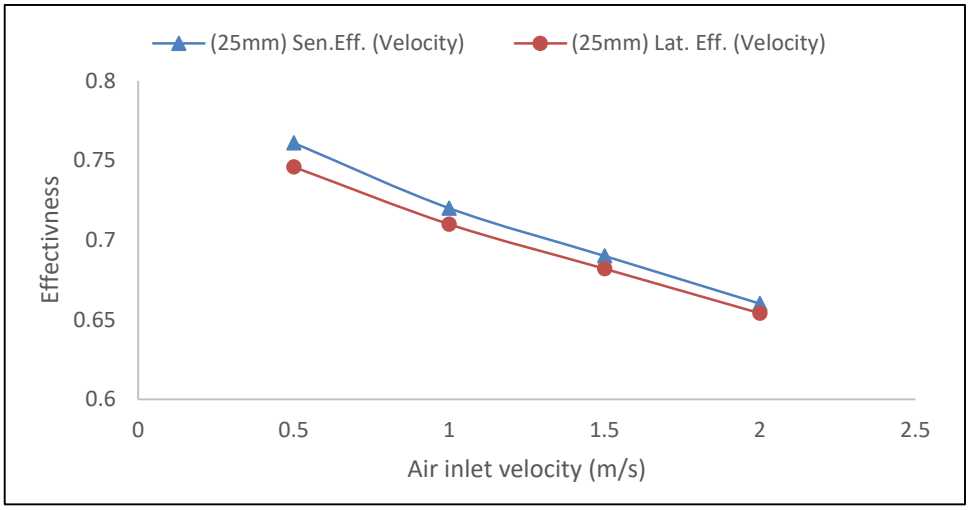


**Figure 4-86: (25 mm) Sensible and latent effectiveness and air inlet velocity (m/s)**

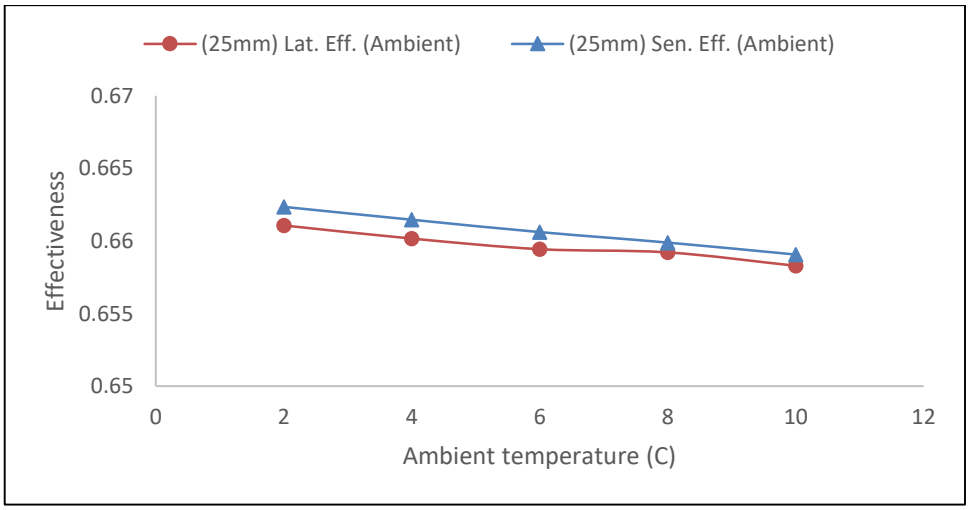


**Figure 4-87: (25 mm) Sensible and latent effectiveness and ambient temperature (C$^{o}$)**

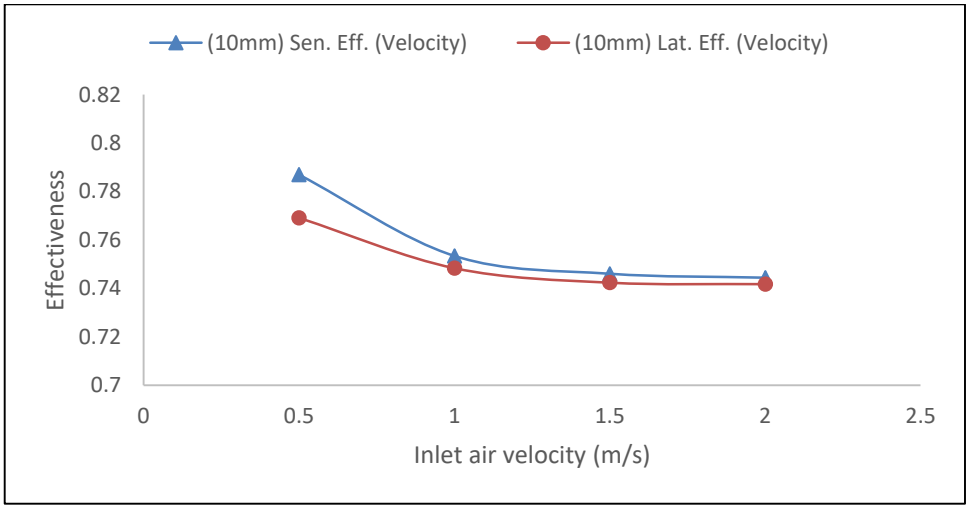


**Figure 4-88: (10 mm) Sensible and latent effectiveness and air inlet velocity (m/s)**

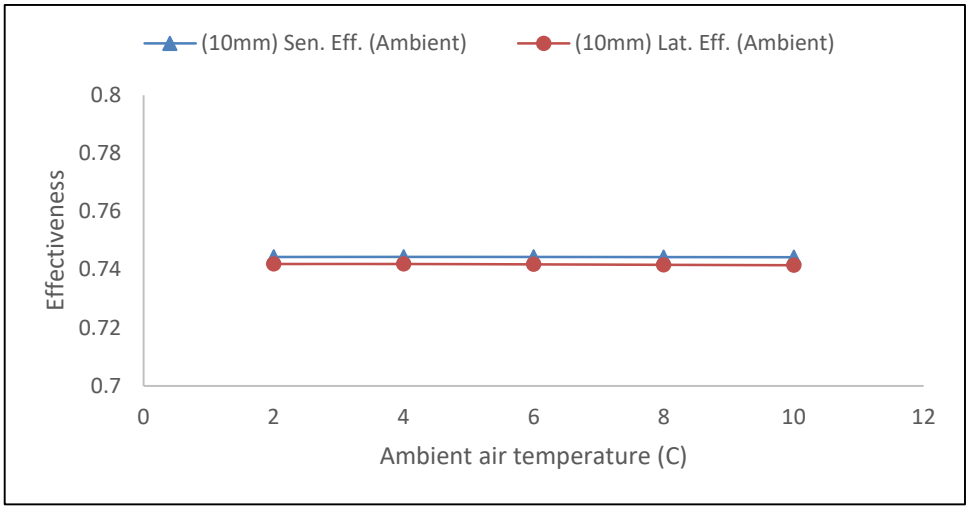


**Figure 4-89: (10 mm) Sensible and latent effectiveness and ambient temperature (Cº)**

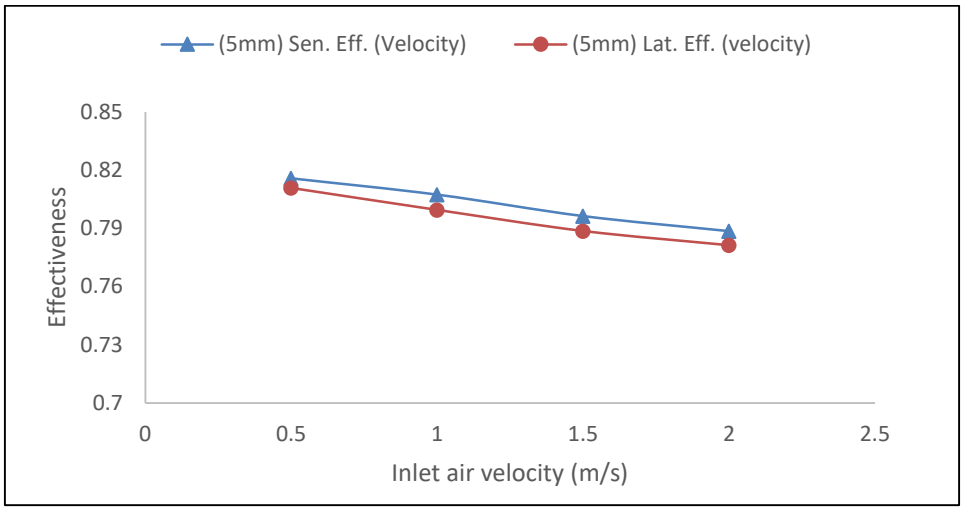


**Figure 4-90: (5 mm) Sensible and latent effectiveness and air inlet velocity (m/s)**

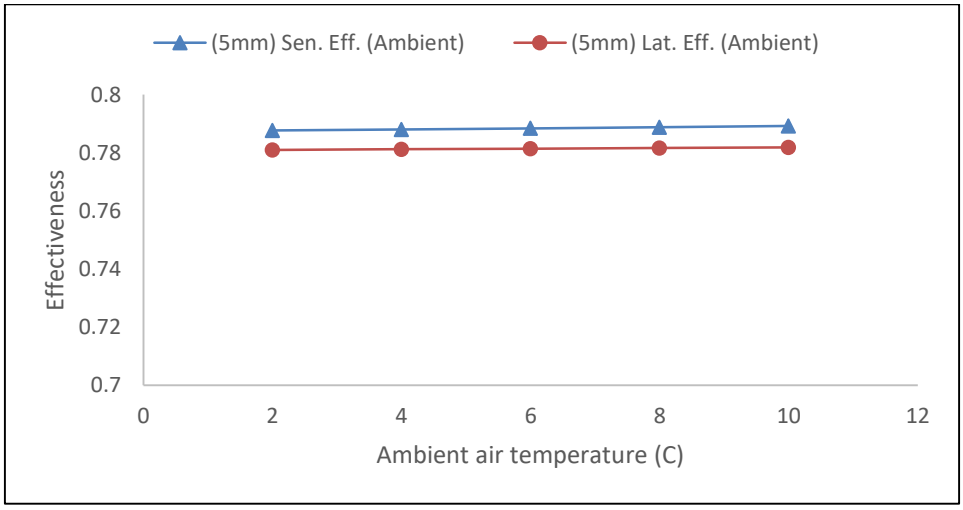


**Figure 4-91: (5 mm) Sensible and latent effectiveness and ambient temperature (Cº)**

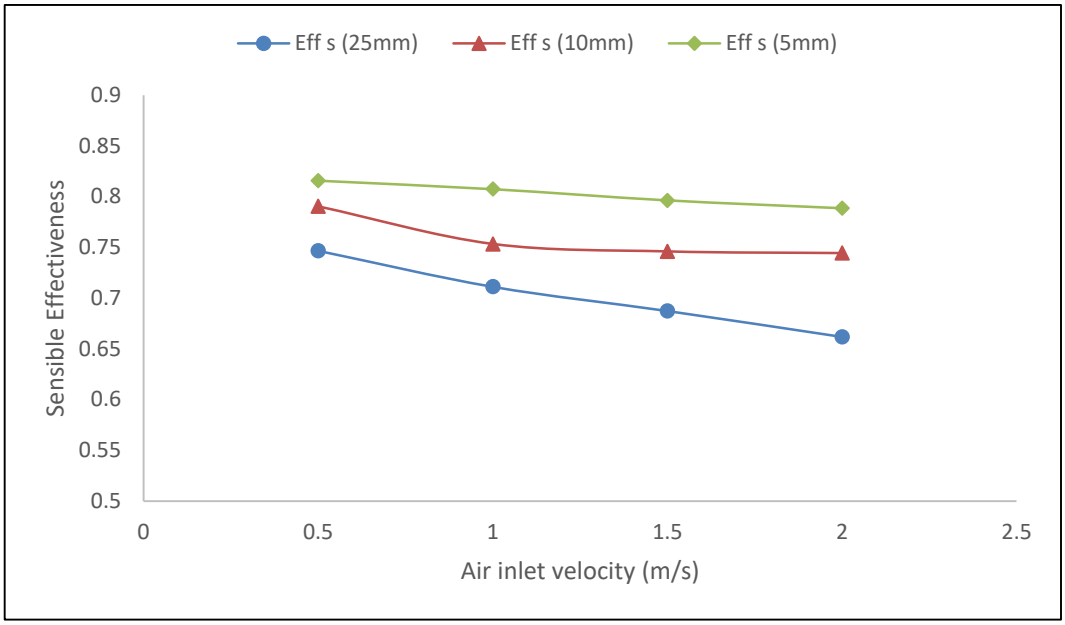


**Figure 4-92: Sensible effectiveness according to the air inlet velocity (m/s) for all three pitch lengths.**

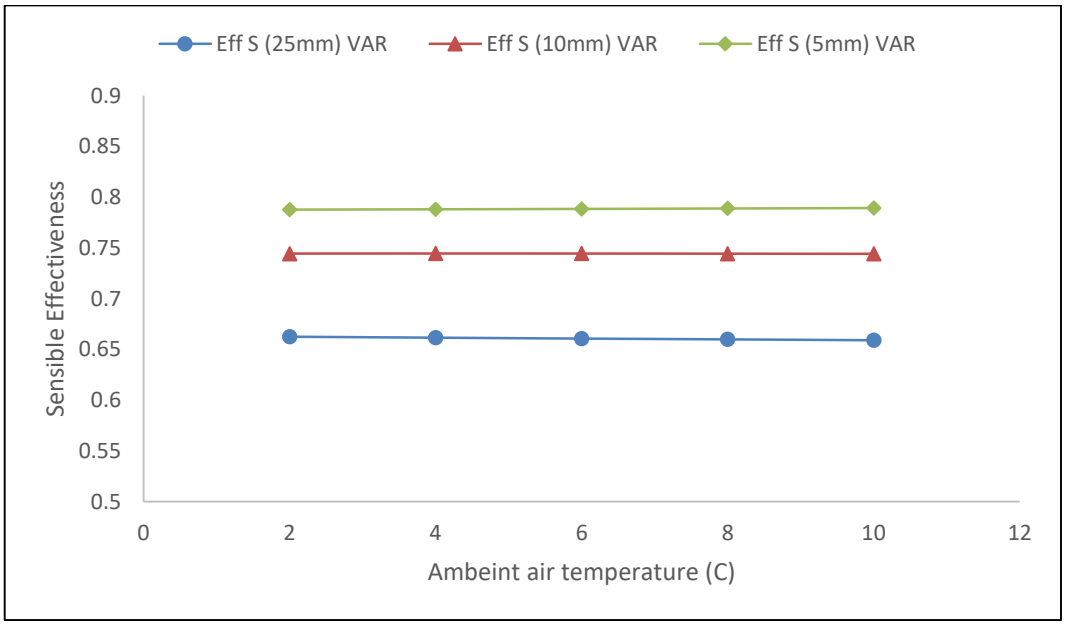


**Figure 4-93: Sensible effectiveness according to the ambient temperature (C$^{o}$) for all three pitch lengths**

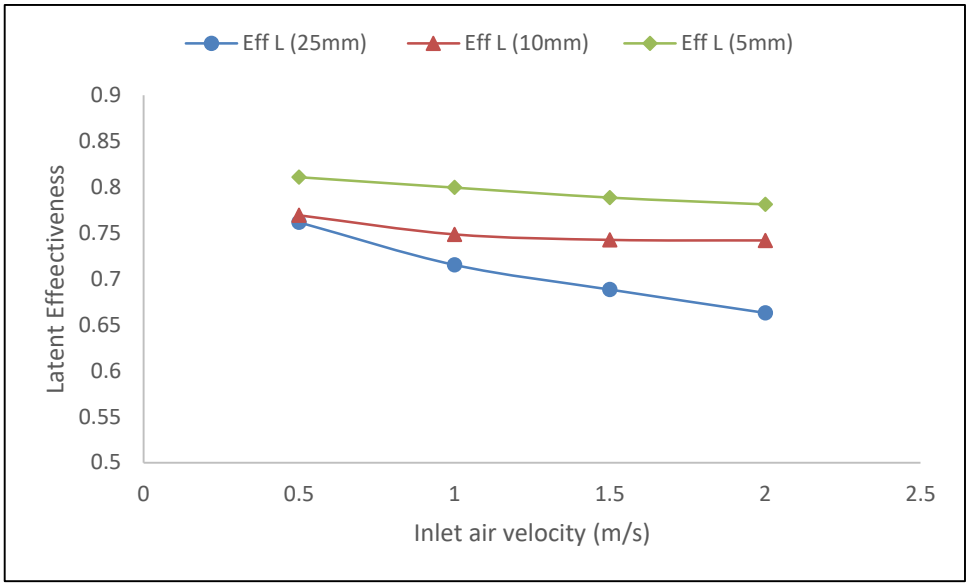


**Figure 4-94: Latent effectiveness according to the air inlet velocity (m/s) for all three pitch lengths**

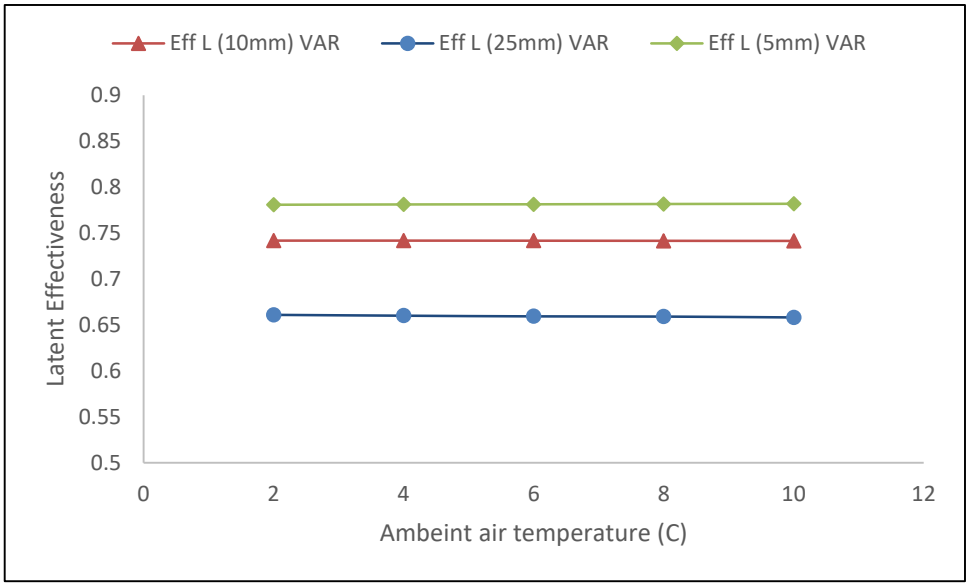


**Figure 4-95: Latent effectiveness according to the ambient temperature (C$^{o}$) for all three pitch lengths**

### 4.9.5 Nusselt Number

In heat transfer at a surface within a fluid, the dimensionless Nusselt number (Nu) is the ratio of convective to conductive heat transfer across (normal to) the boundary. In this context, convection includes both advection and diffusion. The conductive component is measured under the same conditions as the heat convection but with a (hypothetically) stagnant (or motionless) fluid layer.

Figure 4-96 shows the mean Nusselt numbers for each pitch length for different air velocities. At the highest velocity, the mean Nusselt numbers are relatively high. For fully developed flow in straight ducts of constant cross-section the fully developed Nusselt numbers, NuD, is not constant. Rather, it is a variable influenced by the Reynolds number. The Nusselt number is calculated from [181]:

$$Nu = \frac{h_f D_h}{\lambda_a} \tag{4.37}$$

where $\lambda_a$ is thermal conductivity of the air (kW/m.K), $h_f$ is the fresh air side convection heat transfer coefficient (kW/m$^2$.K) and can be calculated from:

$$\frac{1}{h_{tot}} = \frac{1}{h_f} + \frac{\delta}{\lambda_{mem}} + \frac{1}{h_e} \tag{4.38}$$

where $\delta$ is thickness of the membrane (m), $\lambda_{mem}$ is the membrane thermal conductivity (kW/m.K). $h_e$ is the convection heat transfer coefficient on the exhaust air side, and has almost the same value as $h_f$. [181]. The value of $h_{tot}$ can be calculated from:

$$h_{tot} = \frac{Cp_a \rho_a V_a \left(T_{fi} - T_{fo}\right) + \left(T_{ei} - T_{eo}\right)}{2A_{tot}\Delta T_m} \tag{4.39}$$

And

$$\Delta T_m = \psi \frac{\left(T_{fi} - T_{eo}\right) + \left(T_{fo} - T_{ei}\right)}{\ln \frac{\left(T_{fi} - T_{eo}\right)}{\left(T_{fo} - T_{ei}\right)}} \quad 4.40$$

where $Cp_a$ is the specific heat of air, $\rho_a$ is density of the air (kg/m$^3$), $V_a$ is the air flow rate of the fresh air or exhaust air (m$^3$/s). $A_{tot}$ is the total surface area of membrane (m$^2$). $\Delta T_m$ is the log mean temperature difference between the fresh and the exhaust streams. $\psi$ is a correction factor for cross flow, see Li [181], and for this study is about 0.96.

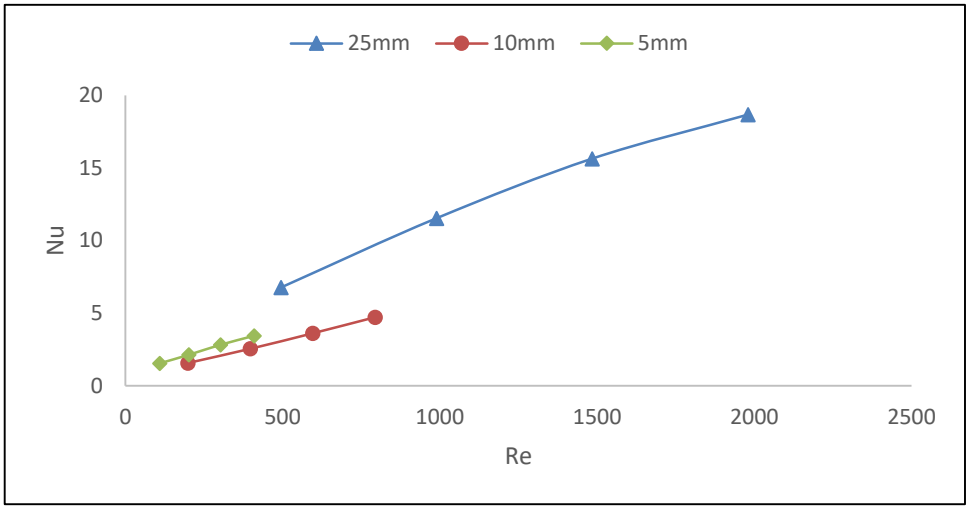


**Figure 4-96: The relation between Nusselt number and Reynolds number for the three pitch lengths**

The Re number varies between the different cases, because although the inlet air velocity range was kept same, the different pitch lengths meant different hydraulic diameters. This meant that the heat transfer by conduction inside the exchanger core increased compared to the convection. This is shown clearly in Figure 4-96, the 25 mm pitch length has the highest Nu compared to the others but all of them have a similar almost linear positive relationship between the values of Nu and Re. The different pitch lengths, and hence different hydraulic diameters. and inlet air velocity are the reasons for the differences between the cases.

### 4.9.6 Sherwood number

Sherwood number is a dimensionless number used in mass-transfer calculations. It represents the ratio of the convective mass transfer to the rate of diffusive mass transport. The Sherwood number is the equivalent of the Nusselt number in heat transfer.

The Sherwood number can be calculated from [181]:

$$Sh = \frac{k_f D_h}{D_{va}} \tag{4.41}$$

where $D_{va}$ is moisture diffusion in air ($m^2/s$), $k_f$ is the fresh air side convection mass transfer coefficient (m/s) and can be calculated from:

$$\frac{1}{k_{tot}} = \frac{1}{k_f} + \frac{\delta}{D_{vm}} + \frac{1}{k_e} \tag{4.42}$$

where $D_{vm}$ is the membrane effective moisture diffusivity ($m^2/s$). $k_e$ is the convection mass transfer coefficient in exhaust air side (m/s), and is almost the same value of $k_f$ [181]. The value of $k_{tot}$ can be calculated from:

$$k_{tot} = \frac{\rho_a V_a \left(w_{fi} - w_{fo}\right) + \left(w_{ei} - w_{eo}\right)}{2 A_{tot} \Delta w_v} \tag{4.43}$$

The log mean humidity ratio difference ($\Delta w_v$) can be calculated from:

$$\Delta w_v = \psi \frac{\left(w_{fi} - w_{eo}\right) + \left(w_{fo} - w_{ei}\right)}{\ln \frac{\left(w_{fi} - w_{eo}\right)}{\left(w_{fo} - w_{ei}\right)}} \tag{4.44}$$

The Sherwood numbers as a function of Re are shown in Figure 4-97, for the three pitch lengths. It can be seen that the values of $Sh$ increase almost linearly with increase of $Re$ for all three values of the pitch length. This was the also the case with $Nu$, and again as with Nu the results for the 25 mm pitch length show much higher values of $Sh$ than the other cases. As with $Nu$, the reason for this behaviour is due to the hydraulic dimeter and the design inlet velocity.

For both $Nu$ and $Sh$, the corrugated design affects them positively because the periodic convergent/divergent motion of the fluid enhances both the heat and the mass transfer in the exchanger core, especially with increase of the inlet air velocity.

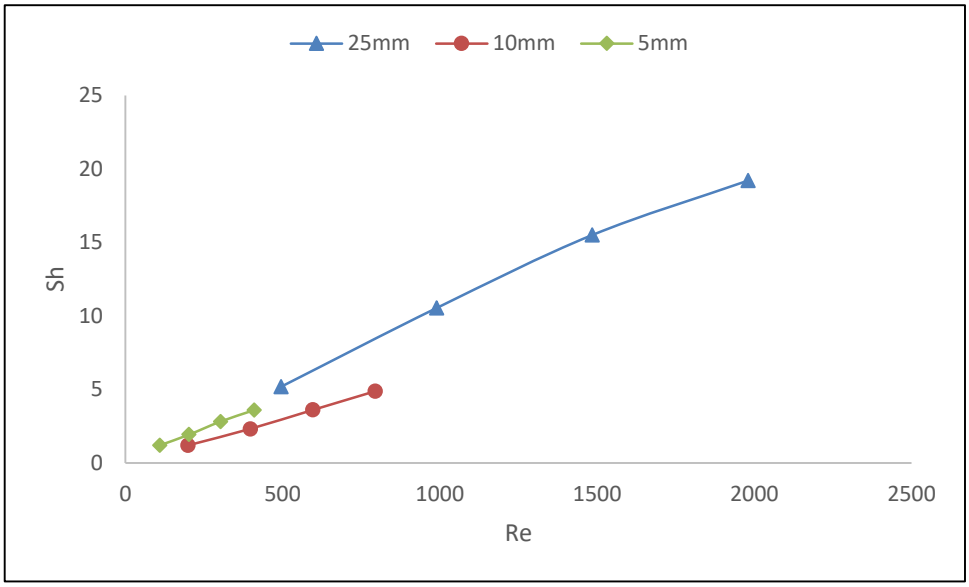


**Figure 4-97: The relation between Sherwood number and Reynolds number.**

### 4.9.7 Pressure drop

The pressure drop across a heat exchanger, the pressure difference between the inlet and the outlet, is considered one of the major design obstacles with heat exchangers. This drop occurs because of the losses inside the core due to friction, and the corrugated core obviously has a higher pressure drop compared to, e.g., flat plate exchanger cores.

The relatively higher pressure drop is an inevitable compromise which needs to be made when choosing this type of exchanger core, but it needs to be minimized. Higher pressure drop means higher energy consumption and bigger, more expensive, fans for the inlet to achieve the ventilation load.

Figure 4-98 shows the pressure drop values for the three pitch lengths for the chosen inlet air flows. In all the cases, the inlet and outlet pressure values were obtained from the CFD simulations using the function calculator in CFDPost17, and the average values were considered in the both the inlet and the outlet of the air streams.

The figure also shows the value for a (250 × 250 × 500) core dimensions for the three pitch lengths and the full range of inlet velocities (0.5, 1.0, 1.5 and 2.0 m/s). The full range of velocities is given for each pitch length in order to examine the performance of the core even at extremes to observe the best thermal and economic performances.

As expected, the duct/channel with the smallest areas (5 mm pitch length) has the highest pressure drop values due to the relative increase in friction forces due to the greater perimeter/cross-sectional area ratio. In addition, there is the relatively large number of corrugations per duct length compared to the 10 mm and 25 mm cases.

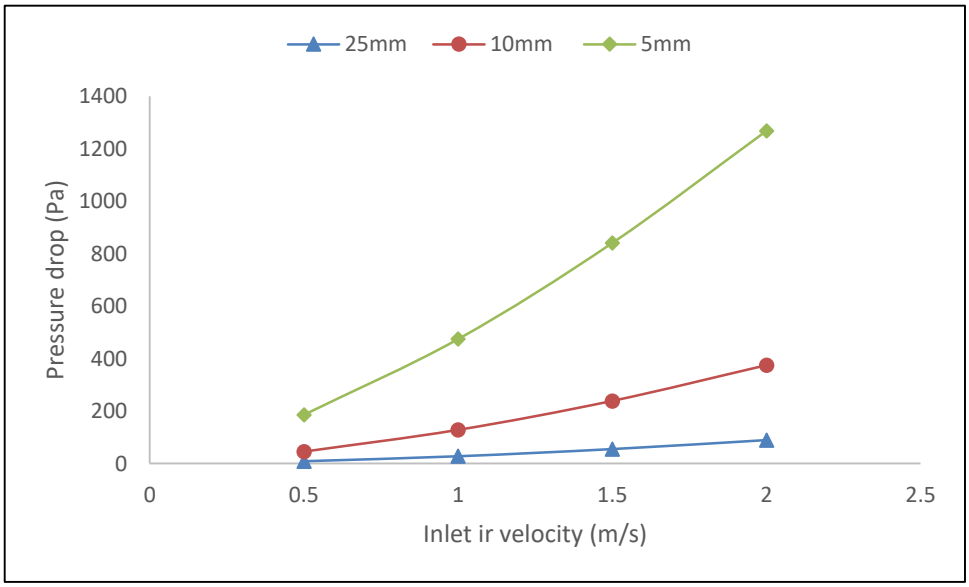


**Figure 4-98 Pressure drop across heat exchanger of (250 × 250 × 500 mm) dimensions for three pitch lengths with change in inlet velocity**

Table 4-16 however, shows the values of the pressure drop for the all of the proposed core designs depending on the inlet air velocity and the number of channels in each core. The dimensions of the exchanger core as mentioned in Chapter three are **(250 × 250 mm) (length × width)**, and these dimensions are the same for the three distinctive designs with the different pitch length. The 25 mm cases show the lowest pressure drop values comparing to the other cases. This table could be expanded as a tool to select for the most appropriate core for the future industrial production.

**Table 4-16: selection table for the presented exchanger core designs.**

| | | **Heat exchanger core height (mm)** | | | | | |
|---|---|---|---|---|---|---|---|
| | | **100** | **200** | **300** | **400** | **500** | |
| **Pitch length (mm)** | **5** | 22 | 42 | 62 | 82 | 102 | **Number of channels/layers** |
| | | 4.5 | 2.3 | 1.5 | 1.1 | 0.9 | **Average Inlet velocity** (m/s) |
| | | 640 | 672 | 515 | 680 | 479 | **Pressure drop** (Pa) |
| | **10** | 12 | 22 | 32 | 42 | 52 | **Number of channels/layers** |
| | | 5.1 | 2.3 | 1.5 | 1.2 | 0.9 | **Average Inlet velocity** (m/s) |
| | | 1200 | 212 | 150 | 197 | 130 | **Pressure drop** (Pa) |
| | **25** | 6 | 10 | 14 | 18 | 22 | **Number of channels/layers** |
| | | 2 | 1 | 0.7 | 0.5 | 0.4 | **Average Inlet velocity** (m/s) |
| | | 25 | 14 | 20 | 10 | 11 | **Pressure drop** (Pa) |

## 4.10 Energetic analysis summery

Having completed the CFD simulations for the cross-corrugated exchanger, the results show that the 5 mm pitch length provides best thermal performance, i.e., temperature and humidity transfer. However, the 5 mm size had two major drawbacks; the first one is the very large pressure drop across the heat exchanger, and the second on is the difficulty in manufacturing membrane sheets with such small pitch length.

The selection process depends on the manufacturer choosing the best core and successfully commercializing it. In this study, the most convenient core with which to achieve the required ventilation loads lies between higher effectiveness for the 10 mm geometry and the lower pressure drop for the 25 mm pitch length.

# 5 EXERGY ANALYSIS

## 5.1 History and Background

Sadi Carnot in 1824 distinguished between the quality of different forms of energy by introducing the relationship between heat and work. The first general relationship of work was introduced by Gibbs in 1873. The word ‘exergy’ was initially suggested by Rant in 1953. Exergy is also known as available energy or availability and is the maximum amount of useful work that may be produced by a system in a reversible operation [133].

Exergy increases as energy is added to a stream and decreases as energy is extracted from the stream. The condition of a system is considered to deviate more from its environment as exergy increases, because at a zero exergy value it achieves equilibrium with the environment: no pressure, temperature, or concentration differences between them. Exergy analysis is used with the principles of conservation of energy and conservation of mass, together with the second law of thermodynamics. Exergy analysis is a useful tool for helping to achieve more efficient use of energy resources. Figure 5-1 shows the portion of total energy that cannot be converted into work, this is called the unavailable energy or in other words, entropy generation [183].

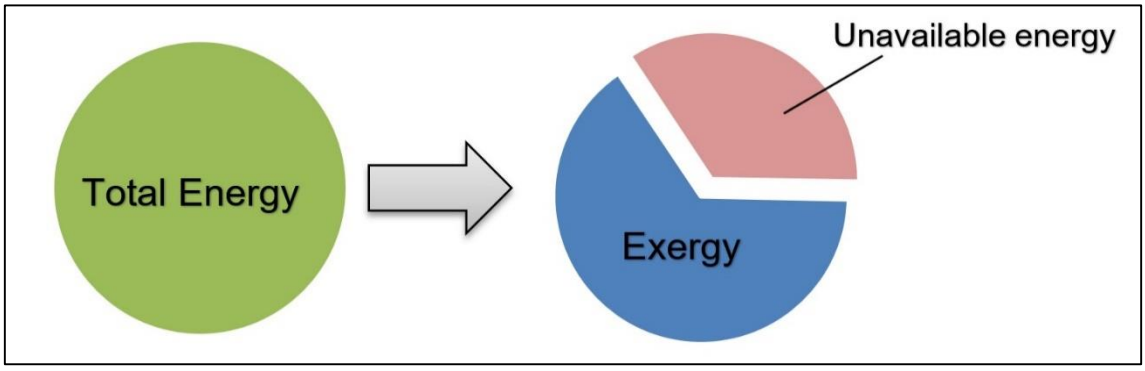


**Figure 5-1: The energy portion that cannot be converted in to work is unavailable energy**

There are many differences between energy and exergy, as illustrated in Table 5-1, the main difference is that exergy can be destroyed.

**Table 5-1 Comparison between ENERGY and EXERGY** [133,183]

| Energy | | Exergy | |
|---|---|---|---|
| **1** | Conserved, based on the first law of thermodynamics | **1** | Not conserved in real processes, based on the second law of thermodynamics |
| **2** | Has a value at equilibrium | **2** | Equal to zero at equilibrium |
| **3** | Cannot be destroyed | **3** | Can be destroyed |
| **4** | Measures quantity only | **4** | Measures both quantity and quality |

## 5.2 The Theory Behind Exergy

The thermodynamics is based on two essential natural laws, known as first law of thermodynamics (FLT) and second law of thermodynamics (SLT). The FLT is simply an expression of the principle of the conservation of energy. The SLT states that energy consists of both quality quantity, and that real thermodynamic processes takes place in the direction of declining the quality of energy: high temperature thermal energy degrades as it transfers to a lower temperature body. The attempt to quantify the quality or work potential of energy in the light of SLT has the result of defining the property named exergy as the useful work potential (also called available energy) of a given amount of energy at a specified state. The work potential of energy contained in a system at a specified state relative to reference (dead state) is simply the maximum amount of useful work that can be obtained from the system [184,185]

The nature of exergy is opposite to that of entropy in that exergy can be destroyed. Therefore, exergy analysis is thermodynamic analysis based on entropy generation minimization (EGM), and provides an alternative and illuminating means of assessing and comparing processes and systems rationally and meaningfully. In particular, exergy analysis yields efficiencies which provide a true measure of how nearly an actual performance approaches the ideal and identifies more clearly than energy analysis the causes and

locations of the thermodynamic losses, and the impact of the built environment on the natural environmental. There will always be a difference, large or small between exergy and the actual work delivered by a device. This difference represents the available room for improvement in the efficiency of the device. Thus exergy analysis can assist in improving and optimizing the design of all energy systems including air conditioning [134].

The exergy change of the system during a process is less than the exergy transfer by an amount equal to the exergy destroyed during the process within the system boundaries. The exergy change is equal to the difference between the net exergy transfer through the system boundaries and exergy destroyed within the system as a result of irreversibilities such as friction, mixing, heat transfer processes, expansion and compression, which always destroy exergy and which always generate entropy. The exergy destroyed is proportional to the entropy generated and EGM is an approach that can be used to optimize the system [133,134].

## 5.3 Ventilation Systems Thermal Analysis

When a system is subject to thermal analysis the result is usually the efficiency of that system. In the case of a total recovery ventilation system the resultant would be the effectiveness of the exchanger core. However, there are two thermodynamic efficiencies, namely the energy and exergy efficiencies. Although energy efficiency is commonly used for performance assessment, exergy efficiency is more beneficial, since it considers irreversibility, and presents the actual performance of the system.

By considering both of these efficiencies, the most effective use of energy can be achieved. Improving efficiency of the heat recovery system is an important challenge for meeting energy conservation objectives. Thus, most industrial companies working in this field have directed their research and development projects to improving design of systems as a whole, as well as improving the performance of the exchanger core. This has meant, for example, reducing the power consumption of the air blowers, and so reducing the pressure across the core, one of the major problems for cross-corrugated exchangers [185].

An engineer designing a system is usually expected to aim for the highest reasonable technical efficiency at the lowest cost under the prevailing technical, economic and legal conditions. Exergy methods can assist in such activities and offer unique insights into possible improvements with special emphasis on the environment and sustainability [185].

## 5.4 Exergetic Analysis

Exergy analysis is a useful tool for analysing the current system by evaluating the locations, types and magnitudes of the losses in the system. Exergy analysis also reveals whether and by how much it is possible to reduce inefficiencies in the design of air conditioning systems [185].

The total heat recovery system is usually evaluated through energetic criteria based on the first law of thermodynamics, but energy analysis cannot provide information about the degradation of energy during a process, nor the quality of various forms of energy. These limitations have been overcome by exergy analysis which can determine the locations and magnitude of degradation in a thermal power system process, revealing the source of irreversibility inefficiencies.

The exergy associated with work, and heat and mass transfer, in the frame of the second law can lead to a clearer understanding of the exergy concept, which is not only critical for plant efficiency but also for the economic and environmental analyses [185].

## 5.5 Exergy Associated with Heat Transfer

A thermodynamic system at a specified temperature and pressure above the ambient conditions will exchange heat with its environment. The system’s internal energy tends to reduce toward equilibrium with the environment. The exergy of heat transfer is the maximum conversion of thermal energy to work. The thermal energy represents the amount of energy transfer to the environment until reaching equilibrium, complying with zeroth law of thermodynamics [183,186].

## 5.6 Exergy Associated with Work

Generally, work is equivalent in magnitude and direction to exergy because it is considered high-energy quality in comparison to heat energy. Exergy associated with work is completely available and has the ability to transform into other forms of energy. [133,134,186].

## 5.7 Types of Exergy

Exergy associated with an open system consists of four components in the absence of nuclear, magnetic, electric, and surface tension effects. These components are physical, kinetic, potential, and chemical. All of them represent the deviation of the system at a specified intensive property with respect to a reference state. The exergy, $\dot{E}_x$, consists of the sum of four distinct components: $\dot{E}_{ph}$ physical exergy, $\dot{E}_{ch}$ chemical exergy, $\dot{E}_{ke}$ kinetic exergy and $\dot{E}_{pe}$ potential exergy. The total value can be expressed as:

$$\dot{E}_x = \dot{E}_{ph} + \dot{E}_{ke} + \dot{E}_{pe} + \dot{E}_{ch} \quad 5.1$$

### 5.7.1 Physical Exergy

Physical exergy ($\dot{E}_{ph}$) is a maximum useful work that can be extracted from a unit mass of substance passing from a specified state ($Ts$, $ps$) to the environmental or reference state ($To$, $po$) in a purely physical process [134]. It also refers to mechanical and thermal energy which is a function of pressure and temperature differences. The physical exergy, defined by the following expression, cannot be entirely converted to useful work due to entropy generation. The physical exergy consists of two parts: mechanical and thermal exergy.

$$\dot{E}_{ph} = \dot{m}[(h_s - h_o) - T_o(s_s - s_o)] \quad 5.2$$

where h is the enthalpy and S is the entropy and both of them are for air, subscripts $s$ and o represent specified stream and reference states respectively.

Once the temperature of a specified stream is equal to the reference state value $Ts = To$ for gases and, based on the ideal gas relation, the equation becomes:

$$\dot{E}_{ph} = \dot{m}_e R T_o ln \frac{P_e}{P_o} \quad 5.3$$

where the symbols have their usual meaning.

### 5.7.2 Chemical Exergy

Chemical exergy ($\dot{E}_{ch}$) is associated with mass flows from an environmental state to a dead state due to differences in concentration and molecular structure. The maximum useful energy that can be extracted during this process represents chemical exergy. This process is limited by the exchange of substances and heat within the environment. In the environmental state, the system is mechanically and thermally, but not chemically, in equilibrium with the local environment. Norio Sato [187] has pointed out that all chemical substances have chemical energy and that exergy is driven by chemical potential. The chemical exergy is divided into two parts. The first part, reactive exergy, is due to differences in the chemical concentration between the system and the environmental state. The second part is purifying exergy, or dilution due to element separation from the composition.

The chemical exergy is very important in the process of humidity transfer in the cross-corrugated membrane core due to the transfer of the water vapour between the two streams. This type of exergy is subjected to degradation and for a gas mixture can be calculated using:

$$E_{ch} = \dot{n}[\sum y_k \, \bar{e}_k^{ch} + \bar{R} T_o \sum y_k \, ln \, y_k] \quad 5.4$$

where $y_k$ and $\bar{e}_k^{ch}$ are molar fraction and molar chemical exergy for component *k* in the mixture, $\bar{R}$ is the gas constant (8.314 J/mol.K) and $T_o$ is the reference temperature. Standard chemical exergy tables show different molar values for chemical exergy based on the particular substance [133].

### 5.7.3 Kinetic Exergy

Kinetic exergy ($\dot{E}_{ke}$) is related to ordered movement. This form of exergy, which does not function as a substance or mixture, depends on mass and velocity and is convertible to work. There are no destruction or entropy generation terms. Kinetic exergy is considered crucial when exhaust gases directly interact with the environment; it is considered separate from exergy loss in most studies.

$$\dot{E}_{ke} = \frac{1}{2}\dot{m}V^2 \qquad 5.5$$

### 5.7.4 Potential Exergy

Potential exergy $\left(\dot{E}_{pe}\right)$ is related to the elevation of particles above a reference level. This form of exergy depends on mass and is fully convertible to work. The potential exergy is similar to kinetic exergy in that it does not depend on substances or mixtures and there is no destruction or entropy generation. Most studies neglect the effect of potential exergy due to its insignificant levels. Accordingly, potential exergy is omitted in the present study.

## 5.8 Reference and Dead State

The thermal power system or its components operate within the surrounding environment. There is a difference between surroundings and the environment; the latter is a portion of the former. The surroundings are not part of the system whereas the environment is. The reference or environment adjacent to the system boundary is assumed to have uniform intensive properties. The phase change in the process has insignificant effects on the environmental state, which is almost free from irreversibility.

At the reference state the system stays mechanically in equilibrium with the environment, (i.e., pressure and temperature are equal). At the dead state the system is mechanically and chemically in equilibrium with environment, (i.e., pressure, temperature, and chemical potential are equal between them).

## 5.9 Waste Exergy

Energy waste in thermal power systems is divided into two parts: exergy destruction, which is directly related to irreversibility within a system, and exergy loss, which is associated with the rejection of energy into the environment at the end of a process.

### 5.9.1 Exergy Losses

Exergy loss is controllable by the designer of the system. Exergy loss is associated with the ejection of energy to the environment at the end of a process and in the current case is the energy ejected into the house.

### 5.9.2 Exergy Destruction

Exergy destruction ($\dot{E}_d$) during a process is proportional to entropy generation due to irreversibilities within each component in the process. There are many sources that cause irreversibility, such as chemical reactions, mixing, friction, heat transfer driven by finite temperature differences, and non-quasi-equilibrium compression or expansion. Tsatsaronis et al., [188,189] split exergy destruction into 'avoidable' and 'un-avoidable' groups in order to relate exergy destruction to economic costs in a thermal power system. This approach to classification of exergy destruction improves our understanding of thermal design systems by providing very useful information about interactions between system components. Kelly et al., [190] have highlighted the importance of beneficial improvements to other components rather than improvements to only the highest exergy destruction component.

The exergy balance equation shows energy degradation due to the irreversibility in the process. For steady-state processes, the balance equation can be expressed as:

$$\dot{E}_d = \sum \dot{E}_i - \sum \dot{E}_e \qquad 5.6$$

where $\dot{E}_i$ and $\dot{E}_e$ are the input and exit exergies.

## 5.10 Exergetic Efficiencies

Exergetic efficiency ($\eta_{ex}$) is a parameter that measures thermodynamic performance of a power system. The exergetic efficiency is also known as rational efficiency or second law efficiency and depends on the fuel used and products produced by the thermal power system. Exergetic efficiency is the ratio of produced exergy ($\dot{E}_p$) to fuel exergy ($\dot{E}_f$) supplied to the system. The quality of energy, exergy waste, and type of component is taken into account in the evaluation. Rephrasing, we can say; the exergetic efficiency is the ratio of total exergy output to total exergy input, i.e.:

$$\eta_{ex} = \frac{\dot{E}_p}{\dot{E}_f} = 1 - \frac{\dot{E}_d + \dot{E}_l}{\dot{E}_f} \qquad 5.7$$

where $\dot{E}_d$ and $\dot{E}_l$ represent the rates of exergy destruction and exergy loss.

## 5.11 Exergetic Analysis Modelling

In this section, the basics of the modelling are explained; including the simulation software and how to achieve the exergetic analysis for total recovery systems. The need for simulation and computational method has become an important factor in most recent studies, in order to save both time and money. With the reliability, repeatability, control and flexibility of these modelling methods, they have proved that it is acceptable to depend on them in order to examine and evaluate the behaviour of system including the current proposed model under a wide range of conditions.

The software used in this study was **IPSEpro**, published by the SimTech Company [191], which provides modelling tools and services for the power industries. IPSEpro is a set of software modules that creates, analyses and utilises models for new or existing process plants throughout their life cycles.

IPSEpro is a very flexible modelling system for calculating heat balances and simulating processes. At the first level, it allows any problem to be represented graphically and mathematically as a network of collected and connected components. This can be carried out by using the model development kit (MDK). At the second level, calculations are performed in the process simulation environment (PSE) from which results are obtained [192,193].

IPESpro is designed to simulate thermal power plants, the developer of this software not only made it possible to accurately simulate heat exchangers but also built into it several modules to predict performance, modify plans to control existing power plants and monitor and optimize plant performance [194]. IPSEpro software has been successfully used by industrial and research companies such as Rolls-Royce and NaREC and It also has the flexibility to work with other thermal processes such as air conditioning systems [192].

Giglmayr, et al. [195], carried out an evaluation of 18 types of simulation software for thermodynamic calculations. The comparison was performed on a two-pressure heat recovery steam generator with a water steam cycle and a heating condenser; design and off-design cases were also used. IPSEpro was proven to be accurate and was recommended for thermodynamic simulations. The output data from the real plant used in this study was collected and modelled accurately using this software [191,196] .

## 5.12 Total Recovery System Modelling

The main energetic analysis, of the heat exchanger core was the focus of the CFD simulation only in order to examine the thermal performance of the exchanger alone. However, the exergy analysis does not operate this way. It was necessary to design a complete system with power input and energy output which behaved like a closed system to make it compatible with the IPSEpro capabilities.

The proposed system consists of the house as the environment, the main heat extraction medium, the membrane core as the working medium and one fan each for the inlet and the outlet air streams which are the power providers to the system. To close the system, the ambient medium is assumed to be at a constant design temperature depending on the particular case studied. Figure 5-2 shows the schematic diagram for the system, all the components and the thermal processes for the exergetic analysis.

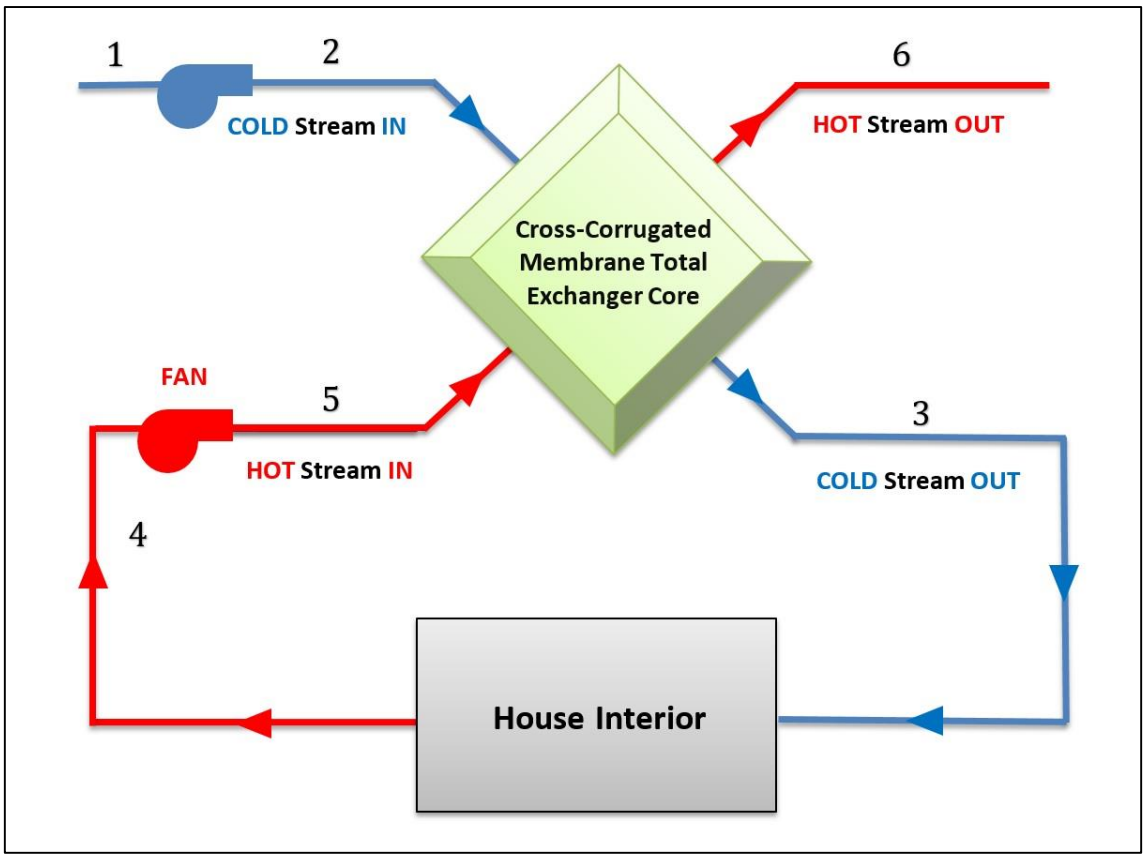


**Figure 5-2 Schematic diagram for the air conditioning system, showing the components and the thermal processes for the exergetic analysis**

### 5.12.1 Modelling Data of the Total Recovery System

The data for this study were collected from CFD simulation using the function calculator in the CFDPost software. This supports the validation of the IPSEpro, which is the main tool used in this study. Since heat recovery exchangers for domestic housings are very small compared to commercial power plants, the opportunity for modelling and simulating such a small-scale exchanger core and its surrounding proposed system has been a great challenge for this exergetic study.

The extracted data from the energetic study were the inlet and outlet temperatures of the air streams, the pressure difference before and after the membrane core the air composition before and after the core, the air mass flow rate before and after the core and for both fresh and exhaust air streams. The air compositions were in the form of mass fractions of Nitrogen, Oxygen and water vapour both before and after the exchanger core.

### 5.12.2 The Process Simulation Environment (PSE)

PSE played an essential role in the IPSEpro modelling [193]. The software has a model library from which component can be extracted to create the system model. This allows optimization of the reliability and accuracy of the mathematical calculations applied to the system components in order to analyze them. The IPSEpro software gives the flexibility to select any component from the model library which could be done with ease using a side bar in the PSE window [196]. Accordingly, any proposed model could be constructed easily in a flow sheet editor even for a one component process. Figure 5-3 shows a selected screen shot of the IPSEpro for a heat exchanger duct of pitch length 25 mm.

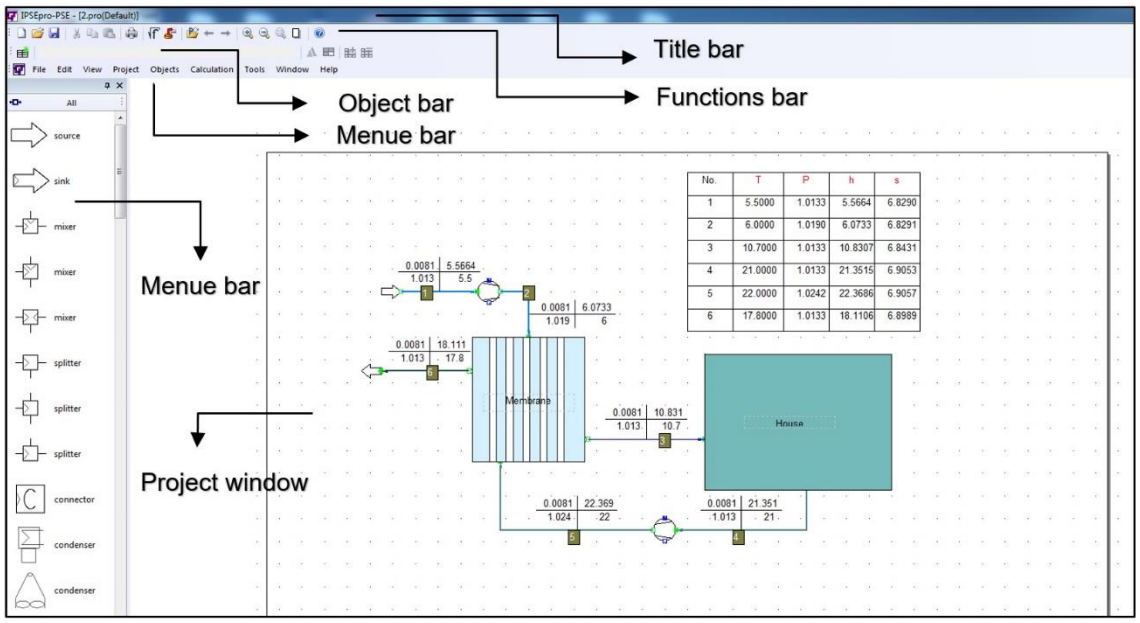


**Figure 5-3 Screen shot of the IPSEpro for a heat exchanger duct of pitch length 25 mm**

The mathematical analysis was carried out by PSE, and the numerical solution produced accordingly. PSE determines a suitable method at the analysis stage that will achieve the optimum solution. PSE has the flexibility to combine several equations simultaneously into groups for the solution stage, and the optimum numerical method would be selected during the analysis stage.

In the numerical solution stage, the parameters and variables in the system undergo an iterative process until the relative change in all the parameters becomes less than a threshold value, $E_x$, or the function residual (the difference between the left and the right side of each equation) is less than a threshold, $E_f$. The PSE uses the X-tolerance ($E_x$) as the total error for all variables, and the Y-tolerance ($E_f$) as the total error for all equations.

Based on the assumption that each variable contributes equally to the system solution, and the total number of variables in the system can be abbreviated as ($n$), the error permitted for a single variable is:

$$\varepsilon_x = \frac{E_x}{\sqrt{n}} \qquad 5.8$$

And the error permitted for a single equation is:

$$\varepsilon_f = \frac{E_f}{\sqrt{n}} \tag{5.9}$$

If an error takes place while the system is in the process of solving the equations, PSE terminates the solution process and issues an error message showing that the system of equations is either structurally or numerically singular, or does not converge within the given number of solution steps, or that an error has occurred in the built-in or external numerical functions.

PSE offers a wide range of controlling and monitoring functions such as: Default value editor, Solver parameters, Free equations editor, Dataset manager, Calculation protocol, Data frame, Data table sheet and Measurement editor.

Default values are used for the default value editor including the variables, parameters, switches and tables in order to reduce the required time for data entering. The default data are taken from the database of the IPSEpro that can be configured using the IPSEpro model development kit (MDK).

The relation between the different entities in the PSE project were established using the free equation editor. This editor is almost like a model equation, however, it does not belong to a single entity, whereas, the free equation editor is associated with an individual PSE project database. The syntax of the free equations and the standard model equations are the same, and the model description language (MDL) is used by both.

The PSE can send and receive any project file to/from any other IPSEpro user via e-mail, allowing the exchange of pre-defined information between the projects using the templates and macros which shortens project work time.

### 5.12.3 Process Simulation MS Excel (PS Excel)

The module PSE-MS Excel can exchange data between PSE and MS Excel. The PS Excel provides a particular MS Excel template and add-on which are (PSExcel.xlt) and (PSExcel.xla) respectively, and which act as the link between the two software packages when exchanging data. The data could be integrated into an MS Excel sheet from the PSE project and used to illustrate the project report. PSE-MS Excel could also change calculations contained in the PSE project by varying the values of some items in the component models.

The variations in data in the PSE project is used in PS Excel with ease, and all the results and variations can be presented in MS Excel in the form of diagrams or charts. The results could be performed for (n) number of variations, for different input data. Thus, all the simulated result from the IPSEpro were transferred to MS Excel sheets using the above integration in order to calculate all the parameters in the exergetic analysis.

## 5.13 Exergetic Analysis Results and Discussion

The variables input to the IPSEpro software are inlet and outlet temperatures ($^{o}$C), inlet and outlet humidity ratios (kg/kg) for the membrane core, and the pressure drop in the core (Pa). All these variables were taken from the CFD simulation in the energetic analysis, using the CFDpost17 function calculation tool and are shown in Appendix A. The air inlet velocity also plays a major role in determining the outcome of the IPSEpro results, however, the software can deal only with mass flow rates. The inlet and outlet mass flow rates (kg/s) for the membrane core were also considered. The CFD results gave the average mass flow rate per channel, so by multiplying this by the number of channels in each design gave the required mass flow rate for the whole membrane core which used in the IPSEpro software. The total recovery system was drawn and illustrated by using the icons in the menu bar in the IPSEpro according to the schematic diagram in Figure 5-2, the outcome of the system model in the software was shown in Figure 5-3 for a 25 mm pitch length. Six air states were considered in the modelling as shown in Table 5-2.

**Table 5-2: Air states points through the system**

| Point | Location |
|---|---|
| 1 | Fresh air inlet - Fan |
| 2 | Fresh air outlet (Fan/inlet) - Membrane |
| 3 | Fresh air outlet - Membrane |
| 4 | Exhaust air inlet - Fan |
| 5 | Exhaust air outlet (Fan/inlet) - Membrane |
| 6 | Exhaust air outlet - Membrane |

The IPSEpro then analysed the system and calculated the properties of all the air states in the system. The most important parameters in the exergy analysis are the entropy (*S*) and the enthalpy (*H*) which are both calculated in Joules since they are both types of energy. These parameters have a significant effect on the exergy analysis. The PSExcel exported and transferred the modelled date to the MS Excel worksheet where the exergy calculations took place. Samples of the modelled case diagrams of the 10 mm and 5 mm pitch lengths in the IPSEpro are shown in Figure 5-4 and Figure 5-5

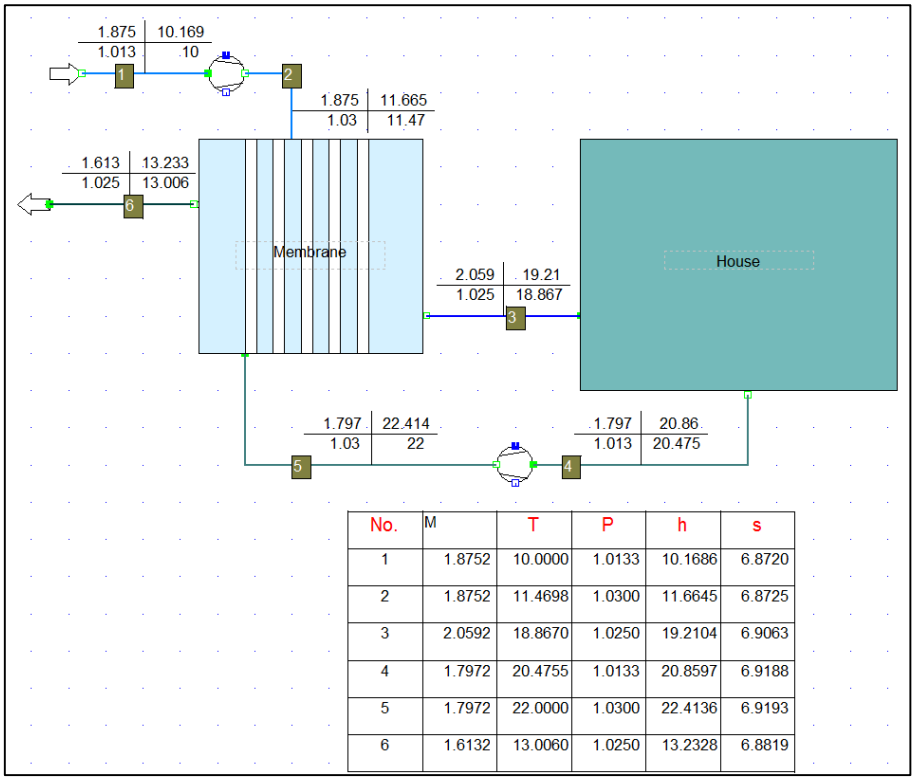


| No. | M | T | P | h | s |
|---|---|---|---|---|---|
| 1 | 1.8752 | 10.0000 | 1.0133 | 10.1686 | 6.8720 |
| 2 | 1.8752 | 11.4698 | 1.0300 | 11.6645 | 6.8725 |
| 3 | 2.0592 | 18.8670 | 1.0250 | 19.2104 | 6.9063 |
| 4 | 1.7972 | 20.4755 | 1.0133 | 20.8597 | 6.9188 |
| 5 | 1.7972 | 22.0000 | 1.0300 | 22.4136 | 6.9193 |
| 6 | 1.6132 | 13.0060 | 1.0250 | 13.2328 | 6.8819 |

**Figure 5-4: Model for 10 mm pitch length in IPSEpro at $10^0$C ambient temperature and 2.0 m/s inlet air velocity.**

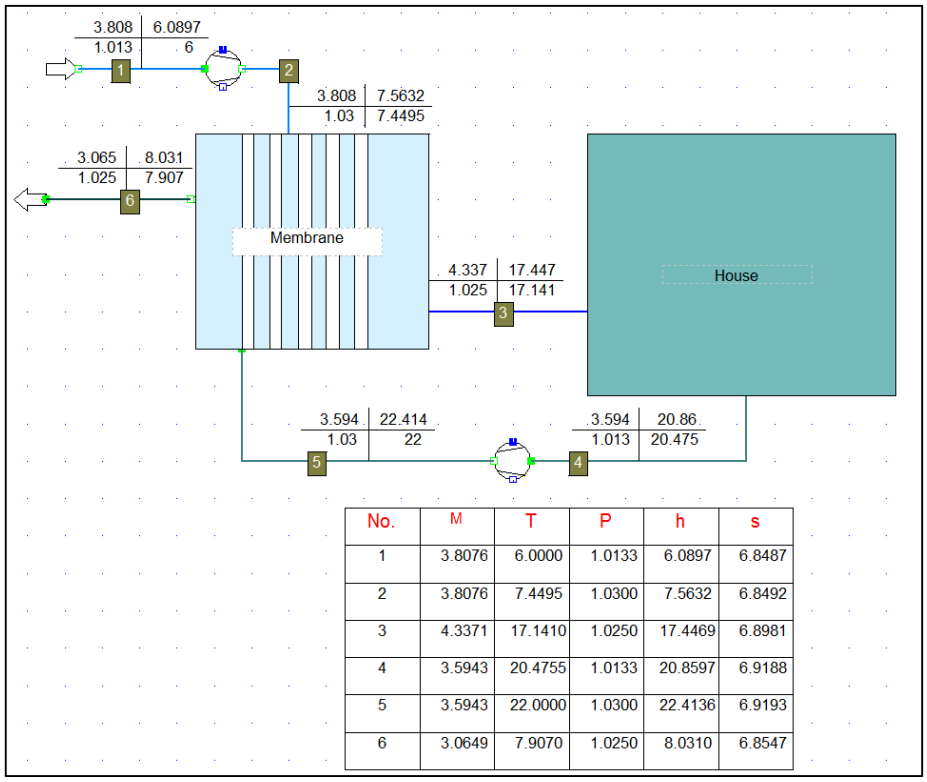


| No. | M | T | P | h | s |
|---|---|---|---|---|---|
| 1 | 3.8076 | 6.0000 | 1.0133 | 6.0897 | 6.8487 |
| 2 | 3.8076 | 7.4495 | 1.0300 | 7.5632 | 6.8492 |
| 3 | 4.3371 | 17.1410 | 1.0250 | 17.4469 | 6.8981 |
| 4 | 3.5943 | 20.4755 | 1.0133 | 20.8597 | 6.9188 |
| 5 | 3.5943 | 22.0000 | 1.0300 | 22.4136 | 6.9193 |
| 6 | 3.0649 | 7.9070 | 1.0250 | 8.0310 | 6.8547 |

**Figure 5-5: Model for 5 mm pitch length in IPSEpro at $6^0$C ambient temperature and 2.0 m/s inlet air velocity.**

### 5.13.1 Exergy Calculations ($\dot{E}$)

As mentioned earlier, the exergy is divided into kinetic, potential, physical and chemical exergy according to the second law of conservation of energy. Since there is neither movement of the system nor any elevation in the particles, the kinetic and the potential exergies were neglected due to their extremely small values. The remaining physical and chemical exergies are the only effective parameters in the calculations. The summation of these individual exergies represents the total exergy in the system.

#### 5.13.1.1 Physical exergy results ($\dot{E}_{ph}$)

The physical exergy mainly depends in the temperature and the pressure throughout the processes in the system, and is considered as the main indication of the useful work in the system, it also refers to the qualitative form of the transferred thermal energy within the system and is calculated using Equation (5-2). The detailed results are to be found in Appendix B.

### 5.13.1.2 Chemical exergy results ($\dot{E}_{ch}$)

Since the moisture transfer as a water vapour is crucial in the designed exchanger, the chemical exergy has a greater effect on the exergetic performance of the system than physical exergy. The calculations of the chemical exergy are quite different from the other types of the exergy and were done in several steps.

The **first step** is to take the values of the molar fraction (humidity ratio) of the air components which are in this case; Nitrogen ($N_2$), Oxygen ($O_2$) and the water vapour ($H_2O$) from the CFDpost17 and establish a reference point for the air composition. Knowing the molar mass of each component in the air (28, 32 and 16 for $N_2$, $O_2$ and $H_2O$ respectively) the total molar mass of the air at the reference point is calculated by multiplying the molar fraction of each component by its molar mass and then summing the results.

The **second step** is to identify the air states in the system. There are four states for the air in the proposed total recovery system, two for the **fresh** air stream (**Air1-P2** before and **Air2-P3** after the exchanger core), and two for the **exhaust** stream (**Air3-P5** before and **Air4-P6** after the exchanger core). Each air state has specific properties and the molar mass can be calculated for each of them in the same way as done in step one above. The chemical exergy was then calculated accordingly. Table 5-3 show the reference composition with air components composition for sample case (25 mm, 6°C and 0.5 m/s).

**Table 5-3: Reference composition and air states 25 mm, 6°C and 0.5 m/s.**

| Reference-Composition | | Air1-P2 | Air2-P3 | Air3-P5 | Air4-P6 | |
|---|---|---|---|---|---|---|
| **Nitrogen** | **0.77371** | 0.76508 | 0.76273833 | 0.76178 | 0.76446586 | Composition ($Y_K$) |
| **Oxygen** | **0.23** | 0.23 | 0.23 | 0.23 | 0.23 | |
| **H2O** | **0.00371** | 0.00492 | 0.00726167 | 0.00822 | 0.00553414 | |
| **Total** | **1.00742** | 1 | 1 | 1 | 1 | |
| **Molar Mass** | **29.083** | 28.861 | 28.833 | 28.821 | 28.854 | |

The **third step** is to use Equation (5-4) to calculate the chemical exergy for each component of the air ($ex_{ch}$) in (J/mol). By summing the values of the $ex_{ch}$, total chemical exergy ($E_{ch\ total}$) (J/mol) is determined. In the end, multiplying the $E_{ch\ total}$ by the term ($\dot{m}_a/molar\ mass$) determines the final chemical exergy rate ($\dot{E}_{ch}$) which is represented in (kW). The standard molar chemical exergy ($\bar{e}_k^{ch}$) is like a property of the air and can be obtained from standard table listing the values of $\bar{e}_k^{ch}$, and the values were obtained from [134]. The values of $\bar{e}_k^{ch}$ are (639, 3951 and 8636 Joule/mole) for the $N_2$, $O_2$ and $H_2O$ respectively. Table 5-4 shows the results of the third step for a sample case (25mm, 6°C and 0.5 m/s). The negative sign in the $H_2O$ chemical exergy means that that the water vapour is adding to the exhaust air stream from the fresh humid air stream. All the detailed results of the other cases are shown in Appendix B.

**Table 5-4: Chemical exergy rate calculations and results (25mm, 6°C and 1.5m/s).**

| | | | | | | |
|---|---|---|---|---|---|---|
| **Air1-P2** | ***Component*** | $\bar{e}_k^{ch}$ | $y_k$ | $ex_{ch}$ | $E_{ch\ total}$ | $\dot{E}_{ch}$ |
| | - | J/mol | Kg/kg | J/mol | J/mol | KW |
| | $N_2$ | 639 | 0.76508 | 13.418 | 119.443 | 1.935 |
| | $O_2$ | 3951 | 0.23 | 124.22 | | |
| | $H_2O$ | 8636 | 0.00492 | -18.194 | | |
| **Air1-P3** | **Component** | $\bar{e}_k^{ch}$ | $y_k$ | $ex_{ch}$ | $E_{ch\ total}$ | $\dot{E}_{ch}$ |
| | $N_2$ | 639 | 0.76274 | 7.947 | 111.877 | 2.043 |
| | $O_2$ | 3951 | 0.23 | 124.22 | | |
| | $H_2O$ | 8636 | 0.00726 | -20.293 | | |
| **Air1-P5** | **Component** | $\bar{e}_k^{ch}$ | $y_k$ | $ex_{ch}$ | $E_{ch\ total}$ | $\dot{E}_{ch}$ |
| | $N_2$ | 639 | 0.76178 | 5.717 | 109.331 | 1.674 |
| | $O_2$ | 3951 | 0.23 | 124.222 | | |
| | $H_2O$ | 8636 | 0.00822 | -20.606 | | |
| **Air1-P6** | **Component** | $\bar{e}_k^{ch}$ | $y_k$ | $ex_{ch}$ | $E_{ch\ total}$ | $\dot{E}_{ch}$ |
| | $N_2$ | 639 | 0.76446 | 11.979 | 117.247 | 1.553 |
| | $O_2$ | 3951 | 0.23 | 124.222 | | |
| | $H_2O$ | 8636 | 0.00553 | -18.954 | | |

The (-ve) refers to the deviation of the values of the calculated state to a value lower than the assumed reference point, but it does not affect the final outcome of the chemical exergy science the exergy is based on the difference between two states rather than an absolute value. The concept of the exergy existence is the existence of a change in the status between two points, and at the reference point the exergy is equal to zero. Consequently, the current case's (-ve) sign means that the air is giving its $H_2O$ to the exchanger which is the purpose of designing this core in the first place.

Figure 5-6 to Figure 5-8 show the effect of the inlet air velocity on the different types of exergy. The total exergy is achieved by summing the chemical and the physical exergies to obtain the total input and the output exergies, into and out of the system.

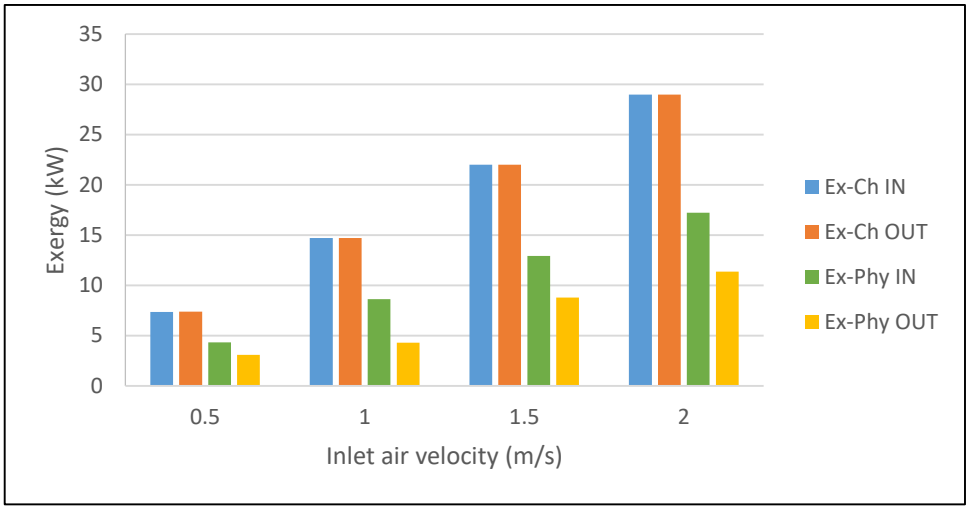


**Figure 5-6: Exergy and inlet air velocity for heat exchanger duct with 5 mm pitch length**

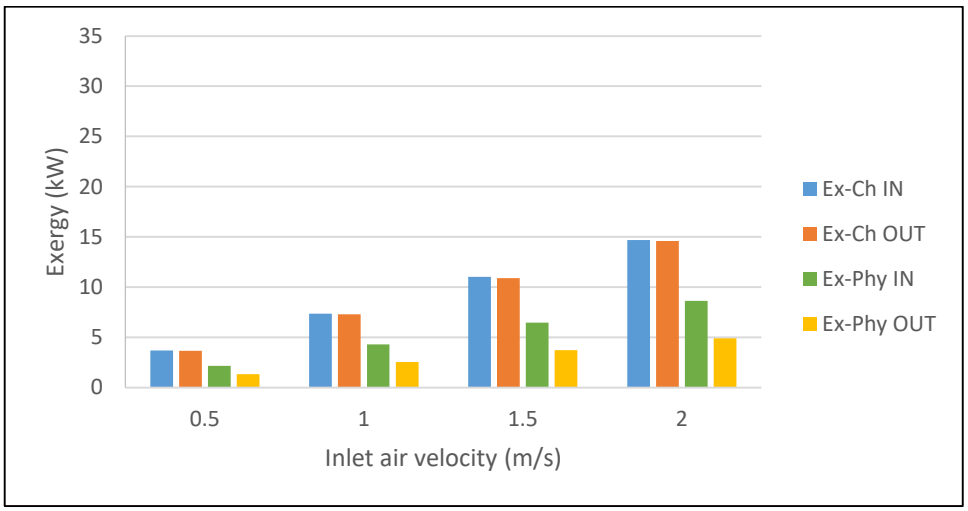


**Figure 5-7: Exergy and inlet air velocity for heat exchanger duct with 10 mm pitch length**

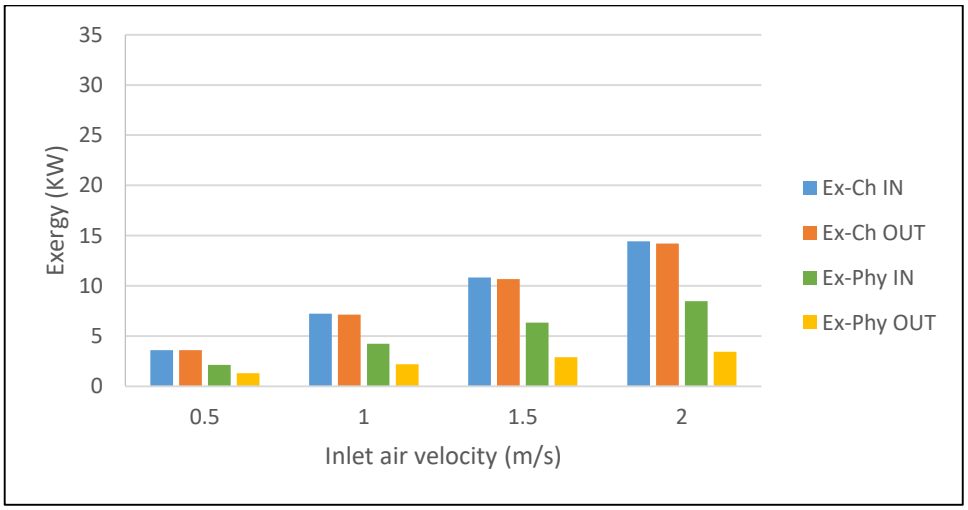


**Figure 5-8: Exergy and inlet air velocity for heat exchanger duct with 25 mm pitch length**

The figures above show that with increase of the inlet air velocity, all the exergies increase but with different percentages. This increase is quite normal because the increase in velocity tends to raise the thermal content of the air, i.e. it raises the enthalpy of the air particles leading to a higher difference in the enthalpy before and after the processes.

The other reason of this positive relationship between the velocity and the exergy is the entropy change that occurs during the processes, which presents as a function of temperature the irreversibility of the process and also the amount of energy which is unavailable to do work. The increase in the velocity increases the enthalpy exchange which increases the exergy. In general, the difference between the input and the output chemical exergy is quite small due to its primarily dependency on the mass transfer apart from other factors. However, a significant decrease in the output physical exergy comparing to the input, is because of the effect of the pressure drop in the exchanger core which increase the entropy generation in the membrane.

The 5 mm pitch length gave the highest exergy comparing to the 10 and 25 mm cases, which are similar in their exergy values (though the values for 10 mm are consistently slightly higher than for 25 mm). The compactness of the 5 mm arrangement makes it a very promising design, however, the practicalities of its construction would be a problem. The increase in the exergy due to the increase of the inlet air velocity from 0.5 m/s to 2.0 m/s is about 4 for all cases.

Figure 5-99 to Figure 5-11 show the negative relationship between exergy and ambient temperature. An increase in ambient temperature leads to a decrease in both forms of exergy. The input chemical exergy has barely noticeable higher values than the corresponding output values, while the difference between the input and output physical exergies is quite significant.

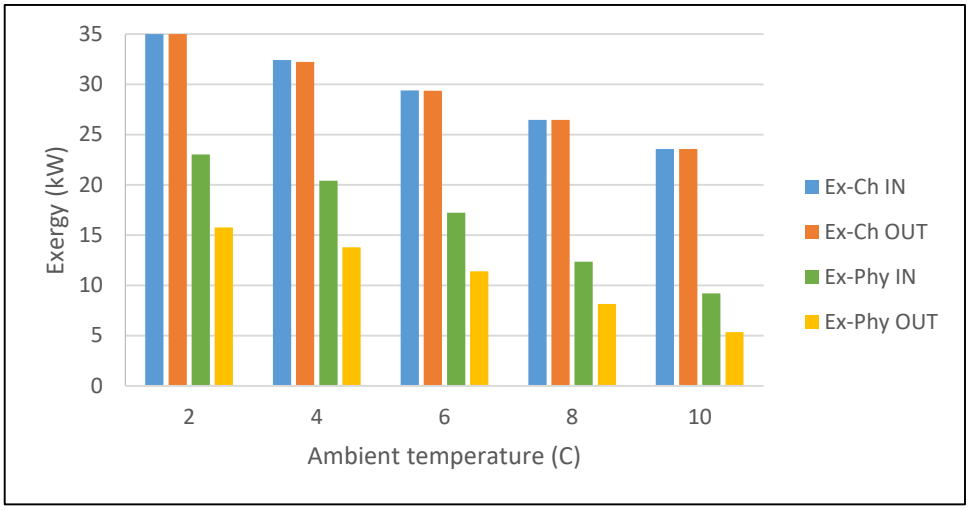


**Figure 5-9: Exergy and ambient temperature for the exchanger core (5 mm) pitch length.**

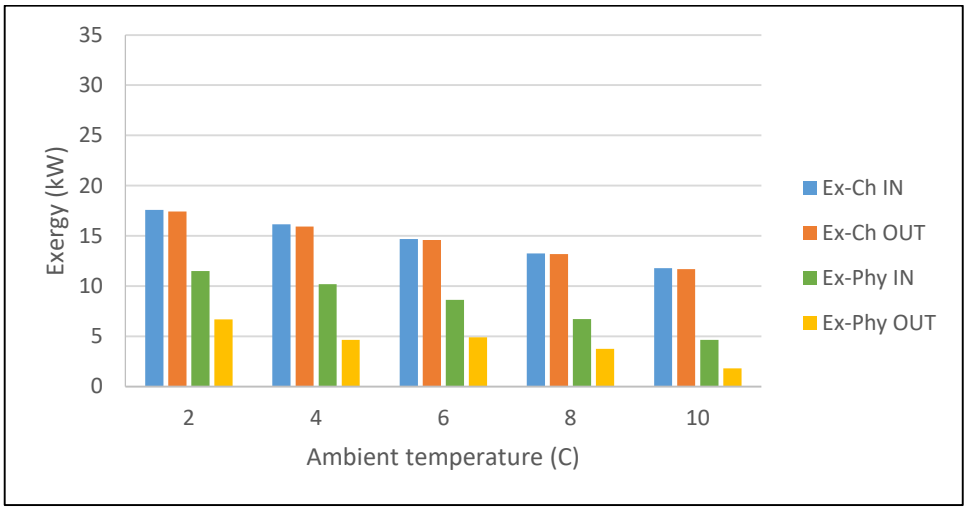


**Figure 5-10: Exergy and ambient temperature for the exchanger core (10mm) pitch length**

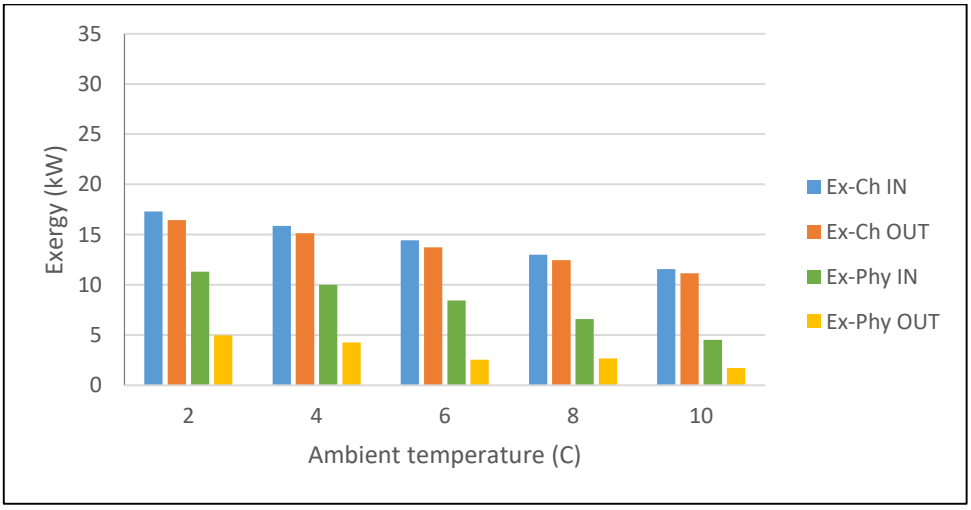


**Figure 5-11: Exergy and ambient temperature for the exchanger core with (25 mm) pitch length.**

For the chemical exergy, the percentage decrease for an increase in ambient temperature from $2^0$C to $10^0$C was about 33% for all cases. For the physical exergy, the percentage decrease was between 55% - 70% depending on the specific case.

The change of the ambient temperature occurred at a constant flow rate which means the same pressure drop for each pitch length of the exchanger core, which means that the temperature in this case plays the main role in determining the value of the exergy, especially physical exergy. Increase in the ambient temperature means the temperature difference across the exchanger core will decrease, this leads to a decrease in the enthalpy difference in the system processes in general but primarily in the membrane core. The entropy difference also decreased with lower temperature difference, leading to lower exergy values.

Again the 5 mm pitch length showed the highest exergy levels comparing to both the 10 mm and 25 mm cases. The reason is due the compactness of this design so the difference in temperature between the ambient and the room has higher influence on its exergetic performance because of the higher difference in the particles' enthalpy.

After comparing the exergy results and their relation with inlet air velocity and ambient temperature, it becomes clear that the effect of change in velocity is much greater than the effect of change in ambient temperature due to higher entropy generation in the membrane core and an increase in the enthalpy difference in the core processes.

### 5.13.2 Exergy Destruction Results ($\dot{E}_{des}$)

As mentioned earlier, the system consists of four parts: the membrane core, the house, the fresh air fan and the exhaust fan. Every component has an input and output total exergy, the difference in these exergies represents the exergy destruction in (kW) and can be calculated using Equation (5-6). The exergy destruction is a measure of the irreversibility of the processes and is considered the best indicator to specify the location of the highest losses in the system. The second main factor in the qualitative exergetic evaluation of any system besides the exergy is the exergetic efficiency.

In order to validate the modelling of the system, a second method was used to determine the exergy destruction value. The second method was based on the fuel-product scheme of evaluation instead of the input and output exergy method, and both methods produced the same exact results. Table 5-5 shows the equations used in the fuel-product method.

**Table 5-5 Equations used in the fuel-product method.**

| | Component | FUEL | PRODUCT | $\dot{E}_{des}$ |
|---|---|---|---|---|
| **1** | Fresh Air Fan | $\dot{m}_{a1}(h_2 - h_1)$ | $\dot{E}_2 - \dot{E}_1$ | *Fuel - Product* |
| **2** | Membrane Core | $\dot{E}_5 - \dot{E}_6$ | $\dot{E}_3 - \dot{E}_2$ | |
| **3** | Exhaust Fan | $\dot{m}_{a5}(h_5 - h_4)$ | $\dot{E}_4 - \dot{E}_5$ | |
| **4** | House | $\dot{E}_3$ | $\dot{E}_4$ | |

where $\dot{m}_{a1}$ and $\dot{m}_{a5}$ are the air mass flow rate (kg/s) , $h_1$ , $h_2$, and $h_4$ and $h_5$ are the enthalpy KJ, $\dot{E}_1, \dot{E}_2, \dot{E}_3, \dot{E}_4, \dot{E}_5$ and $\dot{E}_6$ are the exergy and $\dot{E}_{des}$ is exergy destruction.

The total exergy destruction (kW) was calculated by summing the values of the exergy destruction in all the system components and for all cases. Figure 5-12 show the relation between the total exergy destruction in the system and the inlet air velocity. The 5 mm pitch length shows the highest values which means this design has the highest losses compared to the others. The 10 mm shows the best results of the three geometries with lowest exergy destruction values but the 25 mm case is close behind. From an initial level where the value for the 5 mm case was already significantly larger than the other two, the total exergy destruction increases by factors of 7, 4.5 and 5.5 for the 5 mm, 10 mm and 25 mm pitch lengths respectively, as the inlet air velocity increased from 0.5 to 2.0 m/s. This confirmed that the inlet air velocity is main variable in the model.

In general, for each pitch length the total exergy destruction is proportional to the inlet air velocity, which is as would be expected since the value of the exergy destruction is due to entropy generation within the system, which increases with the increase of the inlet air velocity.

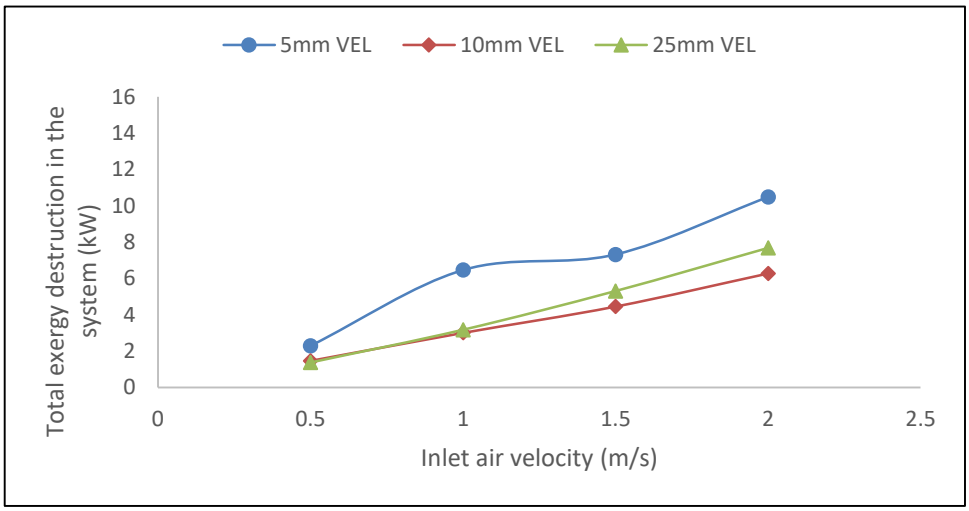


**Figure 5-12: Total exergy destruction in the system as a function of inlet air velocity**

Figure 5-13 shows an indirect proportionality between the total exergy destruction and ambient temperature. Again the 5 mm pitch length shows the highest values, and again the 10 mm case produces least exergy destruction with the 25 mm case close behind. This could be translated to mean that the 10 mm pitch length has least losses compared to the others. For the 5 mm case the total exergy destruction decreased by 43% with increase in ambient temperature from $2^0$C to $10^0$C. The corresponding values for the 10 mm and 25 mm cases were 24% and 33% respectively. The reasons behind the negative relationship between exergy destruction and ambient temperature are; (i) entropy generation decreases with the decrease of the temperature difference in the processes, and (ii) the enthalpy difference also decreases leading to a decrease in the exergy losses in the system.

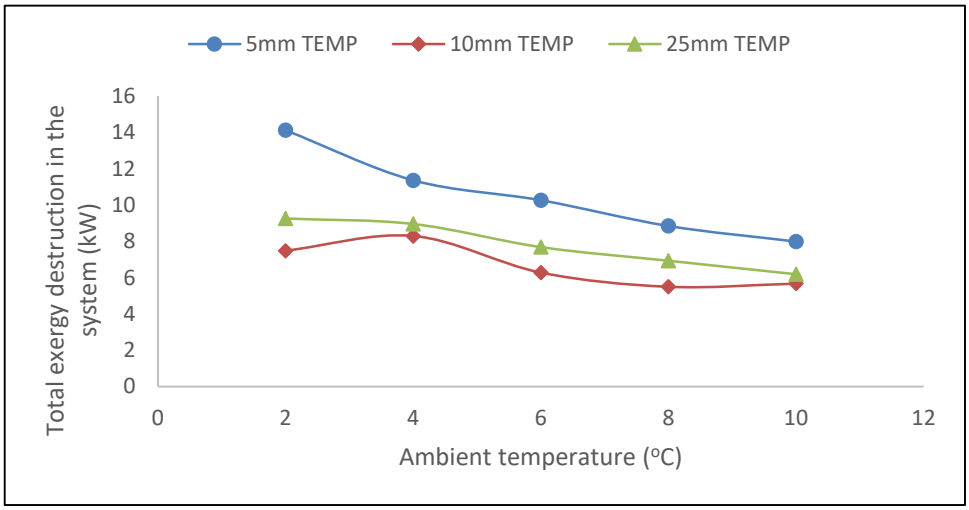


**Figure 5-13: Total exergy destruction in the system with the ambient temperature.**

The exergy destruction could also be used to locate the system components with the highest losses. The exergy destruction percentage is a very most useful parameter by which to achieve this goal by determining the percentage of the total exergy destruction in each of the system's components. Note that the total exergy destruction is always 100%. Figure 5-14 to Figure 5-16 show the exergy destruction percentage in each component with inlet air velocity for all three pitch lengths.

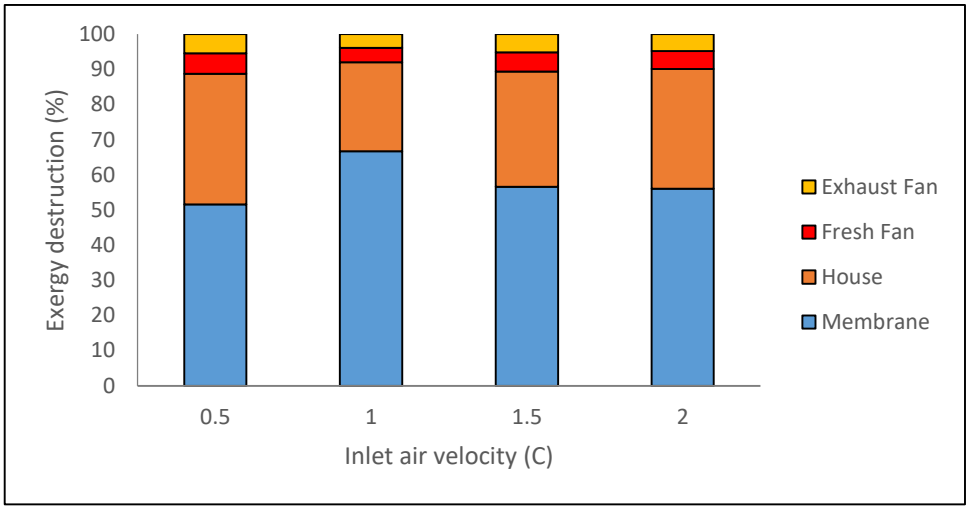


**Figure 5-14: Exergy destruction percentage with the inlet air velocity for system components with 5 mm pitch length**

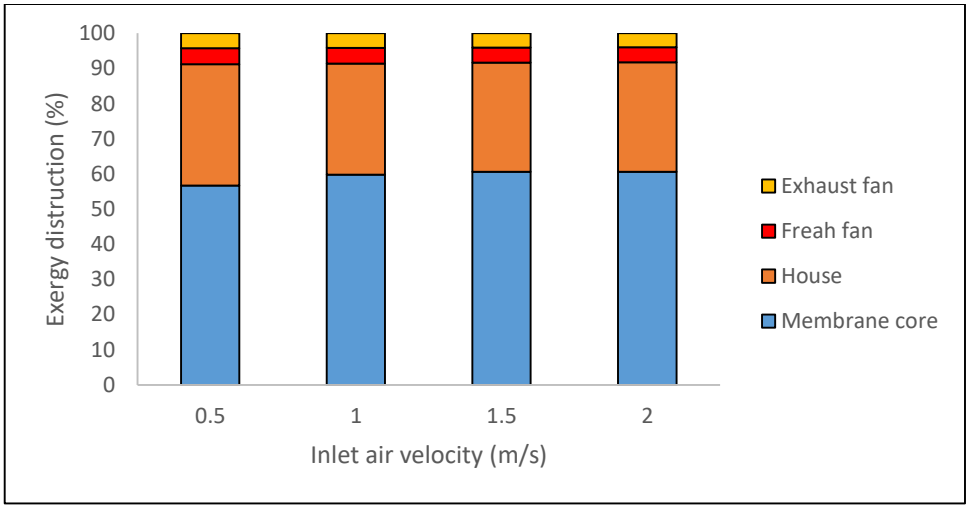


**Figure 5-15: Exergy destruction percentage with the inlet air velocity for system components with 10 mm pitch length.**

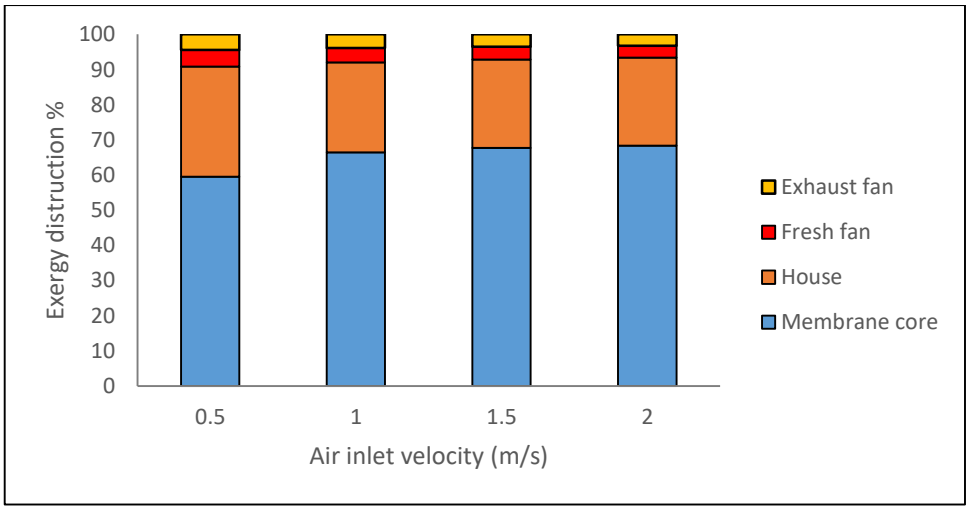


**Figure 5-16: Exergy destruction percentage with the inlet air velocity for system components with 25 mm pitch length.**

In general, the membrane core has the highest percentage of exergy destruction, which means the highest losses occurs in the membrane core - which is as expected because the highest entropy generation occurs within the membrane. There is also the fact that the exchanger core is considered as functioning component of the system and the heat and mass transfer in the membrane core affect the exergy destruction. The percentage exergy destruction has a direct proportional relationship with the inlet air velocity, so as the inlet air velocity increases, the percentage of the exergy destruction increases as well. However, the rate of exergy destruction decreased with increase of inlet velocity.

Figure 5-17, shows the exergy destruction in the membrane for all three pitch lengths as the inlet air velocity increases from 0.5 to 2.0 m/s. It can be seen that for all velocities the greatest exergy destruction is for the 25 mm pitch length followed by the 10 mm and then the 5 mm.

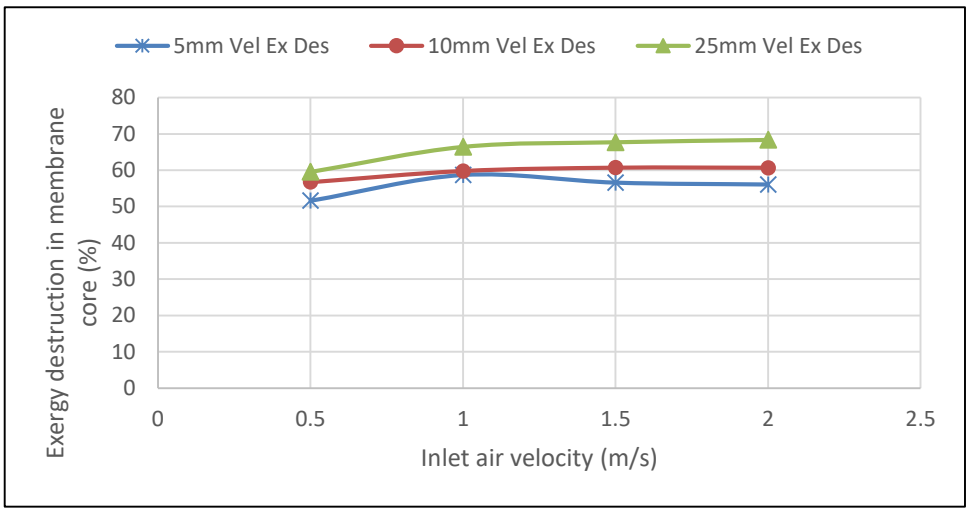


**Figure 5-17: Membrane core's exergy destruction percentage with air inlet velocity.**

Table 5-6 shows in detail the percentage increase in exergy destruction in the core and the decrease in the other components.

**Table 5-6: The differences in the exergy destruction percentage for each component when increasing the inlet air velocity from 0.5 m/s to 2.0 m/s**

| | Membrane core | | House | | Fresh Air Fan | | Exhaust Fan | |
|---|---|---|---|---|---|---|---|---|
| 5 mm | 7.9% | Increase | 8.2% | Decrease | 12.5% | Decrease | 12.5% | Decrease |
| 10 mm | 6.5% | | 9.9% | | 6.2% | | 5.9% | |
| 25 mm | 12.0% | | 19.9% | | 27.9% | | 27.8% | |

The changes in the values of Table 5-6 depend on several factors including the properties of the air, in addition to the proposed geometric changes. For instance, the largest increase in value of the exergy destruction in the membrane core belongs to the 25 mm pitch length, then the 10 mm case and finally the 5 mm which was the lowest. However, for the other components (house, fresh air fan and exhaust fan) the 25 mm case has by far the greatest decrease in exergy destruction.

Figure 5-18 to Figure 5-20 show the relation between the exergy destruction percentage and the ambient temperature. The values show that for the membrane core, the exergy destruction percentage decreases with the increase of ambient temperature, but the values increase with increase of the ambient temperature for the house, fresh air fan and exhaust fan.

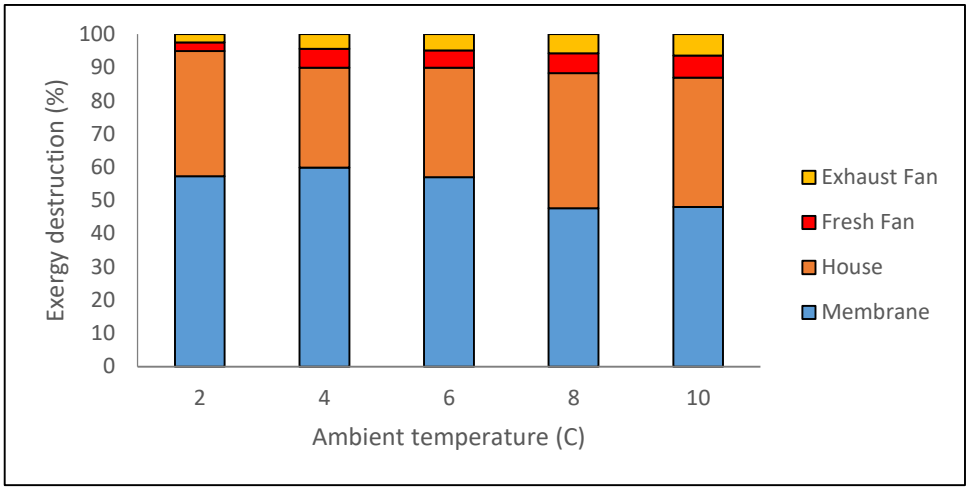


**Figure 5-18: Exergy destruction percentage and the ambient temperature for pitch length 5 mm.**

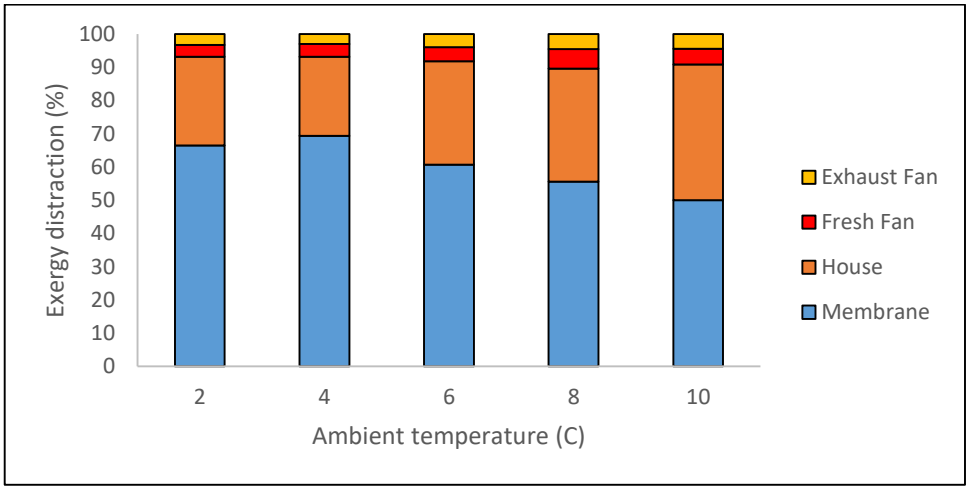


**Figure 5-19: Exergy destruction percentage and the ambient temperature for pitch length 10 mm.**

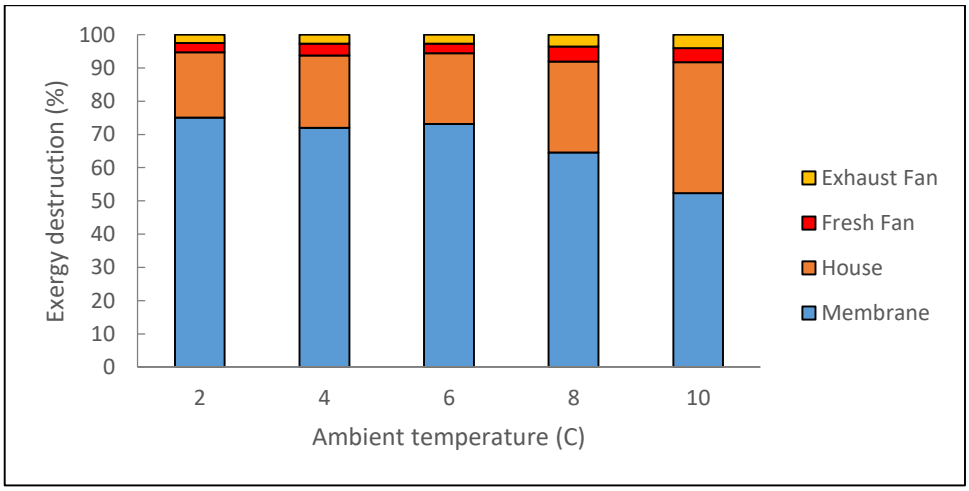


**Figure 5-20: Exergy destruction percentage and the ambient temperature for pitch length 25 mm.**

Figure 5-21 shows the exergy destruction percentages for the membrane are greatest for the 25 mm pitch length, then the 10 mm and finally the 5 mm. The figures also show that exergy destruction in the membrane decreases with increase in ambient temperature. It follows that if the exergy destruction in the membrane decreases then the exergy destruction for the other components increases, see Table 5-5.

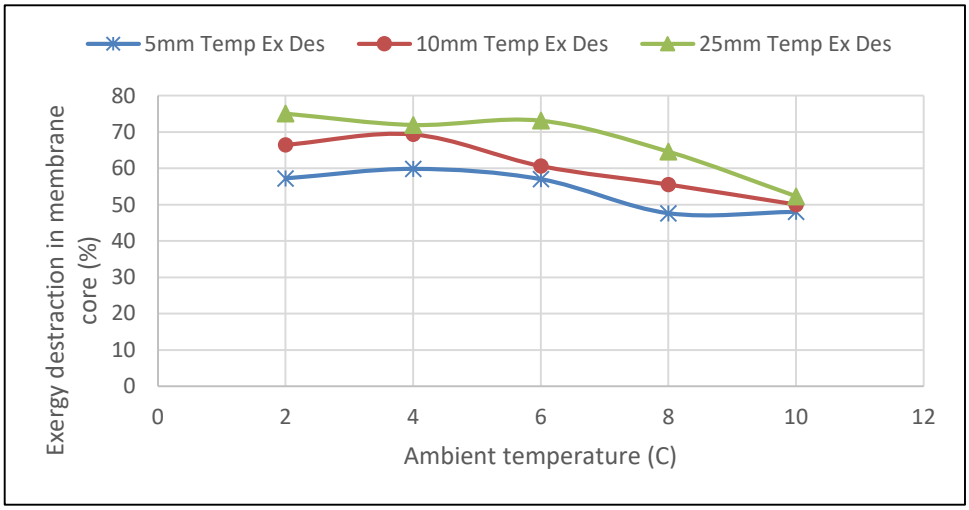


**Figure 5-21: Membrane core's exergy destruction percentage with ambient temperature**

The reason for the decrease in exergy destruction in the membrane is the decrease in temperature difference between the ambient and membrane core. The house and the fans usually supply heat to the membrane core and to the system which increases both the entropy generation and the enthalpy, so it is physically authentic to have higher exergy destruction at higher ambient temperature.

Table 5-7 shows the percentage decreases in exergy destruction in the core and the increase in the other components. The greatest increases are for the 5 mm case, then the 25 mm and finally the 10 mm.

**Table 5-7: The percentage of difference in the exergy destruction percentage for each component when increasing the ambient temperature from 2°C to 10°C.**

| | Membrane core | | House | | Fresh Fan | | Exhaust Fan | |
|---|---|---|---|---|---|---|---|---|
| 5 mm | 16% | Decrease | 33.1% | Increase | 60% | Increase | 61% | Increase |
| 10 mm | 24.8% | | 34.7% | | 24% | | 26.3% | |
| 25 mm | 30% | | 50% | | 35.3% | | 37.2% | |

## 5.14 Exergetic Efficiency Calculations

The exergetic efficiency ($\eta_{ex}$) was calculated for the membrane core and for all three geometries using Equation (5-7). The product-fuel method is also used to determine the efficiencies. The product-fuel method represents the difference in the exergy of the fresh air stream between the inlet and the outlet of the membrane core, while the exergy difference between the inlet and the outlet of the exhaust air stream represents the fuel consumed.

Figure 5-22 shows the results for the exergetic efficiency. It can be seen that they decrease with increase of inlet air velocity. The 5 mm case has the highest values for the exergetic efficiency, then comes the 10 mm and finally the 25 mm. For the 5 mm case the value of the efficiency dropped by 8% as the inlet air velocity increased from 0.5 to 2.0 m/s, for the 10 mm by 4.6%, and for the 25 mm by 26%.

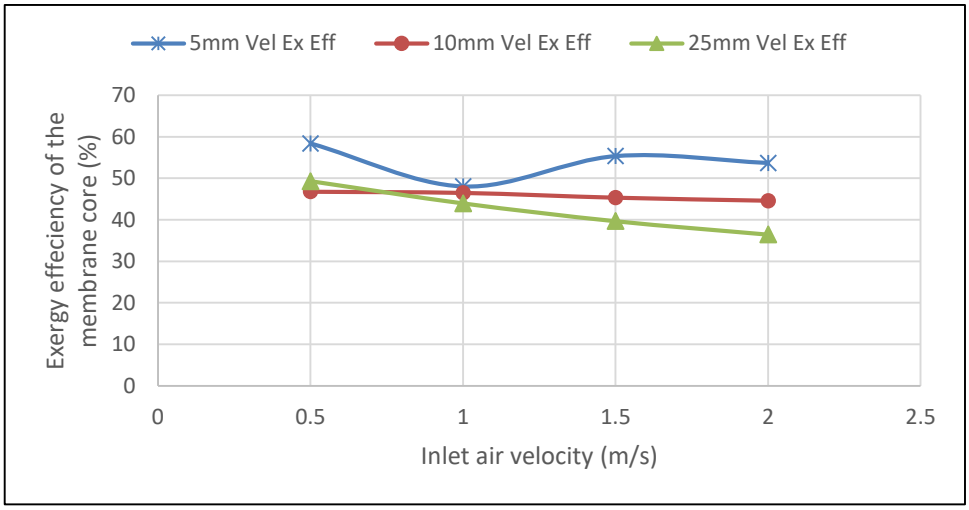


**Figure 5-22: Exergetic efficiency with inlet air velocity for all three duct geometries**

The increase in inlet air velocity leads to increase in entropy generation in the membrane core, which causes the exergy destruction to increase. Therefore, the exergetic efficiency should decrease with increase in air velocity due to the negative relationship between exergy destruction and exergetic efficiency.

Figure 5-23 shows that the exergetic efficiency decreases as ambient temperature increases. Generally, the 5 mm pitch length has the highest values for the exergetic efficiency, then comes the 10 mm case and finally the 25 mm case due the several reasons, the first one is the increment in the total heat transfer area for the 5 mm comparing to the other cases which gives belter heat and mass transfer, the second one is the nature of the small corrugations of the 5 mm cases comparing to the other cases that force the flow to reach the transition region in velocities less than the 10 mm and the 25 mm for the same core height. The percentage decrease in exergy efficiency as the ambient temperature rose from $2^0$C to $10^0$C was 45% for the 5 mm case, 37% for the 10 mm case and 46% for the 25 mm case.

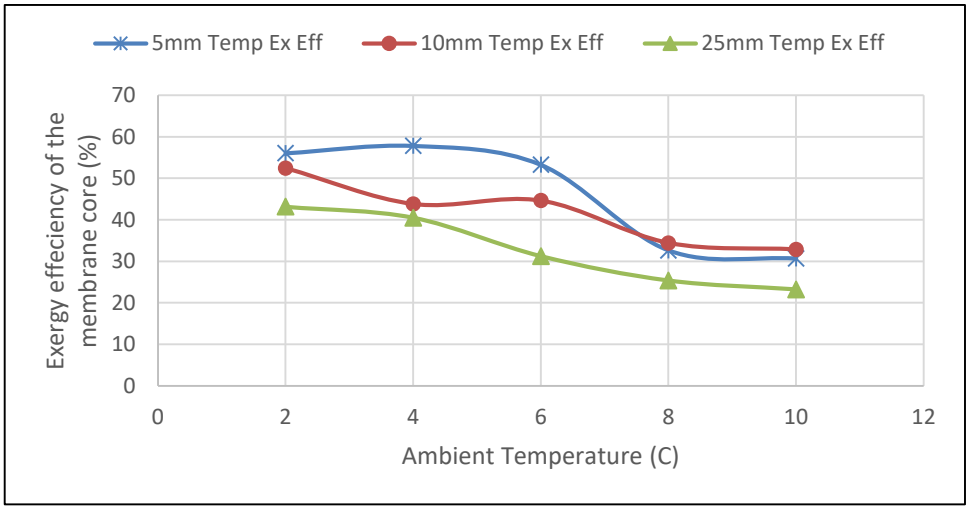


**Figure 5-23: Exergetic efficiency with ambient temperature**

The main variable in these examples is the ambient temperature which means the fresh air inlet temperature. As mentioned earlier the physical exergy is a function of temperature and pressure, and the chemical exergy is function of air composition. The pressure drop remains the same in this case as does the $N_2$ and $O_2$ composition. The remaining two main factors to affect the system's efficiency are the temperature and the $H_2O$ molar fraction and in both cases the physical and the chemical exergies decreased with increase of ambient temperature, leading to a decrease in the exergetic efficiency due to the losses within the system, especially the membrane core. These losses occur with increase of entropy generation in the membrane core because of the increase in fresh air inlet temperature, which leads the thermodynamic process to diverge from the reversible state. These are in addition to the physical losses represented by friction and the pressure drop in the membrane core.

## 5.15 Exergetic Analysis Summary

Having completed the exergetic modelling of the membrane cross-corrugated total recovery system, the values of exergy, exergy destruction of the system, and exergy destruction percentage in the membrane core are seen to increase with increase of both the inlet air velocity and the ambient temperature.

The chemical exergy has the dominant portion of the total exergy compared to the physical exergy, and it increases the total exergy of the membrane-based exchanger as compared to other types of exchangers due to the capability of the membrane exchanger to transfer moisture as well as heat.

The membrane core has the highest percentage of exergy destruction in the system, which can be translated to mean the highest mechanical losses. These losses were clarified in the differences between the values of the input and the output physical exergy, the main two reasons of these losses being pressure drop and entropy generation in the membrane core.

The 5 mm pitch length showed the highest exergetic efficiency comparing to the other geometries, but at the same time had the highest exergy destruction which means the 5 mm case has the highest heat and mass transfer but also the highest losses. The struggle with this design is the practicality of its construction. Comparing the 10 mm and 25 mm pitch lengths we see that the 10 mm case results in a slightly higher performance then the 25 mm. The air velocity and the ambient temperature however show the same effects on system behavior in all the cases.

# 6 CONCLUSIONS AND RECOMMENDATIONS FOR FURTHER WORK

## 6.1 Conclusions

### 6.1.1 Energetic Analysis Conclusions

In this research, fluid flow, heat and mass transfer in a triangular cross-corrugated total recovery exchanger were investigated for application as the core of a domestic ventilation and heat recovery system.

This study proposed three new geometries for the cross-corrugated exchanger core with specified pitch length and apex angle. According to the literature, the current study was the first study simulate the cases using the The Transition-SST model for a range of Reynolds numbers from 100 – 2000 for the CFD simulation of a three-dimensional model of the exchanger core proposed geometries to analyze its sensible and latent thermal performance, and the model was validated using experimental results reported in the literature. The study was also the first to investigate the proposed core arrangement for the UK individual dwellings ventilation demand in the cold and humid winter.

The results showed:

1. That because the flow occurs at low Re values, the Transition-SST model worked well, successfully simulating the thermal and flow behaviour in the proposed exchanger core designs.
2. Comparison of the three pitch lengths proposed for the exchanger geometry (5 mm, 10 mm and 25 mm), showed the 5 mm length had the highest latent and sensible effectiveness. However, it has two downsides: the relatively high pressure drop across the core and the difficulty of its manufacture.
3. Increasing the inlet air velocity from 0.5 – 2.0 m/s, decreased the effectiveness of the core, but the 5 mm pitch showed the least decrease in effectiveness.

4. Increase in ambient temperature from 2 – 10 $^{o}$C had no significant effect on the effectiveness, with the 5 mm pitch maintaining the highest effectiveness with increase in ambient temperature.
5. The 5 mm case showed the most uniform temperature and humidity distribution across the surface of the heat exchanger membrane due to the high number of the corrugations per the membrane sheet.
6. All three pitch lengths showed the same pattern of behaviour of increasing even though they perform in different region of Re values. However, the 25 mm case showed slightly higher values of the Nusselt number suggesting that the convective heat transfer increased relative to the conductive, and similarly for the Sherwood number due to the domination of the convective mass transfer over the diffusion mass transfer.
7. The pressure drop across the exchanger core in all three cases considered was relatively high for a small ventilation exchanger. The 5 mm pitch length showed significant relative increase in pressure drop with the increase in inlet air velocity to the point when the velocity was 2 m/s the pressure drop across the 5 mm exchanger was 1200 Pa compared to 90 Pa for the 25 mm pitch length (both having the same core size - 250 x 250 x 500 mm).

### 6.1.2 Exergetic analysis conclusions

The exergetic analysis for the proposed exchanger core were one of the contributions in the current study by combining the CFD simulations results with the modelling software, the IPSEpro and the PSExcel. This combination has determined the exergetic performance of the exchanger core with its proposed system. The newly proposed system consists of the house, the fresh and exhaust air fans in addition to the membrane core, this makes the system compatible with the IPSEpro software. The house represents the heat source of the system, while the fans represent the power input to the system.

After determining the exergies values and the exergetic efficiencies of all of the cases, a new method (Fuel-Product method) was used to conduct the exergy destruction in the system components as well as validating the results that obtained from the traditional exergy method.

The study concludes the following:

1. The constructed system, comprising the membrane core, the house, and the fresh and exhaust air fans, worked very well with the IPSEpro exergy simulation software.
2. The chemical exergy was the dominant portion of the total exergy rather than the physical exergy. Moisture transfer is the parameter that plays the most important role in the performance of the membrane-based exchanger core.
3. Exergy destruction in the membrane core increased with increase of both the inlet air velocity and the ambient temperature, for all three pitch lengths.
4. In all cases, the membrane core showed the highest percentage of exergy destruction in the system, which can be translated to mean the highest mechanical losses.
5. The pressure drop losses affected the exergy significantly, especially when the physical exergy output from the membrane core decreased dramatically comparing to its input, as happened when the inlet air velocity was increased from 0.5 – 2.0 m/s.
6. The 10 mm pitch length showed the best results for exergetic efficiency and the exergy destruction, located between the higher pressure drop of the 5 mm cases and the less effective 25 mm cases.
7. The 5 mm case showed the highest exergetic efficiency as well as the highest exergy destruction, which puts designers in the position of having to make a compromise.

### 6.1.3 Final Conclusions

1. After taking into consideration both the energetic and exergetic analysis, the membrane based exchanger core showed very promising performance as a total heat and moisture recovery application. Sensible and latent effectiveness varied from 65% to 82%, and the exergetic efficiency varied from 30% to 60% both depending on pitch length and ambient conditions.
2. Decreasing pitch length to increase performance and make the exchanger core more compact is good as a concept, but at a certain point it becomes impractical to manufacture a core with such small channels. Also, smaller channels inevitably mean a higher pressure drop which means a compromise with running costs.
3. Consequently, even with the high performance of the 5 mm pitch length comparing to the others, it is not a practical choice because of high pressure losses even with low Reynold number, and especially at higher inlet air velocities.
4. The 10 mm pitch, provided a better heat and mass transfer performance than the 25 mm pitch, but the difference was not so large that the lower pressure drop across the latter and its relative ease of construction could make it the more practical solution.

## 6.2 Recommendations for the Future Work

1. Conduct experimental work by constructing and testing the proposed geometries, in order to validate the CFD work, and assess the manufacturing difficulties in building exchanger cores of 5 mm, 10 mm and 25 mm pitch length.
2. Increase the quantity of fresh air needed for ventilation, and examine the performance of the proposed cores in different ventilation applications in addition to individual households.
3. Using the same Reynolds number range for all three pitch lengths examine the effects of transitional flow, especially when using the Transition-SST model in the CFD simulations.
4. Investigate the proposed exchanger in a wider range of climate conditions, and examine the performance of the cores in different weathers and seasons in the United Kingdom and Europe.
5. Perform a full economic study including the initial and running costs and ascertain the feasibility of producing such an exchanger core commercially as a future replacement for conventional heat recovery exchangers.

# REFERENCES


1. Zhang L. TOTAL HEAT RECOVERY: HEAT AND MOISTURE RECOVERY FROM VENTILATION AIR. Nova Science Publishers I (ed.) Nova Science Publishers, Inc.; 2008. 316 p.

2. Zhang Y., Yang R., Zhao R. A model for analyzing the performance of photocatalytic air cleaner in removing volatile organic compounds. Atmospheric Environment. August 2003; 37(24): 3395–3399.

3. Mo J., Zhang Y., Yang R. Novel insight into VOC removal performance of photocatalytic oxidation reactors. Indoor air. August 2005; 15(4): 291–300.

4. Xu Y., Zhang Y. An improved mass transfer based model for analyzing VOC emissions from building materials. Atmospheric Environment. June 2003; 37(18): 2497–2505.

5. Xu Y., Zhang Y. A general model for analyzing single surface VOC emission characteristics from building materials and its application. Atmospheric Environment. January 2004; 38(1): 113–119.

6. Liu XH., Zhang Y., Qu KY., Jiang Y. Experimental study on mass transfer performances of cross flow dehumidifier using liquid desiccant. Energy Conversion and Management. September 2006; 47(15–16): 2682–2692.

7. Liu X., Li Z., Jiang Y., Lin B. Annual performance of liquid desiccant based independent humidity control HVAC system. Applied Thermal Engineering. August 2006; 26(11–12): 1198–1207.

8. Zhang L-Z. Progress on heat and moisture recovery with membranes: From fundamentals to engineering applications. Energy Conversion and Management. Elsevier Ltd; November 2012; 63: 173–195.)

9. Mardiana-Idayu a., Riffat SB. Review on heat recovery technologies for building applications. Renewable and Sustainable Energy Reviews. Elsevier Ltd; February 2012; 16(2): 1241–1255.

10. Riffat SB., Gan G. Determination of effectiveness of heat-pipe heat recovery for naturally-ventilated buildings. Applied Thermal Engineering. 1998; 18(3–4): 121–130.

11. Shurcliff WA. Air-to-air heat-exchangers for houses. Annual review of energy. Vol. 13 Annual Reviews Inc., Palo Alto; 1988 pp. 1–22.

12. Department for Business Energy & Industrial Strategy. Energy Consumption in the UK. Energy Consumption in the UK. 2016; (July): 1–39.

13. Mardiana Idayu Ahmad. Novel Heat Recovery Systems for Building Applications. University of Nottingham; 2011.

14. Wu Z., Melnik RVN., Borup F. Model-based analysis and simulation of regenerative heat wheel. Energy and Buildings. May 2006; 38(5): 502–514.

15. Nielsen TR., Rose J., Kragh J. Dynamic model of counter flow air to air heat exchanger for comfort ventilation with condensation and frost formation. Applied Thermal Engineering. Elsevier Ltd; February 2009; 29(2–3): 462–468.

16. Adamski M. Longitudinal flow spiral recuperators in building ventilation systems. Energy and Buildings. January 2008; 40(10): 1883–1888.

17. Yau YH. The use of a double heat pipe heat exchanger system for reducing energy consumption of treating ventilation air in an operating theatre—A full year energy consumption model simulation. Energy and Buildings. January 2008; 40(5): 917–925.

18. Sphaier LA., Worek WM. Parametric analysis of heat and mass transfer regenerators using a generalized effectiveness-NTU method. International Journal of Heat and Mass Transfer. April 2009; 52(9–10): 2265–2272.

19. Dallaire J., Gosselin L., da Silva AK. Conceptual optimization of a rotary

heat exchanger with a porous core. International Journal of Thermal Sciences. February 2010; 49(2): 454–462.

20. Jia CX., Dai YJ., Wu JY., Wang RZ. Use of compound desiccant to develop high performance desiccant cooling system. International Journal of Refrigeration. March 2007; 30(2): 345–353.

21. Simonson CJ., Besant RW. Heat and moisture transfer in energy wheels during sorption, condensation, and frosting conditions. Journal of Heat Transfer. ASME; 1998; 120(3): 699–708.

22. Sphaier LA., Worek WM. Analysis of heat and mass transfer in porous sorbents used in rotary regenerators. International Journal of Heat and Mass Transfer. July 2004; 47(14–16): 3415–3430.

23. Zhang LZ., Niu JL. Indoor humidity behaviors associated with decoupled cooling in hot and humid climates. Building and Environment. January 2003; 38(1): 99–107.

24. Zhang LZ., Niu JL. Performance comparisons of desiccant wheels for air dehumidification and enthalpy recovery. Applied Thermal Engineering. August 2002; 22(12): 1347–1367.

25. For W., Dehumidification AIR., Recoyery E. EFFECTS OF WALL THICKNESS ON THE HEAT ANB MOISTURE TRANSFERS IN DESICCANT WHEELS FOR AIR DEHUMIDIFICATION AND ENTHALPY RECOYERY. 2002; 29(2).

26. Niu JL., Zhang LZ., Zuo HG. Energy savings potential of chilled-ceiling combined with desiccant cooling in hot and humid climates. Energy and Buildings. June 2002; 34(5): 487–495.

27. Vali A., Simonson CJ., Besant RW., Mahmood G. Numerical model and effectiveness correlations for a run-around heat recovery system with combined counter and cross flow exchangers. International Journal of Heat and Mass Transfer. Elsevier Ltd; December 2009; 52(25–26): 5827–5840.

28. Li M., Simonson CJ., Besant RW., Shang W. Run-Around Energy Recovery System for Air-to-Air Applications Using Cross-Flow Exchangers Coupled with a Porous Solid Desiccant — Part I : Model Development and Verification. 2009; (December 2013): 37–41.

29. Riffat SB., Zhao X., Doherty PS. Application of sorption heat recovery systems in heating appliances—Feasibility study. Applied Thermal Engineering. January 2006; 26(1): 46–55.

30. Weixing Y., Yi Z., Xiaoru L., Xiugan Y. Study of a new modified cross-cooled compact solid desiccant dehumidifier. Applied Thermal Engineering. December 2008; 28(17–18): 2257–2266.

31. Zhang LZ. A three-dimensional non-equilibrium model for an intermittent adsorption cooling system. Solar Energy. 2000; 69(1): 27–35.

32. Rose J., Nielsen TR., Kragh J., Svendsen S. Quasi-steady-state model of a counter-flow air-to-air heat-exchanger with phase change. Applied Energy. May 2008; 85(5): 312–325.

33. Liu J., Li W., Liu J., Wang B. Efficiency of energy recovery ventilator with various weathers and its energy saving performance in a residential apartment. Energy and Buildings. January 2010; 42(1): 43–49.

34. Zhong K., Kang Y. Applicability of air-to-air heat recovery ventilators in China. Applied Thermal Engineering. April 2009; 29(5–6): 830–840.

35. Liu S., Zhao X., Riffat S., Yuan Y. Theoretical and experimental investigations of a liquid desiccant filmed cellulose fibre heat and mass exchanger. International Journal of Energy Research. 10 October 2009; 33(12): 1076–1088.

36. Kistler KR., Cussler EL. Membrane Modules for Building Ventilation. Chemical Engineering Research and Design. January 2002; 80(1): 53–64.

37. Min J., Su M. Performance analysis of a membrane-based enthalpy

exchanger: Effects of the membrane properties on the exchanger performance. Journal of Membrane Science. February 2010; 348(1–2): 376–382.

38. Hu T., Min J., Song Y. Modeling and analysis of dynamic adsorption during gas transport through a membrane. Journal of Membrane Science. September 2009; 339(1–2): 204–208.

39. Zhang L-Z. Conjugate Heat and Mass Transfer in Heat Mass Exchanger Ducts. 1st Editio. Boston: Academic Press; 2014. 391 p.

40. Scott K., Lobato J. Mass Transport in Cross-Corrugated Membranes and the Influence of TiO 2 for Separation Processes. Industrial and Engineering Chemistry Research. 2003; 42(22): 5697–5701.

41. Scott K., Mahmood AJ., Jachuck RJ., Hu B. Intensified membrane filtration with corrugated membranes. Journal of Membrane Science. 2000; 173(1): 1–16.

42. ZHANG L. Convective mass transport in cross-corrugated membrane exchangers. Journal of Membrane Science. 1 September 2005; 260(1–2): 75–83.

43. Mardiana a., Riffat SB. Review on physical and performance parameters of heat recovery systems for building applications. Renewable and Sustainable Energy Reviews. Elsevier; December 2013; 28: 174–190.

44. Redring-Xpelair. Redring-Xpelair Company Website. Available at: https://www.redringxpelair.com/

45. Pérez-Lombard L., Ortiz J., Pout C. A review on buildings energy consumption information. Energy and Buildings. January 2008; 40(3): 394–398.

46. Wan KKW., Li DHW., Liu D., Lam JC. Future trends of building heating and cooling loads and energy consumption in different climates. Building and Environment. January 2011; 46(1): 223–234.

47. Shao L., Riffat SB., Gan G. Heat recovery with low pressure loss for natural ventilation. 1998; 28(98).

48. Lazzarin RM., Gasparella A. Technical and economical analysis of heat recovery in building ventilation systems. Applied Thermal Engineering. 1998; 18(1–2): 47–67.

49. Fehrm M., Reiners W., Ungemach M. Exhaust air heat recovery in buildings ´ ration de la chaleur de l ' air extrait pour chauffer des Re habitations. 2002; 25: 439–449.

50. Zhou YP., Wu JY., Wang RZ. Performance of energy recovery ventilator with various weathers and temperature set-points. Energy and Buildings. December 2007; 39(12): 1202–1210.

51. UK Department of Health. UK: Impact Assessment ( IA ) Summary : Intervention and Options Summary : Analysis and Evidence Policy Option 1. Sustainable Development. 2011; (I): 1–42.

52. Min J., Su M. Performance analysis of a membrane-based energy recovery ventilator: Effects of membrane spacing and thickness on the ventilator performance. Applied Thermal Engineering. Elsevier Ltd; June 2010; 30(8–9): 991–997.

53. Lamb BR. Plate heat exchangers-a low-cost route to heat recovery. Journal of Heat Recovery Systems. 1982; 2(3): 247–255.

54. Yau YH. Experimental thermal performance study of an inclined heat pipe heat exchanger operating in high humid tropical HVAC systems. International Journal of Refrigeration. November 2007; 30(7): 1143–1152.

55. Srimuang W., Amatachaya P. A review of the applications of heat pipe heat exchangers for heat recovery. Renewable and Sustainable Energy Reviews. Elsevier Ltd; August 2012; 16(6): 4303–4315.

56. Nóbrega CEL., Brum NCL. Modeling and simulation of heat and enthalpy recovery wheels. Energy. December 2009; 34(12): 2063–2068.

57. Simonson CJ., Besant RW. Energy wheel effectiveness: part I—development of dimensionless groups. International Journal of Heat and Mass Transfer. Elsevier Sci Ltd; June 1999; 42(12): 2161–2170.

58. Seyed-Ahmadi M., Erb B., Simonson CJ., Besant RW. Transient behavior of run-around heat and moisture exchanger system. Part II: Sensitivity studies for a range of initial conditions. International Journal of Heat and Mass Transfer. December 2009; 52(25–26): 6012–6020.

59. Chaudhry HN., Hughes BR., Ghani SA. A review of heat pipe systems for heat recovery and renewable energy applications. Renewable and Sustainable Energy Reviews. Elsevier Ltd; May 2012; 16(4): 2249–2259.

60. Huynh NK., Li H., Soh YC., Cai W. Numerical analysis and model-based control of energy recovery ventilator in HVAC system. 2016 World Congress on Sustainable Technologies, WCST 2016. 2017. pp. 76–77.

61. Caputo a. C., Pelagagge PM. Heat recovery from moving cooling beds: transient modeling by dynamic simulation. Applied Thermal Engineering. January 1999; 19(1): 21–35.

62. Dagdas A. Performance Analysis and Optimization of Double-Flash Geothermal Power Plants. Journal of Energy Resources Technology. 2007; 129(2): 125.

63. Söylemez MS. On the optimum heat exchanger sizing for heat recovery. Energy Conversion and Management. September 2000; 41(13): 1419–1427.

64. Navarro HA., Cabezas-Gómez L. A new approach for thermal performance calculation of cross-flow heat exchangers. International Journal of Heat and Mass Transfer. August 2005; 48(18): 3880–3888.

65. Pongsoi P., Pikulkajorn S., Wongwises S. Effect of fin pitches on the optimum heat transfer performance of crimped spiral fin-and-tube heat exchangers. International Journal of Heat and Mass Transfer. Elsevier Ltd; November 2012; 55(23–24): 6555–6566.

66. Xie G., Wang Q., Sunden B. Parametric study and multiple correlations on air-side heat transfer and friction characteristics of fin-and-tube heat exchangers with large number of large-diameter tube rows. Applied Thermal Engineering. Elsevier Ltd; January 2009; 29(1): 1–16.

67. Manz H., Huber H. Experimental and numerical study of a duct/heat exchanger unit for building ventilation. Energy and Buildings. July 2000; 32(2): 189–196.

68. Nasif M., AL-Waked R., Morrison G., Behnia M. Membrane heat exchanger in HVAC energy recovery systems, systems energy analysis. Energy and Buildings. Elsevier B.V.; October 2010; 42(10): 1833–1840.

69. Yua YH. Theoretical determination of effectiveness for heat pipe heat exchangers operating in naturally ventilated tropical buildings. Proceedings of the Institution of Mechanical Engineers, Part A: Journal of Power and Energy. 1 January 2001; 215(3): 389–397.

70. Dalkilic a. S., Teke I., Wongwises S. Experimental analysis for the determination of the convective heat transfer coefficient by measuring pressure drop directly during annular condensation flow of R134a in a vertical smooth tube. International Journal of Heat and Mass Transfer. Elsevier Ltd; January 2011; 54(4): 1008–1014.

71. Yamaguchi S., Saito K. Numerical and experimental performance analysis of rotary desiccant wheels. International Journal of Heat and Mass Transfer. May 2013; 60: 51–60.

72. Kim S-M., Lee J-H., Kim S., Moon HJ., Cho J. Determining operation schedules of heat recovery ventilators for optimum energy savings in high-rise residential buildings. Energy and Buildings. Elsevier B.V.; March 2012; 46: 3–13.

73. Adamski M. Ventilation system with spiral recuperator. Energy and Buildings. Elsevier B.V.; May 2010; 42(5): 674–677.

74. Zhang L-Z. Heat and mass transfer in plate-fin enthalpy exchangers with

different plate and fin materials. International Journal of Heat and Mass Transfer. May 2009; 52(11–12): 2704–2713.

75. Tang LH., Zeng M., Wang QW. Experimental and numerical investigation on air-side performance of fin-and-tube heat exchangers with various fin patterns. Experimental Thermal and Fluid Science. Elsevier Inc.; July 2009; 33(5): 818–827.

76. Roulet C–., Heidt F., Foradini F., Pibiri M-C. Real heat recovery with air handling units. Energy and Buildings. May 2001; 33(5): 495–502.

77. Laverge J., Janssens a. Heat recovery ventilation operation traded off against natural and simple exhaust ventilation in Europe by primary energy factor, carbon dioxide emission, household consumer price and exergy. Energy and Buildings. Elsevier B.V.; July 2012; 50: 315–323.

78. El Fouih Y., Stabat P., Rivière P., Hoang P., Archambault V. Adequacy of air-to-air heat recovery ventilation system applied in low energy buildings. Energy and Buildings. Elsevier B.V.; November 2012; 54: 29–39.

79. Rasouli M., Ge G., Simonson CJ., Besant RW. Uncertainties in energy and economic performance of HVAC systems and energy recovery ventilators due to uncertainties in building and HVAC parameters. Applied Thermal Engineering. Elsevier Ltd; January 2013; 50(1): 732–742.

80. Dodoo A., Gustavsson L., Sathre R. Primary energy implications of ventilation heat recovery in residential buildings. Energy and Buildings. Elsevier B.V.; July 2011; 43(7): 1566–1572.

81. Kang Y., Wang Y., Zhong K., Liu J. Temperature ranges of the application of air-to-air heat recovery ventilator in supermarkets in winter, China. Energy and Buildings. Elsevier B.V.; December 2010; 42(12): 2289–2295.

82. Incropera FP., DeWitt DP., Bergman TL., Lavine AS. Fundamentals of Heat and Mass Transfer. Incropera FP, Incropera FPFOH, Transfer M (eds.) Water. John Wiley & Sons; 2007. 997 p.

83. Numerical Prediction of Laminar Forced Convection in Triangular Ducts With Unstructured Triangular Grid Method. Numerical Heat Transfer, Part A: Applications. August 2000; 38(2): 209–224.

84. Zhang L-Z. Heat and mass transfer in a cross-flow membrane-based enthalpy exchanger under naturally formed boundary conditions. International Journal of Heat and Mass Transfer. January 2007; 50(1–2): 151–162.

85. Manz H., Huber H., Schälin a., Weber a., Ferrazzini M., Studer M. Performance of single room ventilation units with recuperative or regenerative heat recovery. Energy and Buildings. January 2000; 31(1): 37–47.

86. Liu S. A Novel Heat Recovery / Desiccant Cooling System Thesis by Shuli Liu , BEng , MSc Thesis submitted to the University of Nottingham For the degree of Doctor of Philosophy. 2008; (May).

87. Abd El-Baky M a., Mohamed MM. Heat pipe heat exchanger for heat recovery in air conditioning. Applied Thermal Engineering. March 2007; 27(4): 795–801.

88. Manz H., Huber H. Experimental and numerical study of a duct/heat exchanger unit for building ventilation. Energy and Buildings. Elsevier Sequoia SA; July 2000; 32(2): 189–196.

89. Tadrist L., Miscevic M., Rahli O., Topin F. About the use of fibrous materials in compact heat exchangers. Experimental Thermal and Fluid Science. January 2004; 28(2–3): 193–199.

90. T'Joen C., Park Y., Wang Q., Sommers a., Han X., Jacobi a. A review on polymer heat exchangers for HVAC&R applications. International Journal of Refrigeration. Elsevier Ltd and IIR; August 2009; 32(5): 763–779.

91. Kho T., Zettler H. Effect of flow distribution on scale formation in plate and frame heat exchangers. … Research and Design. 1997; : 0–5.

92. Kragh J., Rose J., Nielsen TR., Svendsen S. New counter flow heat exchanger designed for ventilation systems in cold climates. Energy and Buildings. November 2007; 39(11): 1151–1158.

93. Gendebien S., Bertagnolio S., Lemort V. Investigation on a ventilation heat recovery exchanger: Modeling and experimental validation in dry and partially wet conditions. Energy and Buildings. Elsevier B.V.; July 2013; 62: 176–189.

94. Gendebien S., Bertagnolio S., Lemort V., Guan G., Yang X., Wang R., et al. A review of heat recovery technology for passive ventilation applications. Renewable and Sustainable Energy Reviews. Elsevier B.V.; July 2015; 84: 301–309.

95. Zhao X., Li JM., Riffat SB. Numerical study of a novel counter-flow heat and mass exchanger for dew point evaporative cooling. Applied Thermal Engineering. October 2008; 28(14–15): 1942–1951.

96. Zhao X., Yang S., Duan Z., Riffat SB. Feasibility study of a novel dew point air conditioning system for China building application. Building and Environment. Elsevier Ltd; September 2009; 44(9): 1990–1999.

97. Idicula M., Boudenne A., Umadevi L., Ibos L., Candau Y., Thomas S. Thermophysical properties of natural fibre reinforced polyester composites. Composites Science and Technology. December 2006; 66(15): 2719–2725.

98. Fend T., Hoffschmidt B., Pitz-Paal R., Reutter O., Rietbrock P. Porous materials as open volumetric solar receivers: Experimental determination of thermophysical and heat transfer properties. Energy. April 2004; 29(5–6): 823–833.

99. Liu S., Zhao X., Riffat S., Yuan Y. Comparative study of hydrophilic materials for air-to-air heat/mass exchanger. International Journal of Low-Carbon Technologies. 4 June 2009; 4(2): 120–130.

100. Dallaire J., Gosselin L., da Silva AK. Conceptual optimization of a rotary

heat exchanger with a porous core. International Journal of Thermal Sciences. Elsevier Masson SAS; February 2010; 49(2): 454–462.

101. Zhang L-Z. An analytical solution for heat mass transfer in a hollow fiber membrane based air-to-air heat mass exchanger. Journal of Membrane Science. Elsevier B.V.; September 2010; 360(1–2): 217–225.

102. Zhang L-Z. A fractal model for gas permeation through porous membranes. International Journal of Heat and Mass Transfer. October 2008; 51(21–22): 5288–5295.

103. Zhang LZ., Niu JL. Effectiveness Correlations for Heat and Moisture Transfer Processes in an Enthalpy Exchanger With Membrane Cores. Journal of Heat Transfer. 2002; 124(5): 922.

104. Min J., Su M. Performance analysis of a membrane-based energy recovery ventilator: Effects of membrane spacing and thickness on the ventilator performance. Applied Thermal Engineering. June 2010; 30(8–9): 991–997.

105. Al-Waked R., Nasif MS., Morrison G., Behnia M. CFD simulation of air to air enthalpy heat exchanger. Energy Conversion and Management. Elsevier Ltd; October 2013; 74: 377–385.

106. Niu J. Membrane-based Enthalpy Exchanger: material considerations and clarification of moisture resistance. Journal of Membrane Science. 15 August 2001; 189(2): 179–191.

107. Woods J., Kozubal E. Heat transfer and pressure drop in spacer-filled channels for membrane energy recovery ventilators. Applied Thermal Engineering. Elsevier Ltd; January 2013; 50(1): 868–876.

108. Zhang L-Z. Flow maldistribution and thermal performance deterioration in a cross-flow air to air heat exchanger with plate-fin cores. International Journal of Heat and Mass Transfer. Elsevier Ltd; September 2009; 52(19–20): 4500–4509.

109. Zhang L-Z. A fractal model for gas permeation through porous membranes. International Journal of Heat and Mass Transfer. October 2008; 51(21–22): 5288–5295.

110. Zhang L. Effects of Membrane Parameters on Performance of Vapor Permeation through a Composite Supported Liquid Membrane. Separation Science and Technology. December 2006; 41(16): 3517–3538.

111. Zhang LZ., Jiang Y. Heat and mass transfer in a membrane-based energy recovery ventilator. Journal of Membrane Science. October 1999; 163(1): 29–38.

112. Hemingson HB., Simonson CJ., Besant RW. Steady-state performance of a run-around membrane energy exchanger (RAMEE) for a range of outdoor air conditions. International Journal of Heat and Mass Transfer. Elsevier Ltd; April 2011; 54(9–10): 1814–1824.

113. Ge G., Ghadiri Moghaddam D., Namvar R., Simonson CJ., Besant RW. Analytical model based performance evaluation, sizing and coupling flow optimization of liquid desiccant run-around membrane energy exchanger systems. Energy and Buildings. Elsevier B.V.; July 2013; 62: 248–257.

114. Liu B., Chen J., Du X., Xue L. Poly (vinyl chloride)/montmorillonite hybrid membranes for total-heat recovery ventilation. Journal of Membrane Science. Elsevier; September 2013; 443: 83–92.

115. O'connor D., Calautit JKS., Hughes BR. A review of heat recovery technology for passive ventilation applications. Renewable and Sustainable Energy Reviews. Elsevier; 2016; 54: 1481–1493.

116. Chang WR. Effectiveness Characteristic Measurements of a Membrane-Based Energy Recovery Ventilator for Residential Application. Journal of the Chinese Society of Mechanical Engineers, Transactions of the Chinese Institute of Engineers, Series C/Chung-Kuo Chi Hsueh Kung Ch'eng Hsuebo Pao. 2016; 37(4): 367–375.

117. Chang WR. Experimental study on a membrane dehumidifier for ventilation application. JP Journal of Heat and Mass Transfer. 2016; 13(3): 325–342.

118. Zhang L., Chen Z. Convective heat transfer in cross-corrugated triangular ducts under uniform heat flux boundary conditions. International Journal of Heat and Mass Transfer. January 2011; 54(1–3): 597–605.

119. Han X-H., Cui L-Q., Chen S-J., Chen G-M., Wang Q. A numerical and experimental study of chevron, corrugated-plate heat exchangers. International Communications in Heat and Mass Transfer. Elsevier Ltd; October 2010; 37(8): 1008–1014.

120. Forooghi P., Hooman K. Effect of buoyancy on turbulent convection heat transfer in corrugated channels – A numerical study. International Journal

121. Islamoglu Y., Parmaksizoglu C. Numerical investigation of convective heat transfer and pressure drop in a corrugated heat exchanger channel. Applied Thermal Engineering. January 2004; 24(1): 141–147.

122. Doo JH., Ha MY., Min JK., Stieger R., Rolt a., Son C. An investigation of cross-corrugated heat exchanger primary surfaces for advanced intercooled-cycle aero engines (Part-II: Design optimization of primary surface). International Journal of Heat and Mass Transfer. June 2013; 61: 138–148.

123. Qi Z., Chen J., Chen Z. Parametric study on the performance of a heat exchanger with corrugated louvered fins. Applied Thermal Engineering. February 2007; 27(2–3): 539–544.

124. Zhang G., Li G., Li W., Zhang Z., Leng X., Tian M. Particulate fouling and composite fouling assessment in corrugated plate heat exchangers. International Journal of Heat and Mass Transfer. May 2013; 60: 263–273.

125. Elshafei E a. M., Awad MM., El-Negiry E., Ali a. G. Heat transfer and pressure drop in corrugated channels. Energy. Elsevier Ltd; January 2010; 35(1): 101–110.

126. Fernández-Seara J., Diz R., Uhía FJ., Dopazo A., Ferro JM. Experimental analysis of an air-to-air heat recovery unit for balanced ventilation systems in residential buildings. Energy Conversion and Management. January 2011; 52(1): 635–640.

127. Yaïci W., Ghorab M., Entchev E. Numerical analysis of heat and energy recovery ventilators performance based on CFD for detailed design. Applied Thermal Engineering. Elsevier Ltd; March 2013; 51(1–2): 770–780.

128. Zhang L-Z. An analytical solution for heat mass transfer in a hollow fiber membrane based air-to-air heat mass exchanger. Journal of Membrane Science. September 2010; 360(1–2): 217–225.

129. Nasif M., AL-Waked R., Morrison G., Behnia M. Membrane heat exchanger in HVAC energy recovery systems, systems energy analysis. Energy and Buildings. October 2010; 42(10): 1833–1840.

130. Deshko VI., Karvatskii AY., Sukhodub IO. Heat and mass transfer in cross-flow air-to-air membrane heat exchanger in heating mode. Applied Thermal Engineering. 2016; 100: 133–145.

131. Koester S., Falkenberg M., Logemann M., Wessling M. Modeling heat and mass transfer in cross-counterflow enthalpy exchangers. Journal of Membrane Science. 2017; 525: 68–76.

132. LIANG C., LI Z. Conjugate heat transfer in a total heat exchanger with cross-corrugated triangular ducts in laminar flow. Journal of Thermal Science and Technology. 2015.

133. Bejan A. Entropy generation minimization: The new thermodynamics of finite-size devices and finite-time processes. Journal of Applied Physics. 1996; 79(3): 1191–1218.

134. Bejan A. Fundamentals of exergy analysis, entropy generation minimization, and the generation of flow architecture. International Journal of Energy Research. 2002; 26(7): 0–43.

exchangers. International Journal of Heat and Mass Transfer. 2000; 43(22): 4189–4204. Available at: DOI:10.1016/S0017-9310(99)00364-6

136. Cornelissen RL., Hirs GG. Exergetic optimisation of a heat exchanger. Energy Conversion and Management. 1997; 38(15–17): 1567–1576.

137. Yilmaz M., Sara O., Karsli S. Performance evaluation criteria for heat exchangers based on second law analysis. Exergy, An International Journal. 2001; 1(4): 278–294.

138. Naphon P. Study on the exergy loss of the horizontal concentric micro-fin tube heat exchanger. International Communications in Heat and Mass Transfer. 2011; 38(2): 229–235.

139. Feng X., Zhong G., Zhu P., Gu Z. Cumulative exergy analysis of heat exchanger production and heat exchange processes. Energy & Fuels. 2004; 18(4): 1194–1198.

140. Sukhodub IO., Deshko VI. Exergy analysis of ventilation systems with energy recovery. Magazine of Civil Engineering. 2014; 46(2): 36–74.

141. Mróz TM., Dutka A. Exergy-economic evaluation of heat recovery device in mechanical ventilation system. Energy and Buildings. 2015; 86: 296–304.

142. Ghazikhani M., Khazaee I., Vahidifar S. Exergy analysis of two humidification process methods in air-conditioning systems. Energy and Buildings. Elsevier B.V.; 2016; 124: 129–140.

143. Durmuş A., Benli H., Kurtbaş İ., Gül H. Investigation of heat transfer and pressure drop in plate heat exchangers having different surface profiles. International Journal of Heat and Mass Transfer. 2009; 52(5–6): 1451–1457.

144. Pandey SD., Nema VK. An experimental investigation of exergy loss reduction in corrugated plate heat exchanger. Energy. Elsevier Ltd; 2011; 36(5): 2997–3001.

145. Tiwari AK., Ghosh P., Sarkar J. Combined energy and exergy analysis of a corrugated plate heat exchanger and experimental investigation. International Journal of Exergy. 2014; 15(4): 395–411.

146. Martinaitis V., Bielskus J., Januševičius K., Bareika P. Exergy efficiency of a ventilation heat recovery exchanger at a variable reference temperature. Mechanika. 2017; 23(1): 70–77.

147. Al-Sulaiman FA. Energy and Exergy Analyses of an Air Membrane Heat and Mass Exchanger for Air Conditioning Applications. Journal of Energy Engineering. 2017; 143(5).

148. Jenkins GJ., Perry MC., Prior MJ. The climate of the UK and recent trends. 1st Editio. Met Office Hadley Center. Oxford UK; 2009. 1-122 p.

149. Holman JP. Heat Transfer. 2009; : 752.

150. Gabour LA., Lienhard JH. Wall Roughness Effects on Stagnation-Point Heat Transfer Beneath an Impinging Liquid Jet. Journal of Heat Transfer. 1994; 116(1): 81.

151. Armellini A., Casarsa L., Giannattasio P. Low Reynolds number flow in rectangular cooling channels provided with low aspect ratio pin fins. International Journal of Heat and Fluid Flow. 2010; 31(4): 689–701.

152. Zhang L-Z. Turbulent Three-Dimensional Air Flow and Heat Transfer in a Cross-Corrugated Triangular Duct. Journal of Heat Transfer. 2005; 127(10): 1151.

153. Yang B., Yuan W., Gao F., Guo B. A review of membrane-based air dehumidification. Indoor and Built Environment. 2015; 24(1): 11–26.

154. Woods J. Membrane processes for heating, ventilation, and air conditioning. Renewable and Sustainable Energy Reviews. Elsevier; 2014; 33: 290–304.

155. Metz SJ., Van De Ven WJC., Potreck J., Mulder MH V., Wessling M. Transport of water vapor and inert gas mixtures through highly selective

and highly permeable polymer membranes. Journal of Membrane Science. 2005; 251(1–2): 29–41.

156. Ouyang G., Hussain A., Li J., Li D. Remarkable permeability enhancement of polyethersulfone (PES) ultrafiltration membrane by blending cobalt oxide/graphene oxide nanocomposites. RSC Advances. Royal Society of Chemistry; 2015; 5: 70448–70460.

157. Abdallah H., El-Gendi A., Khedr M., El-Zanati E. Hydrophobic polyethersulfone porous membranes for membrane distillation. Frontiers of Chemical Science and Engineering. 2015; 9(1): 84–93.

158. Kochan J., Wintgens T., Wong JE., Melin T. Properties of polyethersulfone ultrafiltration membranes modified by polyelectrolytes. Desalination. 2010; 250(3): 1008–1010.

159. Versteeg HK., Malaskekera W. An Introduction to Computational Fluid Dynamics. Fluid flow handbook. McGraw-Hill …. 2007. 517 p.

160. Lomax H., Pulliam T., Zingg D., Kowalewski T. Fundamentals of Computational Fluid Dynamics. Applied Mechanics Reviews. 2002. p. B61.

161. Al-Waked R., Nasif MS., Morrison G., Behnia M. CFD simulation of air to air enthalpy heat exchanger: Variable membrane moisture resistance. Applied Thermal Engineering. Elsevier Ltd; 2015; 84: 301–309.

162. Patankar S. Numerical heat transfer and fluid flow. Series in coputational methods in mechanics and thermal sciences. 1980. 1-197 p.

163. Gan G., Riffat SB. Naturally ventilated buildings with heat recovery: CFD simulation of thermal environment. Building Services Engineering Research and Technology. 1997; 18(2): 67–75.

164. ANSYS® WORKBENCH® Academic , Release 17.1, ANSYS, Inc. 2016.

165. ANSYS® Fluent® Academic, Release 17.1, ANSYS, Inc. 2016.

166. CATIA V5. Dassault Systems; 2013.

167. Fluent a. ANSYS Fluent 12.0 user's guide. Ansys Inc. 2009; 15317(November): 1–2498.

168. Menter FR., Langtry R., Völker S., Huang PG. Transition Modelling for General Purpose CFD Codes. Engineering Turbulence Modelling and Experiments 6. 2005; (March): 31–48.

169. Menter FR., Langtry RB., Likki SR., Suzen YB., Huang PG., Völker S. A Correlation-Based Transition Model Using Local Variables—Part I: Model Formulation. Journal of Turbomachinery. 2006; 128(3): 413.

170. Langtry RB., Menter FR., Likki SR., Suzen YB., Huang PG., Völker S. A Correlation-Based Transition Model Using Local Variables-Part II: Test Cases and Industrial Applications. Journal of Turbomachinery. 2006; 128(3): 423.

171. Langtry RB., Menter FR. Correlation-Based Transition Modeling for Unstructured Parallelized Computational Fluid Dynamics Codes. AIAA Journal. 2009; 47(12): 2894–2906.

172. AL-DEROUBI NN. Computational and Experimental Investigation of Drag Reduction for Tractor-Trailer Geometry Using Active Flow Control. University of technology, Baghdad; 2010.

173. Abduljabbar AA. Prediction of Radiant Cooling Panels Performance in Mixed Convection Environments. University of Technology - Baghdad; 2012.

174. Abdulhadi H. Numerical and Experimental Investigation on the Effect of Restriction Shape on Characteristics of Airflow in a Square Duct. University of Technology, Baghdad; 2006.

175. Bahaidarah H. A Numerical Study of Heat and Momentum Transfer Over a Bank of Flat Tubes. A&M Uneversity - Texas; 2004.

176. Nbras H. Effect of riblet geometry on drag reduction and its application on airfoil. University of Tchnology - Baghdad; 2009.

177. Andersson B., Andersson R., Hakansson L., Mortensen M., Sudiyo R., van Wachem B. Computational Fluid Dynamics for Engineers. Cambridge University Press. 2012. 212 p.

178. Hoffmann K a., Chiang ST. Computational Fluid Dynamics Vol.I - Hoffmann.pdf. International Journal of Computational Fluid Dynamics. 2000. pp. 581–594.

179. Tu J., Yeoh G-H., Liu C. Computational Fluid Dynamics: A Practical Approach. Terror and the Postcolonial. 2009. i-xii p.

180. Zhao C., Xue J., Ran F., Sun S. Modification of polyethersulfone membranes – A review of methods. Progress in Materials Science. Elsevier Ltd; January 2013; 58(1): 76–150.

181. Li ZX., Zhong TS., Niu JL., Xiao F., Zhang LZ. Conjugate heat and mass transfer in a total heat exchanger with cross-corrugated triangular ducts and one-step made asymmetric membranes. International Journal of Heat and Mass Transfer. Elsevier Ltd; 2015; 84: 390–400.

182. Zhang L-Z. Heat and mass transfer in a quasi-counter flow membrane-based total heat exchanger. International Journal of Heat and Mass Transfer. November 2010; 53(23–24): 5478–5486.

183. Holman J. Heat Transfer. Mc Graw Hill. 2010. 758 p.

184. Moran MJ., Howard N Shapiro. Fundamentals Of Engineering Thermodynamics. Chemistry & …. 2004; : 845.

185. Alkaesy LA. Modification Analysis and Thermodynamic Modeling of Packaged Unit Air Conditioner Performance. University of Technology, Baghdad; 2012.

186. Cengel YA., Boles MA. Thermodynamics: an Engineering Approach 8th Edition. McGraw-Hill. 2015. 572-575 p.

187. Sato N. Chemical Energy and Exergy : An Introduction to Chemical Thermodynamics for Engineers. Firdt Edit. Amsterdam ; San Diego, CA .

Elsevier, (c); 2014. 149 p.

188. Von V., Diplom-Ingenieur., Andrej J. A novel exergy-based concept of thermodynamic quality and its application to energy system evaluation and process analysis. 2010; : 177. /

189. Tsatsaronis G. Recent developments in exergy analysis and exergoeconomics. International Journal of Exergy. Institute for Energy Engineering, Technische Universität Berlin, Marchstr. 18, 10587 Berlin, Germany; 2008; 5(5–6): 489–499.

190. Kelly S., Tsatsaronis G., Morosuk T. Advanced exergetic analysis: Approaches for splitting the exergy destruction into endogenous and exogenous parts. Energy. 2009; 34(3): 384–391.

191. SimTech. IPSEpro. Available at: http://www.simtechnology.com/CMS/index.php/ipsepro

192. Makhdoum BM. An Energy , Exergy and Economic Modeling Study based on Utilizing waste Heat Energy of a C200 Microturbine to Power ORC, Absorption Chiller and Desalination Units. Newcastle University; 2012.

193. SimTech. PSE: Process Simulation Environment. Available at: http://www.simtechnology.com/CMS/index.php/ipsepro/program-modules/pse

194. Framework IM. IPSEpro - Heat Balance Software for Power Plant Design , Analysis , Optimization and Performance Monitoring IPSEpro - Cloud-Based Computing for Power Plants Open-Equation Modeling Technology. 2012;

195. Giglmayr I., Nixdorf M., Pogoreutz M. Comparison of software for thermodynamic process calculation. VGB PowerTech. 2001. 44-51 p.

196. Sim Tech ST. IPSEpro process simulator manuals: process simulation environment. SimTech Simulation Technology. 2012;

# APPENDICES

# Appendix A ENERGETIC RESULTS

## A.1 (25 mm) Cases with Variable Inlet Air Velocity

**Table 6-1 (25 mm) cases with different INLET AIR VELOCITY**

| | FRESH | | EXHAUST | | FRESH | | EXHAUST | |
|---|---|---|---|---|---|---|---|---|
| **Velocity** | $\dot{m}_{fi}$ | $\dot{m}_{fo}$ | $\dot{m}_{ei}$ | $\dot{m}_{eo}$ | $T_{fi}$ | $T_{fo}$ **average** | $T_{ei}$ | $T_{eo}$ **average** |
| **m/s** | **kg/s** | **kg/s** | **kg/s** | **kg/s** | **C°** | **C°** | **C°** | **C°** |
| **0.5** | 0.467453 | 0.526488 | 0.441271 | 0.382261 | 6 | 17.98 | 22 | 10.089 |
| **1** | 0.934904 | 1.015185 | 0.882538 | 0.802266 | 6 | 18.441 | 22 | 11.682 |
| **1.5** | 1.402357 | 1.505411 | 1.323809 | 1.220764 | 6 | 18.44 | 22 | 12.444 |
| **2** | 1.869808 | 1.995296 | 1.765077 | 1.639602 | 6 | 18.283 | 22 | 13.101 |

**Table 1-2 (25 mm) FRESH Air composition with Variable Inlet Air Velocity**

| | FRESH | | | | | |
|---|---|---|---|---|---|---|
| Velocity | $H_2O_{fi}$ | $H_2O_{fo}$ **average** | $O_{2\,fi}$ | $O_{2\,fo}$ **average** | $N_{2\,fi}$ | $N_{2\,fo}$ **average** |
| m/s | kg/kg | kg/kg | kg/kg | kg/kg | kg/kg | kg/kg |
| **0.5** | 0.00492 | 0.0072616 | 0.23 | 0.230068 | 0.76508 | 0.76267 |
| **1** | 0.00492 | 0.0074656 | 0.23 | 0.229995 | 0.76508 | 0.762539 |
| **1.5** | 0.00492 | 0.0074753 | 0.23 | 0.229996 | 0.76508 | 0.762529 |
| **2** | 0.00492 | 0.0074437 | 0.23 | 0.23 | 0.76508 | 0.762556 |

**Table 1-3 (25 mm) EXHAUST Air composition with Variable Inlet Air Velocity**

| | EXHAUST | | | | | |
|---|---|---|---|---|---|---|
| Velocity | $H_2O_{ei}$ | $H_2O_{eo}$ **average** | $O_{2\,ei}$ | $O_{2\,eo}$ **average** | $N_{2\,ei}$ | $N_{2\,eo}$ **average** |
| m/s | kg/kg | kg/kg | kg/kg | kg/kg | kg/kg | kg/kg |
| 0.5 | 0.00822 | 0.0055341 | 0.23 | 0.229634 | 0.76178 | 0.764832 |
| 1 | 0.00822 | 0.0060436 | 0.23 | 0.230012 | 0.76178 | 0.763944 |
| 1.5 | 0.00822 | 0.0062309 | 0.23 | 0.230007 | 0.76178 | 0.763762 |
| 2 | 0.00822 | 0.0063670 | 0.23 | 0.230002 | 0.76178 | 0.763631 |

## A.2 (25 mm) Cases with Variable AMBIENT TEMPERATURE

**Table 1-4 (25 mm) cases with different AMBIENT TEMPERATURE**

| | FRESH | | EXHAUST | | FRESH | | EXHAUST | |
|---|---|---|---|---|---|---|---|---|
| Amb. Temp. | $\dot{m}_{fi}$ | $\dot{m}_{fo}$ | $\dot{m}_{ei}$ | $\dot{m}_{eo}$ | $T_{fi}$ | $T_{fo}$ average | $T_{ei}$ | $T_{eo}$ average |
| 0C | kg/s | kg/s | kg/s | kg/s | C° | C° | C° | C° |
| 2 | 1.898314 | 2.012414 | 1.765077 | 1.54293 | 2 | 17.304 | 22 | 10.861 |
| 4 | 1.884006 | 2.004791 | 1.765077 | 1.536796 | 4 | 17.783 | 22 | 12.017 |
| 6 | 1.869808 | 1.99694 | 1.765077 | 1.530715 | 6 | 18.262 | 22 | 13.16 |
| 8 | 1.855728 | 1.989097 | 1.765077 | 1.524892 | 8 | 18.74 | 22 | 14.282 |
| 10 | 1.841755 | 1.981397 | 1.765077 | 1.519235 | 10 | 19.215 | 22 | 15.416 |

**Table 1-5 (25 mm) FRESH Air composition with Variable AMBIENT TEMPERATURE**

| | FRESH | | | | | |
|---|---|---|---|---|---|---|
| Amb. Temp. | $H_2O_{fi}$ | $H_2O_{fo}$ average | $O_{2\,fi}$ | $O_{2\,fo}$ average | $N_{2\,fi}$ | $N_{2\,fo}$ average |
| 0C | kg/kg | kg/kg | kg/kg | kg/kg | kg/kg | kg/kg |
| 2 | **0.00371** | 0.00714798 | 0.23 | 0.229999 | 0.76629 | 0.762853 |
| 4 | **0.00427** | 0.00728323 | 0.23 | 0.229999 | 0.76573 | 0.762718 |
| 6 | **0.00492** | 0.00744002 | 0.23 | 0.229999 | 0.76508 | 0.762561 |
| 8 | **0.00565** | 0.0076143 | 0.23 | 0.229998 | 0.76435 | 0.762388 |
| 10 | **0.00647** | 0.00780875 | 0.23 | 0.229998 | 0.76353 | 0.762194 |

**Table 1-6 (25mm) EXHAUST Air composition with Variable AMBIENT TEMPERATURE**

| | EXHAUST | | | | | |
|---|---|---|---|---|---|---|
| Amb. Temp. | $H_2O_{ei}$ | $H_2O_{eo}$ average | $O_{2\,ei}$ | $O_{2\,eo}$ average | $N_{2\,ei}$ | $N_{2\,eo}$ average |
| 0C | kg/kg | kg/kg | kg/kg | kg/kg | kg/kg | kg/kg |
| 2 | 0.00822 | 0.00568355 | 0.23 | 0.230002 | 0.76178 | 0.764314 |
| 4 | 0.00822 | 0.00600766 | 0.23 | 0.230002 | 0.76178 | 0.76399 |
| 6 | 0.00822 | 0.00637999 | 0.23 | 0.230003 | 0.76178 | 0.763617 |
| 8 | 0.00822 | 0.00679249 | 0.23 | 0.230003 | 0.76178 | 0.763205 |
| 10 | 0.00822 | 0.00725205 | 0.23 | 0.230003 | 0.76178 | 0.762745 |

## A.3 (10 mm) Cases with Variable Inlet Air Velocity

**Table 1-7 (10 mm) cases with different INLET AIR VELOCITY**

| | FRESH | | EXHAUST | | FRESH | | EXHAUST | |
|---|---|---|---|---|---|---|---|---|
| **Velocity** | $\dot{m}_{fi}$ | $\dot{m}_{fo}$ | $\dot{m}_{ei}$ | $\dot{m}_{eo}$ | $T_{fi}$ | $T_{fo}$ **average** | $T_{ei}$ | $T_{eo}$ **average** |
| **m/s** | **kg/s** | **kg/s** | **kg/s** | **kg/s** | **C°** | **C°** | **C°** | **C°** |
| **0.5** | 0.475951 | 0.528171 | 0.447769 | 0.395584 | 6 | 17.986 | 22 | 8.689 |
| **1** | 0.951902 | 1.05875 | 0.898583 | 0.791735 | 6 | 17.364 | 22 | 9.255 |
| **1.5** | 1.427853 | 1.57143 | 1.347878 | 1.204301 | 6 | 17.599 | 22 | 9.727 |
| **2** | 1.903804 | 2.071349 | 1.797166 | 1.629628 | 6 | 17.7878 | 22 | 9.968 |

**Table 1-8 (10 mm) FRESH Air composition with Variable Inlet Air Velocity**

| | FRESH | | | | | |
|---|---|---|---|---|---|---|
| Velocity | $H_2O_{fi}$ | $H_2O_{fo}$ **average** | $O_{2\,fi}$ | $O_{2\,fo}$ **average** | $N_{2\,fi}$ | $N_{2\,fo}$ **average** |
| m/s | kg/kg | kg/kg | kg/kg | kg/kg | kg/kg | kg/kg |
| **0.5** | 0.00492 | 0.00723021 | 0.23 | 0.23 | 0.76508 | 0.76277 |
| **1** | 0.00492 | 0.0072526 | 0.23 | 0.23 | 0.76508 | 0.762747 |
| **1.5** | 0.00492 | 0.00730139 | 0.23 | 0.23 | 0.76508 | 0.762699 |
| **2** | 0.00492 | 0.00733993 | 0.23 | 0.23 | 0.76508 | 0.76266 |

**Table 1-9 (10 mm) EXHAUST Air composition with Variable Inlet Air Velocity**

| | EXHAUST | | | | | |
|---|---|---|---|---|---|---|
| Velocity | $H_2O_{ei}$ | $H_2O_{eo}$ **average** | $O_{2\,ei}$ | $O_{2\,eo}$ **average** | $N_{2\,ei}$ | $N_{2\,eo}$ **average** |
| m/s | kg/kg | kg/kg | kg/kg | kg/kg | kg/kg | kg/kg |
| **0.5** | 0.00822 | 0.00545374 | 0.23 | 0.23 | 0.76178 | 0.765112 |
| **1** | 0.00822 | 0.00561322 | 0.23 | 0.23 | 0.76178 | 0.764387 |
| **1.5** | 0.00822 | 0.00570158 | 0.23 | 0.23 | 0.76178 | 0.764298 |
| **2** | 0.00822 | 0.00574402 | 0.23 | 0.23 | 0.76178 | 0.764256 |

## A.4 (10 mm) Cases with Variable AMBIENT TEMPERATURE

**Table 1-10 (10 mm) cases with different AMBIENT TEMPERATURE**

| | FRESH | | EXHAUST | | FRESH | | EXHAUST | |
|---|---|---|---|---|---|---|---|---|
| Amb. Temp. | $\dot{m}_{fi}$ | $\dot{m}_{fo}$ | $\dot{m}_{ei}$ | $\dot{m}_{eo}$ | $T_{fi}$ | $T_{fo}$ average | $T_{ei}$ | $T_{eo}$ average |
| $^0C$ | kg/s | kg/s | kg/s | kg/s | $C^o$ | $C^o$ | $C^o$ | $C^o$ |
| 2 | 1.932833 | 2.084173 | 1.797166 | 1.645826 | 2 | 16.687 | 22 | 6.913 |
| 4 | 1.918259 | 2.077908 | 1.797166 | 1.637524 | 4 | 17.242 | 22 | 8.444 |
| 6 | 1.903804 | 2.071349 | 1.797166 | 1.629628 | 6 | 17.7878 | 22 | 9.968 |
| 8 | 1.889468 | 2.065392 | 1.797166 | 1.621249 | 8 | 18.33 | 22 | 11.49 |
| 10 | 1.875244 | 2.059197 | 1.797166 | 1.613213 | 10 | 18.867 | 22 | 13.006 |

**Table 1-11 (10 mm) FRESH Air composition with Variable AMBIENT TEMPERATURE**

| | FRESH | | | | | |
|---|---|---|---|---|---|---|
| Amb. Temp. | $H_2O_{fi}$ | $H_2O_{fo}$ average | $O_{2\,fi}$ | $O_{2\,fo}$ average | $N_{2\,fi}$ | $N_{2\,fo}$ average |
| $^0C$ | kg/kg | kg/kg | kg/kg | kg/kg | kg/kg | kg/kg |
| 2 | **0.00371** | 0.00700546 | 0.23 | 0.23 | 0.76178 | 0.765177 |
| 4 | **0.00427** | 0.00716204 | 0.23 | 0.23 | 0.76573 | 0.762838 |
| 6 | **0.00492** | 0.00733993 | 0.23 | 0.23 | 0.76508 | 0.76266 |
| 8 | **0.00565** | 0.00753802 | 0.23 | 0.23 | 0.76435 | 0.762462 |
| 10 | **0.00647** | 0.00775759 | 0.23 | 0.23 | 0.76353 | 0.762242 |

**Table 1-12 (10mm) EXHAUST Air composition with Variable AMBIENT TEMPERATURE**

| | EXHAUST | | | | | |
|---|---|---|---|---|---|---|
| Amb. Temp. | $H_2O_{ei}$ | $H_2O_{eo}$ average | $O_{2\,ei}$ | $O_{2\,eo}$ average | $N_{2\,ei}$ | $N_{2\,eo}$ average |
| $^0C$ | kg/kg | kg/kg | kg/kg | kg/kg | kg/kg | kg/kg |
| 2 | 0.00822 | 0.00482334 | 0.23 | 0.23 | 0.76178 | 0.765177 |
| 4 | 0.00822 | 0.00525089 | 0.23 | 0.23 | 0.76178 | 0.764749 |
| 6 | 0.00822 | 0.00574402 | 0.23 | 0.23 | 0.76178 | 0.764256 |
| 8 | 0.00822 | 0.00629588 | 0.23 | 0.23 | 0.76178 | 0.763704 |
| 10 | 0.00822 | 0.0069122 | 0.23 | 0.23 | 0.76178 | 0.763088 |

## A.5 (5 mm) Cases with Variable Inlet Air Velocity

**Table 1-13 (5 mm) cases with different INLET AIR VELOCITY**

| | FRESH | | EXHAUST | | FRESH | | EXHAUST | |
|---|---|---|---|---|---|---|---|---|
| **Velocity** | $\dot{m}_{fi}$ | $\dot{m}_{fo}$ | $\dot{m}_{ei}$ | $\dot{m}_{eo}$ | $T_{fi}$ | $T_{fo}$ **average** | $T_{ei}$ | $T_{eo}$ **average** |
| **m/s** | **kg/s** | **kg/s** | **kg/s** | **kg/s** | **C°** | **C°** | **C°** | **C°** |
| **0.5** | 0.951888 | 1.130276 | 0.898576 | 0.72058 | 6 | 16.467 | 22 | 6.361 |
| **1** | 1.903804 | 2.194668 | 1.797152 | 1.506456 | 6 | 17.007 | 22 | 7.17 |
| **1.5** | 2.85572 | 3.285828 | 2.695756 | 2.265704 | 6 | 17.059 | 22 | 7.576 |
| **2** | 3.807608 | 4.337116 | 3.594332 | 3.064852 | 6 | 17.141 | 22 | 7.907 |

**Table 1-14 (5 mm) FRESH Air composition with Variable Inlet Air Velocity**

| | FRESH | | | | | |
|---|---|---|---|---|---|---|
| Velocity | $H_2O_{fi}$ | $H_2O_{fo}$ **average** | $O_{2\,fi}$ | $O_{2\,fo}$ **average** | $N_{2\,fi}$ | $N_{2\,fo}$ **average** |
| m/s | kg/kg | kg/kg | kg/kg | kg/kg | kg/kg | kg/kg |
| **0.5** | 0.00492 | 0.00700613 | 0.23 | 0.23 | 0.76508 | 0.762962 |
| **1** | 0.00492 | 0.00717563 | 0.23 | 0.23 | 0.76508 | 0.7627 |
| **1.5** | 0.00492 | 0.00718518 | 0.23 | 0.23 | 0.76508 | 0.762815 |
| **2** | 0.00492 | 0.00720007 | 0.23 | 0.23 | 0.76508 | 0.7628 |

**Table 1-15 (5 mm) EXHAUST Air composition with Variable Inlet Air Velocity**

| | EXHAUST | | | | | |
|---|---|---|---|---|---|---|
| Velocity | $H_2O_{ei}$ | $H_2O_{eo}$ **average** | $O_{2\,ei}$ | $O_{2\,eo}$ **average** | $N_{2\,ei}$ | $N_{2\,eo}$ **average** |
| m/s | kg/kg | kg/kg | kg/kg | kg/kg | kg/kg | kg/kg |
| **0.5** | 0.00822 | 0.00495433 | 0.23 | 0.229434 | 0.76178 | 0.764976 |
| **1** | 0.00822 | 0.00519874 | 0.23 | 0.23 | 0.76178 | 0.764859 |
| **1.5** | 0.00822 | 0.00528025 | 0.23 | 0.23 | 0.76178 | 0.764723 |
| **2** | 0.00822 | 0.00534385 | 0.23 | 0.23 | 0.76178 | 0.764656 |

## A.6 (5 mm) Cases with Variable AMBIENT TEMPERATURE

**Table 1-16 (5 mm) cases with different AMBIENT TEMPERATURE**

| | FRESH | | EXHAUST | | FRESH | | EXHAUST | |
|---|---|---|---|---|---|---|---|---|
| Amb. Temp. | $\dot{m}_{fi}$ | $\dot{m}_{fo}$ | $\dot{m}_{ei}$ | $\dot{m}_{eo}$ | $T_{fi}$ | $T_{fo}$ average | $T_{ei}$ | $T_{eo}$ average |
| $^0C$ | kg/s | kg/s | kg/s | kg/s | $C^o$ | $C^o$ | $C^o$ | $C^o$ |
| **2** | 3.865652 | 4.355624 | 3.594332 | 3.104668 | **2** | 15.874 | 22 | 4.364 |
| **4** | 3.836532 | 4.345796 | 3.594332 | 3.084228 | **4** | 16.512 | 22 | 6.141 |
| **6** | 3.807608 | 4.336332 | 3.594332 | 3.065552 | **6** | 17.145 | 22 | 7.915 |
| **8** | 3.778936 | 4.326672 | 3.594332 | 3.046316 | **8** | 17.773 | 22 | 9.685 |
| **10** | 3.750488 | 4.317824 | 3.594332 | 3.02806 | **10** | 18.395 | 22 | 11.452 |

**Table 1-17 (5 mm) FRESH Air composition with Variable AMBIENT TEMPERATURE**

| | FRESH | | | | | |
|---|---|---|---|---|---|---|
| Amb. Temp. | $H_2O_{fi}$ | $H_2O_{fo}$ average | $O_{2\,fi}$ | $O_{2\,fo}$ average | $N_{2\,fi}$ | $N_{2\,fo}$ average |
| $^0C$ | kg/kg | kg/kg | kg/kg | kg/kg | kg/kg | kg/kg |
| **2** | **0.00371** | 0.00681727 | 0.23 | 0.23 | 0.76629 | 0.763183 |
| **4** | **0.00427** | 0.00699999 | 0.23 | 0.23 | 0.76573 | 0.763 |
| **6** | **0.00492** | 0.007205 | 0.23 | 0.23 | 0.76508 | 0.762795 |
| **8** | **0.00565** | 0.00743328 | 0.23 | 0.23 | 0.76435 | 0.762567 |
| **10** | **0.00647** | 0.00768709 | 0.23 | 0.23 | 0.76353 | 0.762313 |

**Table 1-18 (5mm) EXHAUST Air composition with Variable AMBIENT TEMPERATURE**

| | EXHAUST | | | | | |
|---|---|---|---|---|---|---|
| Amb. Temp. | $H_2O_{ei}$ | $H_2O_{eo}$ average | $O_{2\,ei}$ | $O_{2\,eo}$ average | $N_{2\,ei}$ | $N_{2\,eo}$ average |
| $^0C$ | kg/kg | kg/kg | kg/kg | kg/kg | kg/kg | kg/kg |
| **2** | 0.00822 | 0.00428307 | 0.23 | 0.23 | 0.76178 | 0.765717 |
| **4** | 0.00822 | 0.00477823 | 0.23 | 0.23 | 0.76178 | 0.76178 |
| **6** | 0.00822 | 0.00534779 | 0.23 | 0.23 | 0.76178 | 0.764652 |
| **8** | 0.00822 | 0.00598552 | 0.23 | 0.23 | 0.76178 | 0.764014 |
| **10** | 0.00822 | 0.00670055 | 0.23 | 0.23 | 0.76178 | 0.763299 |

# Appendix B EXERGETIC RESULTS

## B.1 (25 mm) Pitch Length Cases with variable Inlet Air Velocity

### B.1.1 (25 mm, 6 $^0$C and 0.5 m/c)

**Table 1-19 Exergy results (25 mm, 6 $^0$C and 0.5 m/c)**

| Point | Location | Mass (Kg/s) | Temp. (C) | H | S | Ex-Phy (W) | Ex-Ch (kW) | Ex (kW) |
|---|---|---|---|---|---|---|---|---|
| 1 | Fresh air inlet- Fan | 0.4675 | 6.00 | 6.0897 | 6.8487 | 0.0000 | **1.93** | **1.93** |
| 2 | Fresh air Outlet- Fan/inlet- Membrane | 0.4675 | 7.45 | 7.5632 | 6.8492 | 0.6236 | **1.93** | **2.56** |
| 3 | Fresh air outlet- Membrane | 0.5265 | 17.98 | 18.3022 | 6.9014 | 1.3156 | **2.04** | **3.36** |
| 4 | Exhaust air inlet- Fan | 0.4413 | 20.48 | 20.8597 | 6.9188 | 2.1175 | **1.67** | **3.79** |
| 5 | Exhaust air Outlet- Fan/inlet- Membrane | 0.4413 | 22.00 | 22.4136 | 6.9193 | 1.4934 | **1.67** | **3.17** |
| 6 | Exhaust air outlet- Membrane | 0.3823 | 10.09 | 10.2515 | 6.8637 | -0.001 | **1.55** | **1.54** |

**Table 1-20 Exergy destruction results (25 mm, 6 $^0$C and 0.5 m/c)**

| No. | Component | Inlet exergy Ein | Outlet exergy Eout | Exergy-Destruction Edes | Exergy Destruction % |
|---|---|---|---|---|---|
| 1 | Fan-1 | 2.62 | 2.56 | 0.07 | 4.72 |
| 2 | Membrane | 5.73 | 4.90 | 0.82 | 59.53 |
| 3 | Fan-2 | 0.69 | 0.62 | 0.06 | 4.45 |
| 4 | House | 3.36 | 3.79 | 0.43 | 31.30 |

**Table 1-21 Exergy destruction (Fuel-Product) results (25 mm, 6 $^0$C and 0.5 m/c)**

| No. | Component | Exergy-Destruction [kw] | Fuel [kw] | Product [kw] | Exergy-Destruction [kw] |
|---|---|---|---|---|---|
| 1 | Fan-1 | 0.07 | 0.69 | 0.62 | 0.07 |
| 2 | membrane | 0.82 | 1.62 | 0.80 | 0.82 |
| 3 | Fan-2 | 0.06 | 0.69 | 0.62 | 0.06 |
| 4 | House | 0.43 | 3.36 | 3.79 | 0.43 |

**Table 1-22 Exergetic efficiency results (25 mm, 6 $^0$C and 0.5 m/c)**

| | |
|---|---|
| Fuel (system) | 3.74 |
| Waste Exergy (system) | 2.93 |
| Fuel (membrane) | 1.62 |
| Product (membrane) | 0.80 |
| Exergy- Destruction (%) | 59.53 |
| **$\eta$ex (%)** | **49.28** |

**Table 1-23 Air composition in all the states (25 mm, 6 $^0$C, 0.5 m/s)**

| Reference-Composition | | Air1-P2 | Air2-P3 | Air3-P5 | Air4-P6 | |
|---|---|---|---|---|---|---|
| Nitrogen | 0.77371 | 0.76508 | 0.76273833 | 0.76178 | 0.76446586 | Composition ($Y_K$) |
| Oxygen | 0.23 | 0.23 | 0.23 | 0.23 | 0.23 | |
| H2O | 0.00371 | 0.00492 | 0.00726167 | 0.00822 | 0.00553414 | |
| Total | 1.00742 | 1 | 1 | 1 | 1 | |
| Molar Mass | 29.08324 | 28.86096 | 28.8328599 | 28.82136 | 28.8535903 | |

**Table 1-24 Chemical exergy calculations and results (25 mm, 6 $^0$C, 0.5 m/s)**

| | Component | $\bar{e}_k^{ch}$ | $y_k$ | $ex_{ch}$ | $E_{ch\ total}$ | $\dot{E}_{ch}$ |
|---|---|---|---|---|---|---|
| | - | J/mol | Kg/kg | J/mol | J/mol | KW |
| Air1-P2 | $N_2$ | 639 | 0.76508 | 13.4147981 | 119.4429239 | 1.93477857 |
| | $O_2$ | 3951 | 0.23 | 124.2225328 | | |
| | $H_2O$ | 8636 | 0.00492 | -18.194407 | | |
| Air1-P3 | Component | $\bar{e}_k^{ch}$ | $y_k$ | $ex_{ch}$ | $E_{ch\ total}$ | $\dot{E}_{ch}$ |
| | $N_2$ | 639 | 0.76273833 | 7.947392943 | 111.8769052 | 2.042918762 |
| | $O_2$ | 3951 | 0.23 | 124.2225328 | | |
| | $H_2O$ | 8636 | 0.00726167 | -20.29302063 | | |
| Air1-P5 | Component | $\bar{e}_k^{ch}$ | $y_k$ | $ex_{ch}$ | $E_{ch\ total}$ | $\dot{E}_{ch}$ |
| | $N_2$ | 639 | 0.76178 | 5.714662251 | 109.3309271 | 1.674027115 |
| | $O_2$ | 3951 | 0.23 | 124.2225328 | | |
| | $H_2O$ | 8636 | 0.00822 | -20.606267 | | |
| Air1-P6 | Component | $\bar{e}_k^{ch}$ | $y_k$ | $ex_{ch}$ | $E_{ch\ total}$ | $\dot{E}_{ch}$ |
| | $N_2$ | 639 | 0.76446586 | 11.97927336 | 117.2470794 | 1.553482876 |
| | $O_2$ | 3951 | 0.23 | 124.2225328 | | |
| | $H_2O$ | 8636 | 0.00553414 | -18.95472678 | | |

## B.1.2 (25 mm, 6 $^0$C and 1.0 m/c)

**Table 1-25 Exergy results (25 mm, 6 $^0$C and 1.0 m/c)**

| Point | Location | Mass (Kg/s) | Temp. (C) | H | S | Ex-Phy (W) | Ex-Ch (kW) | Ex (kW) |
|---|---|---|---|---|---|---|---|---|
| 1 | Fresh air inlet- Fan | 0.9349 | 6.00 | 6.0897 | 6.8487 | 0.0000 | **3.87** | **3.87** |
| 2 | Fresh air Outlet- Fan/inlet- Membrane | 0.9349 | 7.45 | 7.5632 | 6.8492 | 1.2471 | **3.87** | **5.12** |
| 3 | Fresh air outlet- Membrane | 1.0152 | 18.44 | 18.7748 | 6.9042 | 2.8504 | **3.92** | **6.77** |
| 4 | Exhaust air inlet- Fan | 0.8825 | 20.48 | 20.8597 | 6.9188 | 4.2346 | **3.35** | **7.58** |
| 5 | Exhaust air Outlet- Fan/inlet- Membrane | 0.8825 | 22.00 | 22.4136 | 6.9193 | 2.9865 | **3.35** | **6.33** |
| 6 | Exhaust air outlet- Membrane | 0.8023 | 11.68 | 11.8765 | 6.8723 | -0.643 | **3.21** | **2.57** |

**Table 1-26 Exergy destruction results (25 mm, 6 $^0$C and 1 m/c)**

| No. | Component | Inlet exergy Ein | Outlet exergy Eout | Exergy-Destruction Edes | Exergy Destruction % |
|---|---|---|---|---|---|
| 1 | Fan-1 | 5.25 | 5.12 | 0.13 | 4.11 |
| 2 | membrane | 11.45 | 9.34 | 2.11 | 66.43 |
| 3 | Fan-2 | 1.37 | 1.25 | 0.12 | 3.88 |
| 4 | House | 6.77 | 7.58 | 0.81 | 25.58 |

**Table 1-27 Exergy destruction (Fuel-Product) results (25 mm, 6 $^0$C and 1.0 m/c)**

| No. | Component | Exergy-Destruction [kw] | Fuel [kw] | Product [kw] | Exergy-Destruction [kw] |
|---|---|---|---|---|---|
| 1 | Fan-1 | 0.13 | 1.38 | 1.25 | 0.13 |
| 2 | membrane | 2.11 | 3.76 | 1.65 | 2.11 |
| 3 | Fan-2 | 0.12 | 1.37 | 1.25 | 0.12 |
| 4 | House | 0.81 | 6.77 | 7.58 | 0.81 |

**Table 1-28 Exergetic efficiency results (25 mm, 6 $^0$C and 1.0 m/c)**

| | |
|---|---|
| Fuel (system) | 7.43 |
| Waste Exergy (system) | 5.75 |
| Fuel (membrane) | 3.76 |
| Product (membrane) | 1.65 |
| Exergy- Destruction (%) | 66.43 |
| **$\eta$ex (%)** | **43.94** |

**Table 1-29 Air composition in all the states (25 mm, 6 $^0$C, 1.0 m/s)**

| Reference-Composition | | Air1-P2 | Air2-P3 | Air3-P5 | Air4-P6 | |
|---|---|---|---|---|---|---|
| Nitrogen | 0.77371 | 0.76508 | 0.76253434 | 0.76178 | 0.76395638 | Composition ($Y_K$) |
| Oxygen | 0.23 | 0.23 | 0.23 | 0.23 | 0.23 | |
| H2O | 0.00371 | 0.00492 | 0.00746566 | 0.00822 | 0.00604362 | |
| Total | 1.00742 | 1 | 1 | 1 | 1 | |
| Molar Mass | 29.08324 | 28.86096 | 28.83041208 | 28.82136 | 28.84747656 | |

**Table 1-30 Chemical exergy calculations and results (25 mm, 6 $^0$C, 1.0 m/s)**

| | $Component$ | $\bar{e}_k^{ch}$ | $y_k$ | $ex_{ch}$ | $E_{ch\ total}$ | $\dot{E}_{ch}$ |
|---|---|---|---|---|---|---|
| | - | J/mol | Kg/kg | J/mol | J/mol | KW |
| Air1-P2 | $N_2$ | 639 | 0.76508 | 13.4147981 | 119.4429239 | 3.869143284 |
| | $O_2$ | 3951 | 0.23 | 124.2225328 | | |
| | $H_2O$ | 8636 | 0.00492 | -18.19440704 | | |
| Air1-P3 | Component | $\bar{e}_k^{ch}$ | $y_k$ | $ex_{ch}$ | $E_{ch\ total}$ | $\dot{E}_{ch}$ |
| | $N_2$ | 639 | 0.76253434 | 7.471899948 | 111.3113732 | 3.91958692 |
| | $O_2$ | 3951 | 0.23 | 124.2225328 | | |
| | $H_2O$ | 8636 | 0.00746566 | -20.38305958 | | |
| Air1-P5 | Component | $\bar{e}_k^{ch}$ | $y_k$ | $ex_{ch}$ | $E_{ch\ total}$ | $\dot{E}_{ch}$ |
| | $N_2$ | 639 | 0.76178 | 5.714662251 | 109.3309271 | 3.34767489 |
| | $O_2$ | 3951 | 0.23 | 124.2225328 | | |
| | $H_2O$ | 8636 | 0.00822 | -20.606267 | | |
| Air1-P6 | Component | $\bar{e}_k^{ch}$ | $y_k$ | $ex_{ch}$ | $E_{ch\ total}$ | $\dot{E}_{ch}$ |
| | $N_2$ | 639 | 0.76395638 | 10.78925561 | 115.5473241 | 3.213578073 |
| | $O_2$ | 3951 | 0.23 | 124.2225328 | | |
| | $H_2O$ | 8636 | 0.00604362 | -19.4644643 | | |

### B.1.3 (25 mm, 6 $^0$C and 1.5 m/c)

**Table 1-31 Exergy results (25 mm, 6 $^0$C and 1.5 m/c)**

| Point | Location | Mass (Kg/s) | Temp. (C) | H | S | Ex-Phy (W) | Ex-Ch (kW) | Ex (kW) |
|---|---|---|---|---|---|---|---|---|
| 1 | Fresh air inlet- Fan | 1.4024 | 6.00 | 6.0897 | 6.8487 | 0.0000 | **5.80** | **5.81** |
| 2 | Fresh air Outlet- Fan/inlet- Membrane | 1.4024 | 7.45 | 7.5632 | 6.8492 | 1.8707 | **5.80** | **7.68** |
| 3 | Fresh air outlet- Membrane | 1.5054 | 18.44 | 18.773 | 6.9042 | 4.2281 | **5.81** | **10.04** |
| 4 | Exhaust air inlet- Fan | 1.3238 | 20.48 | 20.859 | 6.9188 | 6.3521 | **5.02** | **11.38** |
| 5 | Exhaust air Outlet- Fan/inlet- Membrane | 1.3238 | 22.00 | 22.413 | 6.9193 | 4.4799 | **5.02** | **9.50** |
| 6 | Exhaust air outlet- Membrane | 1.2208 | 12.44 | 12.653 | 6.8761 | -1.324 | **4.86** | **3.54** |

**Table 1-32 Exergy destruction results (25 mm, 6 $^0$C and 1.5 m/c)**

| No. | Component | Inlet exergy Ein | Outlet exergy Eout | Exergy-Destruction Edes | Exergy Destruction % |
|---|---|---|---|---|---|
| 1 | Fan-1 | 7.87 | 7.68 | **0.20** | 3.69 |
| 2 | membrane | 17.18 | 13.58 | **3.60** | 67.71 |
| 3 | Fan-2 | 2.06 | 1.87 | **0.18** | 3.48 |
| 4 | House | 10.04 | 11.38 | **1.33** | 25.13 |

**Table 1-33 Exergy destruction (Fuel-Product) results (25 mm, 6 $^0$C and 1.5 m/c)**

| No. | Component | Exergy-Destruction [kw] | Fuel [kw] | Product [kw] | Exergy-Destruction [kw] |
|---|---|---|---|---|---|
| 1 | Fan-1 | **0.20** | 2.07 | 1.87 | 0.20 |
| 2 | membrane | **3.60** | 5.96 | 2.36 | 3.60 |
| 3 | Fan-2 | **0.18** | 2.06 | 1.87 | 0.18 |
| 4 | House | **1.33** | 10.04 | 11.38 | 1.33 |

**Table 1-34 Exergetic efficiency results (25 mm, 6 $^0$C and 1.5 m/c)**

| | |
|---|---|
| Fuel (system) | 11.26 |
| Waste Exergy (system) | 8.85 |
| Fuel (membrane) | 5.96 |
| Product (membrane) | 2.36 |
| Exergy- Destruction (%) | 67.71 |
| **$\eta$ex (%)** | **39.67** |

**Table 1-35 Air composition in all the states (25 mm, 6 $^0$C, 1.5 m/s)**

| Reference-Composition | | Air1-P2 | Air2-P3 | Air3-P5 | Air4-P6 | |
|---|---|---|---|---|---|---|
| Nitrogen | 0.77371 | 0.76508 | 0.76252462 | 0.76178 | 0.76376908 | Composition (-) |
| Oxygen | 0.23 | 0.23 | 0.23 | 0.23 | 0.23 | |
| H2O | 0.00371 | 0.00492 | 0.00747538 | 0.00822 | 0.00623092 | |
| Total | 1.00742 | 1 | 1 | 1 | 1 | |
| Molar Mass | 29.08324 | 28.86096 | 28.8302954 | 28.82136 | 28.8452289 | |

**Table 1-36 Chemical exergy calculations and results (25 mm, 6 $^0$C, 1.5 m/s)**

| | *Component* | $\bar{e}_k^{ch}$ | $y_k$ | $ex_{ch}$ | $E_{ch\ total}$ | $\dot{E}_{ch}$ |
|---|---|---|---|---|---|---|
| | - | J/mol | Kg/kg | J/mol | J/mol | KW |
| Air1-P2 | $N_2$ | 639 | 0.76508 | 13.4147981 | 119.4429239 | 5.803921855 |
| | $O_2$ | 3951 | 0.23 | 124.2225328 | | |
| | $H_2O$ | 8636 | 0.00492 | -18.19440704 | | |
| Air1-P3 | Component | $\bar{e}_k^{ch}$ | $y_k$ | $ex_{ch}$ | $E_{ch\ total}$ | $\dot{E}_{ch}$ |
| | $N_2$ | 639 | 0.76252462 | 7.449246156 | 111.2847548 | 5.810834311 |
| | $O_2$ | 3951 | 0.23 | 124.2225328 | | |
| | $H_2O$ | 8636 | 0.00747538 | -20.38702417 | | |
| Air1-P5 | Component | $\bar{e}_k^{ch}$ | $y_k$ | $ex_{ch}$ | $E_{ch\ total}$ | $\dot{E}_{ch}$ |
| | $N_2$ | 639 | 0.76178 | 5.714662251 | 109.3309271 | 5.021702006 |
| | $O_2$ | 3951 | 0.23 | 124.2225328 | | |
| | $H_2O$ | 8636 | 0.00822 | -20.60626798 | | |
| Air1-P6 | Component | $\bar{e}_k^{ch}$ | $y_k$ | $ex_{ch}$ | $E_{ch\ total}$ | $\dot{E}_{ch}$ |
| | $N_2$ | 639 | 0.76376908 | 10.3519679 | 114.9481694 | 4.86488512 |
| | $O_2$ | 3951 | 0.23 | 124.2225328 | | |
| | $H_2O$ | 8636 | 0.00623092 | -19.62633139 | | |

### B.1.4 (25 mm, 6 $^0$C and 2.0 m/c)

**Table 1-37 Exergy results (25 mm, 6 $^0$C and 2.0 m/c)**

| Point | Location | Mass (Kg/s) | Temp. (C) | H | S | Ex-Phy (W) | Ex-Ch (kW) | Ex (kW) |
|---|---|---|---|---|---|---|---|---|
| 1 | Fresh air inlet- Fan | 1.8698 | 6.00 | 6.0897 | 6.8487 | 0.0000 | **7.74** | **7.74** |
| 2 | Fresh air Outlet- Fan/inlet- Membrane | 1.8698 | 7.45 | 7.5632 | 6.8492 | 2.4942 | **7.74** | **10.24** |
| 3 | Fresh air outlet- Membrane | 1.9953 | 18.28 | 18.6135 | 6.9035 | 5.5342 | **7.71** | **13.25** |
| 4 | Exhaust air inlet- Fan | 1.7651 | 20.48 | 20.8597 | 6.9188 | 8.4697 | **6.70** | **15.17** |
| 5 | Exhaust air Outlet- Fan/inlet- Membrane | 1.7651 | 22.00 | 22.4136 | 6.9193 | 5.9733 | **6.70** | **12.67** |
| 6 | Exhaust air outlet- Membrane | 1.6396 | 13.10 | 13.3237 | 6.8792 | -2.0988 | **6.51** | **4.41** |

**Table 1-38 Exergy destruction results (25 mm, 6 $^0$C and 2.0 m/c)**

| No. | Component | Inlet exergy Ein | Outlet exergy Eout | Exergy-Destruction Edes | Exergy Destruction % |
|---|---|---|---|---|---|
| 1 | Fan-1 | 10.50 | 10.24 | **0.26** | 3.40 |
| 2 | membrane | 22.91 | 17.66 | **5.25** | 68.35 |
| 3 | Fan-2 | 2.74 | 2.50 | **0.25** | 3.21 |
| 4 | House | 13.25 | 15.17 | **1.92** | 25.04 |

**Table 1-39 Exergy destruction (Fuel-Product) results (25 mm, 6 $^0$C and 2.0 m/c)**

| No. | Component | Exergy-Destruction [kw] | Fuel [kw] | Product [kw] | Exergy-Destruction [kw] |
|---|---|---|---|---|---|
| 1 | Fan-1 | 0.26 | 2.76 | 2.49 | 0.26 |
| 2 | membrane | 5.25 | 8.26 | 3.01 | 5.25 |
| 3 | Fan-2 | 0.25 | 2.74 | 2.50 | 0.25 |
| 4 | House | 1.92 | 13.25 | 15.17 | 1.92 |

**Table 1-40 Exergetic efficiency results (25 mm, 6 $^0$C and 2 m/c)**

| | |
|---|---|
| Fuel (system) | 15.16 |
| Waste Exergy (system) | 12.09 |
| Fuel (membrane) | 8.26 |
| Product (membrane) | 3.01 |
| Exergy- Destruction (%) | 68.35 |
| **$\eta$ex (%)** | **36.45** |

**Table 1-41 Air composition in all the states (25 mm, 6 $^0$C, 2.0 m/s)**

| Reference-Composition | | Air1-P2 | Air2-P3 | Air3-P5 | Air4-P6 | |
|---|---|---|---|---|---|---|
| Nitrogen | 0.77371 | 0.76508 | 0.76273833 | 0.76178 | 0.76446586 | Composition ($Y_K$) |
| Oxygen | 0.23 | 0.23 | 0.23 | 0.23 | 0.23 | |
| H2O | 0.00371 | 0.00492 | 0.00726167 | 0.00822 | 0.00553414 | |
| Total | 1.00742 | 1 | 1 | 1 | 1 | |
| Molar Mass | 29.08324 | 28.86096 | 28.83285996 | 28.82136 | 28.85359032 | |

**Table 1-42 Chemical exergy calculations and results (25 mm, 6 $^0$C, 2.0 m/s)**

| | *Component* | $\bar{e}_k^{ch}$ | $y_k$ | $ex_{ch}$ | $E_{ch\ total}$ | $\dot{E}_{ch}$ |
|---|---|---|---|---|---|---|
| | - | J/mol | Kg/kg | J/mol | J/mol | KW |
| Air1-P2 | $N_2$ | 639 | 0.76508 | 13.4147981 | 119.4429239 | 1.93477857 |
| | $O_2$ | 3951 | 0.23 | 124.2225328 | | |
| | $H_2O$ | 8636 | 0.00492 | -18.19440704 | | |
| Air1-P3 | Component | $\bar{e}_k^{ch}$ | $y_k$ | $ex_{ch}$ | $E_{ch\ total}$ | $\dot{E}_{ch}$ |
| | $N_2$ | 639 | 0.76273833 | 7.947392943 | 111.8769052 | 2.042918762 |
| | $O_2$ | 3951 | 0.23 | 124.2225328 | | |
| | $H_2O$ | 8636 | 0.00726167 | -20.29302063 | | |
| Air1-P5 | Component | $\bar{e}_k^{ch}$ | $y_k$ | $ex_{ch}$ | $E_{ch\ total}$ | $\dot{E}_{ch}$ |
| | $N_2$ | 639 | 0.76178 | 5.714662251 | 109.3309271 | 1.674027115 |
| | $O_2$ | 3951 | 0.23 | 124.2225328 | | |
| | $H_2O$ | 8636 | 0.00822 | -20.60626798 | | |
| Air1-P6 | Component | $\bar{e}_k^{ch}$ | $y_k$ | $ex_{ch}$ | $E_{ch\ total}$ | $\dot{E}_{ch}$ |
| | $N_2$ | 639 | 0.76446586 | 11.97927336 | 117.2470794 | 1.553482876 |
| | $O_2$ | 3951 | 0.23 | 124.2225328 | | |
| | $H_2O$ | 8636 | 0.00553414 | -18.95472678 | | |

## B.2 (25 mm) Pitch Length Cases with variable Ambient Temperature

### B.2.1 (25 mm, 2 $^0$C and 2.0 m/c)

**Table 1-43 Exergy results (25 mm, 2 $^0$C and 2.0 m/c)**

| Point | Location | Mass (Kg/s) | Temp. (C) | H | S | Ex-Phy (W) | Ex-Ch (kW) | Ex (kW) |
|---|---|---|---|---|---|---|---|---|
| 1 | Fresh air inlet- Fan | 1.8983 | 2.00 | 2.0212 | 6.827 | 0.0000 | **9.40** | **9.41** |
| 2 | Fresh air Outlet- Fan/inlet-Membrane | 1.8983 | 3.42 | 3.4628 | 6.8275 | 2.4754 | **9.40** | **11.88** |
| 3 | Fresh air outlet- Membrane | 2.0124 | 17.30 | 17.6121 | 6.8984 | 8.1599 | **9.18** | **17.34** |
| 4 | Exhaust air inlet- Fan | 1.7651 | 20.48 | 20.8597 | 6.9188 | 11.3324 | **7.89** | **19.22** |
| 5 | Exhaust air Outlet- Fan/inlet-Membrane | 1.7651 | 22.00 | 22.4136 | 6.9193 | 8.8325 | **7.89** | **16.72** |
| 6 | Exhaust air outlet- Membrane | 1.5443 | 10.86 | 11.038 | 6.8673 | -3.1994 | **7.27** | **4.07** |

**Table 1-44 Exergy destruction results (25 mm, 2 $^0$C and 2 m/c)**

| No. | Component | Inlet exergy Ein | Outlet exergy Eout | Exergy-Destruction Edes | Exergy Destruction % |
|---|---|---|---|---|---|
| 1 | Fan-1 | 12.14 | 11.88 | **0.26** | 2.73 |
| 2 | membrane | 28.61 | 21.41 | **7.19** | 75.09 |
| 3 | Fan-2 | 2.74 | 2.50 | **0.24** | 2.53 |
| 4 | House | 17.34 | 19.22 | **1.88** | 19.65 |

**Table 1-45 Exergy destruction (Fuel-Product) results (25 mm, 2 $^0$C and 2.0 m/c)**

| No. | Component | Exergy-Destruction [kw] | Fuel [kw] | Product [kw] | Exergy-Destruction [kw] |
|---|---|---|---|---|---|
| 1 | Fan-1 | **0.26** | 2.74 | 2.48 | 0.26 |
| 2 | membrane | **7.19** | 12.65 | 5.46 | 7.19 |
| 3 | Fan-2 | **0.24** | 2.74 | 2.50 | 0.24 |
| 4 | House | **1.88** | 17.34 | 19.22 | 1.88 |

**Table 1-46 Exergetic efficiency results (25 mm, 2 $^0$C and 2 m/c)**

| | |
|---|---|
| Fuel (system) | 16.77 |
| Waste Exergy (system) | 13.65 |
| Fuel (membrane) | 12.65 |
| Product (membrane) | 5.46 |
| Exergy- Destruction (%) | 75.09 |
| **$\eta$ex (%)** | **43.14** |

**Table 1-47 Air composition in all the states (25 mm, 2 $^0$C, 2.0 m/s)**

| Reference-Composition | | Air1-P2 | Air2-P3 | Air3-P5 | Air4-P6 | |
|---|---|---|---|---|---|---|
| **Nitrogen** | 0.77371 | 0.76629 | 0.76285202 | 0.76178 | 0.76431645 | Composition ($Y_K$) |
| **Oxygen** | 0.23 | 0.23 | 0.23 | 0.23 | 0.23 | |
| **H2O** | 0.00371 | 0.00371 | 0.00714798 | 0.00822 | 0.00568355 | |
| **Total** | 1.00742 | 1 | 1 | 1 | 1 | |
| **Molar Mass** | 29.08324 | 28.87548 | 28.83422424 | 28.82136 | 28.8517974 | |

**Table 1-48 Chemical exergy calculations and results (25 mm, 2 $^0$C, 2.0 m/s)**

| | $\bar{e}_k^{ch}$ | $y_k$ | $ex_{ch}$ | $E_{ch\ total}$ | $\dot{E}_{ch}$ |
|---|---|---|---|---|---|
| **Air1-P2** | - | J/mol | Kg/kg | J/mol | J/mol | KW |
| | $N_2$ | 639 | 0.76629 | 23.0300996 | 143.0342587 | 9.403200682 |
| | $O_2$ | 3951 | 0.23 | 135.463908 | | |
| | $H_2O$ | 8636 | 0.00371 | -15.45974891 | | |
| **Air1-P3** | **Component** | $\bar{e}_k^{ch}$ | $y_k$ | $ex_{ch}$ | $E_{ch\ total}$ | $\dot{E}_{ch}$ |
| | $N_2$ | 639 | 0.76285202 | 15.07973045 | 131.4810708 | 9.176335204 |
| | $O_2$ | 3951 | 0.23 | 135.463908 | | |
| | $H_2O$ | 8636 | 0.00714798 | -19.06256758 | | |
| **Air1-P5** | **Component** | $\bar{e}_k^{ch}$ | $y_k$ | $ex_{ch}$ | $E_{ch\ total}$ | $\dot{E}_{ch}$ |
| | $N_2$ | 639 | 0.76178 | 12.6079133 | 128.778026 | 7.886723377 |
| | $O_2$ | 3951 | 0.23 | 135.463908 | | |
| | $H_2O$ | 8636 | 0.00822 | -19.29379529 | | |
| **Air1-P6** | **Component** | $\bar{e}_k^{ch}$ | $y_k$ | $ex_{ch}$ | $E_{ch\ total}$ | $\dot{E}_{ch}$ |
| | $N_2$ | 639 | 0.76431645 | 18.46191792 | 135.7879864 | 7.268087481 |
| | $O_2$ | 3951 | 0.23 | 135.463908 | | |
| | $H_2O$ | 8636 | 0.00568355 | -18.13783945 | | |

## B.2.2 (25 mm, 4 $^0$C and 2.0 m/c)

**Table 1-49 (25 mm, 4 $^0$C and 2.0 m/c)**

| Point | Location | Mass (Kg/s) | Temp. (C) | H | S | Ex-KE(W) | Ex-Phy(W) | Ex-Ch(kW) | Ex (kW) |
|---|---|---|---|---|---|---|---|---|---|
| 1 | Fresh air inlet- Fan | 1.884 | 4.00 | 4.0544 | 6.8376 | 0.0038 | 0.0000 | **8.57** | **8.58** |
| 2 | Fresh air Outlet- Fan/inlet-Membrane | 1.884 | 5.44 | 5.5168 | 6.8382 | 0.0038 | 2.4419 | **8.57** | **11.02** |
| 3 | Fresh air outlet- Membrane | 2.0048 | 17.78 | 18.1019 | 6.9008 | 0.0040 | 6.9534 | **8.45** | **15.40** |
| 4 | Exhaust air inlet- Fan | 1.7651 | 20.48 | 20.8597 | 6.9188 | 0.0035 | 10.0598 | **7.29** | **17.35** |
| 5 | Exhaust air Outlet- Fan/inlet-Membrane | 1.7651 | 22.00 | 22.4136 | 6.9193 | 0.0035 | 7.5616 | **7.29** | **14.86** |
| 6 | Exhaust air outlet- Membrane | 1.5437 | 12.02 | 12.217 | 6.8733 | 0.0031 | -2.6732 | **6.70** | **4.03** |

**Table 1-50 Exergy destruction results (25 mm, 4 $^0$C and 2.0 m/c)**

| No. | Component | Inlet exergy Ein | Outlet exergy Eout | Exergy-Destruction Edes | Exergy Destruction % |
|---|---|---|---|---|---|
| 1 | Fan-1 | 11.33 | 11.02 | **0.31** | 3.50 |
| 2 | membrane | 25.88 | 19.43 | **6.44** | 71.97 |
| 3 | Fan-2 | 2.74 | 2.50 | **0.24** | 2.73 |
| 4 | House | 15.40 | 17.35 | **1.95** | 21.80 |

**Table 1-51 Exergy destruction (Fuel-Product) results (25 mm, 4 $^0$C and 2.0 m/c)**

| No. | Component | Exergy-Destruction [kw] | Fuel [kw] | Product [kw] | Exergy-Destruction [kw] |
|---|---|---|---|---|---|
| 1 | Fan-1 | **0.31** | 2.76 | 2.44 | 0.31 |
| 2 | membrane | **6.44** | 10.83 | 4.38 | 6.44 |
| 3 | Fan-2 | **0.24** | 2.74 | 2.50 | 0.24 |
| 4 | House | **1.95** | 15.40 | 17.35 | 1.95 |

**Table 1-52 Exergetic efficiency results (25 mm, 4 $^0$C and 2 m/c)**

| | |
|---|---|
| Fuel (system) | 16.03 |
| Waste Exergy (system) | 12.98 |
| Fuel (membrane) | 10.83 |
| Product (membrane) | 4.38 |
| Exergy- Destruction (%) | 71.97 |
| **$\eta$ex (%)** | **40.50** |

**Table 1-53 Air composition in all the states (25 mm, 4 $^0$C, 2.0 m/s)**

| Reference-Composition | | Air1-P2 | Air2-P3 | Air3-P5 | Air4-P6 | |
|---|---|---|---|---|---|---|
| **Nitrogen** | 0.77371 | 0.76573 | 0.76271677 | 0.76178 | 0.76399234 | Composition ($Y_K$) |
| **Oxygen** | 0.23 | 0.23 | 0.23 | 0.23 | 0.23 | |
| **H2O** | 0.00371 | 0.00427 | 0.00728323 | 0.00822 | 0.00600766 | |
| **Total** | 1.00742 | 1 | 1 | 1 | 1 | |
| **Molar Mass** | 29.08324 | 28.86876 | 28.83260124 | 28.82136 | 28.84790808 | |

**Table 1-54 Chemical exergy calculations and results (25 mm, 4 $^0$C, 2.0 m/s)**

| | | | | | | |
|---|---|---|---|---|---|---|
| **Air1-P2** | ***Component*** | $\bar{e}_k^{ch}$ | $y_k$ | $ex_{ch}$ | $E_{ch\ total}$ | $\dot{E}_{ch}$ |
| | - | J/mol | Kg/kg | J/mol | J/mol | KW |
| | $N_2$ | 639 | 0.76573 | 18.33403672 | 131.3697767 | 8.57330413 |
| | $O_2$ | 3951 | 0.23 | 129.8432204 | | |
| | $H_2O$ | 8636 | 0.00427 | -16.80748041 | | |
| **Air1-P3** | **Component** | $\bar{e}_k^{ch}$ | $y_k$ | $ex_{ch}$ | $E_{ch\ total}$ | $\dot{E}_{ch}$ |
| | $N_2$ | 639 | 0.76271677 | 11.33240911 | 121.4685738 | 8.446001622 |
| | $O_2$ | 3951 | 0.23 | 129.8432204 | | |
| | $H_2O$ | 8636 | 0.00728323 | -19.70705568 | | |
| **Air1-P5** | **Component** | $\bar{e}_k^{ch}$ | $y_k$ | $ex_{ch}$ | $E_{ch\ total}$ | $\dot{E}_{ch}$ |
| | $N_2$ | 639 | 0.76178 | 9.161287776 | 119.0544766 | 7.291226249 |
| | $O_2$ | 3951 | 0.23 | 129.8432204 | | |
| | $H_2O$ | 8636 | 0.00822 | -19.95003164 | | |
| **Air1-P6** | **Component** | $\bar{e}_k^{ch}$ | $y_k$ | $ex_{ch}$ | $E_{ch\ total}$ | $\dot{E}_{ch}$ |
| | $N_2$ | 639 | 0.76399234 | 14.29301827 | 125.2153171 | 6.70048187 |
| | $O_2$ | 3951 | 0.23 | 129.8432204 | | |
| | $H_2O$ | 8636 | 0.00600766 | -18.92092154 | | |

## B.2.3 (25 mm, 6 $^0$C and 2.0 m/c)

**Table 1-55 (25 mm, 6 $^0$C and 2.0 m/c)**

| Point | Location | Mass (Kg/s) | Temp. (C) | H | S | Ex-Phy (W) | Ex-Ch (kW) | Ex (kW) |
|---|---|---|---|---|---|---|---|---|
| 1 | Fresh air inlet- Fan | 1.8698 | 6.00 | 6.0897 | 6.8487 | 0.0000 | **7.74** | **7.74** |
| 2 | Fresh air Outlet- Fan/inlet- Membrane | 1.8698 | 7.45 | 7.5632 | 6.8492 | 2.4942 | **7.74** | **10.24** |
| 3 | Fresh air outlet- Membrane | 1.9969 | 18.26 | 18.5921 | 6.9034 | 5.5256 | **7.71** | **13.24** |
| 4 | Exhaust air inlet- Fan | 1.7651 | 20.48 | 20.8597 | 6.9188 | 8.4697 | **6.70** | **15.17** |
| 5 | Exhaust air Outlet- Fan/inlet- Membrane | 1.7651 | 22.00 | 22.4136 | 6.9193 | 5.9733 | **6.70** | **12.67** |
| 6 | Exhaust air outlet- Membrane | 1.5307 | 13.16 | 13.3883 | 6.8818 | -2.9715 | **6.01** | **3.04** |

**Table 1-56 Exergy destruction results (25 mm, 6 $^0$C and 2.0 m/c)**

| No. | Component | Inlet exergy Ein | Outlet exergy Eout | Exergy-Destruction Edes | Exergy Destruction % |
|---|---|---|---|---|---|
| 1 | Fan-1 | 10.50 | 10.24 | **0.26** | 2.88 |
| 2 | membrane | 22.91 | 16.29 | **6.62** | 73.14 |
| 3 | Fan-2 | 2.74 | 2.50 | **0.25** | 2.72 |
| 4 | House | 13.24 | 15.17 | **1.92** | 21.26 |

**Table 1-57 Exergy destruction (Fuel-Product) results (25 mm, 6 $^0$C and 2.0 m/c)**

| No. | Component | Exergy-Destruction [kw] | Fuel [kw] | Product [kw] | Exergy-Destruction [kw] |
|---|---|---|---|---|---|
| 1 | Fan-1 | **0.26** | 2.76 | 2.49 | 0.26 |
| 2 | membrane | **6.62** | 9.63 | 3.01 | 6.62 |
| 3 | Fan-2 | **0.25** | 2.74 | 2.50 | 0.25 |
| 4 | House | **1.92** | 13.24 | 15.17 | 1.92 |

**Table 1-58 Exergetic efficiency results (25 mm, 6 $^0$C and 2 m/c)**

| | |
|---|---|
| Fuel (system) | 15.16 |
| Waste Exergy (system) | 12.10 |
| Fuel (membrane) | 9.63 |
| Product (membrane) | 3.01 |
| Exergy- Destruction (%) | 73.14 |
| **$\eta$ex (%)** | **31.23** |

**Table 1-59 Air composition in all the states (25 mm, 6 $^0$C, 2.0 m/s)**

| Reference-Composition | | Air1-P2 | Air2-P3 | Air3-P5 | Air4-P6 | |
|---|---|---|---|---|---|---|
| **Nitrogen** | 0.77371 | 0.76508 | 0.76255998 | 0.76178 | 0.76320751 | Composition ($Y_K$) |
| **Oxygen** | 0.23 | 0.23 | 0.23 | 0.23 | 0.23 | |
| **H2O** | 0.00371 | 0.00492 | 0.00744002 | 0.00822 | 0.00679249 | |
| **Total** | 1.00742 | 1 | 1 | 1 | 1 | |
| **Molar Mass** | 29.08324 | 28.86096 | 28.83071976 | 28.82136 | 28.83849012 | |

**Table 1-60 Chemical exergy calculations and results (25 mm, 6 $^0$C, 2.0 m/s)**

| | *Component* | $\bar{e}_k^{ch}$ | $y_k$ | $ex_{ch}$ | $E_{ch\ total}$ | $\dot{E}_{ch}$ |
|---|---|---|---|---|---|---|
| | - | J/mol | Kg/kg | J/mol | J/mol | KW |
| **Air1-P2** | $N_2$ | 639 | 0.76508 | 13.4147981 | 119.4429239 | 7.738286569 |
| | $O_2$ | 3951 | 0.23 | 124.2225328 | | |
| | $H_2O$ | 8636 | 0.00492 | -18.19440704 | | |
| **Air1-P3** | **Component** | $\bar{e}_k^{ch}$ | $y_k$ | $ex_{ch}$ | $E_{ch\ total}$ | $\dot{E}_{ch}$ |
| | $N_2$ | 639 | 0.76255998 | 7.531658863 | 111.3817312 | 7.714624567 |
| | $O_2$ | 3951 | 0.23 | 124.2225328 | | |
| | $H_2O$ | 8636 | 0.00744002 | -20.37246055 | | |
| **Air1-P5** | **Component** | $\bar{e}_k^{ch}$ | $y_k$ | $ex_{ch}$ | $E_{ch\ total}$ | $\dot{E}_{ch}$ |
| | $N_2$ | 639 | 0.76178 | 5.714662251 | 109.3309271 | 6.695729121 |
| | $O_2$ | 3951 | 0.23 | 124.2225328 | | |
| | $H_2O$ | 8636 | 0.00822 | -20.60626798 | | |
| **Air1-P6** | **Component** | $\bar{e}_k^{ch}$ | $y_k$ | $ex_{ch}$ | $E_{ch\ total}$ | $\dot{E}_{ch}$ |
| | $N_2$ | 639 | 0.76320751 | 9.041514283 | 113.2292307 | 6.010022809 |
| | $O_2$ | 3951 | 0.23 | 124.2225328 | | |
| | $H_2O$ | 8636 | 0.00679249 | -20.03481646 | | |

## B.2.4 (25 mm, 8 $^0$C and 2.0 m/c)

**Table 1-61(25 mm, 8 $^0$C and 2.0 m/c)**

| Point | Location | Mass (Kg/s) | Temp. (C) | H | S | Ex-Phy (W) | Ex-Ch (kW) | Ex (kW) |
|---|---|---|---|---|---|---|---|---|
| 1 | Fresh air inlet- Fan | 1.8557 | 8.00 | 8.1276 | 6.8601 | 0.0000 | **6.90** | **6.91** |
| 2 | Fresh air Outlet- Fan/inlet-Membrane | 1.8557 | 9.46 | 9.6123 | 6.8607 | 2.4421 | **6.90** | **9.35** |
| 3 | Fresh air outlet- Membrane | 1.9891 | 18.74 | 19.0816 | 6.906 | 3.8803 | **6.98** | **10.87** |
| 4 | Exhaust air inlet- Fan | 1.7651 | 20.48 | 20.8597 | 6.9188 | 6.6569 | **6.10** | **12.76** |
| 5 | Exhaust air Outlet- Fan/inlet-Membrane | 1.7651 | 22.00 | 22.4136 | 6.9193 | 4.1622 | **6.10** | **10.27** |
| 6 | Exhaust air outlet- Membrane | 1.5249 | 14.28 | 14.5305 | 6.8857 | -1.2116 | **5.48** | **4.27** |

**Table 1-62 Exergy destruction results (25 mm, 8 $^0$C and 2.0 m/c)**

| No. | Component | Inlet exergy Ein | Outlet exergy Eout | Exergy-Destruction Edes | Exergy Destruction % |
|---|---|---|---|---|---|
| 1 | Fan-1 | 9.66 | 9.35 | **0.31** | 4.52 |
| 2 | membrane | 19.61 | 15.14 | **4.48** | 64.60 |
| 3 | Fan-2 | 2.74 | 2.49 | **0.25** | 3.58 |
| 4 | House | 10.87 | 12.76 | **1.89** | 27.30 |

**Table 1-63 Exergy destruction (Fuel-Product) results (25 mm, 8 $^0$C and 2.0 m/c)**

| No. | Component | Exergy-Destruction [kw] | Fuel [kw] | Product [kw] | Exergy-Destruction [kw] |
|---|---|---|---|---|---|
| 1 | Fan-1 | **0.31** | 2.76 | 2.44 | 0.31 |
| 2 | membrane | **4.48** | 6.00 | 1.52 | 4.48 |
| 3 | Fan-2 | **0.25** | 2.74 | 2.49 | 0.25 |
| 4 | House | **1.89** | 10.87 | 12.76 | 1.89 |

**Table 1-64 Exergetic efficiency results (25 mm, 8 $^0$C and 2 m/c)**

| | |
|---|---|
| Fuel (system) | 14.30 |
| Waste Exergy (system) | 11.20 |
| Fuel (membrane) | 6.00 |
| Product (membrane) | 1.52 |
| Exergy- Destruction (%) | 64.60 |
| **$\eta$ex (%)** | **25.35** |

**Table 1-65 Air composition in all the states (25 mm, 8 $^0$C, 2.0 m/s)**

| Reference-Composition | | Air1-P2 | Air2-P3 | Air3-P5 | Air4-P6 | |
|---|---|---|---|---|---|---|
| **Nitrogen** | 0.77371 | 0.76435 | 0.7623857 | 0.76178 | 0.76320751 | Composition ($Y_K$) |
| **Oxygen** | 0.23 | 0.23 | 0.23 | 0.23 | 0.23 | |
| **H2O** | 0.00371 | 0.00565 | 0.0076143 | 0.00822 | 0.00679249 | |
| **Total** | 1.00742 | 1 | 1 | 1 | 1 | |
| **Molar Mass** | 29.08324 | 28.8522 | 28.8286284 | 28.82136 | 28.8384901 | |

**Table 1-66 Chemical exergy calculations and results (25 mm, 8 $^0$C, 2.0 m/s)**

| | $Component$ | $\bar{e}_k^{ch}$ | $y_k$ | $ex_{ch}$ | $E_{ch\ total}$ | $\dot{E}_{ch}$ |
|---|---|---|---|---|---|---|
| | - | J/mol | Kg/kg | J/mol | J/mol | KW |
| **Air1-P2** | $N_2$ | 639 | 0.76435 | 8.293136791 | 107.3288326 | 6.903117083 |
| | $O_2$ | 3951 | 0.23 | 118.6018453 | | |
| | $H_2O$ | 8636 | 0.00565 | -19.56614944 | | |
| **Air1-P3** | **Component** | $\bar{e}_k^{ch}$ | $y_k$ | $ex_{ch}$ | $E_{ch\ total}$ | $\dot{E}_{ch}$ |
| | $N_2$ | 639 | 0.7623857 | 3.686215084 | 101.2299889 | 6.984604614 |
| | $O_2$ | 3951 | 0.23 | 118.6018453 | | |
| | $H_2O$ | 8636 | 0.0076143 | -21.05807145 | | |
| **Air1-P5** | **Component** | $\bar{e}_k^{ch}$ | $y_k$ | $ex_{ch}$ | $E_{ch\ total}$ | $\dot{E}_{ch}$ |
| | $N_2$ | 639 | 0.76178 | 2.268036725 | 99.60737768 | 6.100231992 |
| | $O_2$ | 3951 | 0.23 | 118.6018453 | | |
| | $H_2O$ | 8636 | 0.00822 | -21.26250433 | | |
| **Air1-P6** | **Component** | $\bar{e}_k^{ch}$ | $y_k$ | $ex_{ch}$ | $E_{ch\ total}$ | $\dot{E}_{ch}$ |
| | $N_2$ | 639 | 0.76320751 | 5.612188941 | 103.6154007 | 5.478897263 |
| | $O_2$ | 3951 | 0.23 | 118.6018453 | | |
| | $H_2O$ | 8636 | 0.00679249 | -20.59863348 | | |

## B.2.5 (25 mm, 10 $^0$C and 2.0 m/c)

**Table 1-67 (25 mm, 10 $^0$C and 2.0 m/c)**

| Point | Location | Mass (Kg/s) | Temp. (C) | H | S | Ex-Phy (W) | Ex-Ch (kW) | Ex (kW) |
|---|---|---|---|---|---|---|---|---|
| 1 | Fresh air inlet- Fan | 1.8418 | 10.00 | 10.1686 | 6.872 | 0.0000 | **6.07** | **6.07** |
| 2 | Fresh air Outlet- Fan/inlet-Membrane | 1.8418 | 11.47 | 11.6645 | 6.8725 | 2.4944 | **6.07** | **8.57** |
| 3 | Fresh air outlet- Membrane | 1.9814 | 19.22 | 19.2104 | 6.9063 | 1.3280 | **6.26** | **7.59** |
| 4 | Exhaust air inlet- Fan | 1.7651 | 20.48 | 20.8597 | 6.9188 | 4.5192 | **5.50** | **10.03** |
| 5 | Exhaust air Outlet- Fan/inlet-Membrane | 1.7651 | 22.00 | 22.4136 | 6.9193 | 2.0263 | **5.50** | **7.53** |
| 6 | Exhaust air outlet- Membrane | 1.5192 | 15.42 | 13.2328 | 6.8819 | 0.3965 | **4.88** | **5.28** |

**Table 1-68 Exergy destruction results (25 mm, 10 $^0$C and 2.0 m/c)**

| No. | Component | Inlet exergy Ein | Outlet exergy Eout | Exergy-Destruction Edes | Exergy Destruction % |
|---|---|---|---|---|---|
| 1 | Fan-1 | 8.83 | 8.57 | **0.26** | 4.22 |
| 2 | membrane | 16.10 | 12.87 | **3.23** | 52.29 |
| 3 | Fan-2 | 2.74 | 2.49 | **0.25** | 4.04 |
| 4 | House | 7.59 | 10.03 | **2.44** | 39.45 |

**Table 1-69 Exergy destruction (Fuel-Product) results (25 mm, 10 $^0$C and 2.0 m/c)**

| No. | Component | Exergy-Destruction [kw] | Fuel [kw] | Product [kw] | Exergy-Destruction [kw] |
|---|---|---|---|---|---|
| 1 | Fan-1 | **0.26** | 2.76 | 2.49 | 0.26 |
| 2 | membrane | **3.23** | 2.26 | -0.98 | 3.23 |
| 3 | Fan-2 | **0.25** | 2.74 | 2.49 | 0.25 |
| 4 | House | **2.44** | 7.59 | 10.03 | 2.44 |

**Table 1-70 Exergetic efficiency results (25 mm, 10 $^0$C and 2 m/c)**

| | |
|---|---|
| Fuel (system) | 14.01 |
| Waste Exergy (system) | 11.46 |
| Fuel (membrane) | 3.23 |
| Product (membrane) | 0.98 |
| Exergy- Destruction (%) | 52.29 |
| **$\eta$ex (%)** | **43.40** |

**Table 1-71 Air composition in all the states (25 mm, 10 $^0$C, 2.0 m/s)**

| Reference-Composition | | Air1-P2 | Air2-P3 | Air3-P5 | Air4-P6 | |
|---|---|---|---|---|---|---|
| Nitrogen | 0.77371 | 0.76353 | 0.76219125 | 0.76178 | 0.76274795 | Composition ($Y_K$) |
| Oxygen | 0.23 | 0.23 | 0.23 | 0.23 | 0.23 | |
| H2O | 0.00371 | 0.00647 | 0.00780875 | 0.00822 | 0.00725205 | |
| Total | 1.00742 | 1 | 1 | 1 | 1 | |
| Molar Mass | 29.08324 | 28.84236 | 28.826295 | 28.82136 | 28.8329754 | |

**Table 1-72 Chemical exergy calculations and results (25 mm, 10 $^0$C, 2.0 m/s)**

| | *Component* | $\bar{e}_k^{ch}$ | $y_k$ | $ex_{ch}$ | $E_{ch\ total}$ | $\dot{E}_{ch}$ |
|---|---|---|---|---|---|---|
| Air1-P2 | - | J/mol | Kg/kg | J/mol | J/mol | KW |
| | $N_2$ | 639 | 0.76353 | 2.943122973 | 95.02570647 | 6.068100744 |
| | $O_2$ | 3951 | 0.23 | 112.9811577 | | |
| | $H_2O$ | 8636 | 0.00647 | -20.89857422 | | |
| Air1-P3 | Component | $\bar{e}_k^{ch}$ | $y_k$ | $ex_{ch}$ | $E_{ch\ total}$ | $\dot{E}_{ch}$ |
| | $N_2$ | 639 | 0.76219125 | -0.210836423 | 91.00468911 | 6.25528501 |
| | $O_2$ | 3951 | 0.23 | 112.9811577 | | |
| | $H_2O$ | 8636 | 0.00780875 | -21.76563218 | | |
| Air1-P5 | Component | $\bar{e}_k^{ch}$ | $y_k$ | $ex_{ch}$ | $E_{ch\ total}$ | $\dot{E}_{ch}$ |
| | $N_2$ | 639 | 0.76178 | -1.178588801 | 89.88382824 | 5.504734864 |
| | $O_2$ | 3951 | 0.23 | 112.9811577 | | |
| | $H_2O$ | 8636 | 0.00822 | -21.91874067 | | |
| Air1-P6 | Component | $\bar{e}_k^{ch}$ | $y_k$ | $ex_{ch}$ | $E_{ch\ total}$ | $\dot{E}_{ch}$ |
| | $N_2$ | 639 | 0.76274795 | 1.100020606 | 92.60459175 | 4.879305511 |
| | $O_2$ | 3951 | 0.23 | 112.9811577 | | |
| | $H_2O$ | 8636 | 0.00725205 | -21.47658657 | | |